Development of a functional screen for MreB mutants in Bacillus subtilis and characterization of a putative MreB effector

Alba De San Eustaquio Campillo

NNT : 2017SACLS071

THESE DE DOCTORAT
DE
L'UNIVERSITE PARIS-SACLAY
PREPAREE A
L'UNIVERSITE PARIS-SUD

ECOLE DOCTORALE N° 577
Structure et Dynamique des Systèmes Vivants

Spécialité de doctorat : Sciences de la Vie et de la Santé

Par

Mme Alba de San Eustaquio Campillo

Development of a functional screen for MreB mutants in *Bacillus subtilis* and characterization of a putative MreB effector

Thèse présentée et soutenue à Jouy en Josas, le 27 Mars 2017 :

Composition du Jury :

Pr. Bayan, Nicolas	PR, Université Paris Sud	Président du jury
Dr. Buddelmeijer, Nienke	DR, Institut Pasteur	Examinatrice
Dr. Galinier, Anne	DR, Université Aix-Marseille	Rapportrice
Dr. Mignot, Tam	DR, Université Aix-Marseille	Rapporteur
Dr. Chastanet, Arnaud	CR1, INRA	Directeur de thèse

Université Paris-Saclay
Espace Technologique / Immeuble Discovery
Route de l'Orme aux Merisiers RD 128 / 91190 Saint-Aubin, France

Synthèse en français

Introduction

La majorité des cellules bactériennes sont entourées d'une enveloppe. Cette enveloppe est une structure complexe qui sépare la cellule de son environnement, agit comme une barrière de diffusion et une interface de communication et qui contrecarre la forte pression de turgescence interne (Radeck, Fritz, & Mascher, 2016). La structure de l'enveloppe divise la plupart des bactéries en mono derme ou Gram-positives (G+) et di derme ou Gram-négatives (G-) (Dufresne & Paradis-Bleau, 2015). Chez les bactéries G+, l'enveloppe est formée par une membrane cytoplasmique et une paroi cellulaire (CW) multicouches. L'enveloppe des G- a une membrane cytoplasmique ou intérieure, une membrane externe supplémentaire et une CW entre elles, plus mince que celles des G+s (Dufresne & Paradis-Bleau, 2015).

Les parois des G+s et G-s sont principalement formées de peptidoglycan, ainsi que de molécules chargées négativement (acides téichoïques) chez les bactéries G+. Le peptidoglycan (PG) forme un maillage macromoléculaire dont la structure est critique pour le maintien de l'intégrité cellulaire (van Heijenoort, 1998), dont la synthèse est assurées par des machineries de synthèse du PG. Les protéines cytosquelettiques constituent un élément important de ces machineries de synthèse du PG en permettant lier tous les protéines nécessaires à ce procès. On peut cependant différencier deux types de machinerie de synthèse de fonctions différentes et présentant des protéines cytosquelettiques caractéristiques : celles permettant la synthèse de la paroi latérale lors de l'élongation (élongasome) et celles réalisant la synthèse du septum pendant la division (divisome). L'élongasome comporte un homologue procaryote de l'actine, MreB. Le divisome a comme élément le plus caractéristique FtsZ, un homologue procaryote de la tubulin (Egan, Cleverley, Peters, Lewis, & Vollmer, 2016). On pense que ces protéines cytosquelettiques bactériennes créent des échafaudages, positionnant les machineries de synthèse du PG pendant l'allongement et la division cellulaire, respectivement (Egan et al., 2016).

Les protéines impliquées dans la synthèse du PG ont fait l'objet d'études approfondies depuis longtemps. Néanmoins, il existe encore de nombreuses questions sans réponses. L'absence ou la malformation de cette barrière du PG essentielle provoque la perte de forme et, en fin de compte, la lyse des cellules. L'intégrité de la paroi est donc une question d'importance vitale pour les bactéries. La composition et le fonctionnement précis des mécanismes de synthèse du PG pendant l'allongement ne sont pas complètement compris, mais ils dépendent d'un acteur clé: MreB. J'ai utilisé *Bacillus subtilis*, le modèle des bactéries G+, pour mieux comprendre le rôle de MreB dans la morphogenèse bactérienne. Dans ce but, j'ai caractérisé un opéron de fonction inconnu dont l'expression est

dépendante de MreB et j’ai développé un crible génétique qui m’a permis de sélectionner des mutants de perte de fonction de *mreB*.

Résultats

Étude d'un effecteur potentiel de MreB

Des résultats non publiés de notre groupe ont révélé l'existence d'un opéron non caractérisé (*ydcFGH*), dont l'expression est fortement induite en absence de *mreB*. Un certain nombre d'expériences ont été menées afin de caractériser l'opéron *ydcFGH*, sa régulation et le lien entre cet opéron et MreB. Les conclusions tirées des expériences menées sont:

1. YdcH: un répresseur / activateur régulateur de la transcription du type MarR?

L'approche globale que nous avons utilisée a révélé un très grand nombre de gènes affectés, positivement et négativement, par YdcH (Figure 1). Bien que surprenant, plusieurs hypothèses peuvent expliquer ces résultats. Une possibilité simple serait qu’YdcH affecte l'activité d'autres régulateurs. Cela peut être soit par activation ou répression directe des gènes impliqués dans la régulation d'autres procès, soit parce que les modifications physiologiques de l'absence d’*ydcH*, à leur tour, ont activé ou désactivé ces régulateurs. Nous ne pouvions pas trouver des régulons complets régulés vers le haut ou vers le bas, mais tels régulons peuvent être partiellement cachés par des régulations croisés de leurs gènes.

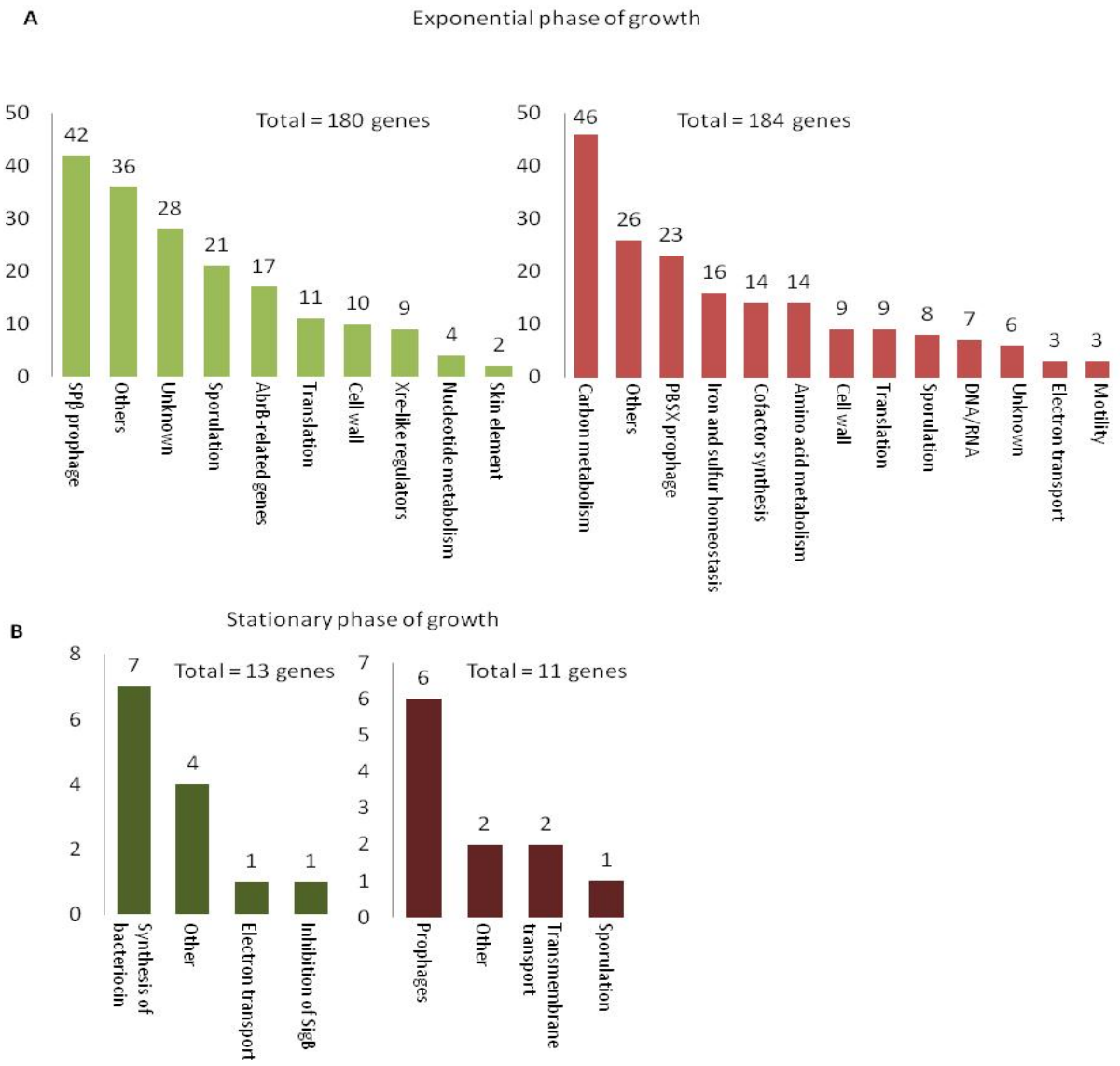

Figure 1. Differentially expressed genes in absence of *ydcH*. Results from the RNAseq experiment comparing gene expression levels in a WT (ABS2005) and a Δ*ydcH* strain (ASEC56) show that, in absence of *ydcH*, during exponential growth (**A**), there are 180 unrepressed genes (green) and 184 down-regulated genes (red); during stationary growth (**B**) there are 13 up-regulated (dark green) and 11 down-regulated genes (dark red).

Une autre hypothèse est qu'YdcH pourrait agir à la fois comme un répresseur et un activateur de l'expression des gènes. La plupart des régulateurs de transcription du type MarR (ce qu'YdcH semble être) décrits agissent comme des répresseurs et quelques-uns comme activateurs (Grove, 2013). Il n'y a que deux régulateurs de transcription du type MarR connus qui ont les deux activités (Oh, Shin, & Roe, 2007; Tran et al., 2005). Ils agissent comme des répresseurs en se liant à des séquences d'ADN proches des régions promotrices des gènes réprimés. Lorsque les conditions environnementales sont modifiées, ils subissent une modification structurelle qui entraîne une réduction de leur affinité pour l'ADN et leur permet de lier l'ARN polymérase, ce qui améliore sa liaison à la région promotrice du

gène régulé. Par conséquent, c'est une possibilité qui vaut la peine d'être vérifiée dans le futur pour YdcH.

2. YdcH: un nouveau régulateur de l'état de transition

Plusieurs lignes de preuve préconisent qu'YdcH soit un nouveau régulateur de l'état de transition qui pourrait aider à la cellule à s'adapter aux changements environnementaux, de manière similaire à celle de AbrB ou SigH (Britton et al., 2002; Phillips & Strauch, 2002). Tout d'abord, le profil d'expression d'*ydcFGH* montre que le point culminant de l'expression (probablement lorsque YdcH est inactif) coïncide avec la transition entre la phase de croissance exponentielle et stationnaire. Ceci est bien confirmé par la différence dramatique entre les profils globaux d'expression génique pendant la phase de croissance exponentielle et la phase stationnaire. Ceux-ci montrent que l'énorme regulon d'YdcH est dérégulé une fois que les cellules ont entrées en phase stationnaire (presque pas de différences entre WT et Δ*ydcH*). Il n'est pas surprenant que plusieurs gènes régulés par un autre régulateur de l'état de transition, par AbrB, soient également affectés en l'absence d'YdcH. Deuxièmement, il existe une grande diversité de fonctions affectées par YdcH conduisant à une reprogrammation globale de l'expression des gènes, typique de ces régulateurs (Strauch & Hoch, 1993). Troisièmement, parmi ces nombreux gènes, un grand sous-ensemble est impliqué dans le métabolisme du carbone ou des acides aminés, tous ces deux étant considérablement affectés à l'entrée en phase stationnaire en raison de l'épuisement de certaines sources de carbone. Fait intéressant, nous avons remarqué de nombreux gènes du regulon d'YdcH liés à la synthèse de plusieurs bacteriotoxins: *albABCDEFG* (bacteriocine antilistérienne subtilosine), *ntdR* (antibiotique kanosamine), *sdpA*, *sdpI* et *yknW* (toxine de SdpC) et *yydGHIJ* (contrôle du système LiaR-LiaS comme réponse à la bacitracine). Cela pourrait être une stratégie pour la cellule pour récupérer de nouvelles ressources à partir d'un environnement appauvri (Abriouel, Franz, Ben Omar, & Galvez, 2011). Tous ensemble, nos résultats suggèrent que, lors de la transition de la phase exponentielle à la phase stationnaire de croissance, la répression d'YdcH est partiellement libérée (comme l'a observé l'étude de l'expression de P_{ydc1}) conduisant à l'activation ou répression d'un grand ensemble de gènes, entraînant potentiellement une reprogrammation de la cellule. Nous faisons l'hypothèse qu'YdcH agit comme un régulateur de l'état de transition chez *B. subtilis*, agissant peut-être à la fois comme activateur et répresseur. Nous pouvons imaginer qu'YdcH soit actif pendant la croissance exponentielle, réprime sa propre expression et celle d'autres régulateurs de transcription. Pendant la phase stationnaire, YdcH est inactive. Cela entraînerait l'activation de ces régulateurs de transcription qui pourraient alors agir positivement ou négativement sur les plus de 300 gènes qui apparaissent différemment exprimés dans la souche Δ*ydcH* par rapport au WT pendant la phase stationnaire.

Pour aller plus loin dans notre compréhension d'YdcH et de ses fonctions et pour vérifier notre hypothèse, nous devrions identifier la séquence d'ADN à laquelle YdcH se lie, la "boîte d'YdcH ",

dans P_{ydc1}. Nous pourrions alors effectuer une prédiction *in silico* des "boîtes d'YdcH" dans d'autres promoteurs afin d'essayer une caractérisation plus précise du regulon d'YdcH. Si YdcH provoque un effet large dans la cellule, en utilisant l'approche de RNAseq nous récupérerons les données de tous les changements produits dans la cellule: ceux qui sont directement liés à YdcH et ceux qui sont causés indirectement (par des gènes contrôlés par YdcH). Les expériences de démonstration pourraient également nous fournir des informations sur la fonction et les effecteurs d'YdcH.

Etude de structure-fonctionne de MreB

1. Une bibliothèque de mutants de MreB avec affectation de sa fonctionne

Nous avons développé une méthodologie pour obtenir des mutants de MreB (MreB*s) et un criblage pour leur sélectionner selon leur perte de fonctionnalité grâce à l'activation de P_{mreBH}. Bien qu'il soit difficile d'obtenir MreB*s avec un seul résidu modifié en raison de l'acquisition spontanée de mutations supplémentaires ou de mutations suppresseurs, nous avons construit avec succès une collection de mutants présentant une variété de phénotypes (Figure 2). À l'avenir, en utilisant différents rapporteurs de la fonctionnalité de MreB, nous pourrions agrandir notre bibliothèque et avoir une vision complète de la manière dont MreB exerce son activité. L'addition de Mg^{+2} et de sucres (regarder la prochaine sectionne) pendant le processus de mutagenèse pourrait aider à récupérer des mutants supplémentaires. Enfin, ces mutants seront un atout pour les futures études biochimiques afin de déterminer les propriétés biochimiques de MreB chez *B. subtilis*. L'interaction des protéines pourrait également être étudiée à travers des expériences de pull down ou du système des doubles hybrides chez la levure.

	MreB*	Mutation	Activation of P_{mreBH} (1)	Protein levels (2)	Growth		Cell morphology (5)	GFP-MreB (6)		
					CH (3)	LB (4)		Localization	Velocity	Density
WT-like	B1	I242N	L	+++	WT	WT	WT	P	WT	WT
	B2	N88I	L	+++	WT	WT	WT	P	WT	WT
	B7	E243G	L	+++	WT	WT	Interm	P	WT	WT
	B11	T41A	L	+++	WT	WT	WT	P	WT	WT
	B15	I142T	L	+++	WT	WT	WT	P	WT	WT
	B16	G216R	L	+++	WT	WT	WT-ish	P	WT	WT
	B18	V72I	L	+++	WT	WT	WT-ish	P	WT	WT
	B20	E31G	L	+++	WT	WT	WT	P	WT	WT
	B23	K52R	L	+++	WT	WT	Interm	P	WT	WT
	B25	S33T	L	+++	WT	WT	WT	P	WT	WT
	B27	I174M	L	+++	WT	WT	WT	P	WT	WT
	B28	D189G	L	+++	WT	WT	Interm	P	WT	WT
	B29	R66C	L	+++	WT	WT	Interm	P	WT	WT
	B37	T79M	L	+++	WT	WT	WT	P	WT	WT
	B39	D121E	L	+++	WT	WT	WT	P	WT	WT
	B41	I134V	L	+++	WT	WT	WT	P	WT	WT
	B44	P32L	L	+++	WT	WT	WT	P	WT	WT
	B52	N49S	L	+++	WT	WT	WT	P	WT	WT
Intermediates	B5	K197E	H	+++	Δ*mreB*	WT	Interm	P	WT	WT
	B14	V114A	H	+++	Δ*mreB*	WT	Interm.	Dif & P	WT	Very low
	B21	V182A	H	+++	Δ*mreB*	WT	WT	P	WT	WT
	B26	A51V	H	+++	WT	WT	Interm.	P	WT	WT
	B42	P151Q	H	+++	Δ*mreB*	WT	Interm.	Dif & P	Static	Low
	B47	M155V	H	++	atypical	WT	Interm.	P	WT	WT
	B53	G60R	H	+++	Δ*mreB*	WT	Interm.	P	WT	WT
Δ*mreB*-like	B6	G160R	H	++	Δ*mreB*	Δ*mreB*	Interm.	Dif	-	-
	B19	G231D	H	++	Δ*mreB*	Δ*mreB*	Δ*mreB*	Dif	-	-
	B22	G14E	H	+	Δ*mreB*	Δ*mreB*	Interm.	Dif	-	-
	B4	G56R	H	+++	Δ*mreB*	WT	Δ*mreB*	Dif & P	-	Very low
	B58	I168F I169W	H	+	Δ*mreB*	Δ*mreB*	Δ*mreB*	Dif & P	Static	Very low
WeB	B10	S109P	H	+	WeB	WeB	Interm	Dif & P	Some static	Very low
	B17	A276G	H	+++	WeB	WeB	Interm	P	Some static	WT
	B30	I279V	H	+++	WeB	WeB	Interm	P	WT	WT
	B46	V72A	H	+++	WeB	WeB	Interm	P	WT	WT
	B32	L171P	H	+	WeB	WT	WeB	Dif	-	-

Figure 2. Classification of MreB*s based on their phenotypic characterization. (1) Expression of P_{mreBH} based on the color of the colony on LB plates supplemented with Xgal; L, low; H, high. (2) Estimated relative protein levels during exponential growth, based on western blot analysis. (3) Growth curve of cells grown in CH media at 37 °C; WeB stands for "Worst than Δ*mreB*". (4) Growth curve of cells grown in LB media at 37 °C. (5) Morphology of exponentially grown cells in CH media at 37 °C observed with bright field microscopy; interm. stands for intermediate phenotype between that of WT and Δ*mreB* strains. (6) GFP-MreB localization and dynamic properties qualitatively analyzed from TIRFM acquisitions; P, patches; Dif, diffusive.

2. MreB peut jouer un rôle dans la synthèse de la CW, la morphologie cellulaire et le métabolisme cellulaire

Malgré des années d'efforts prolongés, la (les) fonction (s) exacte (s) de MreB restent insaisissables. En créant un criblage génétique qui sélectionne des mutants de MreB de perte de fonctionne dans la bactérie G+ *B. subtilis*, nous avons pu contourner cette problématique et établir des liens entre la structure et la fonction de MreB. Il est difficile d'extraire des conclusions solides de nos résultats

préliminaires, mais nous avons réussi à l'acquisition d'un groupe très intéressant de mutants de MreB qui indiquent que MreB a plus d'une fonction chez *B. subtilis*.

Les corrélations structure-fonctionne nous permettent d'extraire des conclusions. Les mutants $MreB^{G160R}$ et $MreB^{G14E}$, avec un phénotype similaire a ce du Δ*mreB*, sont localisés dans le site putatif de liaison nucléotidique de MreB. En combinant la localisation et les résultats qui prouvent la perte de fonctionne de ces mutations, on peut en déduire que cette zone et, éventuellement l'activité de liaison des nucléotides de MreB, sont importantes pour le bon fonctionnement de la protéine. MreB*s $MreB^{G231D}$, $MreB^{G56R}$, avec un phénotype similaire a ce du Δ*mreB*, et $MreB^{L171P}$, avec un phénotype plus sévère que ce du Δ*mreB*, se trouvent à proximité immédiate de la zone putatif de formation du protofilament (les monomères de MreB se lient à d'autres monomères de MreB pour former des chaînes ou protofilaments). Ces trois mutants, comme ceux mentionnés ci-dessus, montrent une fonction MreB altérée et on peut donc déduire que cette zone, et probablement la capacité de polymérisation de MreB, sont importantes pour le bon fonctionnement de la protéine.

Il est intéressant de noter que certains mutants montrent un désaccouplement des défauts de forme et une déficience de la croissance. Quatre des MreB*s avec un phénotype plus sévère que ce du Δ*mreB* ($MreB^{S109P}$, $MreB^{A276G}$, $MreB^{I279V}$ et $MreB^{V72A}$) ont une morphologie WT et une localisation de MreB faiblement perturbées pendant que la croissance cellulaire, à la fois dans les milieux CH et LB, est très fortement perturbée. L'utilisation de *E. coli* montre que LB a présument des faibles quantités de sucres (estimées <100 μM). Leur épuisement marque la fin de la phase exponentielle de croissance des bactéries, moment où les cellules passent à la consommation d'acides aminés (Sezonov, Joseleau-Petit, & D'Ari, 2007). Lorsque *B. subtilis* est cultivé dans du LB, un diauxie peut être observé autour de $OD_{600\ nm}$ ~ 0,5, ce qui est vraisemblablement dû à l'épuisement des sucres du milieu aussi. C'est précisément le moment où la croissance des mutants $MreB^{S109P}$, $MreB^{A276G}$, $MreB^{I279V}$ et $MreB^{V72A}$ commence à se dégrader. $MreB^{S109P}$ et $MreB^{V72A}$ sont localisés à la surface de MreB, à proximité immédiate de l'interface putatif d'interaction interprotofilament; $MreB^{A276G}$ est localisé près de la zone putative de protofilament. Enfin, $MreB^{I279V}$ est muté dans un résidu interne, près de la zone supposée de polymérisation de MreB. Notre hypothèse est que ces mutations de MreB, d'une certaine manière, empêchent la cellule de passer de la glycolyse à la gluconéogenèse. Une possibilité tentante est que MreB agirait comme un point de contrôle reliant le métabolisme cellulaire et la synthèse de la CW. On sait que MreB interagit avec les protéines impliquées dans la synthèse des précurseurs de la CW (Favini-Stabile, Contreras-Martel, Thielens, & Dessen, 2013; Rueff et al., 2014) et nous pensons qu'il existe un équilibre entre MreB associée à la membrane et polymérisée et MreB qui est cytosolique. Il pourrait être possible que MreB agit comme un senseur du statut métabolique cellulaire pour coordonner la synthèse de la CW avec les besoins de la cellule. Cela pourrait expliquer pourquoi les défauts de forme et de croissance pourraient être désaccouplés.

Cette hypothèse est encore renforcée par les résultats obtenus avec le mutant MreB^{L171P}. Dans ce cas, nous perdons la morphologie WT et la localisation de MreB. En outre, une forte concentration de Mg^{+2} récupère son défaut de forme (come pour le Δ*mreB*), mais pas ses anomalies de croissance. D'autre part, l'addition de sucres améliore sa croissance sans affecter sa morphologie. On a déjà signalé des signes d'association entre la synthèse de la CW et le métabolisme cellulaire dans les bactéries. Il a été démontré que FtsZ est sensible aux niveaux de pyruvate et que la suppression d'un gène codant pour une kinase du pyruvate (pyk) chez *B. subtilis* affecte la formation du Z-ring et, par conséquent, la division (Monahan, Hajduk, Blaber, Charles, & Harry, 2014). La synthèse latérale de la CW a également été reliée au métabolisme cellulaire (Foulquier, Pompeo, Bernadac, Espinosa, & Galinier, 2011; Gorke, Foulquier, & Galinier, 2005). YvcK a deux rôles distincts, l'un dans le métabolisme du carbone et un autre dans la synthèse de la CW. La modification de ses niveaux de phosphorilation découpe les deux fonctionnes. Bien que sa fonctionne dans le métabolisme du carbone ne soit pas affectée par ses niveaux de phosphorilation, sa capacité à positionner correctement PBP1 est réduite. Ce qui est encore plus intéressant, c'est qu'YvcK, lorsqu'il est surproduit, est capable de sauver le mutant Δ*mreB*.

Compte tenu de toutes ces données, nous supposons que MreB peut servir de point de contrôle entre la synthèse latérale de la CW et le métabolisme cellulaire. MreB pourrait avoir une deuxième fonctionne dans le métabolisme des acides aminés qui est modifié par nos mutations avec un phénotype plus sévère que ce du Δ*mreB*. L'ajout de sucres permettrait à ces mutants de surmonter les effets négatifs d'un métabolisme des acides aminés altéré. Une vérification plus poussée sera faite pour l'identification du processus du métabolisme spécifiquement lié à MreB. Pour poursuivre la compréhension de MreB, si nous avons découplé le rôle de la protéine dans la morphologie cellulaire et le métabolisme cellulaire, nous pouvons la faire croitre dans des milieux minimaux définis complétés par différentes sources de carbone et monitoriser sa croissance. Nous profiterons également du MreB^{L171P} qui se développe comme la souche WT dans du LB pour élucider ce qui est nécessaire pour que ce mutant récupère la morphologie des cellules WT et la dynamique de la protéine MreB.

Possibilité de connexion entre la suppression de *mreB* et l'apparition de la mutation dans *ydcH*

Au début de ce projet, l'induction spécifique de l'opéron d'*ydcFGH* avait été observée en absence de *mreB*, appelant à l'élucidation de la fonctionne de cet effecteur potentiel spécifique de MreB, ainsi que son mode d'induction. Le résultat, dans les dernières semaines du doctorat, était inattendu.

La souche 3725 (Δ*mreB*) est censée être un parent direct du *B. subtilis* 168 de type sauvage et a été utilisée pendant de nombreuses années dans des laboratoires européens. En notant plusieurs mutations familières dans la liste des SNP présents dans cette souche, nous avons réalisé qu'une de ces

mutations, SepF^{M11T} était nécessaire pour que *B. subtilis* forme des formes L (Dominguez-Cuevas, 2011), tandis que plusieurs autres (*sigI, walR, accC*) affectent des gènes connus ou soupçonnés d'être impliqués dans la forme L et / ou d'être des gènes suppresseurs de défauts de Δ*mreB* (Dominguez-Cuevas, 2011; Schirner, 2009; Mercier, 2013).

Bien qu'il ne soit pas possible de suivre complètement la chaîne d'événements menant à l'apparition de tant de mutations dans la souche 3725, elles apparurent toutes dans un temps et un lieu (Oxford) où la forme L et le gène essentiel de MreB étaient étudiés. Il est concevable qu'ils aient été involontairement sélectionnés comme suppresseurs. À l'heure actuelle, on ne sait pas si la mutation dans *ydcH* était fortuite ou sélectionnée car elle améliore le phénotype du Δ*mreB*. Mais on peut spéculer que, si YdcH joue un rôle dans la régulation de l'état métabolique cellulaire, facilitant l'adaptation de la cellule aux conditions changeantes, y compris l'appauvrissement du carbone comme dans la transition de phase (agissant sur ~ 60 gènes impliqués dans le métabolisme du carbone) et si MreB relie la croissance cellulaire au métabolisme du carbone (voir les section sur YdcH et la mutagenèse de MreB), cette mutation peut donc augmenter la survie de la souche Δ*mreB* en modifiant le métabolisme du carbone et / ou des acides aminés et peut ne pas être accidentelle.

Bibliography

Abriouel, H., Franz, C. M., Ben Omar, N., & Galvez, A. (2011). Diversity and applications of *Bacillus* bacteriocins. *FEMS Microbiol Rev, 35*(1), 201-232. doi: 10.1111/j.1574-6976.2010.00244.x

Britton, R. A., Eichenberger, P., Gonzalez-Pastor, J. E., Fawcett, P., Monson, R., Losick, R., & Grossman, A. D. (2002). Genome-wide analysis of the stationary-phase sigma factor (sigma-H) regulon of *Bacillus subtilis*. *J Bacteriol, 184*(17), 4881-4890.

Dufresne, K., & Paradis-Bleau, C. (2015). Biology and assembly of the bacterial envelope. *Adv Exp Med Biol, 883*, 41-76. doi: 10.1007/978-3-319-23603-2_3

Egan, A. J., Cleverley, R. M., Peters, K., Lewis, R. J., & Vollmer, W. (2016). Regulation of bacterial cell wall growth. *FEBS J*. doi: 10.1111/febs.13959

Favini-Stabile, S., Contreras-Martel, C., Thielens, N., & Dessen, A. (2013). MreB and MurG as scaffolds for the cytoplasmic steps of peptidoglycan biosynthesis. *Environ Microbiol, 15*(12), 3218-3228. doi: 10.1111/1462-2920.12171

Foulquier, E., Pompeo, F., Bernadac, A., Espinosa, L., & Galinier, A. (2011). The YvcK protein is required for morphogenesis via localization of PBP1 under gluconeogenic growth conditions in *Bacillus subtilis*. *Mol Microbiol, 80*(2), 309-318. doi: 10.1111/j.1365-2958.2011.07587.x

Gorke, B., Foulquier, E., & Galinier, A. (2005). YvcK of *Bacillus subtilis* is required for a normal cell shape and for growth on Krebs cycle intermediates and substrates of the pentose phosphate pathway. *Microbiology, 151*(Pt 11), 3777-3791. doi: 10.1099/mic.0.28172-0

Grove, A. (2013). MarR family transcription factors. *Curr Biol, 23*(4), R142-143. doi: 10.1016/j.cub.2013.01.013

Monahan, L. G., Hajduk, I. V., Blaber, S. P., Charles, I. G., & Harry, E. J. (2014). Coordinating bacterial cell division with nutrient availability: a role for glycolysis. *MBio, 5*(3), e00935-00914. doi: 10.1128/mBio.00935-14

Oh, S. Y., Shin, J. H., & Roe, J. H. (2007). Dual role of OhrR as a repressor and an activator in response to organic hydroperoxides in *Streptomyces coelicolor*. *J Bacteriol, 189*(17), 6284-6292. doi: 10.1128/JB.00632-07

Phillips, Z. E., & Strauch, M. A. (2002). *Bacillus subtilis* sporulation and stationary phase gene expression. *Cell Mol Life Sci, 59*(3), 392-402.

Radeck, J., Fritz, G., & Mascher, T. (2016). The cell envelope stress response of *Bacillus subtilis*: from static signaling devices to dynamic regulatory network. *Curr Genet*. doi: 10.1007/s00294-016-0624-0

Rueff, A. S., Chastanet, A., Dominguez-Escobar, J., Yao, Z., Yates, J., Prejean, M. V., . . . Carballido-Lopez, R. (2014). An early cytoplasmic step of peptidoglycan synthesis is associated to MreB in *Bacillus subtilis*. *Mol Microbiol, 91*(2), 348-362. doi: 10.1111/mmi.12467

Sezonov, G., Joseleau-Petit, D., & D'Ari, R. (2007). *Escherichia coli* physiology in Luria-Bertani broth. *J Bacteriol, 189*(23), 8746-8749. doi: 10.1128/JB.01368-07

Strauch, M. A., & Hoch, J. A. (1993). Transition-state regulators: sentinels of *Bacillus subtilis* post-exponential gene expression. *Mol Microbiol, 7*(3), 337-342.

Tran, H. J., Heroven, A. K., Winkler, L., Spreter, T., Beatrix, B., & Dersch, P. (2005). Analysis of RovA, a transcriptional regulator of *Yersinia pseudotuberculosis* virulence that acts through antirepression and direct transcriptional activation. *J Biol Chem, 280*(51), 42423-42432. doi: 10.1074/jbc.M504464200

van Heijenoort, J. (1998). Assembly of the monomer unit of bacterial peptidoglycan. *Cell Mol Life Sci, 54*(4), 300-304. doi: 10.1007/s000180050155

Acknowledgements

I would like to thank all the people whose contribution, advice and support made the realization of this work possible. I would also like to acknowledge the following people, without whom, this adventure wouldn't have been possible:

- Dr. Arnaud Chastanet for his way of making everything seem like a game and his enthusiasm. But most of all, for his patience, never giving up in trying to make me a better scientist, support and guidance. Thank you.

- Dr. Rut Carballido Lopez for giving me the opportunity to come to her lab and sharing with me her never ending enthusiasm for science.

- All the Proced members, current and former, with whom I have shared the past years. Thank you for all the personal and professional advice, for making the everyday of this PhD so much easier.

- Colleagues from INRA that gave valuable help.

- My family, near and far, but always standing next to me.

Thank you all for making the past years such a great experience.

Abbreviations

CFU: colony forming unit

CH: casein hydrolysate medium

CM: cytoplasmic membrane

CP: carboxipeptidases

CSM: cell wall synthetic machinery

CW: cell wall

ddH_2O: distilled water

DSM: Difco sporulation medium

EP: endopeptidases

G-: Gram-negative bacteria

G+: Gram-positive bacteria

IF: intermediate filaments

LB: Luria Bertani medium

LPS : lipopolysaccharides

LPS: lipopolysaccharides

LTA: lipoteichoic acids

M/S: monomers of PG per strand

MC: competence medium

MSM: minimal salt medium

NAG-NAM: N-acetyl glucosamine-N-acetyl muramic acid

o/n: over night

OM: outer membrane

orf: open reading frame

PBP: penicillin binding protein

PG: peptidoglycan

polyGroP: polyglycerol phosphate

polyRboP : polyribitol phosphate

SNP: single nucleotide polymorphism

TA: teichoic acids

TG: transglycosilation

TP: transpeptidation

UDP-GlcNAc: UDP-*N*-acetylglucosamine

UDP-MurNAc: UDP-*N*-acetylmuramic acid

WTA: wall teichoic acids

Table of Contents

List of tables

List of figures

1. Introduction

1. Introduction

Free-living bacterial cells are surrounded by an envelope. This envelope is a complex structure that separates the cell from its environment, acts as a diffusive barrier and communication interface and counteracts the high internal turgor pressure (Radeck, Fritz, & Mascher, 2016). The structure of the envelope divides most of the bacteria in monoderm or Gram-positives (G+) and diderm or Gram-negatives (G-) (Dufresne & Paradis-Bleau, 2015). In Gram-positive bacteria, the envelope is formed by a cytoplasmic membrane (CM) and a multilayered cell wall (CW). Gram-negative's envelope has a cytoplasmic or inner membrane (IM), an additional outer membrane (OM), and a CW in between, thinner than in Gram-positives (Figure 1) (Dufresne & Paradis-Bleau, 2015).

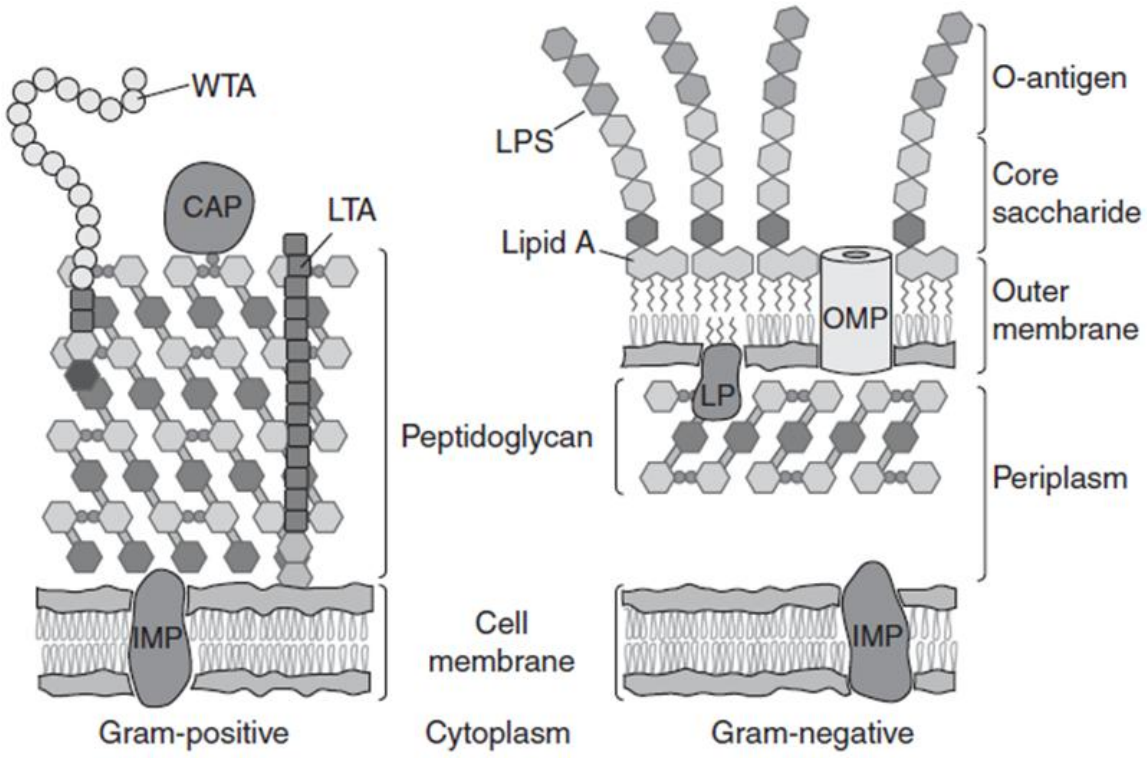

Figure 1 Depiction of Gram-positive and Gram-negative cell walls (modified from (Silhavy, Kahne, & Walker, 2010)). CAP, covalently attached protein; IMP, integral membrane protein; LTA, lipoteichoic acid; WTA, wall teichoic acid; LP, lipoprotein; OMP, outer membrane protein; LPS, lipopolysaccharide.

Both G+'s and G-'s CW are mainly formed of peptidoglycan and negatively charged molecules, in G+ bacteria (teichoic acids). Peptidoglycan forms a macromolecular mesh whose structure is crucial to maintaining cell integrity (J. van Heijenoort, 1998). Cytoskeletal proteins connect PG synthetic machineries to cytosolic processes. These machineries vary depending on whether the CW is being formed during elongation (elongasome) or division (divisome). Even though the process of PG synthesis follows the same steps, the proteins involved in it vary depending on the moment of the cell cycle (Egan, Cleverley, Peters, Lewis, & Vollmer, 2016).

1.1. Bacterial envelope

1.1.1 Cytoplasmic membrane

Gram-positive and Gram-negative bacteria have very similar CM. It is a symmetrical phospholipid bilayer carrying undecaprenyl-phosphate (lipid II carrier; see section 2.2.2), teichoic acid precursor carriers in G+ bacteria, intramembrane α-helice proteins and lipoproteins (Dufresne & Paradis-Bleau, 2015). Proteins in the CM are involved in many metabolic processes and look either towards the periplasm in G- (the space between the CM and OM) or the cytoplasm (Silhavy et al., 2010).

1.1.2 Cell wall

The CW is mainly formed of peptidoglycan (PG, also called murein) both in Gram-positive and Gram-negative bacteria. PG forms a polymeric macromolecule of various layers called sacculus. It is thought to be thicker in G+ bacteria than in G- (Gan, Chen, & Jensen, 2008; Hayhurst, Kailas, Hobbs, & Foster, 2008). It is formed by linear chains of the disaccharide N-acetyl glucosamine-N-acetyl muramic acid (NAG-NAM), cross-linked by pentapeptide bridges (Figure 2; see section 1.2) (Vollmer, Blanot, & de Pedro, 2008). The flexibility of the sacculus is given by the pentapeptide bond that can expand and shrink, whereas the glycan strand is rigid (Cava & de Pedro, 2014).

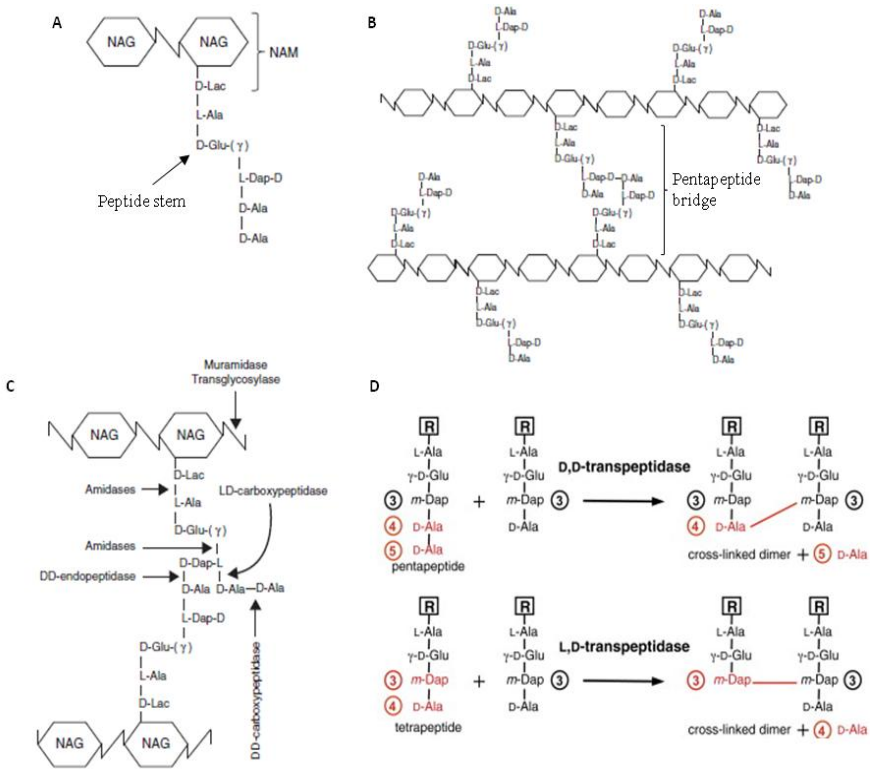

Figure 2 Peptidoglycan composition (modified from (Cava & de Pedro, 2014)). **A**. Chemical composition of the PG subunit. **B**. Fragment of the PG mesh with the glycan chains interconnected by a pentapeptide bridge. **C**. Site of action of PG hydrolases. **D**. Modified from (Lecoq et al., 2012). DD- and LD-transpeptidation. NAG, N-acetyl-glucosamine; NAM, N-acetyl muramic acid; D-Lac, D-lactate; L-Ala, L-alanine; D-Glu-(γ), D-gamma glutamate; L-Dap-D, meso-diamino pimelic acid; D-Ala, D-alanine; R, glycan strand.

Gram-positive bacteria have an extra CW component that isn't present in Gram-negatives, teichoic acids (TA). They constitute about 30-60 % of the CW mass, the rest being PG (Neuhaus & Baddiley,

2003). TA are anionic polymers with a short saccharidic linkage unit and multiple hydroxyl functional groups. They can be divided into wall teichoic acids (WTA) and lipoteichoic acids (LTA) (Neuhaus & Baddiley, 2003). There is a large variety of WTAs. They bind covalently to PG and go past it towards the exterior of the cell (Dufresne & Paradis-Bleau, 2015). The most common WTAs have a disaccharide attached to a polyribitol phosphate (polyRboP) or a polyglycerol phosphate (polyGroP) chain with a maximum of 60 repeats. The hydroxyl groups are modified with different molecules. These make WTAs such a varied class (Silhavy et al., 2010). LTAs are shorter than WTAs and have different chirality. They bind to the cytoplasmic membrane and don't stretch beyond the PG mesh (Dufresne & Paradis-Bleau, 2015). LTAs are always formed by polyGroP and have modified hydroxyl groups, as WTAs. TAs are essential to determine bacterial surface charge and hydrophobicity (Brown et al., 2013). They are also involved in the regulation of cell division, PG synthesis and morphogenesis (Brown, Santa Maria, & Walker, 2013). LTAs are also implicated in divalent cation homeostasis and membrane physiology (Percy & Grundling, 2014).

G- CW is formed of a thin layer of PG. It does not have TA anchored on the CW, but instead has another negatively charged lipidic molecule attached to the OM, the lipopolysaccharides (LPS, see section 1.3). In these organisms, the CW is located in the periplasm, the space between the CM and the OM. PG composition in G- bacteria is similar to that of G+s, but less cross-linked (Vollmer et al., 2008).

1.1.3 Outer membrane

Gram-negatives have an extra layer, the OM, that is not present in Gram-positives. It is porous to certain substances and is capable of transporting others, an aspect needed to allow cell metabolism and growth (Beveridge, 1999; Dufresne & Paradis-Bleau, 2015). It has intramembrane β-barrel proteins and specific lipoproteins organized in an asymmetrical lipid bilayer (Dufresne & Paradis-Bleau, 2015). The inner leaflet is formed by phospholipids while the outer leaflet is composed of anionic glycolipids, principally lipopolysaccharides (LPS) (Figure 1).

LPS are most commonly made of an anchor of lipid A (glucosamine-based phospholipid) that binds to the outer leaflet, a core oligosaccharide and a highly variable chain of oligosaccharides named O-antigen (Silhavy et al., 2010). The oligosaccharide core is divided into inner and outer core. The inner core links to lipid A and is formed by negatively charged sugars. The outer core is more diverse and links with the O-antigen, which is, again, highly variable. LPS are negatively charged and very abundant in the outer leaflet of the OM. The negative charges are counterbalanced by divalent cations like Mg^{2+} and Ca^{2+} (Dufresne & Paradis-Bleau, 2015). As TA in Gram-positive bacteria, LPS are determinants of surface charge and hydrofobicity in Gram-negative bacteria.

I will now focus on PG, the most important structural element of the bacterial envelope that is common to both G+ and G- bacteria. Its structure and synthesis are key for bacterial survival (Typas, Banzhaf, Gross, & Vollmer, 2011).

1.2. Peptidoglycan

PG, besides being such an important molecule in bacteria, is unique to bacteria (Bern, Beniston, & Mesnage, 2016). This makes it the target of many antibiotics. Even though it is common to most free-living bacteria, it presents some differences depending on the species (Bern et al., 2016) and in response to environmental conditions (Ruiz, 2016). There are two moments during the cell cycle in which PG is synthesized: cell division (at the septum) and cell elongation (at the side wall). The machineries in charge of the synthesis share most of their components, but some are specific for either division or elongation (Chastanet & Carballido-Lopez, 2012). For a more detailed description of these machineries see section 1.2.2.4.

1.2.1 Peptidoglycan structural models

The length of the glycan strand varies in different strains and growth conditions. Most Gram-negative bacteria have 20-100 monomers of PG per strand (M/S), but there is a preference for the lower values, 20-40 M/S (de Pedro & Cava, 2015). Entry into stationary phase causes a progressive reduction of PG strand length in both G+ and G- bacteria. This adaptation is due to post-synthesis processing of the macromolecule, rather than modification of the PG termination process (Pisabarro, de Pedro, & Vazquez, 1985).

The 3D structural organization of the PG is still unknown, but three main theoretical models have been proposed: 1. the horizontal layer model in which the strands run parallel to the cell surface, forming a circumference, 2. the scaffold model with PG strains running perpendicularly to the membrane and 3. the coiled-coil model with glycan strands forming a "rope" that surrounds the cell perpendicularly to the cell long axis (Figure 3).

1.2.1.1 Horizontal layered model:

Electron cryotomography studies performed on *Escherichia coli* and *Caulobacter crescentus* sacculi show glycan strands running parallel to the cell surface, wrapping the cell (Figure 3A) (Gumbart, Beeby, Jensen, & Roux, 2014). In this study, they advocate for a single layered PG CW in G- bacteria where glycan strains have a low level of organization. Another study showed similar results also in *E. coli*, with new PG being inserted in strands or patches (Typas et al., 2011).

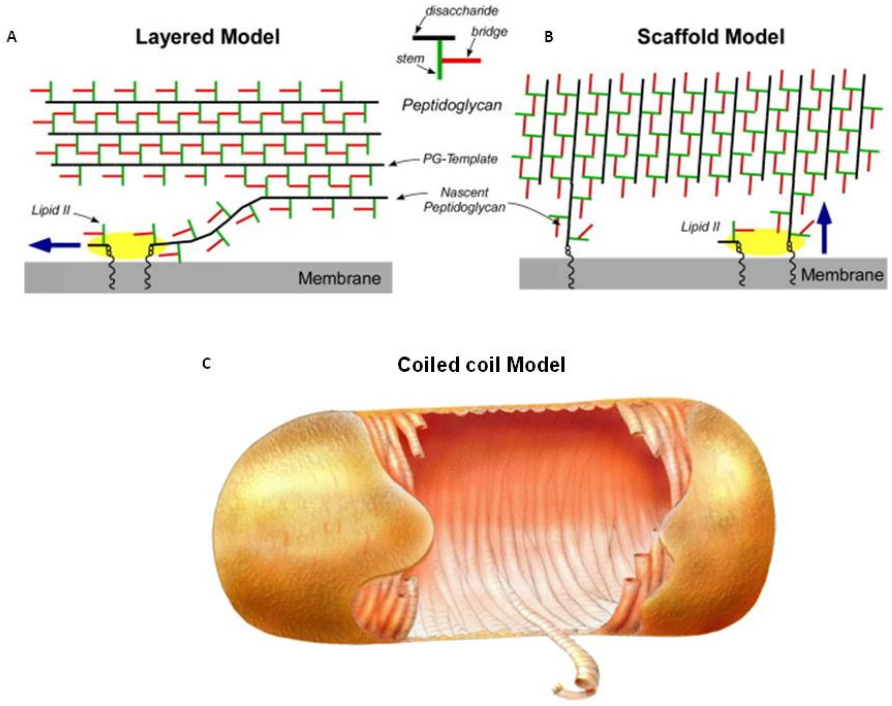

Figure 3 Peptidoglycan structure models (modified from (Kim, Chang, & Singh, 2015) and (Hayhurst et al., 2008)). **A**. Layered model with PG strands running parallel to the cytoplasmic membrane. **B**. Scaffold model with PG strands perpendicular to the cytoplasmic membrane. **C**. Coiled coil model with PG strands acting as ropes, surrounding the cell.

Studies on the 3D structure of PG in Gram-positive bacteria have to overcome the difficulty of a thick PG mesh. Fortunately, innovative techniques are starting to attenuate these difficulties. Recent results from Kim and coworkers (Kim et al., 2015) using solid-state NMR have demonstrated that PG strands in *Staphylococcus aureus* follow the layered model, as Gram-negative bacteria, but are highly ordered and packed, contrary to the data from studies on G-s (Gumbart et al., 2014; Kim et al., 2015).

1.2.1.2 Scaffold model:

The scaffold model was proposed using Gram-negative CW as a model. It describes glycan strands as perpendicular to the cytoplasmic membrane, growing towards the outside of the cell, and pentapeptide bonds parallel to it (Figure 3B) (Dmitriev et al., 2003). In the scaffold model, the cross-linking rate of glycan strands would be higher closer to the cytoplasmic membrane than towards the OM, contemplating the possibility of the PG tips being free, with no pentapeptide bonds. The authors accept that it is difficult to reconcile this idea with cell division in *E. coli* and *Bacillus subtilis* (the G+ bacterium model). However, it is supported by the existence of spheroid bacteria with alternate division planes (Dmitriev et al., 2003). The problematic of cell division is still ongoing and further

studies will be necessary to fully understand the process. Other results go against the scaffold model in the G- bacterium *E. coli* (Vollmer & Holtje, 2004). According to their results derived from the analysis from multiple measurements including PG thickness, strand length and degree of cross-linkage, the scaffold model is highly unlikely.

1.2.1.3 Coiled-coil model:

The coiled-coil model advocates that the glycan strands act as a guide for the synthesis of new PG (Figure 3C) (Turner, Hobbs, & Foster, 2016). AFM studies on *B. subtilis* have shown helical "cables" surrounding the cell, parallel to the cytoplasmic membrane (Hayhurst et al., 2008). According to this hypothesis, during PG synthesis, glycan strands are polymerized and cross-linked in groups to form a "rope" that will then be attached to preexisting PG with a helical pattern (Hayhurst et al., 2008).

There are still many open questions about PG 3D structure. What is accepted by all the scientific community is that the steps taken to synthesize PG are conserved in all bacteria. I will now proceed to describe this process.

1.2.2 Peptidoglycan synthesis

PG synthesis is a highly controlled process as it has to adapt to growth changes like transition from exponential growth to stationary phase or cell division without compromising cellular integrity. This process is very similar between Gram-positive and Gram-negative bacteria. During elongation, PG synthesis takes place along the cell cylinder and is controlled by the elongasome, the cell wall synthetic machinery (CSM) regulating CW formation during cell growth. During division, it takes place at the septum, controlled by the divisome, the CSM that regulates septum formation during division. Even though the synthesis of PG in both cases follows the same process, some of the components of the CSM regulating it vary (Bhavsar & Brown, 2006). Broadly, PG synthesis can be divided into three different stages: stage 1. synthesis of the cytoplasmic precursor lipid II, stage 2. flipping of lipid II across the membrane and stage 3. assembly of PG (Figure 4) (Siegel, Liu, & Ton-That, 2016).

1.2.2.1 Stage 1, synthesis of the cytoplasmic precursor lipid II

The synthesis of lipid II is accomplished stepwise (Figure 4). First, MurAA and MurB catalyze the transformation of UDP-*N*-acetylglucosamine (UDP-GlcNAc) and phosphoenolpyruvate into UDP-*N*-acetylmuramic acid (UDP-MurNAc) (Bhavsar & Brown, 2006). Then, MurC, MurD, MurE and MurF,

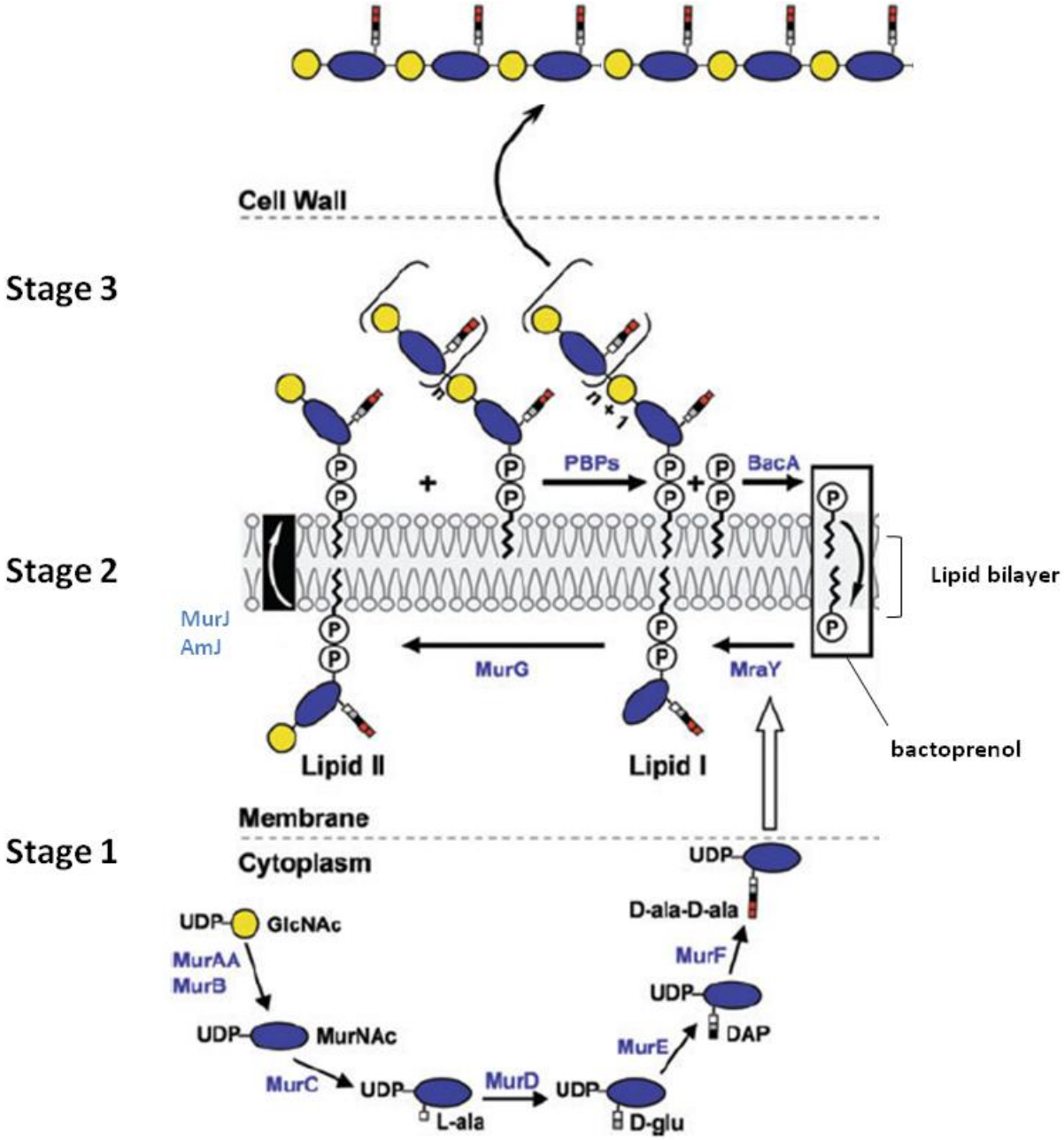

Figure 4 Peptidoglycan synthesis (modified from (Bhavsar & Brown, 2006)). Solid arrows denote catalysis of the reactions by the indicated enzyme. Block arrows denote where activated substrate is utilized in the biosynthesis pathway. The distinction between the reactions taking place in the cytosol and the membrane is denoted by a dashed grey line.

one after the other, will bind L-alanine (L-ala), D-glutamate (D-glu), diaminopimelic acid (DAP) and the D-ala-D-ala dipeptide (forming the pentapeptide) to ADP-MurNAc. These four enzymes are ATP-dependent amino acid ligases. UDP-MurNAc-pentapeptide is then bound covalently to undecaprenyl-phosphate (also known as bactoprenol) by MraY in the membrane, forming lipid I. Finally, MurG binds Glc-NAc from UDP-GlcNAc, forming lipid II, the disaccharide-pentapeptide building block of PG.

1.2.2.2 Stage 2, flipping of lipid II across the membrane

In stage 2, lipid II is translocated from the inner leaflet of the cytoplasmic membrane to the exterior (Figure 4). It has been estimated that there are 1000-2000 lipid II molecules in exponentially growing *E. coli* (Y. van Heijenoort, Gomez, Derrien, Ayala, & van Heijenoort, 1992). According to this study, in order to keep up with growth rate, the flipping of lipid II to the exterior of the cell must be fast. It is accepted that this process requires the action of flippase(s) that would form a channel through which lipid II would cross the cytoplasmic membrane, easing the process. The hydrophilic part of lipid II would cross the membrane while the hydrophobic moiety would remain in the membrane (Kramer et al., 2004). The identity of the flippase(s) has been the focus of a number of studies. There are three identified flippases: FtsW, MurJ and AmJ (Meeske et al., 2015; Young, 2014).

FtsW, a protein required for cell septation, and its paralog RodA, required for lateral PG synthesis, were the first proteins lipid II flippases in *E. coli* (Ehlert & Holtje, 1996). It is only recently that Mohammadi and coworkers performed *in vitro* experiments with FtsW suggesting that the protein could flip lipid II in liposomes (Mohammadi et al., 2011).

A decade ago, another study in *E. coli* had proposed MurJ to be the lipid II flippase based on an informatic approach (Ruiz, 2015). But its activity was demonstrated *in vivo* only recently in *E. coli* and in *B. subtilis*(Meeske et al., 2015). Recently, they showed that MurJ is needed for PG synthesis and deleting it causes an increase in the accumulation of lipid-linked PG precursors in the G- bacterium model (Sham et al., 2014), questioning the role of FtsW/RodA. However, it does not flip lipid II *in vitro*, as FtsW does, maintaining some suspense on which, between FtsW and MurJ is the flippase.

In *B. subtilis*, the situation is even more intricate, with the presence of FtsW and RodA, a homolog of MurJ (YtgP), and three paralogs. When deleting the four *murJ* paralogs in *B. subtilis*, the strain was still viable, going against the hypothesis of MurJ being the lipid II flippase (Sham et al., 2014). But a recent work from Meeske and collaborators reinforced the hypothesis of MurJ being a candidate for lipid II flippases (Meeske et al., 2015). They identified AmJ ("Alternate to *murJ*") in *B. subtilis*, a functionally redundant protein with MurJ. A strain lacking the four *murJ* paralogs and *amj* was shown to be lethal. Furthermore, AmJ can substitute native MurJ in *E. coli*. AmJ is a very different protein to MurJ and its expression is activated in absence of YtgP, which might benefit the organism during MurJ inhibiting conditions (Meeske et al., 2015). It is possible that MurJ and AmJ act in the same process, under different conditions.

Despite all efforts, it is still unclear which of these proteins are the lipid II flippases in G+ and G- bacteria or if all of them flip lipid II across the cytoplasmic membrane depending on growth conditions.

1.2.2.3 Stage 3, assembly of peptidoglycan

The final step of PG synthesis is stage 3, where the PG precursor is linked to existing glycan strands (Figure 4). Glc-NAc from the lipid II is bound by transglycosilation to the reducing part of the growing strand. A molecule of undecaprenyl-pyrophosphate is liberated and dephosphorylated to form bactoprenol, which becomes available to form lipid I again. This is a critical step as it will limit the formation of PG precursors. The PG subunit is then linked to the preexisting PG mesh by PBPs, penicillin binding proteins. As their name suggests, PBPs are the target of the antibiotic penicillin and its derivatives. Penicillin resembles to the D-ala-D-ala moiety of the PG pentapeptide. Therefore, penicillin can bind the active site of PBPs, inactivating them permanently (Tipper & Strominger, 1965). PBPs have been studied for a long time, and their nomenclature is confusing. In what follows, I will summarize what is known about PBPs here.

Some PBPs have both transglycosilation (TG) and transpeptidation (TP) activities. It is thought that most of the peptide bonds are created at the same time as TG happens, but some peptide bonds can be formed by other PBPs after TG (see section 1.2.2.3.1) (Bhavsar & Brown, 2006). A study showed that PBP1b from *E. coli* performs TG and TP simultaneously (Bertsche, Breukink, Kast, & Vollmer, 2005) while, in another study, PBP1a from *E. coli* showed a preference for peptides from elongating glycan strands (Born, Breukink, & Vollmer, 2006). TP takes place between the pentapeptide moieties of neighboring strands, but not all pentapeptide moieties form a pentapeptide bond and the percentage of TP varies between strains (de Pedro & Cava, 2015). PBPs are multidomain proteins. Most of them have a cytoplasmic tail, a transmembrane domain and two domains looking at the periplasmic area, where the PG synthesis takes place (Sauvage, Kerff, Terrak, Ayala, & Charlier, 2008). The amount of PBPs and their activity vary depending on the strain (Table 1). I will continue with a short classification of PBPs and their activity.

1.2.2.3.1 Transpeptidases

The C-terminal domain of PBPs, the penicillin-binding (PB) domain, is in charge of the peptide cross-linking of the sacculus, the TP. PBPs that present TP activity are called high molecular mass PBPS or HMM (Sauvage & Terrak, 2016). In *B. subtilis*, there are ten HMM PBPs (Table 1). These can be divided into class A (PBP1, PBP2c, PBP2d and PBP4) and class B (PBP2a, PBP2b, PBP3, PBP4b, PbpH and SpoVD). Proteins in class A have both TP and TG activities while those in class B only perform TP.

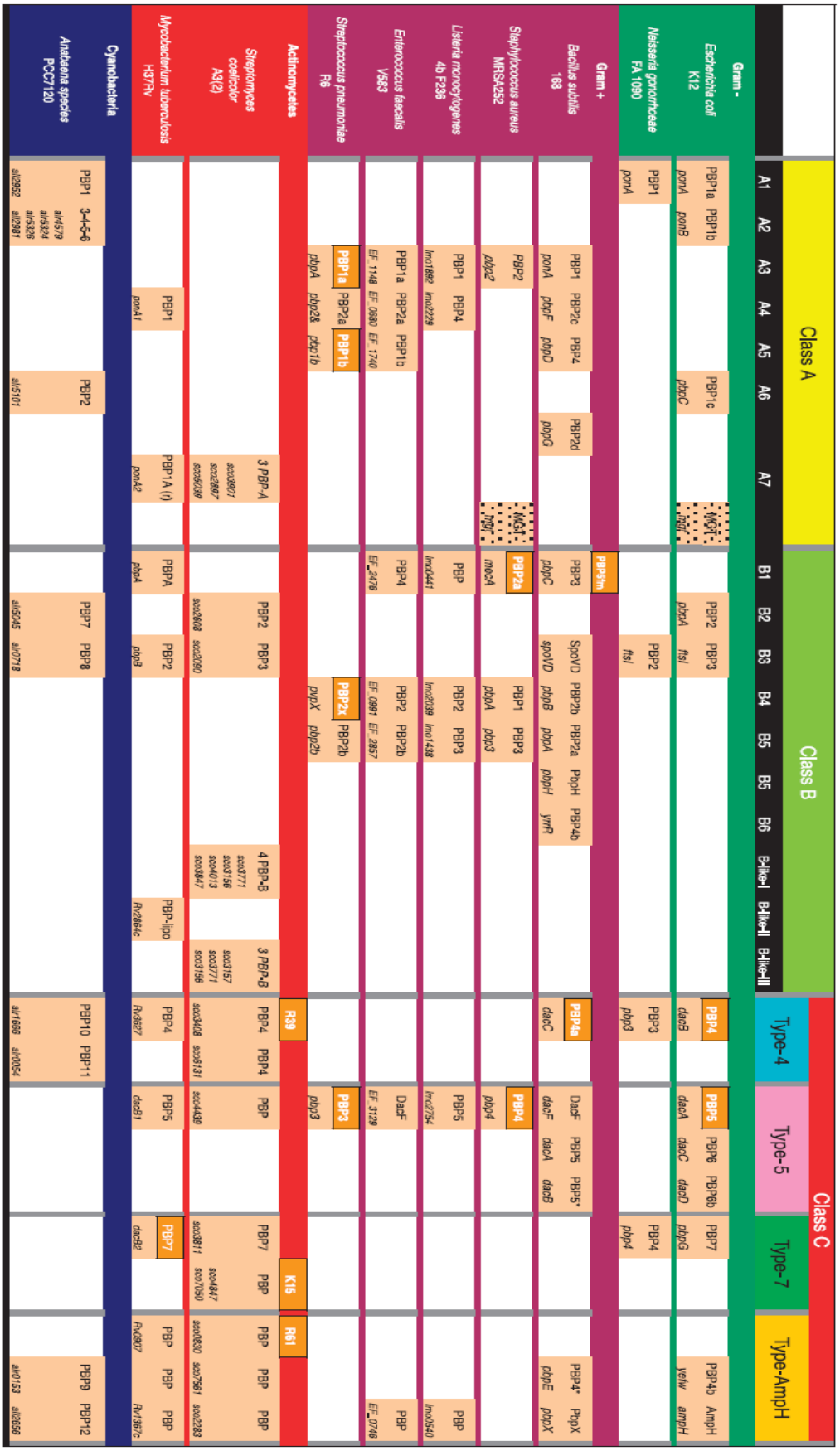

Table 1 PBPs classification (modified from (Sauvage et al., 2008)).

The most common TP reaction is DD-TP. In this reaction the enzyme binds to the D-ala-D-ala moiety of the peptide stem, releases the last D-ala and binds the penultimate one to the terminal DAP of a neighbour acceptor PG strand (Sauvage et al., 2008). The second most extended way of transpeptidation that happens in bacteria is LD-TP (Figure 2D). In this case, it is DAP-D-ala from the donor that binds to the DAP from the acceptor. LD cross-linking isn't universal nor essential for bacteria and, in those bacterial species with both DD- and LD-TP, the relative abundance for each type is variable (de Pedro & Cava, 2015).

1.2.2.3.2 Transglycosylases

Some PBPs have an N-terminal domain with glycosyltransferase activity (TG). These also have a C-terminal TP domain and are, therefore, bifunctional PBPs. They fall into the HMM class A category and, in *B. subtilis*, there are four of them: PBP1, PBP2c, PBP2d and PBP4 (Table 1) (Sauvage & Terrak, 2016). These form glycan strands with varying lengths. PBP1a from *E. coli* forms glycan strands of about 20 disaccharides while PBP1b would form strands with more than 25 disaccharides on average (Sauvage et al., 2008).

1.2.2.3.3 Carboxypeptidases and endopeptidases

In *B. subtilis*, there are six carboxipeptidases (CP) or endopeptidases (EP) PBPs (also called class C or low molecular mass PBPs - LMM): PBP4*, PBP4a, PBP5, PBP5*, DacF and PbpX PBPs (Table 1). They can be linked to the cytoplasmic membrane or interact directly with either PG or TA. These enzymes modify the peptide stem of existing PG at the CW. Their exact role isn't established, but PG modifications allow the introduction of new PG to the mesh and cell division. They are thought to be involved in cell morphology, competence, cell motility, germination and biofilm formation (Frirdich & Gaynor, 2013).

1.2.2.4 Cell wall synthetic machineries

During the cell cycle, a bacterial cell has to grow and form two daughter cells. To do so, the continuous PG macromolecule (sacculus) has to be enlarged and then divided without compromising cell integrity. CSM are multiprotein complexes that ensure this process. They are formed of PG synthases (most of the PBPs), hydrolases and other morphoproteins. Depending on when they're active, we can divide CSM into elongasome and divisome. Some of the enzymes are present in both complexes but some are specific to each CSM. The most characteristic element of elongasomes is the presence of MreB, an actin-like protein, highly conserved in rod-like bacteria, while in the case of divisomes, it is FtsZ, the first described bacterial tubulin homolog (Bhavsar & Brown, 2006; Jones,

Carballido-Lopez, & Errington, 2001). Cytoskeletal proteins are thought to create scaffolds, positioning CSMs during elongation and cell division (Egan et al., 2016).

1.3. Bacterial cytoskeleton

Eukaryotic cells have a filament system that acts as an organization center for a number of essential cellular processes like cell division, chromosome segregation, cell polarity and intracellular traffic (Howard & Hyman, 2003). It is a complex and dynamic system formed of three main filaments: actin microfilaments, tubulin microtubules and intermediate filaments (IF). For a long time, it was believed that only eukaryotic cells had a cytoskeleton, but the first prokaryotic homologs of cytoskeletal proteins were discovered two decades ago, and members of all three eukaryotic filament family have now been discovered in bacteria (Cabeen & Jacobs-Wagner, 2010). Furthermore, bacteria contain additional specific cytoskeletal proteins absent from eukaryotes (Ingerson-Mahar & Gitai, 2012). Before that, the bacterial cell was thought to be an unorganized bag, but it has been demonstrated that there is an intricate organization in bacterial cells, forming supramolecular assemblies in the cytoplasm or associated with the membrane (Govindarajan & Amster-Choder, 2016). An example of this organization is the localization of specific proteins to the cell poles. Bacteria have different ways to attain this organization, which is thought to enable the integration of extracellular information and optimize producing a correct response (Govindarajan & Amster-Choder, 2016). There is a very interesting and well written review covering this aspect from the Jacobs-Wagner group (Laloux & Jacobs-Wagner, 2014).

By organizing the cell, the bacterial cytoskeleton is crucial for virulence, cell shape maintenance, growth and motility. Cytoskeletal proteins also help by forming an organized structure that enables molecular transport. I will now make a more detailed description of these prokaryotic cytoskeletal proteins.

1.3.1 Bacterial cytoskeletal proteins

1.3.1.1 Actin-like proteins

Actin is the most abundant protein in eukaryotic cytoplasms. It presents a characteristic fold, with four domains stabilized in the center by an ADP molecule. Actin polymerizes in the presence of ATP and can be found in two conformations: globular or G-actin and filamentous or F-actin (Ingerson-Mahar & Gitai, 2012). Actin-like proteins are present in every known cell, from eukaryotic cells to prokaryotic, including archaeal cells (Petek & Mullins, 2014). Several bacterial proteins belonging to the actin family have been described, and are involved in many cellular processes. Some examples are FtsA that participates in cell division (Pichoff & Lutkenhaus, 2005), MreB who is involved in CW synthesis and

cell morphology (Dominguez-Escobar et al., 2011; Garner et al., 2011; van Teeffelen & Gitai, 2011), some Alp proteins and ParM that play key roles in plasmid segregation (Cabeen & Jacobs-Wagner, 2010) and MamK, closely related with organelle organization (Toro-Nahuelpan et al., 2016).

ParM and MreB only share ~11% and ~15% similarity, respectively, with eukaryotic actin, but do contain its characteristic 3D fold formed by subdomains IA, IB, IIA and IIB that correspond to subdomains 1, 2, 3 and 4 in actin (Carballido-Lopez, 2006; van den Ent, Amos, & Lowe, 2001) (Figure 5).

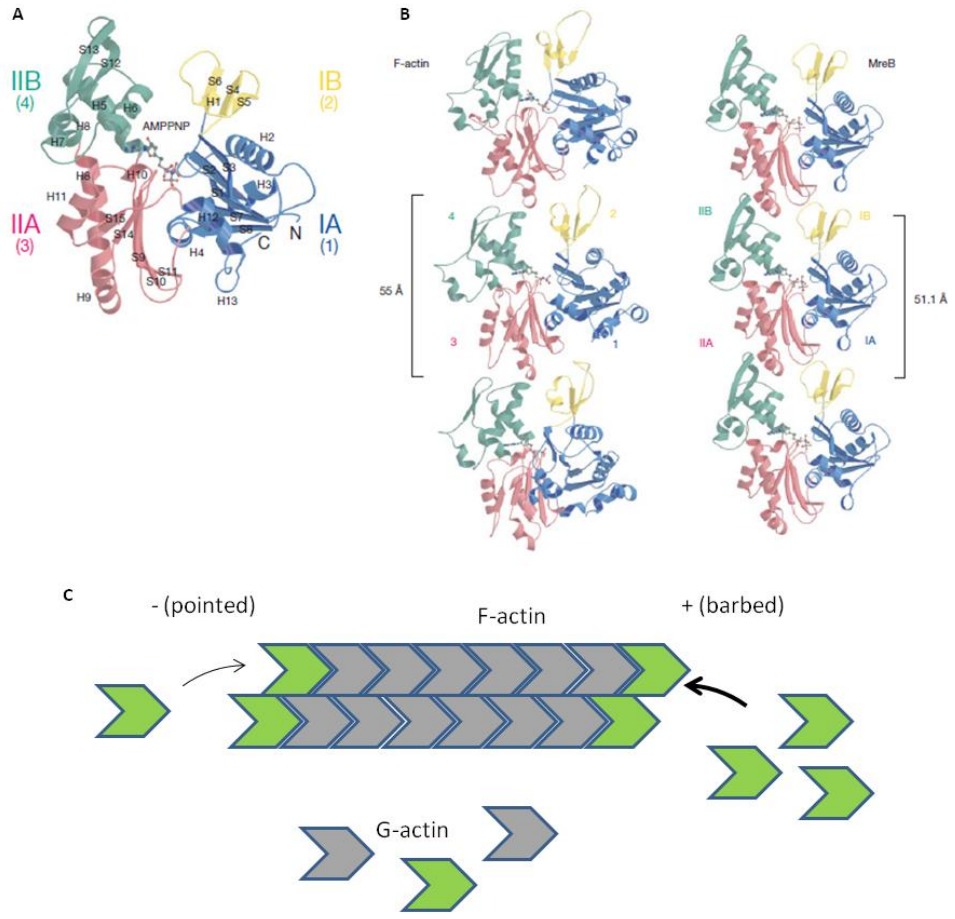

Figure 5 Crystal structure of *T. maritima* MreB monomer and polymer and a scheme of actin treadmilling. A. Ribbon representations of *T. maritima* MreB monomer. MreB crystallized with AMPPNP and magnesium. The four domains (IA, IB, IIA, IIB) correspond to those in actin (1, 2, 3, 4). AMPPNP binds at the nucleotide binding site formed by the four domains. **B**. Comparison of yeast F-actin and *T. maritima* MreB polymers. The tip residues of domains IA and IIA go into the cleft formed by IB and IIB of MreB in the same manner as those from domains 1 and 3 of actin go into the cleft formed by 2 and 4. **A** and **B** are adapted from (van den Ent et al., 2001). **C**. Polymerization of Actin. ATP-bound monomers are in green, and ADP-bound in grey. The process of polymerization is much faster on the + end than in the - end., giving a directionality to the polymerization process (treadmilling).

Actin microtubules polymerize from both ends, but each end has a different affinity for the addition of monomers. We can distinguish a slow growing end (- or pointed) and a fast growing end (+ or barbed) (Figure 5). Depending on the local concentration of the protein, actin can undergo polymerization, called treadmilling (that is an equilibrium between the loss of monomers at the - end and gain at the + end), steady state or a rapid depolymerization called catastrophe (Cleveland, 1982). *In vivo* polymerization studies of MreB and Mbl in *B. subtilis* ruled out treadmilling as their source of processive movement, which does not exclude the possibility that treadmilling exists at a different timescale (Dominguez-Escobar et al., 2011). ParM polymerization is driven by treadmilling where the stabilization of the polymers by ATP binding and instability due to hydrolysis of the nucleotide give a directionality to ParM polymerization, as in actin.

1.3.1.2 Tubulin-like proteins

Tubulin microtubules in eukaryotes are formed of α- and β-tubulin. They are dynamic, GTP-dependent and serve as tracks for other motor proteins (Lowe & Amos, 2009). The first bacterial cytoskeleton-like protein to be described was FtsZ, a tubulin homologue (Figure 6A) (Bi, Dai, Subbarao, Beall, & Lutkenhaus, 1991). It is conserved in the majority of free-living bacteria. It forms linear filaments in a GTP-dependent manner that localize at the cell division site forming a structure called the Z-ring (Erickson, Anderson, & Osawa, 2010). It is used as a cytokinetic scaffold to which other proteins of the cell division complex bind. It has also been showed that FtsZ uses GTP hydrolysis to bend the linear filaments, pulling the membrane inward to help septum formation (Li, Trimble, Brun, & Jensen, 2007). A recent study from the Xiao group suggests that FtsZ polymerization (highly regulated both by positive and negative regulators) can be fashioned to allow cell division to happen at the correct place and timing (Coltharp & Xiao, 2017). According to this study, FtsZ regulators modify the Z-ring structure and dynamics which, in turn, acts as a signal integrator and transduction system for cell wall and cell division.

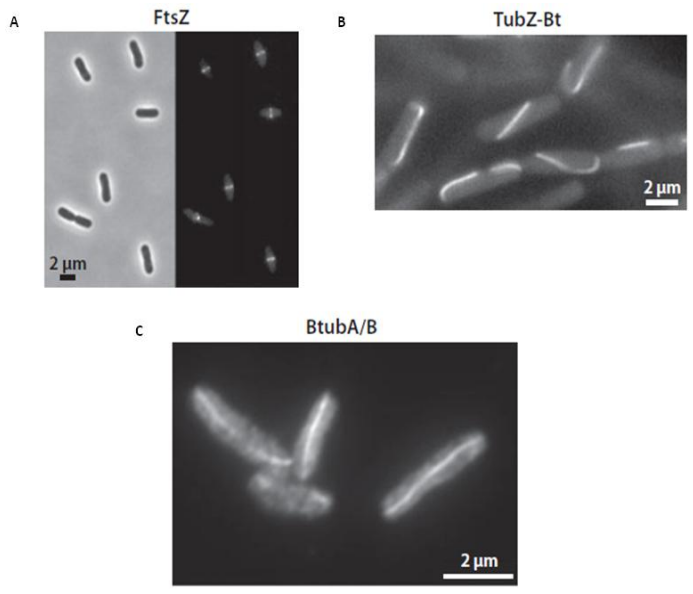

Figure 6 Bacterial tubulin-like homologs (modified from (Cabeen & Jacobs-Wagner, 2010)). **A**. FtsZ-GFP in *E. coli*. Same field is shown as phase contrast (left panel) or fluorescent image (right panel). FtsZ forms a ring-like structure (the Z-ring) at mid-cell marking the division sites. **B**. TubZ-GFP forming a filament in *Bacillus thuringiensis*. **C**. Immunofluorescence images of BtubA/B in *E. coli*.

Using bioinformatic tools, two FtsZ-like protein families were discovered. One of them, the FtsZ1 family, is present in over 120 bacterial and archaeal species, but their function is not well known. They are normally found in operons with genes that share homology with eukaryotic genes involved in vesicle trafficking and membrane remodeling (Makarova & Koonin, 2010). The other family of proteins is even less well understood.

There are also plasmid encoded bacterial tubulin homologs that may play a role in their plasmid partitioning. TubZ is an example from *Bacillus thuringiensis*, encoded on the virulence plasmid pBToxis (Figure 6B). Interestingly, it forms double-helical filaments that show treadmilling *in vivo* and are more similar to actin filaments than to tubulin microtubules (Larsen et al., 2007). Another plasmid-encoded tubulin-like protein is RepX, encoded in the plasmid pX01 from *Bacillus anthracis*. It has been identified to have a role in plasmid replication (Pogliano, 2008).

Another family of prokaryotic tubulin homologs was identified in some *Prosthecobacter* bacteria. It includes the proteins BtubA and BtubB (Figure 6C). They actually have a higher similarity with alpha and beta tubulin than FtsZ or TubZ, but their function remain unknown (Ingerson-Mahar & Gitai, 2012).

1.3.1.3 IF-like proteins

IF proteins in eukaryotes share a rod-like domain between two variable domains. The most common IF proteins are keratin and lamin. They self-assemble in a nucleotide-independent manner (Lowe & Amos, 2009). The most studied IF-like bacterial protein is crescentin (CreS), from *Caulobacter crescentus* (Figure 7A). It was the first IF-like protein to be discovered, in 2003 (Ausmees, Kuhn, & Jacobs-Wagner, 2003). It has mild sequence similarity with eukaryotic IF, but does not depend on nucleotides to form slightly curved filaments *in vitro*, as eukaryotic IFs. Lack of CreS causes *Caulobacter* to lose its typically curved form and to become a straight rod (Ingerson-Mahar & Gitai, 2012).

The main similarity between IF and CreS is that they are coiled coil-rich proteins. There are a number of coiled coil-rich proteins in bacteria that self-assemble into filaments in a nucleotide-independent manner. Some act as scaffolds or localization factors of other proteins, but their exact functions are still unknown (Lin & Thanbichler, 2013). FilP is an example of a coiled coil-rich protein from *Streptomyces coelicolor* that plays a role in the formation of hyphae (Figure 7B). Deletion of *filP* induces abnormal hyphal morphology and decreased stability (Cabeen & Jacobs-Wagner, 2010). Other examples are RsmP from *Corynebacterium glutamicum* and Ccrp from *Bdellovibrio bacteriovorus* (Ingerson-Mahar & Gitai, 2012).

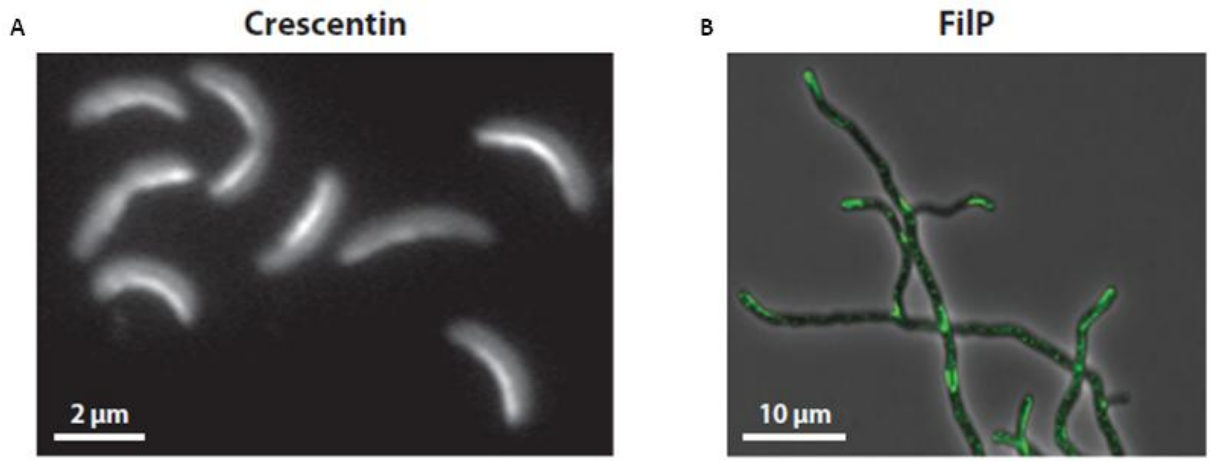

Figure 7 Bacterial intermediate filaments-like homologs (modified from (Cabeen & Jacobs-Wagner, 2010)). **A**. Fluorescence micrograph of FIAsH-stained crescentin-TC in *C. crescentus.* **B**. FilP-GFP in *S. coelicolor*.

1.3.1.4 Endosomal Sorting Complexes Required for Transport proteins (ESCRTs)

ESCRT proteins are present in eukaryotic cells where they are involved in the late stages of mammalian cytokinesis. They are also present in archaea and some bacterial species like *Chlamydia* that do not have FtsZ (Ingerson-Mahar & Gitai, 2012). ESCRTs may be linked with cell division.

1.3.1.5 Prokaryotic-specific cytoskeleton proteins

It was believed that cytoskeletal proteins fitted into the previous three groups: actin, tubulin and intermediate filaments. Nevertheless, other cytoskeletal proteins have been discovered that could have a role in cellular organization and cell form, only present in bacterial cells.

1.3.1.5.1 Walker A Cytoskeletal ATPases (WACAs)

Walker A Cytoskeletal ATPases (WACAs) are a subfamily of the P-loop NTPase family; which includes GTPases, signal recognition particle proteins and eukaryotic cytoskeleton-associated proteins. WACAs are found in most bacteria and some archaea. The two main examples of the WACA proteins are ParA and MinD (Ingerson-Mahar & Gitai, 2012).

ParA is a plasmid and chromosome segregation protein that determines the position of other proteins in the cell (Pogliano, 2008). In its free state, it is a monomer that dimerizes and then polymerizes when bound to ATP. It also associates with additional factors like DNA and ParB, that stimulates ATP hydrolysis and the dissociation of the filament (Ingerson-Mahar & Gitai, 2012). It seems that in *Caulobacter* and *Vibrio cholerae*, ParA binds the *parS origin*-proximal region and its polymerization-

depolymerization pulls the chromosome through the cell during its segregation. There are other ParA homologs implicated in plasmid segregation (Ingerson-Mahar & Gitai, 2012).

MinD polymerizes at the inner leaflet of the cytoplasmic membrane, attached to it by an amphipatic helix, in an ATP-dependent manner (Figure 8) (Lowe & Amos, 2009). It associates with MinC and, together, they inhibit FtsZ polymerization, acting as spatial regulators of the site of cell division (Lutkenhaus, 2007). In *E. coli*, MinE binds to MinD and promotes ATP hydrolysis, creating a gradient of MinD bound to the membrane and allowing the polymerization of FtsZ at midcell. *B. subtilis* lacks MinE, but it still recruits MinD to the cell poles and recent division sites.

C. crescentus does not have the Min system, but has a different WACA protein, namely MipZ, that disables the mislocalization of FtsZ (Ingerson-Mahar & Gitai, 2012). At the beginning of the cell cycle, MipZ binds the origin of replication (*oriC*) of the chromosome via ParB. After DNA replication, one of the daughter origins migrates to the opposite cell pole with MipZ, activating the release of FtsZ from the area. This mechanism creates a gradient of proteins from both cell poles, directing FtsZ assembly at mid-cell (Pogliano, 2008).

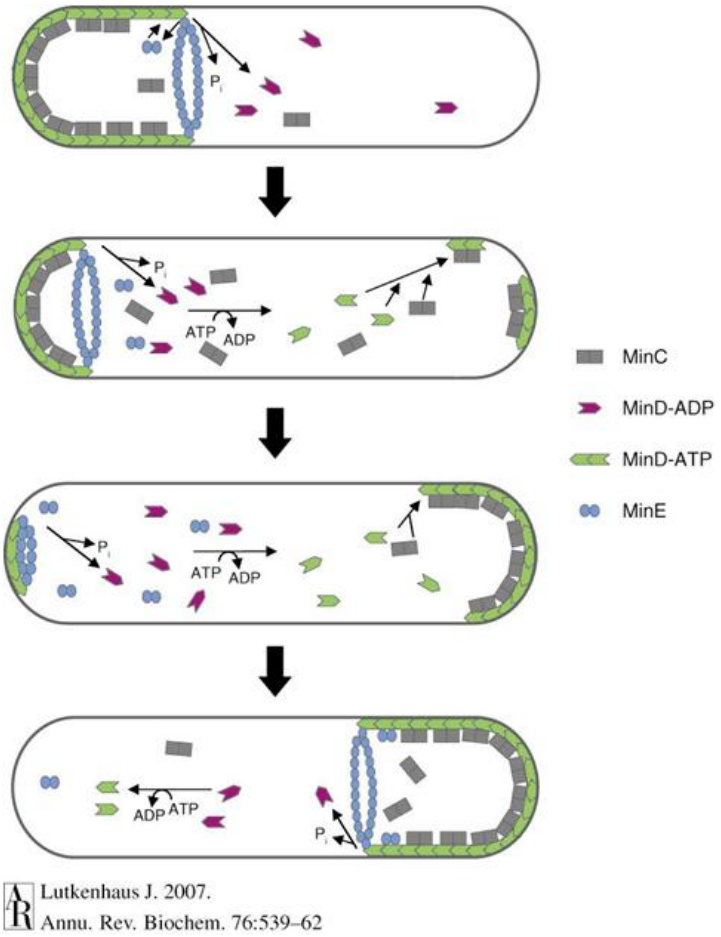

Figure 8 Dynamics of the Min proteins in *E. coli* (modified from (Lutkenhaus, 2007)).

1.3.1.5.2 Bactofilins

Bactofilins are conserved in most bacteria and may perform varied cellular roles in each species. In *Myxococcus xanthus*, they regulate motility and morphogenesis (Ingerson-Mahar & Gitai, 2012) while they organize stalk biogenesis in *C. crescentus* (Kuhn et al., 2010). The most studied bactofilins are BacA and BacB from *C. crescentus*. They form filaments *in vitro* and linear structures when overexpressed.

1.3.1.5.3 CtpS

CtpS is an ubiquitous protein that synthesizes CTP from UTP, ATP and glutamine. It has also been shown that it polymerizes forming linear filaments, which might be used to regulate its enzymatic activity. It is thought to also have a role in *C. crescentus'* shape determination as it is localized at the inner cell curvature, its overexpression forms straighter cells and the curvature of the cell increases in absence of CtpS (Ingerson-Mahar, Briegel, Werner, Jensen, & Gitai, 2010). In addition, CtpS and CreS co-localize in *C. crescentus* but can form filaments independently from one another. Also, point mutations of CtpS that abolish its enzymatic activity do not have an effect on *C. crescentus* cell shape (Ingerson-Mahar et al., 2010).

1.3.2 Bacterial actin homologs

1.3.2.1 MreB

MreB is the first discovered and certainly the better studied member of the family of prokaryotic actin-like proteins (Figure 9A). This protein will be further described in section 1.4. Since its discovery, several other bacterial actin-like proteins have been characterized. I will pursue with their description now.

1.3.2.2 MamK

Magnetospirillum magneticum has two actin-like genes: *mreB* and *mamK* (Figure 9B). MamK forms linear filaments and filament bundles that organize magnetosomes in the bacteria. Magnetosomes are vesicles arranged in chains that enclose a magnetite crystal. Magnetotactic bacteria take advantage of them as a cellular compass to sense the geomagnetic field (Bennet et al., 2015; Pradel, Santini, Bernadac, Fukumori, & Wu, 2006). In absence of MamK, magnetosomes are disordered and no filaments are seen (Cabeen & Jacobs-Wagner, 2010). MamK has another key role in magnetosome organization as it is hypothesized that it recruits magnetosomes to the division site and ensures equal inheritance of the organelles (Toro-Nahuelpan et al., 2016).

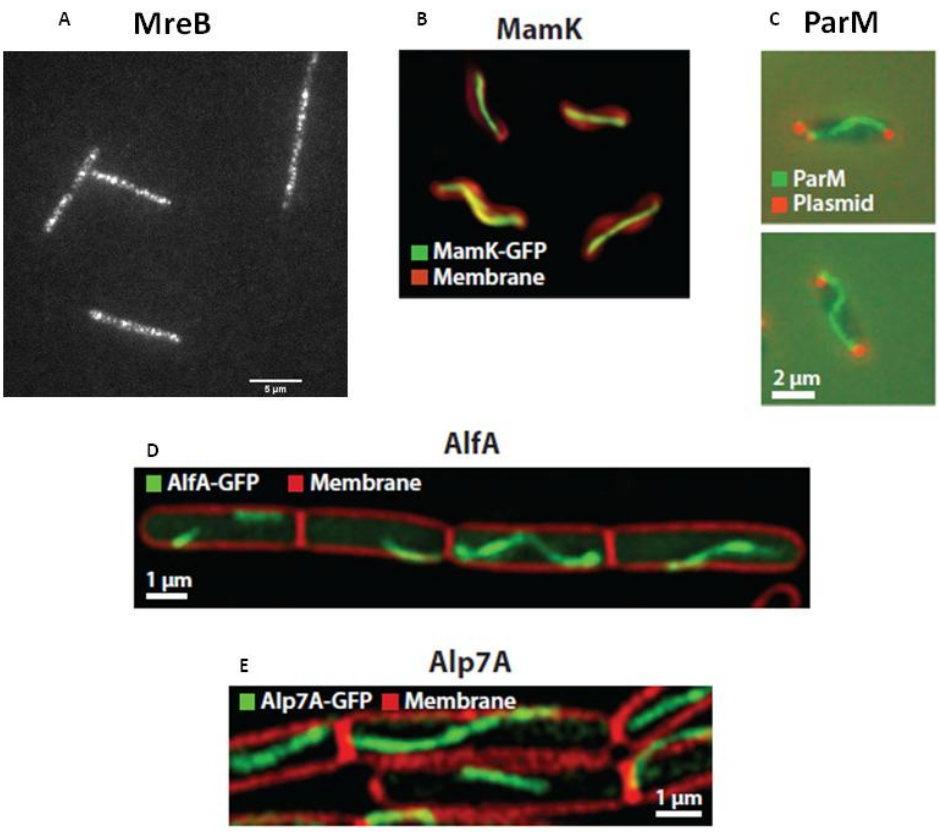

Figure 9 Bacterial actin homologs A. TIRFM image of GFP-MreB *B. subtilis* cells. **B.** Composite fluorescence micrograph of *M. magneticum* cells (3-4 µm in length) producing MamK-GFP. **C.** Immunofluorescence images of ParM (green) segregating LacI-GFP-labeled plasmids (red) in *E. coli*. **D**. AlfA-GFP fluorescence in *B. subtilis*. **E**. Fluorescence micrograph of Alp7A-GFP in *B. subtilis* cells. (**A** personal data; **B-E** modified from (Cabeen & Jacobs-Wagner, 2010)).

1.3.2.3 ParM

ParM is the best studied plasmid-encoded actin-like protein. It is one of the three components of the plasmid partitioning system: ParM (motor), *cis*-acting DNA region *parC* and the repressor that binds to *parC*, ParR (Figure 9C). ParM forms left-handed helices with a high dynamic instability that are stabilized by ParR/*parC*. When bound to the *parC* sites, ParM polymerizes and pulls the plasmids apart, growing from the ParR/*parC*-bound sites. If ParM's ATPase site is mutated the otherwise curved and dynamic filament will become straight and stable and plasmid partitioning will be defective (Cabeen & Jacobs-Wagner, 2010).

1.3.2.4 FtsA

One of the elements of the divisome, together with the tubulin-like protein FtsZ, is FtsA. FtsA filaments are polar, dynamic and depend on ATP for their formation. They act as a scaffold for FtsZ,

together with the membrane. At the same time, both the cytoplasmic membrane and FtsZ act as a scaffold for FtsA (Mura et al., 2016). They are called "collaborative filaments" (Fink, Szewczak-Harris, & Lowe, 2016). In absence of FtsA, septation isn't achieved and cells lyse (Mura et al., 2016).

1.3.2.5 AlfA

AlfA is similar to ParM in that it is another plasmid-encoded actin-like protein linked to plasmid segregation; pLS32 from *B. subtilis*, specifically (Figure 9D). It also forms left-handed helices along the cell long axis, but they do not present dynamic instability as ParM filaments. AlfA helices group in bundles of mixed polarity. AlfA forms part of a three components system where AlfB acts as a repressor of *alfA* expression and binds to a three tandem repeat upstream of the *alfA* promoter, *parN* (Becker et al., 2006).

1.3.2.6 Actin-like protein (Alp) families

After the discovery of AlfA, BLAST studies revealed the existence of 35 actin-like protein (Alp) families. Some Alps are encoded in chromosome genes, but the majority of them are on plasmids, phage genomes and integrating conjugative elements (Cabeen & Jacobs-Wagner, 2010). The Alp protein that has been studied the most is Alp7A (Figure 9E). It forms filaments that are involved in plasmid segregation in a similar way as ParM, but with in a treadmilling fashion (Derman et al., 2009).

1.4. MreB

MreB has been considered as the main prokaryotic actin-like protein for a long time. Nevertheless controversial results from the past few years are raising doubts about how similar these two proteins really are. Actin forms dynamic filaments that are involved in intracellular trafficking, cell shape maintenance, cytokinesis (cell division) and cell movement. MreB is also a dynamic, polymeric protein, but not all of actin's functions are covered by MreB. Furthermore, many of its functions are species-specific.

1.4.1 MreB isoforms

There are three MreB isoforms in *B. subtilis*: MreB, MreBH (MreB homolog) and Mbl (MreB-like). They have overlapping functions, even though there are some differences between them that still remain unexplained.

In many bacteria *mreB* is upstream of the highly conserved morphogenes *mreC* and *mreD*. In *B. subtilis*, the three genes are co-transcribed and essential (Formstone, Carballido-Lopez, Noirot, Errington, & Scheffers, 2008). They are important for cell wall synthesis and cell morphology, although their exact functions remain unclear. The genes encoding MreBH and Mbl are positioned separately from the *mreBCD* operon.

Deletion of each of the paralogs causes slightly different phenotypes (Figure 10), although bulging and loss of cell form is common to all three (depending on the growth conditions), but the deletion of *mreBH* causes a much milder phenotype than those linked to the deletion of *mreB* or *mbl*. These defects are all rescued by elevated concentration of Mg^{+2} or (for *mreB* and *mbl* mutants) deletion of *ponA*, the gene encoding for PBP1 (Carballido-Lopez, 2006; Dominguez-Cuevas, Porcelli, Daniel, & Errington, 2013; Kawai, Daniel, & Errington, 2009). The only viable double deletion mutant is Δ*mbl* Δ*mreBH* (Kawai, Asai, & Errington, 2009), even in the presence of Mg^{+2}. Therefore, under native conditions, MreB is the only of the three isoforms that can support growth and viability on its own, always with high Mg^{+2} concentrations. In a different study from the Errington group (Schirner & Errington, 2009), a triple deletion mutant was created, but in a very specific background. The viability of this mutant is possible because of an extragenic suppressor mutation causing the overexpression of SigI (by the deletion of *rsgI*, gene encoding an anti-sigma factor that controls SigI expression). The resultant strain (Δ*mreB* Δ*mbl* Δ*mreBH* Δ*rsgI*) generates more or less spherical cells that can divide, also Mg^{+2}-dependent (Kawai, Asai, et al., 2009; Schirner & Errington, 2009).

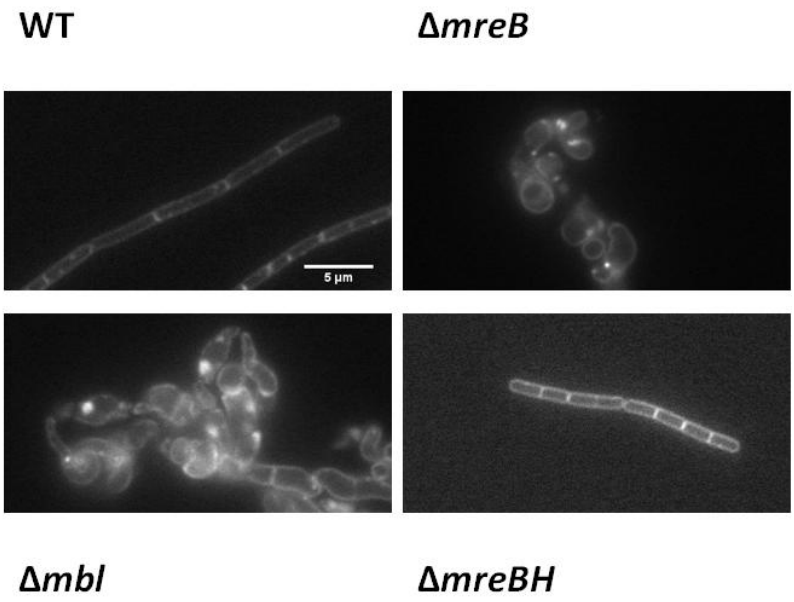

Figure 10 Effects of the deletion of each of the *mreB* paralogues in *B. subtilis*. Fluorescent membrane dye FM1-43 images of wild type *B. subtilis* (168; RCL44), Δ*mreB* (RCL423), Δ*mbl* (RCL78) and Δ*mreBH* (RCL49).

Not only the absence of the isoforms is deleterious for the cell, but the overexpression of MreB or MreBH too (although surprisingly Mbl's overproduction does not have deleterious effects on cell growth or shape) (Kawai, Asai, et al., 2009). The interactions of the actin-like isoforms in *B. subtilis* with other proteins are also different. All three isoforms interact between them and with RodZ (Defeu Soufo et al., 2010; Dominguez-Escobar et al., 2011; Muchova, Chromikova, & Barak, 2013). MreBH interacts with LytE, a major autolysin in *B. subtilis* involved both in cell elongation and division (Carballido-Lopez et al., 2006). As for MreB, there are results suggesting its interaction with TufA, TagT, TagU, PBP1, DapI and ComGA (Kawai, Daniel, et al., 2009; Mirouze, Ferret, Yao, Chastanet, & Carballido-Lopez, 2015; Rueff et al., 2014).

On the other hand, there may be an overlap of function as all three proteins, MreB, Mbl and MreBH, colocalize at the cell-side wall together with other elements of the elongasome and present the same velocity and directionality of movement (Dominguez-Escobar et al., 2011; Formstone & Errington, 2005). This suggests that all three are involved in the same process. In line with the common function hypothesis, the results from (Kawai, Asai, et al., 2009) show that, when expressed at the correct level, each MreB isoform is capable of maintaining WT growth and cell shape on their own. They constructed strains with only one of each paralog gene under the control of an IPTG inducible promoter: MreB-only, Mbl-only and MreBH-only. Each gene needs a different induction level to compensate for the loss of the other two, demonstrating that, even though all three proteins have overlapping functions, some differences exist. Likewise, each of the resulting strains (MreB-only, Mbl-only or MreBH-only) has different survival rates when grown in different stress conditions. The MreBH-only strain is the most affected, showing lower endurance than WT to alkaline, salt and heat stress; MreB-only is impaired during alkaline and salt stress and Mbl-only has a decreased survival upon salt stress.

The amino acid sequence of the three proteins is different, we can see in Table 2 the percentage of homology between them. This points too towards a differentiation of their function(s). Probably MreB, Mbl and MreBH have a common, main activity linked to CW synthesis and maintenance of cell morphology. Nevertheless, the mode of action might be different between them and they may come in during different conditions. It is also possible that each of them have different secondary function(s) that haven't been identified yet.

Isoform	Mbl	MreBH
MreB	52.41	51.20
Mbl		56.12

Table 2 Percentage of amino acid identity between the three MreB isoforms in *B. subtilis*: MreB, Mbl and MreBH. Obtained with ClustalO (Sievers et al., 2011).

1.4.2 Biochemical properties of MreB

MreB biochemistry has proven to be a though area of investigation. It is a difficult protein to purify in its soluble, active form. This explains why for a long time MreB's biochemistry was entirely studied on the thermophilic organism *T. maritima* (Bean & Amann, 2008; Esue, Cordero, Wirtz, & Tseng, 2005; Popp et al., 2010). With years, more MreBs have been purified in *E. coli*, *Leptospira interrogans*, *Magnetospirillium gryphiswaldense*, *Candidatus* Magnetobacterium casensis (Mcas), *Chlamydophila pneumoniae* (Barko et al., 2016; Bean & Amann, 2008; Deng et al., 2016; Gaballah, Kloeckner, Otten, Sahl, & Henrichfreise, 2011; Nurse & Marians, 2013; Sonkaria et al., 2012). Still, only a single -and controversial- publication has been released in a Gram-positive organism, *B. subtilis* (Mayer & Amann, 2009). Table 3 summarizes the biochemical properties of the MreBs studied and mentioned above.

	Organism						
Condition	*E. Coli*[6]	*T. Maritima*[7]	*L. Interrogans*[8]	*C. Pneumoniae*[9]	*M. gryphiswaldense*[10]	Mcas[11]	*B. Subtilis*[12]
ATP[1]	+	+	+	-	+	+	-
Magnesium[2]	+	+	+	+	+	+	+
Monovalent salt[3]	Max. 25 mM Inh. 200 mM	Inh. by high concentration	Max 300 mM	Inh. by high concentration		Inh. by high concentration	Inh. by high concentration
pH[4]		Max pH = 5 Inh. pH = 8		Inh. pH = 8		Max. pH = 5,5 Inh. pH = 8,5	Max. pH = 5,5-6 Inh. pH = 9
Verification of polymerization[5]	Yes (EM)	Yes (FL)	Yes (EM)	No	Yes (EM)	Yes (EM)	No

Table 3 Summary of biochemical properties of MreB in different organisms. (1) Dependence on ATP for polymerization. (2) Dependence on Mg for polymerization. (3) Dependence on monovalent ion; max., maximal polymerization; Inh., polymerization inhibited. (4) pH at which polymerization was maximal (max.) or inhibited (inh.). (5) Method used to differentiate between aggregation and polymerization; EM, electron microscopy; FL, fluorescent labelling. (6) (Nurse & Marians, 2013). (7) (Bean & Amann, 2008). (8) (Barko et al., 2016). (9) (Gaballah et al., 2011). (10) (Sonkaria et al., 2012). (11) (Deng et al., 2016). (12) (Mayer & Amann, 2009).

The only studies that didn't differentiate polymerization from aggregation by further analyzing light scattering and sedimentation results where those performed on *B. subtilis* MreB (Bs-MreB) and *C. pneumoniae* MreB (Cp-MreB) (Gaballah et al., 2011; Mayer & Amann, 2009). What is most striking is that these two studies are the only ones to defend that MreB's polymerization/aggregation is non-dependent on ATP. It is very interesting to note that A22, an inhibitor of MreB polymerization, does not affect neither Bs-MreB (Noguchi et al., 2008) nor Cp-MreB (Gaballah et al., 2011) while it

inhibits MreB polymerization in many other organisms (Noguchi et al., 2008). A22 binds to the nucleotide binding (NB) pocket of MreB preventing ATP binding and inhibiting MreB polymerization (Bean et al., 2009). The NB pocket is highly conserved in all MreBs, however, the protein conformation could vary in each MreB in a way that it prevents A22 binding to this NB pocket. *C. pneumoniae* is a coccoid, intracellular bacteria and no peptidoglycan has been reliably detected in its CW. It is thought that MreB is needed in these bacteria to maintain the proper functionality of the divisome.

1.4.3 Localization and dynamics of MreB

MreB's localization is one of its most polemic aspects. The subcellular localization of MreB was first performed in 2001 by the Errington group (Jones et al., 2001). This work, together with results from another group on MreB, Mbl and MreBH of *B. subtilis* (Defeu Soufo & Graumann, 2004), described the MreB proteins to form filaments in the cytoplasm, very close to the membrane. These filaments followed a helical pattern along the cell long axis and were dynamic. Further confirmation came from studies on MreB from *E. coli* and *C. crescentus* (Figge, Divakaruni, & Gober, 2004; Kruse, Moller-Jensen, Lobner-Olesen, & Gerdes, 2003). However, a decade after the first localization study of MreB was published, three independent groups reported results contradicting the helical pattern of MreB and the formation of micrometer long filaments (Dominguez-Escobar et al., 2011; Garner et al., 2011; van Teeffelen et al., 2011). They observed MreB homologs forming discrete patches that moved along the cell circumference, perpendicularly to the cell long axis, in *B. subtilis* and in *E. coli*. These results were supported by works from the Jensen group who, moreover, demonstrated that the strain used to study MreB in *E. coli*, MC1000/pLE7, caused artifacts due to the YFP fusion of the protein (Swulius et al., 2011; Swulius & Jensen, 2012). Since then, new publications have argued against this model, showing high resolution pictures of long structures (Olshausen et al., 2013). Based on these, a new model reviving "the helices" was proposed (Errington, 2015). There is still an ongoing conflict between helices vs. perpendicular tracks and filaments vs. diffraction-limited clusters. It must be noted that, because of the resolution power of microscopes, a "diffraction limited" object only means that it is the smallest form distinguishable by a microscope. As a consequence, everything smaller than this limit (~ 300 nm), no matter its shape or level of organization, will look like a globular 300 nm patch and smaller filaments will also look as round blobs. Therefore, the debate between filaments and patches is not about the existence of filamentous structures but rather about their size.

- Helix vs. perpendicular tracks:

While original observations made with epifluorescence microscopy suggested helical structures (Defeu Soufo & Graumann, 2004; Jones et al., 2001), TIRF and confocal microscopy images showed movements along perpendicular tracks (Dominguez-Escobar et al., 2011; Garner et al., 2011; van

Teeffelen et al., 2011). New results using single-molecule tracking experiments have confirmed these observations in *E. coli* with MreB^{SW}-PAmCherry (PAm-cherry sandwich fusion) (Lee et al., 2014) and a monomeric Venus sandwich fusion of *mreB* (MreB^{mVenus}) (Ursell et al., 2014).

Even in new reports claiming the existence of long filaments, those ring shaped, discontinuous structures are oriented perpendicularly to the cell long axis, with a Gaussian distribution around 90° (Olshausen et al., 2013; Reimold, Defeu Soufo, Dempwolff, & Graumann, 2013).

In conclusion, all recent data agrees about the orientation of the movement, leaving aside the length of the structures.

- Long vs. short structures

Graumann's group has showed that GFP (green fluorescent protein)- and YFP (yellow fluorescent protein)-MreB and GFP-Mbl from *B. subtilis* and MreB^{SW}-RFP (sandwich red fluorescent protein) from *E. coli*, in exponential growth, form filaments longer than the diffraction limit and up to 1.5 µm (about half a circumference of a typical *B. subtilis* cell). These were seen with SIM (structured illumination microscopy), STED (stimulated emission depletion) and TIRF-SIM (total internal reflection fluorescent-SIM) superresolution techniques. They also indicate that filaments were disassembled upon cell stress, forming small clusters, and reassembled when optimal growth conditions were renewed (Olshausen et al., 2013; Reimold et al., 2013). YFP-MreB was shown to be an exception among these fusions because it is non-functional and the YFP tag seems to over-stabilize the MreB polymers, generating artificially long filaments (Figure 11) (Swulius & Jensen, 2012). Observations from Olshausen, Reimold and coworkers with GFP and RFP fusions are much puzzling since these fusions have been used in other labs, including ours, producing drastically different results showing light-diffraction limited structures (Dominguez-Escobar et al., 2011; Garner et al., 2011). However, in *E. coli*, the most recent study using the less perturbing fluorescent MreB fusion to date in this bacterium (a monomeric superfolder GFP sandwiched into MreB) reported filaments of 500 ± 10 nm in minimal media (Ouzounov et al., 2016).

The ability to form filaments is not the core of the debate since *in vitro* works support the existence of MreB polymers (see section 1.4.2). The questions are: 1. how long are the structures, 2. what is their orientation relative to their movement and to the cell long axis, 3. is their length correlated with other parameters (speed, direction, density of protein in the cell, growth rate...) and 4. what is their ultrastructure, specially when they are shorter than the diffraction limit (polymer of monomers, polymer of dimers, bundle, parallel or antiparallel sheets...).

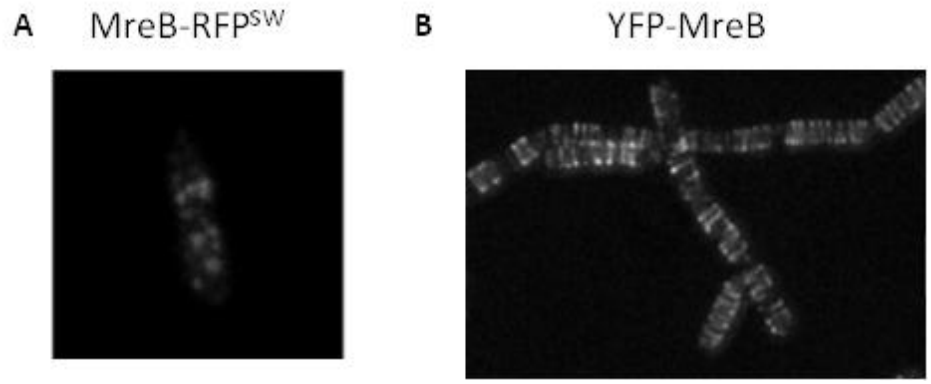

Figure 11 Filaments and diffraction-limited clusters (modified from (Swulius & Jensen, 2012) and (Reimold et al., 2013)). **A.** Clusters of MreB-RFP^{SW} in *E. coli*. **B**. Filaments of YFP-MreB in *E. coli*.

An interesting result from our lab, to be published, comparing different strains from various labs under different growth conditions, suggests that over-accumulation of MreB above natural levels leads to the formation of long filaments in *B. subtilis* (Chastanet et al., unpublished results). This suggests that protein expression levels could be key to understand MreB filament length.

1.4.4 Role of MreB in cell shape determination and cell wall synthesis

The most obvious phenotype and probably the primary function of MreB, seems to be the control of rod shape during elongation, although its precise role and way of action are not known. Curiously, most non rod-shaped bacteria lack *mreB*, but have *mreC* and *mreD*. We could hypothesize that MreB is linked to lateral CW elongation in rods and that is why it is absent in non-rods, but there are some exceptions of coccoids with MreB (Ouellette, Karimova, Subtil, & Ladant, 2012) and this explanation wouldn't fit those cases. Anyway, from pioneering studies on MreB, the shape defect of *mreB* was reported (Doi et al., 1988; Wachi et al., 1987). These mutants have a characteristic phenotype, they bulge and curve, even forming telephone cord-like cell chains, and, finally, they lyse (Figure 10). A study from the Shaevitz group (Ouzounov et al., 2016) uses sub-lethal concentrations of A22 (a drug that inhibits MreB polymerization) and a series of MreB mutants to study the polymerization properties of MreB and its effect in cell shape in *E. coli*. They obtained a number of MreB point mutations that caused a higher resistance to A22. This allowed them to find two exciting correlations, the strongest being between cell diameter and MreB polymer angle and the second between cell diameter and polymer number. Interestingly, their data shows that a reduction of the helical angle of MreB entails an increase of cell width.

Cell wall integrity is tightly linked to cell morphology. An impressive study from (Ursell et al., 2014) measures simultaneously cell shape dynamics, CW insertion and cytoskeletal localization in *E. coli*.

Their conclusions are that MreB's localization is biased to negatively curved areas along the cell cylinder, directing PG insertion to those areas, causing the straightening of the cell. There are multiple evidences of MreB from different organisms (including *B. subtilis*) interacting with Mur and DAP proteins as well as with proteins from the CW machinery (Divakaruni, Baida, White, & Gober, 2007; Favini-Stabile, Contreras-Martel, Thielens, & Dessen, 2013; Gaballah et al., 2011; Rueff et al., 2014; White, Kitich, & Gober, 2010). Kawai and co-workers showed that the localization and correct function of PBP1 is MreB-dependant (Kawai, Daniel, et al., 2009). Also, in pulldown assays, both MreB and Mbl associate with PBP1, PBP2a, PBP4 and possibly PBP5, independently (Kawai, Asai, et al., 2009). Furthermore, PbpH, PBP2a, MreC, MreD and RodA move similarly and colocalize with the MreB/Mbl/MreBH complex (Dominguez-Escobar et al., 2011; Garner et al., 2011). Further validation of these results comes from single-molecule experiments that revealed how PBP2 and MreB colocalize transiently to coordinate cell wall synthesis (Lee et al., 2014). Their results show how, by PBP2 having a diffusive motion and MreB following directed paths, their transitory interactions are beneficial to buffer growth through variable enzyme abundances and changing environmental conditions. It is possible that MreB acts as the link between PG precursor synthesis and its insertion to the CW.

1.4.5 Other roles of MreB

MreB has been linked to motility in *Myxococcus xanthus*, spore formation in *Streptomyces* and chromosome segregation and cell polarity in various bacteria (Chastanet & Carballido-Lopez, 2012). In *B. subtilis*, it has only been shown to, may be, have a role in chromosome segregation and viral DNA and replication proteins localization.

1.4.5.1 Chromosome segregation

For some time, MreB was thought to have a role in DNA segregation and that the state of the chromosome affected MreB polymerization (Defeu Soufo & Graumann, 2005). Once in-frame deletions of *mreB* were created, avoiding polar effects on downstream genes, the impact on chromosomal segregation wasn't detectable (Formstone et al., 2008).

1.4.5.2 Viral DNA and replication proteins localization

Efficient ϕ29 DNA replication requires functional MreB proteins in *B. subtilis*. Interestingly, it needs the presence of all three MreB paralogs (Munoz-Espin, Serrano-Heras, & Salas, 2012). This is the first example of non-redundancy of the three MreB paralogs until now.

1.4.5.3 Cell division

Until recently, there was no established link between the different cytoskeletal elements in bacteria. In (Fenton & Gerdes, 2013) it is demonstrated that MreB and FtsZ interact and that this interaction is essential for the correct localization of the divisome and septum synthesis. It seems that MreB, besides interacting with FtsZ, recruits PBP1B and PBP2 to the divisome, which is an essential step to pursue with cell division.

1.4.5.4 Pathogenicity

A very interesting study in *Bdellovibrio bacteriovorus*, a predatory bacterium with two *mreB* genes, *mreB1* and *mreB2*, has demonstrated a link between the actin-like protein and predatory rate (Fenton, Lambert, Wagstaff, & Sockett, 2010). Both genes are essential in *B. bacteriovorus*, but they succeeded in creating GFP fusions of each protein with partial functionality that allowed them to study the role of MreB1 and MreB2 independently. MreB1 is implicated in the early differentiation of predatory cells while MreB2 is involved in the late differentiation of those. Addition of A22 helps those cells with partially functional MreB1, most likely because it stabilizes its polymers. In the other hand, addition of A22 during the late stages of WT attack-phase cells didn't have an effect, while it did affect cells with partially functional MreB2. This suggests that, in this condition, MreB2 continued to be active in CW turnover for longer than in the WT strain.

Another example of MreB being involved in pathogenicity comes from a study performed in *Pseudomonas aeruginosa* (Cowles & Gitai, 2010). They discovered that pilus localization and its correct function are MreB-dependent. They also saw that this is a secondary function of MreB, separate from cell shape maintenance. This is evident through the addition of low concentrations of A22 that don't cause a morphology defect while it alters pilus localization.

1.4.5.5 Gliding

Bacteria have different motility systems that allow them to change location allowing them to go to more beneficial zones or to develop a different physiological state. Gliding is a type of motility that takes place on surfaces and doesn't involve the development of appendages on the cell (Islam & Mignot, 2015). Studies performed on *M. xanthus* have described MglA, a cytoplasmic Ras-like GTPase, as a key factor in the organization of gliding motion (Hodgkin & Kaiser, 1979; Mauriello et al., 2010). The interaction of MglA with MreB promotes the assembly of the gliding machinery at the leading cell pole according to movement directionality (Islam & Mignot, 2015).

1.5. Aims of the thesis

MreB has been studied for a long time, but it seems that there are more and more open questions than solid answers. No one doubts the role of MreB in cell shape and CW synthesis. The three MreB paralogs in *B. subtilis*, MreB, Mbl and MreBH, although highly overlapping, have paralog-specific functions that were revealed when cells underwent stress conditions (Kawai, Asai, et al., 2009). These secondary functions remain unknown.

The main aim of the thesis was to understand the specific function of MreB in *B. subtilis* that isn't shared with its two other paralogs, Mbl and MmreBH. To do so we took advantage of an operon, *ydcFGH*, that showed high levels of induction in absence of *mreB*. The problematic was approached through the characterization of the three genes in the *ydcFGH* operon, the study of the regulatory link between these and *mreB* and building a screen to select loss-of-function point mutants of MreB by means of the promoter region of the *ydcFGH* operon.

2. Materials and Methods

2. Materials and Methods

2.1. Media Composition:

Lysogeny broth (LB) medium has a composition as in (Sezonov, Joseleau-Petit, & D'Ari, 2007). Casein hydrolysate (CH) medium has a composition as in (Formstone et al., 2008).

2.2. Media supplements:

Supplements added to the media and the concentration they were used at are in Table 4.

Table 4 Media supplements

Supplement	**Stock concentration**	**Final concentration**	
		B. subtilis	***E. coli***
Antibiotics			
Ampicillin	100 mg/mL	-	100 µg/mL
Chloramphenicol	10 mg/mL	5 µg/mL	-
Erythromycin	10 mg/ml	1 µg/mL	-
Kanamycin	25 mg/mL	5 µg/mL	-
Phleomycin	5 mg/mL	0.2 µg/mL	-
Spectinomycin	100 mg/mL	100 µg/mL	-
Amino acids			
Tryptophan	1%	0.01%	-
Threonine	1%	0.01%	-
Other supplements			
$MgSO_4$	1 M	20 mM	-
Fructose	20 %	1.50%	-
Glucose	20 %	1.50%	-
Xylose	20%	0.50%	-
X-Gal	20 mg/mL	2.5 mg/mL	

2.3. Strains and plasmids

Bacterial strains and plasmids used in this study are given in Table 5 and 6, respectively.

Table 5 Strains used in this study

Name	**Genotype**	**Construction*, reference**
	Bacillus subtilis strains	
168	*trpC2*	Laboratory stock
RCL45	*trpC2* Δ*mreB::neo*	Laboratory stock**
RCL413	*trpC2* Δ*mreB::neo*	Laboratory stock
RCL329	*trpC2 gfp-mreB (neo)*	Laboratory stock
ASEC341	*trpC2 gfp-mreB (neo) thrC::*P_{ydc1}*-lacZ (erm)*	This study ABS1990 → RCL329
RCL414	*trpC2 neo*Ω*mreB*	A. Chastanet not published
ASEC12	*trpC2 neo*Ω*mreB thrC::*P_{ydc1}*-lacZ (erm)*	This study RCL414 → ABS1990
ABS2054	*trpC2* Δ*mreB::neo thrC::*P_{ydc1}*-lacZ (erm)*	A. Chastanet not published

Table 5 Strains used in this study (continuation)		
Name	**Genotype**	**Construction*, reference**
Bacillus subtilis strains		
ABS1987	*trpC2 amyE::*P_{xyl}*-gfp-mreB (spc)*	A. Chastanet not published
ASEC9	*trpC2 ΔmreB::neo thrC::*P_{ydc1}*-lacZ (erm) amyE::*P_{xyl}*-gfp-mreB (spc)*	This study ABS1987 → ABS2054
ABS2005	*trpC2 sacA::*P_{ydc1}*-lux (cat)*	A. Chastanet not published
ABS1990	*trpC2 thrC::*P_{ydc1}*-lacZ (erm)*	A. Chastanet not published
ASEC16	*trpC2 ΔmreB::neo thrC::*P_{ydc1}*-lacZ (erm) amyE::*P_N*-mreB (spc)*	This study pDG1730 → ABS2054
ABS1463	*trpC2 bkdB::tn917::amyE::cat*	A. Chastanet not published
ASEC211	*trpC2 ΔmreB::neo thrC::*P_{ydc1}*-lacZ (erm) bkdB::tn917::amyE::cat*	This study ABS1463 → ABS2054
ASEC234	*trpC2 ΔmreB::neo thrC::*P_{ydc1}*-lacZ (erm) bkdB::tn917::amyE::cat::*P_{xyl}*-gfp-mreB (spc)*	This study ABS1987 → ASEC211
ASEC42	*trpC2 amyE::*P_N*-mreB (spc)*	This study pDG1730.1 → RCL44
ASEC236	*trpC2 ΔmreB::neo thrC::*P_{ydc1}*-lacZ (erm) bkdB::tn917::amyE::cat::*P_N*-mreB (spc)*	This study ASEC42 → ASEC211
ASEC18	*trpC2 ΔminC::km*	This study Gibson → 168
ASEC342	*trpC2 ΔminC::km thrC::*P_{ydc1}*-lacZ (erm)*	This study ABS1990 → ASEC18
ASEC266	*trpC2 amyE::Km-*P_{xyl}*-pep thrC::*P_{ydc1}*-lacZ (erm)*	This study Gibson → ABS1990
ABS1400	*trpC2 ΔmreB::neo amyE::*P_N*-mreBCD (spc)*	A. Chastanet not published
ASEC20	*trpC2 ΔmreB::neo amyE::*P_N*-mreBCD (spc) thrC::*P_{ydc1}*-lacZ (erm)*	This study ABS1400 → ABS1990
ASEC35	*trpC2 amyE::*P_N*-mreBCD (spc) ΔmreBCD::km*	This study ΔmreBCD::neo Gibson PCR → ABS1397
ASEC40	*trpC2 amyE::*P_N*-mreBCD (spc) ΔmreBCD::km thrC::*P_{ydc1}*-lacZ (erm)*	This study ABS1990 → ASEC35
RCL82	*trpC2 ΔmreC::km*	Laboratory stock
ASEC7	*trpC2 ΔmreC::km thrC::*P_{ydc1}*-lacZ (erm)*	This study ABS1990 → RCL82
RCL181	*trpC2 mreC*ΩP_{xyl}*-gfp-mreCmreD (cat)*	Laboratory stock
ASEC115	*trpC2 mreC*ΩP_{xyl}*-gfp-mreCmreD (cat) thrC::*P_{ydc1}*-lacZ (erm)*	This study ABS1990 → RCL181
RCL180	*trpC2 mreD*ΩP_{xyl}*-gfp-mreD (cat)*	Laboratory stock
ASEC168	*trpC2 mreD*ΩP_{xyl}*-gfp-mreD (cat) thrC::*P_{ydc1}*-lacZ (erm)*	This study ABS1990 → RCL180
RCL131	*trpC2 amyE::*P_{xyl}*-gfp-mreC (spc)*	Laboratory stock
ASEC109	*trpC2 amyE::*P_{xyl}*-gfp-mreC (spc) thrC::*P_{ydc1}*-lacZ (erm)*	This study ABS1990 → RCL131
RCL132	*trpC2 amyE::*P_{xyl}*-gfp-mreD (spc)*	Laboratory stock
ASEC111	*trpC2 amyE::*P_{xyl}*-gfp-mreD (spc) thrC::*P_{ydc1}*-lacZ (erm)*	This study ABS1990 → RCL132
NC101	*trpC2* ΔSPβ *Δskin* ΔPBSX *upp::*P_{lambda}*-neo*	N. Mirouze not published
ASEC24	*trpC2* ΔSPβ *Δskin* ΔPBSX *upp::*P_{lambda}*-neo ΔydcF*	This study *ydcF* clean deletion → NC101
ASEC5	*trpC2 ΔSPβ Δskin ΔPBSX upp::Plambda-neo ΔydcG*	This study *ydcG* clean deletion → NC101
ABS1381	*trpC2 ΔydcH::spc*	A. Chastanet not published
ASEC56	*trpC2 ΔydcH::spc sacA::Pydc1-lux (cat)*	This study ABS1381 → ABS2005
ASEC58	*trpC2 ΔSPβ Δskin ΔPBSX upp::Plambda-neo ΔydcG sacA::Pydc1-lux (cat)*	This study ABS2005 → ASEC5
ASEC60	*trpC2 ΔSPβ Δskin ΔPBSX upp::Plambda-neo ΔydcF sacA::Pydc1-lux (cat)*	This study ABS2005 → ASEC24

Table 5 Strains used in this study (continuation)		
Name	**Genotype**	**Construction*, reference**
Bacillus subtilis strains		
ABS1798	*trpC2* Δ*ydcH::spc::erm*	A. Chastanet not published
BKE04650	Δ*ydcF::erm*	BGSE centre
BKE04760	Δ*ydcG::erm*	BGSE centre
BKE04770	Δ*ydcH::erm*	BGSE centre
ASEC275	*trpC2* Δ*ydcF::erm*	This study BKE04750 → RCL44
ASEC277	*trpC2* Δ*ydcG::erm*	This study BKE04760 → RCL44
ASEC279	*trpC2* Δ*ydcH::erm*	This study BKE04770 → RCL44
ASEC287	*trpC2* Δ*ydcF*	This study pDR244 → ASEC275
ASEC289	*trpC2* Δ*ydcG*	This study pDR244 → ASEC277
ASEC293	*trpC2* Δ*ydcH*	This study pDR244 → ASEC279
ABS2084	*trpC2 sacA::*P_{ydc1}*-lacZ (cat)*	A. Chastanet not published
ASEC281	*trpC2 sacA::*P_{ydc1}*-lacZ (cat)* Δ*ydcF*	This study ABS2084 → ASEC287
ASEC283	*trpC2 sacA::*P_{ydc1}*-lacZ (cat)* Δ*ydcG*	This study ABS2084 → ASEC289
ASEC285	*trpC2 sacA::*P_{ydc1}*-lacZ (cat)* Δ*ydcH*	This study ABS2084 → ASEC293
ASEC311	*trpC2 sacA::*P_{ydc1}*-luxABCDE (cat)* Δ*ydcF::erm*	This study ABS2005 → ASEC275
ASEC313	*trpC2 sacA::*P_{ydc1}*-luxABCDE (cat)* Δ*ydcG::erm*	This study ABS2005 → ASEC277
ASEC315	*trpC2 sacA::*P_{ydc1}*-luxABCDE (cat)* Δ*ydcH::erm*	This study ABS2005 → ASEC279
ASEC317	*trpC2 sacA::*P_{ydc1}*-luxABCDE (cat)* Δ*ydcF*	This study pDR244 → ASEC311
ASEC319	*trpC2 sacA::*P_{ydc1}*-luxABCDE (cat)* Δ*ydcG*	This study pDR244 → ASEC313
ASEC321	*trpC2 sacA::*P_{ydc1}*-luxABCDE (cat)* Δ*ydcH*	This study pDR244 → ASEC315
ABS1761	*trpC2 amyE::*P_{ydc1}*-lacZ (spc)*	A. Chastanet not published
CCBS213	*trpC2* Δ*mreB::neo amyE::*P_{ydc1}*-lacZ (spc)*	This study ABS1761 → RCL413
ABS1763	*trpC2 amyE::*P_{ydc2}*-lacZ (spc)*	A. Chastanet not published
ABS1765	*trpC2 amyE::*$P_{ydc1\text{-}2}$*-lacZ (spc)*	A. Chastanet not published
ABS1767	*trpC2 amyE::*P_{ydc0}*-lacZ (spc)*	A. Chastanet not published
ABS1764	*trpC2 amyE::*P_{ydc2}*-lacZ (spc)* Δ*mreB::neo*	A. Chastanet not published
ABS1766	*trpC2 amyE::*$P_{ydc1\text{-}2}$*-lacZ (spc)* Δ*mreB::neo*	A. Chastanet not published
ABS1768	*trpC2 amyE::*P_{ydc0}*-lacZ (spc)* Δ*mreB::neo*	A. Chastanet not published
RCL78	*trpC2* Δ*mbl::cat*	Laboratory stock
ABS1769	*trpC2* Δ*mbl::cat amyE::*P_{ydc1}*-lacZ (spc)*	A. Chastanet not published
ABS1770	*trpC2* Δ*mbl::cat amyE::*$P_{ydc1\text{-}2}$*-lacZ (spc)*	A. Chastanet not published
RCL49	*trpC2* Δ*mreBH::cat*	Laboratory stock
ABS1824	*trpC2* Δ*mreBH::cat amyE::Pydc1-lacZ (spc)*	A. Chastanet not published
ABS1825	*trpC2* Δ*mreBH::cat amyE::Pydc1-2-lacZ (spc)*	A. Chastanet not published
ABS1821	*trpC2* Δ*ydcH::spc::erm amyE::Pydc1-lacZ (spc)*	A. Chastanet not published
ABS1822	*trpC2* Δ*ydcH::spc::erm amyE::Pydc1-2-lacZ*	A. Chastanet not published
ABS1823	*trpC2* Δ*ydcH::spc::erm amyE::Pydc0-lacZ*	A. Chastanet not published
ASEC337	*trpC2 amyE::Pydc2-lacZ (spc)* Δ*ydcH*	This study ABS1763 → ASEC293
ASEC335	*trpC2 amyE::Pydc2-lacZ (spc)* Δ*ydcG*	This study ABS1763 → ASEC289

Table 5 Strains used in this study (continuation)		
Name	**Genotype**	**Construction*, reference**
Bacillus subtilis strains		
ASEC333	*trpC2 amyE::*P_{ydc2}*-lacZ (spc) ΔydcF*	This study ABS1763 → ASEC287
CCBS194	*trpC2 neoΩmreB*-3STOP *thrC*::P_{ydc1}*-lacZ* (*erm*)	C. Cornilleau not published
CCBS202	*trpC2 ΔmreB::neo*-3STOP *thrC*::P_{ydc1}*-lacZ* (*erm*)	C. Cornilleau not published
ABS1755	*trpC2 thrC::*P_{mreBH}*-lacZ (spc)*	A. Chastanet not published
ABS1756	*trpC2 thrC::*P_{mreBH}*-lacZ (spc) ΔmreB::neo*	A. Chastanet not published
RCL422	*trpC2 thrC::*P_{mreBH}*-lacZ (cat)*	This study pDag32 → ABS1755
RCL423	*trpC2 thrC::*P_{mreBH}*-lacZ (cat) ΔmreB::neo*	This study pDag32 → ABS1756
ABS1749	*trpC2 thrC::*P_{fru}*-lacZ (spc)*	A. Chastanet not published
ABS1750	*trpC2 thrC::*P_{fru}*-lacZ (spc) ΔmreB::neo*	A. Chastanet not published
RCL424	*trpC2 thrC::*P_{mreBH}*-lacZ (cat) mreB::km-*P_N*optrbsgfp-mreB*^{WT}	This study CCBS170 → RCL422
CCBS170	*trpC2 mreB::km-*P_N*optrbsgfp-mreB*^{WT}	C. Cornilleau not published
RCL425	*trpC2 thrC::*P_{mreBH}*-lacZ (cat) mreB::km-*P_N*optrbsgfp-mreB*^{I242N}	This study CCBS170 → RCL422
RCL426	*trpC2 thrC::*P_{mreBH}*-lacZ (cat) mreB::km-*P_N*optrbsgfp-mreB*^{N88I}	This study CCBS170 → RCL422
RCL427	*trpC2 thrC::*P_{mreBH}*-lacZ (cat) mreB::km-*P_N*optrbsgfp-mreB*^{G56R}	This study CCBS170 → RCL422
RCL428	*trpC2 thrC::*P_{mreBH}*-lacZ (cat) mreB::km-*P_N*optrbsgfp-mreB*^{K197E}	This study CCBS170 → RCL422
RCL429	*trpC2 thrC::*P_{mreBH}*-lacZ (cat) mreB::km-*P_N*optrbsgfp-mreB*^{G160R}	This study CCBS170 → RCL422
RCL430	*trpC2 thrC::*P_{mreBH}*-lacZ (cat) mreB::km-*P_N*optrbsgfp-mreB*^{E243G}	This study CCBS170 → RCL422
RCL431	*trpC2 thrC::*P_{mreBH}*-lacZ (cat) mreB::km-*P_N*optrbsgfp-mreB*^{S109P}	This study CCBS170 → RCL422
RCL432	*trpC2 thrC::*P_{mreBH}*-lacZ (cat) mreB::km-*P_N*optrbsgfp-mreB*^{T41A}	This study CCBS170 → RCL422
RCL433	*trpC2 thrC::*P_{mreBH}*-lacZ (cat) mreB::km-*P_N*optrbsgfp-mreB*^{V114A}	This study CCBS170 → RCL422
RCL434	*trpC2 thrC::*P_{mreBH}*-lacZ (cat) mreB::km-*P_N*optrbsgfp-mreB*^{I142T}	This study CCBS170 → RCL422
RCL435	*trpC2 thrC::*P_{mreBH}*-lacZ (cat) mreB::km-*P_N*optrbsgfp-mreB*^{G216R}	This study CCBS170 → RCL422
RCL436	*trpC2 thrC::*P_{mreBH}*-lacZ (cat) mreB::km-*P_N*optrbsgfp-mreB*^{A276G}	This study CCBS170 → RCL422
RCL437	*trpC2 thrC::*P_{mreBH}*-lacZ (cat) mreB::km-*P_N*optrbsgfp-mreB*^{V72I}	This study CCBS170 → RCL422
RCL438	*trpC2 thrC::*P_{mreBH}*-lacZ (cat) mreB::km-*P_N*optrbsgfp-mreB*^{G231D}	This study CCBS170 → RCL422
RCL439	*trpC2 thrC::*P_{mreBH}*-lacZ (cat) mreB::km-*P_N*optrbsgfp-mreB*^{E31G}	This study CCBS170 → RCL422
RCL440	*trpC2 thrC::*P_{mreBH}*-lacZ (cat) mreB::km-*P_N*optrbsgfp-mreB*^{V182A}	This study CCBS170 → RCL422
RCL441	*trpC2 thrC::*P_{mreBH}*-lacZ (cat) mreB::km-*P_N*optrbsgfp-mreB*^{G14E}	This study CCBS170 → RCL422
RCL442	*trpC2 thrC::*P_{mreBH}*-lacZ (cat) mreB::km-*P_N*optrbsgfp-mreB*^{K52R}	This study CCBS170 → RCL422
RCL443	*trpC2 thrC::*P_{mreBH}*-lacZ (cat) mreB::km-*P_N*optrbsgfp-mreB*^{S33T}	This study CCBS170 → RCL422

Table 5 Strains used in this study (continuation)		
Name	**Genotype**	**Construction*, reference**
Bacillus subtilis strains		
RCL444	*trpC2 thrC::*P_{mreBH}*-lacZ (cat) mreB::km-*P_N*optrbsgfp-mreB*^{A51V}	This study CCBS170 → RCL422
RCL445	*trpC2 thrC::*P_{mreBH}*-lacZ (cat) mreB::km-*P_N*optrbsgfp-mreB*^{I174M}	This study CCBS170 → RCL422
RCL446	*trpC2 thrC::*P_{mreBH}*-lacZ (cat) mreB::km-*P_N*optrbsgfp-mreB*^{D189G}	This study CCBS170 → RCL422
RCL447	*trpC2 thrC::*P_{mreBH}*-lacZ (cat) mreB::km-*P_N*optrbsgfp-mreB*^{R66C}	This study CCBS170 → RCL422
RCL448	*trpC2 thrC::*P_{mreBH}*-lacZ (cat) mreB::km-*P_N*optrbsgfp-mreB*^{I279V}	This study CCBS170 → RCL422
RCL449	*trpC2 thrC::*P_{mreBH}*-lacZ (cat) mreB::km-*P_N*optrbsgfp-mreB*^{L171P}	This study CCBS170 → RCL422
RCL450	*trpC2 thrC::*P_{mreBH}*-lacZ (cat) mreB::km-*P_N*optrbsgfp-mreB*^{T79M}	This study CCBS170 → RCL422
RCL451	*trpC2 thrC::*P_{mreBH}*-lacZ (cat) mreB::km-*P_N*optrbsgfp-mreB*^{D121E}	This study CCBS170 → RCL422
RCL452	*trpC2 thrC::*P_{mreBH}*-lacZ (cat) mreB::km-*P_N*optrbsgfp-mreB*^{I134V}	This study CCBS170 → RCL422
RCL453	*trpC2 thrC::*P_{mreBH}*-lacZ (cat) mreB::km-*P_N*optrbsgfp-mreB*^{P151Q}	This study CCBS170 → RCL422
RCL454	*trpC2 thrC::*P_{mreBH}*-lacZ (cat) mreB::km-*P_N*optrbsgfp-mreB*^{P32L}	This study CCBS170 → RCL422
RCL455	*trpC2 thrC::*P_{mreBH}*-lacZ (cat) mreB::km-*P_N*optrbsgfp-mreB*^{V72A}	This study CCBS170 → RCL422
RCL456	*trpC2 thrC::*P_{mreBH}*-lacZ (cat) mreB::km-*P_N*optrbsgfp-mreB*^{M155V}	This study CCBS170 → RCL422
RCL457	*trpC2 thrC::*P_{mreBH}*-lacZ (cat) mreB::km-*P_N*optrbsgfp-mreB*^{N49S}	This study CCBS170 → RCL422
RCL458	*trpC2 thrC::*P_{mreBH}*-lacZ (cat) mreB::km-*P_N*optrbsgfp-mreB*^{G60R}	This study CCBS170 → RCL422
RCL461	*trpC2 thrC::*P_{mreBH}*-lacZ (cat) mreB::km-*P_N*optrbsgfp-mreB*^{I168FI169W}	This study CCBS170 → RCL422
Escherichia coli strains		
AEC1013	*DH5*α pAC824	A. Chastanet not published
AEC955	*DH5*α pAC772	A. Chastanet not published
AEC958	*DH5*α pAC775	A. Chastanet not published
AEC961	*DH5*α pAC778	A. Chastanet not published
AEC966	*DH5*α pAC783	A. Chastanet not published
AEC1021	*DH5*α pAC832	A. Chastanet not published

* Resistance gene abbreviations: neo, neomycin; kan, kanamycin; spc, spectinomycine; cat, chloramphenicol; erm, erythromycin. Other abbreviations: Δ, deletion; Ω, insertion. ** Δ*mreB* strain 3725. X → Z depicts construction procedure, where X could be plasmid or chromosomal DNA and Z is the recipient strain transformed by X.

Table 6 Plasmids used in this study

Plasmid	Characteristics	Source
pDG1730	*bla spc amyE*	Laboratory stock
pDG1730.1	*bla spc amyE3'*P_N*mreBamy5'*	This study
pDR244	*bla cre spc cop repF*	Laboratory stock
pDG1663	*bla thrC 3' erm lacZ thrC 5'*	Laboratory stock
pAC824	*bla thrC 3' erm* P_{ydc1}*lacZ thrC 5'*	This study
pDG1728	*bla amyE 3' spc lacZ amyE 5'*	Laboratory stock
pAC772	*bla amyE 3' spc* P_{ydc2}*lacZ amyE 5'*	This study
pAC775	*bla amyE 3' spc* $P_{ydc1\text{-}2}$*lacZ amyE 5'*	This study
pAC778	*bla amyE 3' spc* P_{ydc0}*lacZ amyE 5'*	This study
pAC783	*bla amyE 3' spc* P_{fruRKA}*lacZ amyE 5'*	This study
pDG1729	*bla thrC 3' spc lacZ thrC 5'*	Laboratory stock
pDag32	*bla spc::cat*	Laboratory stock
pAH328	*bla sacA 3' cat luxABCDE sacA 5'*	Laboratory stock
pAC832	*bla sacA 3' cat* P_{ydc1}*luxABCDE sacA 5'*	This study

2.4. Experimental procedures

2.4.1 Cloning procedures:

2.4.1.1 Oligonucleotides:

Oligonucleotides were designed using the Clone Manager 9 PE and purchased from Eurofins MWG. 100 pmol/µL aliquots were stored at -20 °C. Oligonucleotides used in this study are given in Table 7.

Table 7 Oligonucleotides used in this study

Primer	Description	Sequence 5' → 3'	Restriction sites/homology	Used for
AC1345	Rv at *mreC*	AAGTCACTCAGTAATAACCGC	-	verifications at *mreBCD* locus and *mreB* random mutagenesis
AC1335	Fw at *maf*	TCGATCAAGCCGTAGCCTTTGCTG	-	verifications at *mreBCD* locus and *mreB* random mutagenesis
CC181	Fw at *maf*	GTCATGGGCCTTCCTATATC	-	*mreB* directed mutagenesis
RK14	Rv at *mreC*	AATTCGAGCAGACAGACAGCCAGAAC	-	*mreB* directed mutagenesis
AC1240	Fw	GTAGAATTCGCTGAAAATGTATACG ACATCGAG	EcoRI	amplify P_{ydc1} and P_{ydc1-2}
AC1241	Rv	GGAGGATCCCCGTCGGCATGTCTTT AGACAGT	BamHI	amplify P_{ydc1} and P_{ydc0}
AC1242	Rv	GGAGGATCCGGCAGCGCCTTTTAAT ACATGTT	BamHI	amplify P_{ydc2} and P_{ydc1-2}
AC1243	Fw	GAAGAATTCACTTATCATTCTGGGA GCTTATGGG	EcoRI	amplify P_{ydc1} and P_{ydc0}
AC1248	Fw	GATGAATTCCAGTTTTTAATTG AATCAGTCG	EcoRI	amplify P_{fru}
AC1249	Rv	GGAGGATCCAACGTATTCATTTTGA ATACAATTT	BamHI	amplify P_{fru}
AC1246	Fw	GATGAATTCTTCATCTACTTTTCTCA CAACA	EcoRI	amplify P_{mreBH}
AC1247	Rv	GGAGGATCCCCTAATTTAATATGAT TCTACATTT	BamHI	amplify P_{mreBH}
ASEC19	Fw at *ydcF*	AGCTGTGAAGAAGCTCAGAGAGGC CTTGAT	-	PI-PO *ydcF*
ASEC20	Rv at *ydcH*	ACACATAAAAAAAGACAGCTGGCG CTGCCC	-	PI-PO *ydcF*
ASEC21	Rv at *ydcF*	CGACCTGCAGGCATGCAAGCTCCTT GCAGAAGCAATGTTCCTTCCGTTCC A	cassette phleomycin	PI-PO *ydcF*
ASEC22	Fw at *ydcF*	CGACGTCGAATTCACTGGCCGTCTG GAACGGAAGGAACATTGCTTCTGCA AGGGCCGACGGCTGTCAGCAGGCTT GTCCATCT	C1 and *ydcF* 5'	PI-PO *ydcF*
ASEC23	Fw at *ydcG*	GTAATCAGGCGATGAAAAACAAAA GAGGCG	-	PI-PO *ydcG*
ASEC48	Rv at *ydcG*	GTCAGGATATAGTCGGCAAGCGGCT CAAGG	-	PI-PO *ydcG*
ASEC25	Rv at *ydcG*	CGACCTGCAGGCATGCAAGCTTCTG ACACAACGCCGATCCAGTAATTT	cassette phleomycin	PI-PO *ydcG*

Table 7 Oligonucleotides used in this study (continuation)				
Primer	**Description**	**Sequence 5' → 3'**	**Restriction sites/homology**	**Used for**
ASEC47	Fw at *ydcG*	CGACGTCGAATTCACTGGCCGTCGAAATTACTGGATCGGCGTTGTGTCAGAAAAAAAGATTTTTTGACAATAGCACAAGCGATGGG	C1 and *ydcG* 5'	PI-PO *ydcG*
ASEC69	Fw at *radC*	TAAGACAGAAGTTGCGTTTTGGTCCCTCAG		Δ*mreBCD*
ASEC70	Rv at 5' *mreB*	AGCCCAAGCTCTAGACCAAGGTCTCTAGCACCAATTCCAAACATA	5' neomycin cassette	Δ*mreBCD*
ASEC71	Fw neomycine	TCTAGAGCTTGGGCTGCAGGTCG	5' neomycin cassette	Δ*mreBCD*
ASEC72	Rv neomycine	GTAACCAACATGATTAACAATTATTAGAGGTCATCGTTCAAA	3' neomycin cassette	Δ*mreBCD*
ASEC73	Fw 3' *mreD*	TTAATCATGTTGGTTACGTAAAAAGGATTTTATCTTTTTTTGACGAAATGAGTATGTTGTTGAG	3' neomycin cassette	Δ*mreBCD*
ASEC74	Rv *minC*	CTCCAGCAGTCCTATAATACGGTCAGCATC		Δ*mreBCD*
ASEC87	Rv *mreB*	TTTTTTATGGCCTGAATGATGTAATATTTCATCATCG	MreB* N88I	B2
ASEC88	Fw *mreB*	GAAATATTACATCATTCAGGCCATAAAAAATAAAGG	MreB* N88I	B2
ASEC91	Rv *mreB*	GCCCGGTGTCCGTCTAATCATATTTTTCGC	MreB* G56R	B4
ASEC92	Fw *mreB*	ATATGATTAGACGGACACCGGGCAACGTGG	MreB* G56R	B4
ASEC95	Rv *mreB*	GTACCGCCCCTGATATCAACAACCATGCTTCC	MreB* G160R	B6
ASEC96	Fw *mreB*	TGTTGATATCAGGGGCGGTACGACAGAAGTTGC	MreB* G160R	B6
ASEC97	Rv *mreB*	TTCCTGTAATTCCAATTGTTTTCGGCAAACCTG	MreB* E243G	B7
ASEC98	Fw *mreB*	AAAACAATTGGAATTACAGGAAAAGAGATTTCTAACGCTCTACGCGACAC	MreB* E243G	B7
ASEC154	Rv *mreB*	CAGCTGCTGAAGAACGCGCTGTTATCGATGCGACAAGACAGG	MreB* V114A	B14
ASEC155	Fw *mreB*	CGCGTTCTTCAACAGCTGTAATGCCTGATGGG	MreB* V114A	B14
ASEC156	Rv *mreB*	GATTGGCTCCGGTTGCTGCGGCAAAAGGCTCTTC	MreB* I142T	B15
ASEC157	Fw *mreB*	GCCGCAGCAACCGGAGCCAATCTGCCAGTTTGGG	MreB* I142T	B15
ASEC160	Rv *mreB*	TCAGCGATAATGCCGTCTTTCATCGGGCGAAGAG	MreB* G216R	B16
ASEC161	Fw *mreB*	GAAAGACGGCATTATCGCTGATTATGAAA	MreB* G216R	B16
ASEC170	Rv *mreB*	GTAATGCCTGGTGGGACACATACCATTAC	MreB* S109P	B10
ASEC171	Fw *mreB*	ATGTGTCCCACCAGGCATTACAGC	MreB* S109P	B10

Table 7 Oligonucleotides used in this study (continuation)				
Primer	**Description**	**Sequence 5' → 3'**	**Restriction sites/homology**	**Used for**
ASEC172	Rv *mreB*	ATCGATTTCGCATCCGTCTGCAAAGC	MreB* T41A	B11
ASEC173	Fw *mreB*	TTGTCGCTTTGCAGACGGATGCGAAAT	MreB* T41A	B11
ASEC174	Fw *mreB*	CCTGAGCTTGGAGCAGATATCATGGACA GAGGTA	MreB* A276G	B17
ASEC175	Rv *mreB*	GATATCTGCTCCAAGCTCAGGCGGTGTTT TTTCG	MreB* A276G	B17
ASEC176	Fw *mreB*	GAAATCCGCGACCGCGATTTGCTCACAG GTTTGC	MreB* G231D	B19
ASEC177	Rv *mreB*	CGCGGTCGCGGATTTCCATGTTG	MreB* G231D	B19
ASEC178	Rv *mreB*	CTGACGGCCCTCTCACAACAATTCCTTTT CCTTTT	MreB* E31G	B20
ASEC179	Fw *mreB*	GTTGTGAGAGGGCCGTCAGTTGTCGCTTT GCAG	MreB* E31G	B20
ASEC180	Fw *mreB*	TCAATCCGTGCAGCCGGTGATGAGATGG ATGACGC	MreB* V182A	B21
ASEC181	Rv *mreB*	ATCACCGGCTGCACGGATTGACTGAGAC GTTACGA	MreB* V182A	B21
ASEC182	Fw *mreB*	ATAGATCTTGAAACTGCGAATACGCTTGT TTTTGT	MreB* G14E	B22
ASEC183	Rv *mreB*	TTCGCAGTTTCAAGATCTATACCAAGGTC TC	MreB* G14E	B22
ASEC184	Rv *mreB*	GGTTTGCCGAAAACAAATGAAATTACAG GAAAAGAGATTTCTA	MreB* I242N	B1
ASEC185	Fw *mreB*	CTTTTCCTGTAATTTCATTTGTTTTCGGCA AACCTGTGAGC	MreB* I242N	B1
ASEC186	Rv *mreB*	ATCAGATTGTACGTTTCTCTGATGTAGTT	MreB* K197E	B5
ASEC187	Fw *mreB*	ATTATCAACTACATCAGATAAACGTACA	MreB* K197E	B5
ASEC257	Fw *mreB*	GAAAGACGGCGCTATCGCTGATTATG	MreB* V72I	B18
ASEC258	Rv *mreB*	TCAGCGATAGCGCCGTCTTTCATCGGG	MreB* V72I	B18
ASEC211	Fw *mreB*	AATGATGCGAGAAATATGATTGG	MreB* K52R	B23
ASEC212	Rv *mreB*	ATCATATTTCTCGCATCATTTCCGAC	MreB* K52R	B23
ASEC215	Fw *mreB*	TGAGAGAGCCGACAGTTGTCGC	MreB* S33T	B25
ASEC216	Rv *mreB*	GCGACAACTGTCGGCTCTCTCAC	MreB* S33T	B25
ASEC217	Fw *mreB*	GAAATGATGTGAAAAATATGATTG	MreB* A51V	B26
ASEC218	Rv *mreB*	CATATTTTTCACATCATTTCCGAC	MreB* A51V	B26
ASEC219	Fw *mreB*	CGGAGGCATGGTAACGTCTCAG	MreB* I174M	B27
ASEC220	Rv *mreB*	GAGACGTTACCATGCCTCCGAGGGAAAT A	MreB* I174M	B27
ASEC221	Fw *mreB*	AGATGGATGGCGCGATTATCAACTACA	MreB* D189G	B28
ASEC222	Rv *mreB*	GATAATCGCGCCATCCATCTCATCAC	MreB* D189G	B28
ASEC223	Fw *mreB*	GTGGCTCTTTGCCCGATGAAAGAC	MreB* R66C	B29
ASEC224	Rv *mreB*	TTCATCGGGCAAAGAGCCACCAC	MreB* R66C	B29
ASEC225	Fw *mreB*	GCAGCAGATGTCATGGACAGAG	MreB* I279V	B30
ASEC226	Rv *mreB*	CTGTCCATGACATCTGCTGCAAGCTC	MreB* I279V	B30
ASEC229	Fw *mreB*	TTATTTCCCCCGGAGGCATCGTAACGTC	MreB* L171P	B32
ASEC230	Rv *mreB*	GATGCCTCCGGGGGAAATAATC	MreB* L171P	B32

Table 7 Oligonucleotides used in this study (continuation)				
Primer	**Description**	**Sequence 5' → 3'**	**Restriction sites/homology**	**Used for**
ASEC239	Fw *mreB*	ATGAAACAATGGCGACGATGATG	MreB* T79M	B37
ASEC240	Rv *mreB*	CATCGTCGCCATTGTTTCAT	MreB* T79M	B37
ASEC243	Fw *mreB*	TGTTATCGAAGCGACAAGACAGGCG	MreB* D121E	B39
ASEC244	Rv *mreB*	GTCTTGTCGCTTCGATAACAGCGCGT	MreB* D121E	B39
ASEC247	Fw *mreB*	GACGCGTATCCGGTTGAAGAGCCTTT	MreB* I134V	B41
ASEC248	Rv *mreB*	GGCTCTTCAACCGGATACGCGTCAC	MreB* I134V	B41
ASEC249	Fw *mreB*	TTTGGGAACAGACTGGAAGCATGG	MreB* P151Q	B42
ASEC250	Rv *mreB*	GCTTCCAGTCTGTTCCCAAACTGGC	MreB* P151Q	B42
ASEC253	Fw *mreB*	TGAGAGAGCTGTCAGTTGTCGCTT	MreB* P32L	B44
ASEC254	Rv *mreB*	GACAACTGACAGCTCTCTCACAAC	MreB* P32L	B44
ASEC257	Fw *mreB*	GAAAGACGGCGCTATCGCTGATTATG	MreB* V72A	B46
ASEC258	Rv *mreB*	TCAGCGATAGCGCCGTCTTTCATCGGG	MreB* V72A	B46
ASEC259	Fw *mreB*	CCGACTGGAAGCGTGGTTGTTGATATCGG	MreB* M155V	B47
ASEC260	Rv *mreB*	TCAACAACCACGCTTCCAGTCGG	MreB* M155V	B47
ASEC269	Fw *mreB*	CGCTGTCGGAAGTGATGCGAAAAAT	MreB* N49S	B52
ASEC270	Rv *mreB*	TTTCGCATCACTTCCGACAGCGACAA	MreB* N49S	B52
ASEC271	Fw *mreB*	ACGGACACCGCGCAACGTGGTGG	MreB* G60R	B53
ASEC272	Rv *mreB*	ACCACGTTGCGCGGTGTCCGTC	MreB* G60R	B53
ASEC196	Rv	TTCCAAACATCCTAGGAATCTCCTTTCT	5' Δ*mreB*	*amyE*::P_{xyl}*pep*
ASEC197	Fw	GATTCCTAGGATGTTTGGAATTGGTGCTAGA	3' P_{xyl}	*amyE*::P_{xyl}*pep*
ASEC198	Rv	TATCAAGCTTTTATCTAGTTTTCCCTTTGAAAAGATG	5' amyE	*amyE*::P_{xyl}*pep*
ASEC199	Fw	AACTAGATAAAAGCTTGATATCGAATTCTAGTT	3' Δ*mreB*	*amyE*::P_{xyl}*pep*

2.4.1.2 Polymerase chain reaction (PCR):

PCR reactions were set up on ice and performed according to manufacturer's recommendations. Taq DNA polymerase was used to confirm insertions or deletions and for mutagenesis; Phusion (NEB) DNA polymerase was used for cloning in *B. subtilis* and sub-cloning in *E. coli*.

2.4.1.3 Polymerase chain reaction on *B. subtilis* colonies (cPCR):

50 µL LB cultures were inoculated with the colony of interest and incubated at 37 °C for 30 min. Reactions were set up on ice using Taq DNA polymerase, following manufacturer's recommendations. The DNA was introduced by adding 1 µL of the culture to the PCR mix.

2.4.1.4 Agarose gel electrophoresis of DNA fragments:

Agarose gel electrophoresis was performed in 1 % (w/v) agarose gels containing 1 % (v/v) ethidium bromide (Euromedex) in 1X TBE buffer. DNA samples were mixed at a 6:1 ratio with DNA loading buffer (30 % (v/v) glycerol, 0.25 % (w/v) bromophenol blue, 0.25 % (w/v) xylene cyanol FF) prior to loading. The voltage used for electrophoresis was 120 V.

2.4.1.5 Purification of DNA:

-DNA fragments:

Following PCR reactions or subsequent enzymatic reactions, DNA fragments are purified using the QIAquick PCR Purification Kit (QIAGEN), according to manufacturer's recommendations.

- Plasmids:

Plasmids are purified from *E. coli* strains containing it using a QIAprep Spin Miniprep Kit (QIAGEN), according to manufacturer's recommendations.

2.4.1.6 Estimation of DNA concentration:

Concentration of DNA in solution was determined by the use of a NanoDrop spectrophotometer (Thermo Scientific). The blank used was pure water. DNA solutions were assumed to be largely free of contaminating proteins if the ratio of absorbance at 260:280 nm was > 1.6.

2.4.1.7 Isothermal assembly of DNA fragments:

Isothermal assembly was performed mainly as described in Gibson *et al*., (Gibson et al., 2009) with minor modifications. In brief, DNA fragments are amplified adding homologous regions t their extremities, a 5' exonuclease creates long overhangs, a polymerase fills in the gaps of the annealed single strand regions, and a DNA ligase seals the nicks of the annealed and filled-in gaps.

2.4.1.8 General strategy for sub-cloning DNA fragments into plasmids in *E. coli*:

PCR-generated DNA fragments were purified as in 2.4.1.5, restriction digests were performed as per the manufacturers recommendations followed by dialysis against ddH_2O for 30 min. Dephosphorylation was performed with SAP (shrimp alkaline phosphate) as per manufacturers recommendations to then perform a ligation for 1 h at RT and transformation in competent DH5α

E.coli grown under selective pressure and saved as glycerol stock at -80 °C. Checking of the construction was performed by PCR and sequencing (see next section).

2.4.1.9 DNA sequencing:

1. Following sub-cloning in *E. coli* and cloning into *B. subtilis*, the complete plasmidic or chromosomal DNA regions that were subject to PCR or isothermal assembly, were sequenced to ensure the complete absence of unwanted mutations. For this, primers upstream and downstream of the inserted area were used. Sequencing of PCR products was performed by the sequence facility of Eurofins MWG and according to their recommendations.

2. Complete genome sequencing of *B. subtilis*: Chromosomal DNA of exponentially grown *B. subtilis* was extracted (2.4.2.4). The subsequent steps were subcontracted to GATC Biotech SARL (Mulhouse). For this, 200 ng of DNA was sent for construction of a genomic library. Sequencing was performed using Illumina technology, with paired-ends, 125bp long reads and 5 million read pairs. A pre-analysis (with with semi-automatic detection and mapping) with mapped SNPs and InDels was delivered. We further analyzed the data with the Tablet software (REF: Milne I, et al. Briefings in Bioinformatics 14(2) 193-202).

2.4.1.10 Random mutagenesis:

Random mutagenesis was performed by amplifying DNA fragments through PCR reactions. The frequency of mutations was favored by the use of a DNA polymerase devoid of proof-reading ability (Taq) and the presence of $MnCl_2$.

PCRs were performed as in 2.3.1.2 except that 0-0.4 mM $MnCl_2$ prepared freshly, were added to the mix. Next, PCR products were dialyzed against ddH_2O and used to transform *B. subtilis* competent cells (strain RCL422). Transformations were plated on LB-agar plates supplemented with kanamycin, $MgSO_4$ and X-gal. Mutants with MreB-impaired functionality formed bleu colonies (due to the activation of P_{mreBH} *lacZ*).

2.4.1.11 Directed mutagenesis PCR:

Site directed mutagenesis (Figure 21) is performed by “Gibson” assembly of PCR fragments generated on DNA from a strain bearing a *km* resistance cassette before the natural *mreB* promoter, and the *gfp* gene fused in 5’ of the *mreB* gene (RCL424). Two intermediate PCR products are generated using CC181/Rv mutation primer and Fw mutation primer/RK14, the mutation to introduce being bear on

the overlapping forward and reverse primers. PCRs were performed with Phusion (NEB) DNA polymerase, according to manufacturer's recommendations. Next, the PCR reaction was cooled down at RT and 1 µL of restriction enzyme DpnI was added and incubated at 37 °C for 1 h to digest methylated DNA (used as template and non-mutated). PCR products were purified as in 2.4.1.5 and DNA concentration was measured as in 2.3.1.6. Then, equivalent molecule quantities of the fragments were mixed to a total volume of 5 µL, added to 15 µL of joining mix (5 % w/v PEG-8000, 100 mM Tris-HCl pH = 7.5, 10 mM $MgCl_2$, 10 mM DTT, 1 mM NAD, 0.2 mM each dNTP, 25 U/mL T5 exonuclease, 50 U/mL Pfu DNA polymerase, 6667 U/mL Taq DNA ligase) and incubated 20 min at 50 °C to form a single DNA molecule (2.4.1.7). 10 µL of the joining reaction was used to transform competent *B. subtilis* cells.

2.4.1.12 Construction of plasmids with transcriptional fusion reporters:

- P_{ydc1}*lacZ*: A DNA fragment containing the putative P_{ydc1} promoter was PCR-amplified (see 2.4.1.3) using oligonucleotides AC1240 and AC1241and purified DNA (2.4.2.4) from WT strain RCL44 as template. The purified product (2.4.1.5) along with plasmid pDG1663 (containing the reporter gene *lacZ*), were subject to *Eco*RI/*BamH*I digestions (according to manufacturer's instructions) prior ligation and transformation in *E. coli*, generating pAC824.

- P_{ydc1}*luxABCDE*: A DNA fragment containing the putative P_{ydc1} promoter was PCR-amplified (see 2.4.1.3) using oligonucleotides AC1240 and AC1286 and purified DNA (2.4.2.4) from WT strain RCL44 as template. The purified product (2.4.1.5) along with plasmid pAH328 (containing the reporter gene *luxABCDE*), were subject to *Spe*I/*Eco*RI digestions (according to manufacturer's instructions) prior ligation and transformation in *E. coli*, generating pAC832.

- P_{ydc2}*lacZ*: A DNA fragment containing the putative P_{ydc2} promoter was PCR-amplified (see 2.4.1.3) using oligonucleotides AC1242 and AC1243 and purified DNA (2.4.2.4) from WT strain RCL44 as template. The purified product (2.4.1.5) along with plasmid pDG1728 (containing the reporter gene lacZ), were subject to *Eco*RI/*BamH*I digestions (according to manufacturer's directions) prior ligation and transformation in *E. coli*, generating pAC772.

- $P_{ydc1\text{-}2}$*lacZ*: A DNA fragment containing the putative $P_{ydc1\text{-}2}$ promoter was PCR-amplified (see 2.4.1.3) using oligonucleotides AC1240 and AC1242 and purified DNA (2.4.2.4) from WT strain RCL44 as template. The purified product (2.4.1.5) along with plasmid pDG1728 (containing the reporter gene lacZ), were subject to *Eco*RI/*BamH*I digestions (according to manufacturer's directions) prior ligation and transformation in *E. coli*, generating pAC775.

- P_{ydc0}*lacZ*: A DNA fragment containing the putative P_{ydc0} promoter was PCR-amplified (see 2.4.1.3) using oligonucleotides AC1243 and AC1241 and purified DNA (2.4.2.4) from WT strain RCL44 as template. The purified product (2.4.1.5) along with plasmid pDG1728 (containing the reporter gene lacZ), were subject to *Eco*RI/*BamH*I digestions (according to manufacturer's directions) prior ligation and transformation in *E. coli*, generating pAC778.

- P_{fruRKA}*lacZ*: A DNA fragment containing the putative P_{fruRKA} promoter was PCR-amplified (see 2.4.1.3) using oligonucleotides AC1248 and AC1249 and purified DNA (2.4.2.4) from WT strain RCL44 as template. The purified product (2.4.1.5) along with plasmid pDG1728 (containing the reporter gene lacZ), were subject to *Eco*RI/*BamH*I digestions (according to manufacturer's directions) prior ligation and transformation in *E. coli*, generating pAC783.

- P_{mreBH}-*lacZ*: A DNA fragment containing the putative P_{mreBH} promoter was PCR-amplified (see 2.4.1.3) using oligonucleotides AC1246 and AC1247 and purified DNA (2.4.2.4) from WT strain RCL44 as template. The purified product (2.4.1.5) along with plasmid pDG1729 (containing the reporter gene lacZ), were subject to *Eco*RI/*BamH*I digestions (according to manufacturer's directions) prior ligation and transformation in *E. coli*, generating pAC783.

2.4.2 Manipulation in *B. subtilis*

2.4.2.1 Preparation of *B. subtilis* competent cells:

To make *B. subtilis* competent for the uptake of DNA, 500 µL of MC medium per transformation were inoculated with a colony of a freshly streaked strain and incubated at 37 °C until $OD_{600\ nm}$ = 1-1.5.

2.4.2.2 Transformation of *B. subtilis* competent cells:

400 µL competent *B. subtilis* cells were mixed with 1 µg of chromosomal or PCR DNA, incubated 2 h at 37 °C and plated on selective medium and incubated o/n at 37 °C. Four colonies per transformation were checked by colony PCR.

2.4.2.3 Cloning of DNA fragments at ectopic loci:

DNA fragments were cloned at the *amyE* , *thrC*, *sacA*, and *bkdE* loci, using *B. subtilis* competent cells (2.4.2.1). DNA were either plasmids (from *E. coli* subcloning), PCR-generated fragments or product of isothermal assembly; the last two were subject to a purification test (2.4.1.5) or dialysis prior transformation. Following the transformation step, selection was performed on antibiotic resistance

plus *amy* minus phenotype tested on starch plate for *amyE* clonings; test on minimal medium for *thr* minus strains.

2.4.2.4 Preparation of chromosomal DNA:

To isolate genomic DNA, 3 mL of LB medium with the appropriate antibiotic were inoculated with a single colony from a freshly streaked strain and incubated either at 30 °C o/n or at 37 °C for 7 h. Two mL of cell culture were pelleted and resuspended in 450 µL of 50 mM EDTA with 10 µL of lysozyme (100 µg/µL stock). The sample was incubated 20 min at 37 °C. Then 600 µL of Nuclei Lysis Solution (Promega) were added and mixed gently. 200 µL of Protein Precipitation Solution (Promega) were added. The sample was mixed by vortexing and incubated at 4 °C for 5 min. The sample was then centrifuged at 13000 rpm. The supernatant was added to 700 µL of isopropanol and mixed gently. DNA was pelleted, washed with 600 µL of 70 % (w/v) ethanol and rehydrated with 200 µL of pure water.

2.4.2.5 Creation of marker-less mutants with pop-in, pop-out method:

Marker-less deletion mutants were created mainly as described in (Tanaka et al., 2013), with minor modifications (Figure 13). In brief the gene of interest is substituted by a phleomycine cassette linked to the c1 gene at a strain containing P_{λ}*neo* at *upp*. Selection is possible as C1 inhibits the activation of P_{λ}. Homologous regions at both sides of the pleo-c1 cassette allow a recombination process that exiceses the cassette, producing a clean deletion of the gene of interest leaving no scar.

2.4.2.6 Creation of marker-less mutants from BKE strains:

BKE knockouts are made by replacing the gene of interest by an erythromycin cassette flanked by *loxP* sites. The plasmid pDR244 contains a ***cre*** gene that catalyzes a site-specific recombination between the ***lox*** sites. We can then cure the strain of plasmid pDR244 by growing it at high temperatures. BKE knockout strains were transformed with plasmid pDR244 and selected for spectinomycin resistance at 30 °C, the plasmid replication permissive temperature. Selected colonies were grown it in LB media at 42 °C. Serial dilutions were plated on LB-agar plates and incubated o/n at 42 °C.

2.4.2.7 Test of *lacZ* expression:

Strains bearing the *lacZ* reporter gene were grown in LB cultures at 37 °C for < 8 h and spotted on LB-agar plates supplemented with X-gal. Plates were incubated o/n at 37 °C. If *lacZ* was expressed,

X-gal will have been metabolized and the colony will present a blue coloration. If *lacZ* is not expressed, the colony will be white.

2.4.2.8 Growth curves

A single colony from a freshly streaked strain was inoculated in 3 mL of the appropriate medium with supplements and incubated o/n at 30 °C. The precultures were diluted into fresh media to an $OD_{600\ nm}$ 0.005 and incubated at 37 °C until $OD_{600\ nm} \approx 0.2$. They were then re-diluted into a 96 well plate to $OD_{600\ nm}$ 0.005 and incubated in a plate reader where $OD_{600\ nm}$ was measured every 5 min for a maximum of 24 h.

This methodology was used to test growth phenotypes in different media, osmotic pressure resistance and resistance to different antibiotics.

2.4.2.9 Disk diffusion test:

To test the resistance of *B. subtilis* cells to H_2O_2, we performed a disk diffusion assay. The strains were grown in CH media supplemented with the correct selective pressure, o/n, at 30 °C. The cultures were diluted to $OD_{600\ nm} = 0.005$ in CH medium and grown at 37 °C until $OD_{600\ nm} = 0.2$. 0.5 mL aliquots of the cultures were plated on LB-agar plates and a sterile disk of filter paper was placed on top of it with 5 µL of 30 % H_2O_2. Plates were incubated o/n at 37 °C. H_2O_2 diffuses from the paper disk creating a gradient. Cells start growing forming a halo around the disk. The size of the halo depends on their resistance to the substance.

2.4.2.10 Viability test:

Cells were grown in CH at 37 °C and aliquots of the culture were taken at $OD_{600\ nm} = 0.3$ (exponential phase of growth), $OD_{600\ nm} = 1.2$ (growth phase transition) and $OD_{600\ nm} = 2,1$ (stationary phase of growth). Serial dilutions were made in fresh CH media and plated on DSM-agar plates. After an incubation of 12 h at 37 °C, colony forming units (CFU)/mL were calculated.

2.4.2.11 Transformation efficiency:

Strains were transformed with DNA from strain ABS1990 carrying a erythromycin marker. Transformation was performed as in (Mirouze et al., 2015).

2.4.2.12 Sporulation efficiency:

Strains were grown in DSM medium during 30 h at 37 C. Serial dilutions were plated on DSM-agar plates before and after a 20 min heat shock at 80 °C. Sporulation efficiency was calculated as the

percentage of the vegetative cells that undergo a complete sporulation process yielding heat resistant spores and was calculated as the ratio between the spore concentration and total cell concentration.

2.4.3 Protein procedures:

2.3.3.1 Sodium Dodecyl Sulfate Poly-Acrylamide Gel Electrophoresis (SDS-PAGE):

SDS-PAGE gels at 11 % were used. Samples were mixed 1:6 with protein loading buffer (0.5 M Tris-HCl pH = 6.8, 1 M β-mercaptoethanol, 20 % (v/v) SDS, 0.2 % (v/v) bromophenol blue, 12.5 % (v/v) glycerol), incubated 10 min at 65 °C and electrophoresis was performed in Laemmli 1X buffer (15 % glycerol, 0,7 % sodium dodecyl sulfate), at 200 V. Protein sizes were estimated relative to a protein marker ladder. The gel was washed before staining with ddH_2O.

2.4.3.2 Western blot:

Strains were grown in CH media at 37 °C until $OD_{600\ nm}$ = 0.2 – 0.3. 2 mL aliquots of the cultures were spun down at 13000 rpm for 10 min. The pellet was either used to continue with the process or frozen at -20 °C. The pellet as resuspended in 25µL resuspension buffer (50 mM glucose, 1 mM EDTA, 50 mM Tris pH = 8,0, 1 mg/mL lysozyme, protease inhibitors) and incubated for 5 min at RT. Then 25 µL of ice-cold lysis buffer (500 mM NaCl, 1 % NP40, 50 mM tris pH = 8,0, 5 mM $MgCl_2$, 0,05 % benzonase) is added and incubated on ice for 20 min. The clear lysate is used for SDS-PAGE (see 2.3.3.1). The proteins on the SDS-PAGE are transfered to a nitrocellulose membrane during 2 h, at 140 mA. The membrane is then blocked in TBST buffer (0,2 M Tris base, 1,5 M NaCl, 0,05 % Tween 20) with 5 % milk for 1 h, at RT. Three rounds of 10 min washing are performed afterwards with TBST buffer and then the incubation of the primary antibody is performed o/n at RT at a ratio of 1/10000 in TBST buffer. Another three rounds of 10 min washing are performed with TBST buffer and then an incubation of the secondary antibody in TBST at a ratio of 1/10000 for 1 h at RT. The membrane was developed using ECL Bio-Rad reagents as per the manufacturer on a Chemidoc imaging system.

2.4.4 RNA procedures:

2.4.4.1 Cell culture for RNA extraction:

Inoculate 200 mL CH media to $OD_{600\ nm}$=0.005 from an o/n culture. Incubate at 37 °C and 200 rpm. At $OD_{600\ nm}$=0.2 and $OD_{600\ nm}$=2, collect 70 mL and mix with 30 mL ice-cold killing buffer (20 mM Tris-

HCl pH = 7.5; 5 mM $MgCl_2$, 20 mM NaN_3). Centrifuge 10 min at 4700 rpm and 4 °C. Freeze pellet in liquid nitrogen and save at -80 °C.

2.4.4.2 RNA extraction:

Resuspend frozen bacterial pellet in 200 µL ice-cold killing buffer (20 mM Tris-HCl pH = 7.5, 5 mM $MgCl_2$, 20 mM NaN_3). Add 500 µL of small glass beads and 1 mL of lysis buffer (4 M guanidine-thiocyanate, 25 mM sodium acetate pH = 5.2, 0.5 % N-lauroylsarcosinate). Disrupt cells with a Fastprep with carbon ice for 30 sec at power 6.5. Centrifuge at maximum speed for 3 min at 4 °C. Add 1 mL of acid phenol to the supernatant and mix for 5 min at 1400 rpm. Add 1 mL of chlorophorm/isoamyl-alcohol 24:1 and mix 5 min at 1400 rpm. Centrifuge at maximum speed for 5 min at 4 °C. Wash twice the aqueous phase with equivalent volumes of chlorophorm/isoamyl-alcohol. Add 1/10 volume of 3 M sodium acetate and mix by vortexing. Add 1 mL isopropanol, vortex and leave o/n at -20 °C. Centrifuge 15 min at 15000 rpm at 4 °C. Wash RNA pellet with 1 mL 70 % ethanol and centrifuge 15 min at 15000 rpm at 4 °C. Dry the pellet at 37 °C for 1 min and resuspend it in 75 µL H_2O for 3h at 4 °C and 30 min at RT. Treat the sample with QIAGen RNase-Free DNase set as per manufacturer's instructions. Clean the sample with Norgen Concentration Micro Kit as per manufacturer's instructions.

2.4.4.3 RNAseq

WT strain (ABS2005) and Δ*ydcH* strain (ASEC56) were grown as in 2.4.4.1 and RNA was extracted as in 2.4.4.2. Samples were processed by the platform Imagif (Gif sur Yvette) to generate a library of RNA fragments that were then sequenced using the NEXT SEQ SR 150 nt method. Treatment of this data was performed by collaboration with C. Guerin from the Maiage team at INRA, Jouy en Josas.

2.4.5 Microscopy methods:

2.4.5.1 Sample preparation for microscopy

For sample preparation, pre-cultures of *B. subtilis* were grown o/n in CH medium supplemented with 20 mM $MgSO_4$ and appropriate antibiotic selection, from -80 °C stocks, at 30 °C. Pre-cultures were diluted in CH media to an $OD_{600\ nm}$ = 0,005 and incubated at 37 °C without antibiotics and without supplementations, except if specified. Samples for microscopic observation were taken during exponential growth ($OD_{600\ nm} \approx$ 0,2 - 0,3) and mounted on CH-1 % agarose pads freshly made.

2.4.5.2 Total internal fluorescence microscopy

Time-lapse TIRFM movies were acquired at least two different days for each strain and condition. 1 µL of culture was spotted on thin agarose pad (1 % agarose in CH media), topped by a coverslip and immersion oil and mounted immediately in the temperature-controlled microscope stage. For all TIRFM acquisitions, exposure time was 100 ms. Inter-frame intervals were 1 s over 1 min movies (2 min for B30 and B46). Imaging was performed on an inverted microscope (Nikon Ti-E) equipped with an Apo TIRF 100x oil objective (Nikon, NA 1.49), with an iLas2 laser coupling system from Roper Scientific (150 mW, 488 nm). Images were collected with an electron-multiplying charge-coupled device (EMCCD) camera (iXON3 DU-897, Andor) at maximum gain setting (300) attached to a 2.5X magnification lens. Final pixel size was 64 nm. Image acquisition was controlled by a Metamorph v.7 software package.

3. Results

3. Results

Previous data from our group (E. Marchadier, unpublished) had revealed in a whole-genome transcriptional analysis that the *ydcFGH* operon was highly overexpressed in absence of MreB (Figure 12). This characteristic was specific for the deletion of *mreB* as the operon's expression was not modified in absence of Mbl or MreBH, the two isoforms of MreB present in *B. subtilis*. It suggested that MreB may have a specific property leading to the repression of *ydcFGH* that was not shared by the two other actin-like proteins. We decided to undertake a comprehensive analysis aiming to both, reveal the function of this operon and to decipher the regulatory mechanism linking the presence of *mreB* with the expression of these genes. Using a variety of genetic techniques, we showed i- that YdcH is a probable transcriptional repressor controlling its own expression, ii- that this regulator may constitute a new transition state regulator in *B. subtilis*, and iii- that a frameshift mutation in *ydcH* is probably responsible for the deregulation of the operon in our Δ*mreB* laboratory strain.

As a second but parallel part of the project, in a first attempt, we used the promoter of *ydcFGH*, highly activated in absence of *mreB*, to create a genetic screen of randomly generated loss-of-function MreB mutants. Because we demonstrated that the link between *ydcFGH* and MreB was not direct, the genetic screen was finally performed by means of a different upregulated gene in absence of *mreB* (*mreBH*, Figure 12). MreB's function remains elusive despite two decades of extensive efforts both in Gram-positive and Gram-negative models (see Introduction) therefore the characterization of these mutants through the study of their cell growth, cell morphology and MreB dynamics, revealed very promising results. We show critical residues that uncouple the growth of *B. subtilis* to its ability to form actively moving directional patches, and suggest that MreB could act as a link between cell metabolism and CW synthesis.

By combining all these data and techniques, we have acquired a better understanding of MreB and some insights on the *ydcFGH* operon in *B. subtilis*. Although a subset of the results was, at the time, somewhat disappointing, it led us to very interesting and promising preliminary conclusions that may allow us to pin point the so long searched MreB's function(s).

A

Gene	Function or prediction	Expression Ratio
ftsX	ABC transporter required for CwlO activity (CW synthesis)	4.012
mreBH	CW biosynthesis, mreB homolog	4.111
fruK	fructose catabolism	4.127
catE	catechol resistance	4.314
fruR	Transcriptional regulator (Fructose catabolism)	4.412
cwlO	CW biosynthesis (endopeptidase)	5.280
cydD	ABC transporter, requires for Cytochrome expression	5.592
cydC	ABC transporter, requires for Cytochrome expression	6.736
fruA	fructose uptake	8.487
ydcF	unknown	15.633
ydcH	unknown	23.358
ydcG	unknown	24.014

B

Gene	Function or prediction	Expression Ratio
pstBA	P uptake ABC transporter	5.133
thrB	Threonine biosynthesis (homoserine kinase)	6.221
fruK	fructose catabolism	10.087
gruR	Transcriptional regulator (Fructose catabolism)	10.288

Figure 12 Most overexpressed genes in Δ*mreB* (A) and Δ*mbl* (B) in LB medium. Unpublished data from Marchadier E. et al.

3.1. Functional analysis of *ydcF*, *ydcG* and *ydcH*.

3.1.1 The *ydcFGH* operon is composed of three genes of unknown functions.

To get clues about the potential function of this operon, we first performed an *in silico* analysis using the BLAST (looking for sequence similarities) and Phyre2 (searching for protein fold conservation) web tools on each gene of the operon (Altschul et al., 1997; Kelley, Mezulis, Yates, Wass, & Sternberg, 2015). The first gene, *ydcF*, a small 292 nucleotides long orf (open reading frame), encodes a protein carrying a domain (residues 20-53) similar to the relaxase superfamily as predicted by BLAST. Proteins in this superfamily are involved in secretion (type IV systems), horizontal gene transfer and nicking of ssDNA (Balzer, Pansegrau, & Lanka, 1994). The second orf encodes YdcG, a protein predicted to have an EVE domain: potentially a RNA-binding domain present in proteins with broad types of functions (Bertonati et al., 2009). Finally YdcH was predicted, with a very strong confidence, to be a MarR-type transcription regulator (TR). MarR TRs are usually involved in the response to environmental changes, helping cells to improve their survival. They are frequently linked to multiple antibiotic, salt and aromatic molecules resistance as well as to virulence (Chang, Chen, Ko, Chang-Chien, & Wang, 2013; Ellison & Miller, 2006; Grove, 2013; Vazquez-Torres, 2012).

3.1.2 Construction of knock-out mutants of *ydcF*, *ydcG* and *ydcH*

To understand what *ydcF*, *ydcG* and *ydcH* are involved in, we created a series of strains inactivated for each of the genes separately. *ydcH* was inactivated by replacement with a spectinomycin resistance cassette (ABS1381) while *ydcF* and *ydcG*, to prevent polar effect on downstream gene(s), were inactivated by marker-less deletions following the pop-in pop-out method (see Materials and Methods), generating strains ASEC24 and ASEC5 respectively (Figure 13).

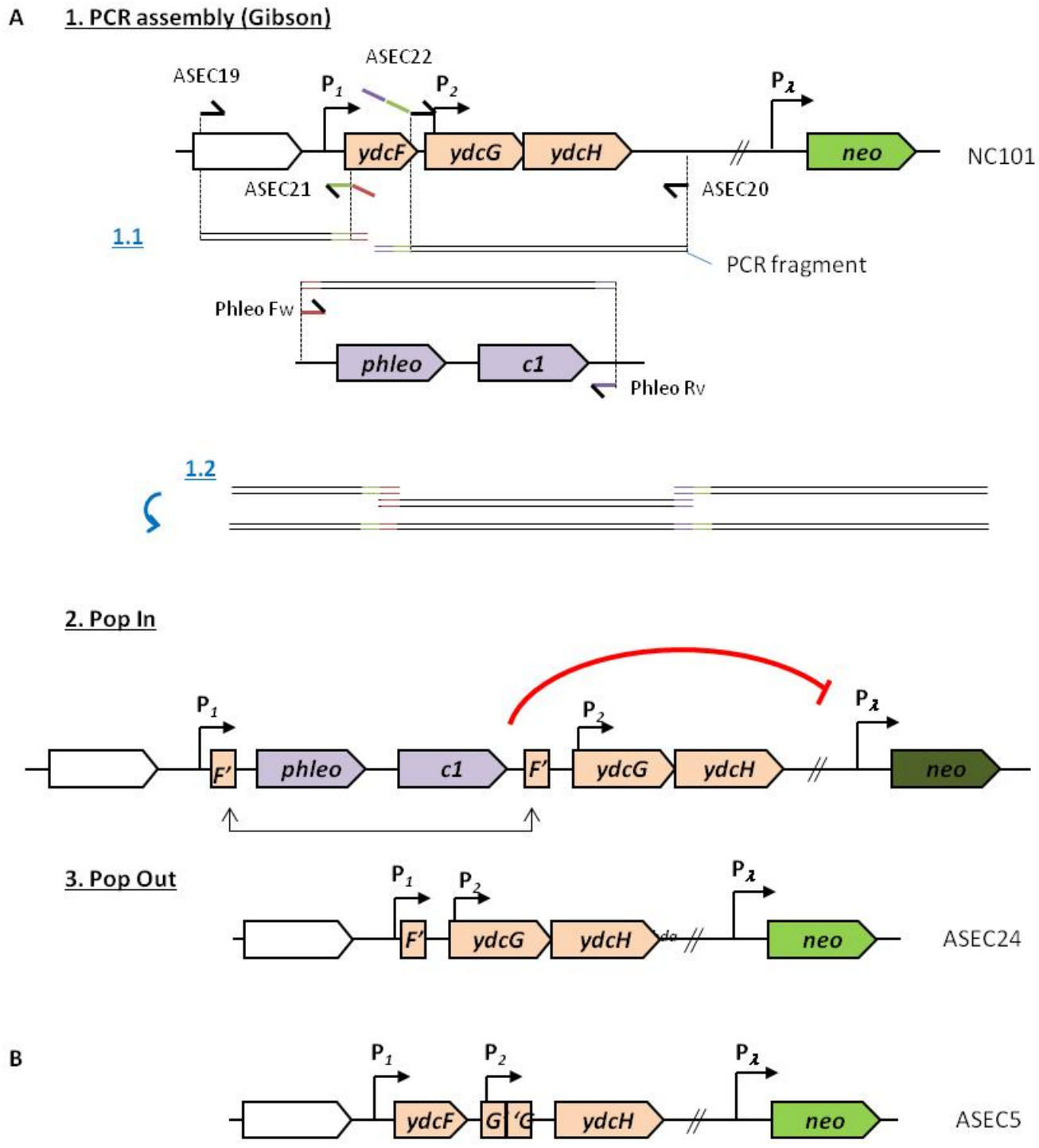

Figure 13 Pop-In Pop-Out Δ*ydcF* and Δ*ydcG*. Described in (Tanaka et al., 2013). **A**. Example of "Pop-In Pop-Out" marker-less deletion procedure on the *ydcF* gene. Upstream (oligonucleotides ASEC19+ASEC20) and downstream (ASEC22+ASEC20) fragments of *ydcF* are PCR-amplified, introducing homologous extremities to the extremities of the *phleo-c1* cassette, which is also amplified (oligonucleotides Phleo Fw +Phleo Rv). The three fragments were assembled and used to transform strain NC101 (*upp*::P$_{\lambda}$*neo*). Eviction of phleo-c1 is achieved by recombination of homologous regions at both sides of the cassette, leaving a clean deletion of *ydcF* (ASEC24). **B**. Genetic map of the *ydcFGH* locus after the "Pop-In Pop-Out " deletion of *ydcG* (in Δ*ydcG* strain ASEC5).

3.1.3 Phenotypic characterization of *ydc* genes exposes an inappropriate strain frame

The three mutant strains were used along the WT 168, in a variety of assays in order to fully characterize the *ydcFGH* operon. These experiments strongly suggested that deletion mutants of *ydcF* and *ydcG* were affected in several stationary phase events including cell survival and sporulation (see Appendix 1). But by the end of this study, an ultimate whole genome transcriptomic profiling experiment (section 3.3) revealed, to our surprise, the presence of significant gaps, covering more than 200 genes, in the genome of the two strains constructed via the "pop-in pop-out" method. This unveiled that the strain NC101 bearing P_{λ}*neo* required for this approach (and increasingly used in our lab) had been cured of its prophages SPβ, PBSX and the Skin element. Suspecting that at least some of the phenotypes we had observed could be due to the difference of background between these strain and the WT reference, we generated new marker-less deletion mutants. This time we used mutants constructed as part of a comprehensive knock-out library (BKE) that were recently made available by the Bacillus Genetic Stock Centre. Each of these "BKE" strains has a single orf replaced by an erythromycin cassette that can be evicted easily (see Materials and Methods for details), creating new marker-less mutants for *ydcF* (ASEC287) and *ydcG* (ASEC289). We also took this opportunity to make a marker-less mutant of *ydcH* (ASEC293).

None of the phenotypes previously observed with the original *ydcF* and *ydcG* knock-out mutants could be confirmed in the newly constructed deletion strains (see Appendix 1 for details), and as shown on Figure 14, all three mutants grew as the wild type strain in a variety of media, from exponential to stationary phase of growth.

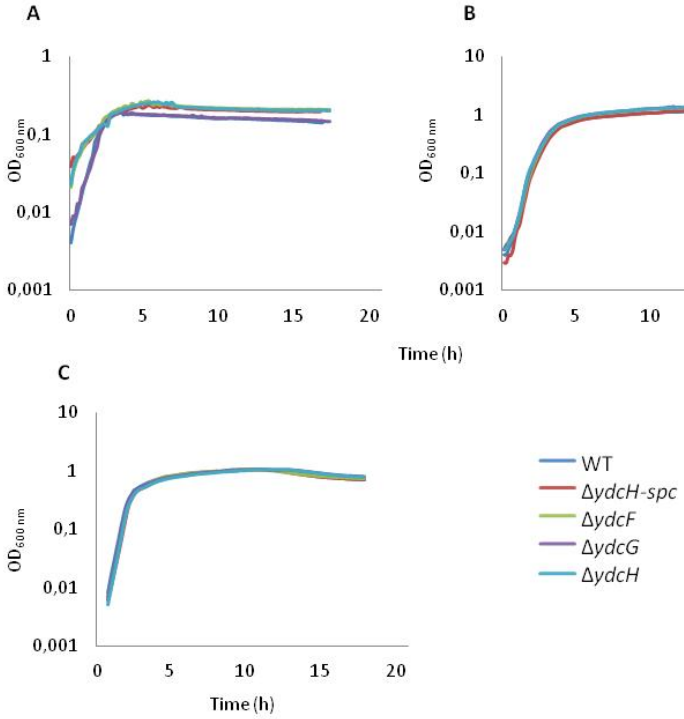

Figure 14 Growth of deletion mutants of *ydcF*, *ydcG* and *ydcH* derived from BKE strains in different media. WT cells (ABS2005), the deletion-replacement mutant of *ydcH* (ASEC56) and the marker-less deletion mutants of *ydcF* (ASEC317), *ydcG* (ASEC319), and *ydcH* (ASEC321) were grown in MSM media (**A**), CH media (**B**) and LB media (**C**). Δ*ydcF*, Δ*ydcG* and both Δ*ydcH* strains have a WT growth phenotype in all media tested.

3.1.4 YdcF, YdcG and YdcH are not involved in stress resistance

YdcH is predicted to be a TR of the MarR family. MarR TRs are DNA-binding proteins that regulate the expression of genes by binding as dimers to a palindromic sequence in their promoters (Grove, 2013). Most MarR TRs act as repressors and usually control their own expression in addition to that of other genes. Accordingly, as we will show below (section 3.2.2), YdcH is involved in its own repression, reinforcing this prediction. Since MarR TRs are implicated in the response to multiple environmental adaptations as antibiotic stress, oxidative stress, synthesis of virulence factors and degradation of aromatic compounds (Krasper et al., 2016), we decided to test the effect of deleting *ydcH* on the adaptive ability of *B. subtilis* to various stresses.

We first tested high osmolarity by growing cells in rich CH medium supplemented with NaCl ranging from 1 to 2 M (see Materials and Methods). As seen in Figure 15A, no impact on growth, relative to that of the wild type strain, could be detected with any of the concentrations tested. Similarly, cells were tested for resistance to oxidative stress using H_2O_2 in a disc diffusion assay (see Materials and Methods; Figure 15E). The halos of both strains presented no differences, suggesting identical resistance to H_2O_2 between the deletion mutant and the WT. Finally, we tested the resistance of the deletion mutant to a set of antibiotics (vancomycin, methicillin, D-cycloserine and rifampicin) by growing cells in liquid rich CH medium supplemented with increasing concentrations of each antibiotic (see Materials and Methods; Figure 15B-D). Again, no benefits or impairments could be observed in the mutants, relatively to the wild type strain.

Together, these results show no involvement of YdcH in a broad range of stress conditions known to affect other MarR-type TR mutants. This suggests that YdcH is either involved in resistance to more exotic stresses, or in a completely different function.

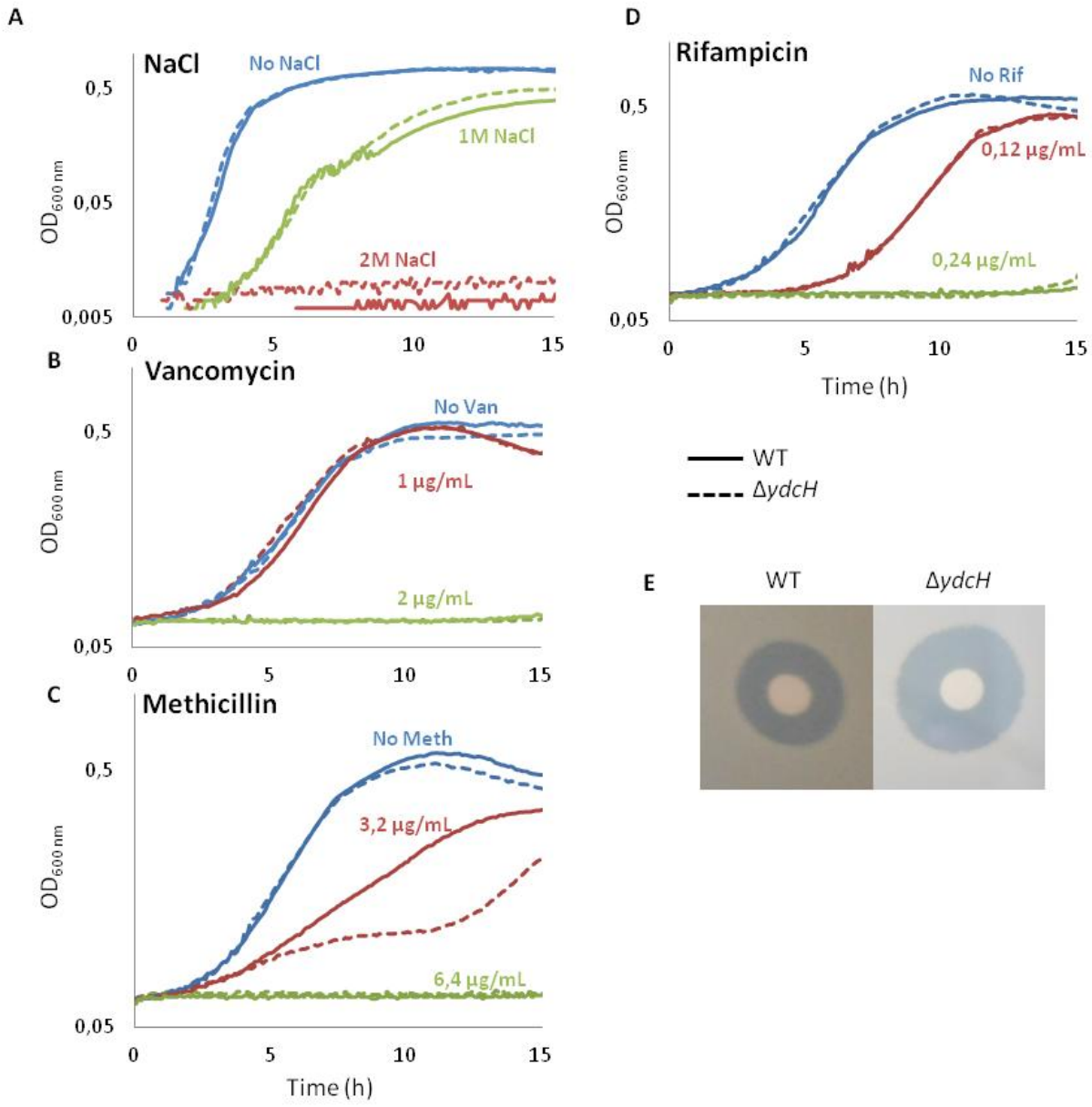

Figure 15 The Δ*ydcH* strain is not affected by salt, oxidative or antibiotic stresses. A-D. *ydcH* mutant resistance to NaCl and antibiotics. WT (RCL44; continuous lines) and Δ*ydcH* (ABS1381; dotted lines) cells were grown in CH media supplemented with NaCl (**A**), vancomycin (**B**), methicillin (**C**) or rifampicin (**D**). **F**. Resistance to H_2O_2 was tested on LB plates via a disk diffusion assay with 30 % H_2O_2.

3.2. Transcriptional study of *ydcFGH*

Fuctional characterization of the genes in the *ydcFGH* operon did not shed any light on their link with MreB or their function. We therefore decided to focus on undersanding the regulatory relation that caused the increase of expression of the *ydcFGH* operon in absence of *mreB* (Marchandier et al., unpublished, Figure 12).

3.2.1 *ydcH* is under the control of two promoters

The genome-wide transcriptional analysis by tilling array done by Nicolas and coworkers (Nicolas et al., 2012), suggested the existence of two promoters. One, located in front of *ydcF* (hereafter named P_{ydc1}), that would initiate the expression of a long transcript including the three orfs, and a second (P_{ydc2}) lying in the *ydcG* coding region which would allow only the expression of *ydcH* (Figure 16).

We initially constructed four reporter transcriptional fusions to *lacZ* (Figure 16; see Materials and Methods): P_{ydc1} corresponding to 303 bp in front of the *ydcF* orf and potentially containing the first promoter; P_{ydc2} extending from 153 bp upstream *ydcF* to 56 bp into *ydcG*, excluding the first and containing the putative second promoter; P_{ydc1-2} containing both putative promoter regions; and P_{ydc0} containing none of them. As shown on Figure 16A, in a WT background, no expression could be detected from P_{ydc0} and P_{ydc1}, while a weak expression could be observed with P_{ydc2} and P_{ydc1-2}. Therefore, we concluded that the expression of the *ydcFGH* operon mainly originates from P_{ydc2} in a WT background, and is maintained at a very low level of expression.

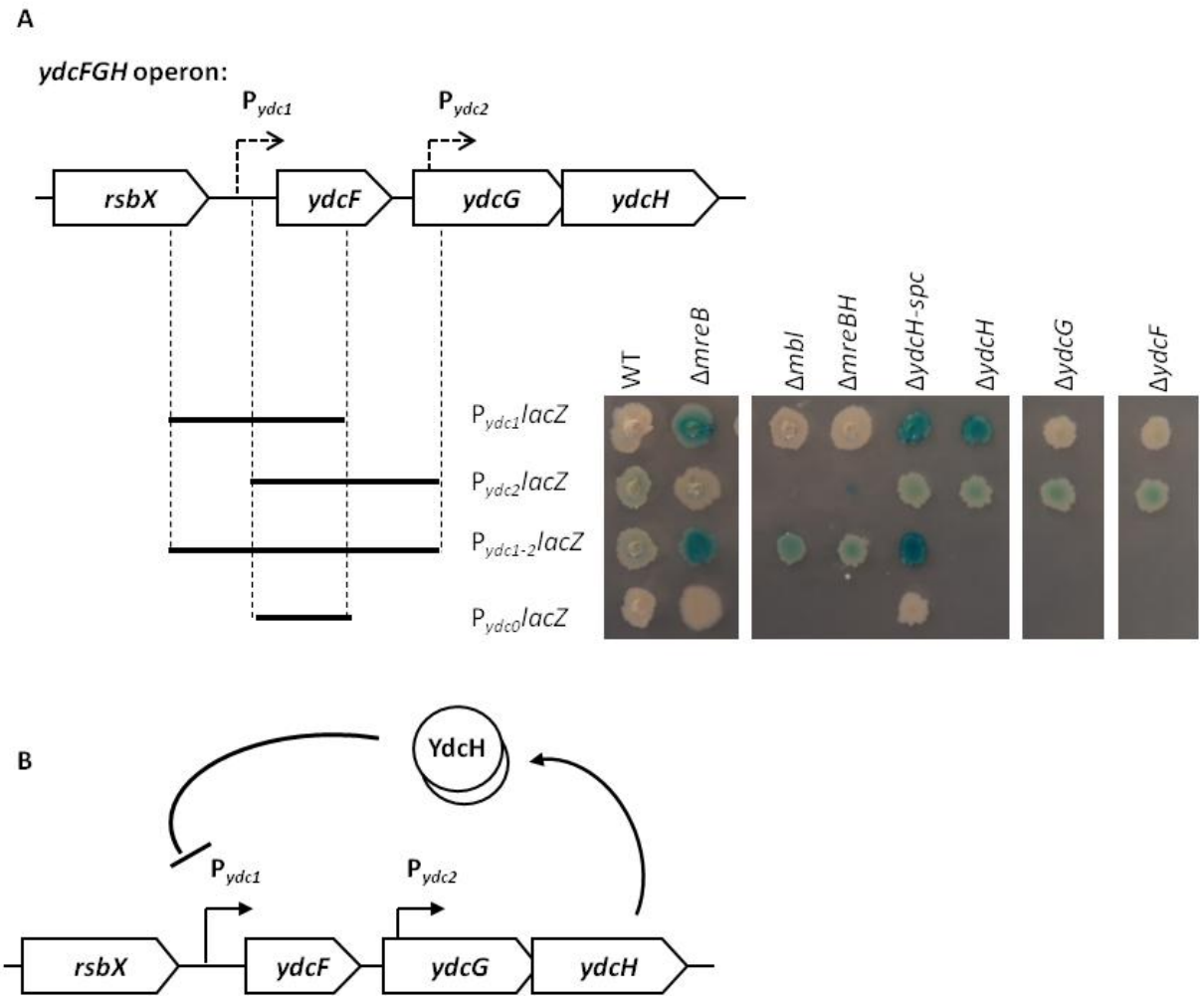

Figure 16 The *ydcFGH* operon. A. The *ydcFGH* operon is formed by three genes: *ydcF*, *ydcG* and *ydcH*. The expression of these genes is driven by two promoters: P_{ydc1} and P_{ydc2}. Transcriptional fusions with the reporter gene *lacZ* and the first promoter (P_{ydc1}*lacZ*), the second promoter (P_{ydc2}*lacZ*), both of them ($P_{ydc1\text{-}2}$*lacZ*) or the region in between (P_{ydc0}*lacZ*) confirm that the expression of the operon, in WT conditions, is regulated by a low, basal activation of P_{ydc2}. P_{ydc1} is activated in the absence of *mreB* (strain ABS1762) or *ydcH* (replaced with *spc* (ABS1820), or in a marker-less strain (ASEC305)) but not in absence of *mbl* (ABS1769), *mreBH* (ABS1824), *ydcF* (ASEC297) *or ydcG* (ASEC301). **B**. YdcH may act as a repressor of its own operon's expression through the repression of P_{ydc1}.

3.2.2 YdcH, but not YdcF nor YdcG, is involved in the control of P_{ydc1} expression

When *ydcH* is inactivated, P_{ydc1} and $P_{ydc1\text{-}2}$ are strongly activated while P_{ydc2} maintains a low basal level of activation (Figure 16A), suggesting that most of the transcripts initiate from the first promoter in this context. However, inactivation of *ydcF* or *ydcG* had no impact on either P_{ydc1} or $P_{ydc2.}$ Taken together, our results draw a model (Figure 16B) in which YdcH is produced from constitutively low expressed transcripts originating from P_{ydc2} and represses the expression of the whole *ydcFGH* operon in a negative regulatory feedback loop acting on P_{ydc1}. The prediction of YdcH as a TR strongly suggests that the repression occurs directly through the binding of the protein to its own promoter.

3.2.3 The absence of MreB is not responsible for P_{ydc1} induction

We next tested the impact of the deletion of the *mreB* paralogs on the expression of the two *ydc* promoters. Similar results to that obtained with the *ydcH* deletion are obtained when the reporters are introduced into the Δ*mreB* 3725 strain (Figure 16A), while deleting *mbl* or *mreBH* had no impact. These results suggest a repressing effect of MreB on the expression of the first promoter of *ydcFGH*, confirming previous genome wide expression data from E. Marchadier (unpublished).

We next tried to unveil the link between its expression and the absence of the *mreB* gene. A puzzling result was obtained when *mreB* was cloned back at an ectopic locus in the genome under a xylose inducible or its natural promoter, in the strain 3725 deleted for *mreB*. In these trans-complemented strains, the *lacZ* reporter was still activated suggesting that the sole absence of the MreB protein was not responsible for P_{ydc1} induction. It should be noted that at this step, many alternative hypotheses were envisioned and tested to explain this puzzling result, which are described in Appendix 2. By the end of our investigation, we suspected that a mutation unlinked to *mreB* was responsible of the induction of the expression of *ydcFGH*.

We then decided to realize a complete sequencing of the Δ*mreB* strain (3725). As shown on table 8, and to our astonishment, this strain bears more than 50 mutations compared to its supposedly parent strain 168. Among them, we noticed a single nucleotide deletion in the *ydcH* orf. The deletion has occurred in a potentially sliding stretch of A and led to a frameshift. The resulting YdcH protein is predicted to be truncated of more than half its full size. Based on our transcriptional study (see Figure 16), we know that the absence of functional YdcH leads to induction of P_{ydc1}, which is the most probable cause for the overexpression of the *ydcFGH* operon in strain 3725 (Δ*mreB*).

Intragenic mutations	Gene	Amino acid change
snps	*parC*	S288L
snps	*accC*	D248G
indel	*yesY*	Frameshift
indel	*glcK*	Frameshift
snps	*gltA*	A1181V
snps	*ilvC*	A268
snps	*sacA*	L448F
snps	*rluD*	P287S
snps	*trmD*	H227Y
snps	*oppD*	V357G
snps	*gerAA*	T299A
indel	*pksN*	Frameshift
snps	*yoqA*	L23P
snps	*yqbS*	Y60H
snps	*yutE*	A37T
indel	***ydcH***	**Frameshift**
snps	*walR*	R203C
snps	*sigI*	L198R
snps	*sepF*	M11T
snps	*bscR*	I160R
snps	*ytpS*	P375S
snps	*panE*	A76T
snps	*mmgA*	M115R
snps	*yuxG*	G573R
snps	*comP*	E628G
snps	*yhgE*	G228E
snps	*yisQ*	D51N
snps	*yjcM*	K216N
snps	*ymfD*	A319T
snps	*epsC*	A276V
snps	*yxbD*	V9I

Intergenic mutations	Gene	Amino acid change
indel	S1255 & *sspG*	Codon deletion
snps	?	NA
snps	int *bsrB/yvrM*	NA
snps	S1101 (5' UTR *citZ*)	NA
snps	S1101 (5' UTR citZ)	NA
indel	S125 (5' UTR hxlR)	
indel	S352 (3' UTR *yhaH*)	
snps	BSU_misc_RNA_20	NA
snps	S486 (5' UTR *mtnE)*	NA
indel	BSU_misc_RNA_28	
indel	S596 (5'UTR *ylxY*)	
indel	S736	
indel	int *yorN/M*	
snps	S1123 (5' UTR *nifZ*) / S1124 (5'UTR *braB*)	NA
indel	S1145 (5' UTR *ytnP*)	

Silent mutations	Gene	Amino acid change
snps	*ygaN*	S31
snps	*yozT*	D43
snps	*rluB*	Q189
snps	*yqeZ*	A225
snps	*pgdS*	L210

Table 8 Mutations found in the Δ*mreB* strain (3725). Sequencing of strain 3725 revealed the existence of 52 SNPs, 27 introducing an amino-acid change and 4 a frameshift, including one in *ydcH* (bold).

3.3. YdcH, a new regulator for carbon metabolism?

So far, we were not able to infer the function of the *ydcFGH* operon nor the regulatory link between the operon and *mreB* or why this operon was upregulated in the Δ*mreB* strain. Because YdcH is probably a putative TR, a prediction reinforced by our transcriptional analysis of its promoters, we reasoned that clues on its role could emerge from uncovering the genes potentially under its control. For this, we performed a whole genome expression analysis by an RNAseq analysis, comparing Δ*ydcH* and WT cells. In order to find the most appropriate time point for this experiment, we first monitored the expression of *ydcFGH* all along the growth phase, using a transcriptional reporter fusion with *luxABCDE* (Meighen, 1993) (see Materials and Methods). The expression of *ydcFGH*

increases all along the exponential growth phase. Its maximal expression occurs during the transition from exponential to stationary phases (Figure 17).

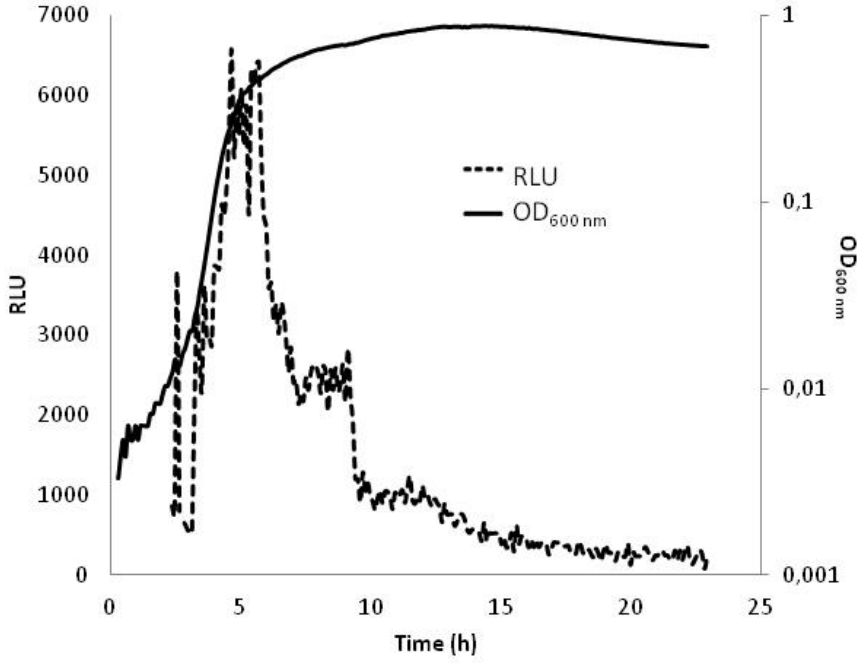

Figure 17 Expression of *ydcFGH* peaks at the transition from exponential to stationary phase. Strain ABS1990 (WT; P_{ydc1}-*luxABCDE*) was grown in CH media at 37 °C.

We decided to compare the expression between both strains when the differences should be maximum, before and after the transition, in exponential ($OD_{600\ nm} \approx 0.2$) and stationary ($OD_{600\ nm} \approx 2$-2.3) phases of growth. With a threshold of 2x difference in gene expression, we observed a total of 364 affected genes during exponential phase, 180 de-repressed and 184 down-regulated genes in Δ*ydcH* (Figure 18; Appendix 3). During stationary phase, a different set composed of only a limited number of genes were differentially expressed (13 overexpressed and 11 down-regulated genes). As expected, *ydcH* appears as one of the most repressed genes both during stationary and exponential growth.

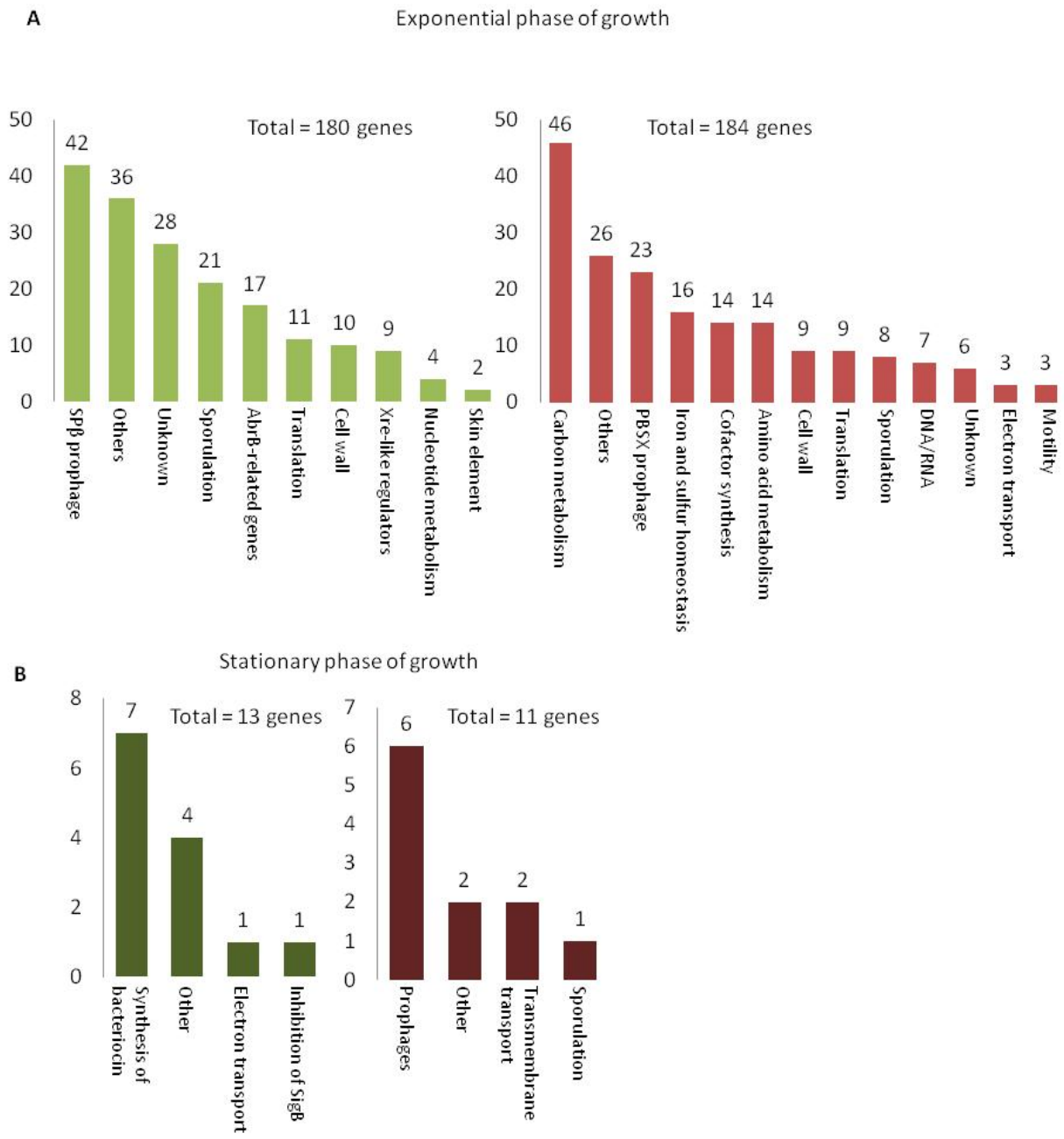

Figure 18 Differentially expressed genes in absence of *ydcH*. Results from the RNAseq experiment comparing gene expression levels in a WT (ABS2005) and a Δ*ydcH* strain (ASEC56) show that, in absence of *ydcH*, during exponential growth (**A**), there are 180 unrepressed genes (green) and 184 down-regulated genes (red); during stationary growth (**B**) there are 13 up-regulated (dark green) and 11 down-regulated genes (dark red). For more details, see appendix 4.

The two largest functional groups of genes affected by YdcH are prophages (44 down and 23 up-regulated) and carbon/amino-acids metabolism (60 upregulated genes) genes. A number of other functions are also affected including sporulation (29), cell wall (19), metal homeostasis (16) and translation (19).

The large number of significantly affected genes (> 350, including numerous down-regulated genes) observed in the Δ*ydcH* strain (in particular during exponential growth) comes a bit as a surprise for a putative transcriptional repressor. This strongly advocates for indirect effects through, potentially, other regulators. Some genes coding for known regulators and three other uncharacterized putative MarR TRs (*yisI*, *ypoP*, and *ykvN*) appear to be affected in absence of YdcH. They may contribute to the extent of the impact of the *ydcH* deletion. We also imagined that, without affecting the transcription of regulators, their activity could be modified in this context, but a systematic check for known regulations affecting the 350 genes failed to reveal the induction or repression of any complete regulons. The largest affected regulon found was that of the transition state regulator, AbrB, with 37 genes impacted (on a total of 249 genes controlled by AbrB).

Thus, so far, it is unclear how the expression of such a large number of genes can be affected by the absence of *ydcH*, but a direct control can't be excluded. The most striking characteristics of the YdcH regulon are the fairly large number of genes from the prophages and carbon metabolism categories it contains, and the various functional categories that are affected.

3.4. MreB mutagenesis

In order to get new insight into MreB, we used a genetic approach based on previous data from the group (Marchandier et al., unpublished, Figure 12) that allowed us to identify key residues. We designed a genetic screen to obtain a collection of randomly generated loss-of-function MreB mutants. After generating fusions of these MreB mutants to the green fluorescent protein (GFP), we performed a full characterization of these strains, including cell growth, cell morphology and MreB dynamics. The results generated are revealing critical residues uncoupling the growth of *B. subtilis* to its ability to form actively moving directional patches, and suggest that MreB could act as a link between cell metabolism and CW synthesis.

3.4.1. Setting up a genetic screen for MreB loss-of-function mutants

In order to create a genetic screen that would enable us to identify *mreB* mutants affected in their function(s), we needed a reporter gene that would be activated in absence of functional MreB. For this purpose, we took advantage of an unpublished investigation performed in our lab (Marchadier et al., unpublished) in which the impact of the absence of each of the actin-like proteins of *B. subtilis* (MreB, Mbl and MreBH) on gene transcription at the genome-wide level was characterized. To create a reporter gene for MreB functionality, we planned to fuse the promoter region of one of the genes overexpressed in absence of MreB to *lacZ*. This gene encodes the β-galactosidase enzyme from *E. coli*, that cleaves lactose into glucose and galactose, or the lactose surrogate Xgal, freeing an insoluble blue product (Juers, Matthews, & Huber, 2012) (see Materials and Methods for details).

In a first attempt, we created a reporter gene by fusing the promoter region of the operon *ydcFGH* (P_{ydc1}) to *lacZ* (see Materials and Methods and *ydcFGH* operon section). *ydcF*, *ydcG* and *ydcH* are the three most overexpressed genes in the absence of *mreB* (15, 23 and 24 fold induction respectively, Figure 12), and were an obvious first choice as a reporter candidate. While we started investigating the promoter structure and characteristics of the *ydcFGH* operon (see results from *ydcFGH* operon above), it quickly appeared that this reporter remained activated in cells deleted for *mreB* but complemented in *trans* with a *gfp-mreB* fusion. Induction of this reporter in the presence of a wild type GFP-MreB fusion made it improper for the screening purpose and other candidate reporters were investigated.

We then turned on other strongly induced genes on the list: *mreBH* and the *fruRKA* operon. Our previous transcriptional analysis indicated that *fruR*, *fruK* and *fruA* are induced 4 to 8 times, and *mreBH* 4 times in absence of *mreB* (Figure 12). We created two transcriptional fusions with *lacZ*: one (P_{fru}) with a region encompassing the three predicted promoters of the *fru* operon (Nicolas et al., 2012) and one (P_{mreBH}) with the promoter region of *mreBH*. Both fusions were introduced into the WT and Δ*mreB* backgrounds and compared by plating strains on plates supplemented with Xgal. While differences in P_{fru} *lacZ* expression between the strains happened to be too subtle for an efficient screen (Figure 19), differences of P_{mreBH} expression in a WT strain and in a Δ*mreB* strain could be easily perceived. We therefore retained this reporter fusion to screen for MreB loss-of-function mutants.

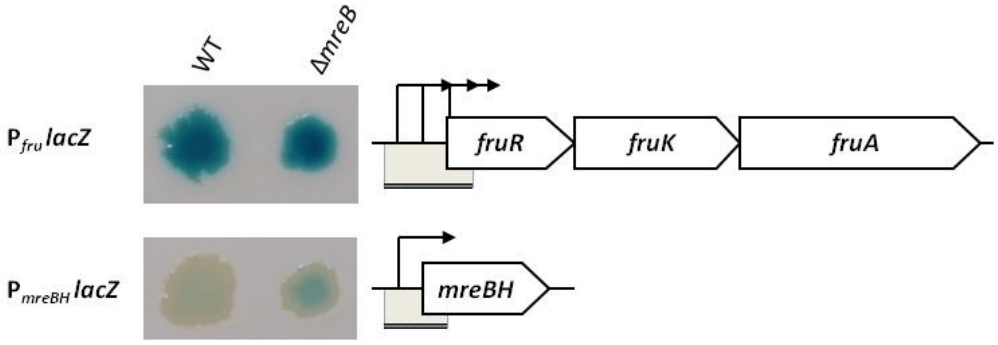

Figure 19 Expression of P_{mreBH} and P_{fru} transcriptional fusions to *lacZ* in presence and absence of *mreB*. The promoter regions of the *fruRKA* operon and the *mreBH* gene were cloned as transcriptional fusions with *E. coli lacZ*. Resulting constructions were independently inserted into wild type (WT) or mutant for *mreB* (Δ*mreB*) *B. subtilis* strains. ABS1749 (WT, P_{fru}*lacZ*), ABS1750 (Δ*mreB*, P_{fru}*lacZ*), RCL422 (WT, P_{mreBH}*lacZ*) and RCL423 (Δ*mreB*, P_{mreBH}*lacZ*) were spotted on LB-agar plates supplemented with Xgal. The promoter regions used for the reporter constructions are drawn as green-shaded areas on the corresponding right hand cartoons. Activation of the promoter region P_{fru} is too high, both in a WT and a Δ*mreB* background, to easily differentiate between them. However the difference of expression of P_{mreBH} *lacZ* between WT and Δ*mreB* allows an easy screening of the colonies.

3.4.2. Random mutagenesis of *mreB*

Next, we realized a random mutagenesis selectively on the *mreB* locus (see Materials and Methods). Briefly, we performed a mutagenic PCR that produced a DNA fragment containing the end of *maf*, *radC*, a kanamycin resistance cassette, *mreB* and the beginning of *mreC* (Figure 20). The resulting product was transformed and integrated in a single step into a *B. subtilis* strain containing the above-mentioned reporter. Blue colonies, indicating activation of P_{mreBH}, were selected.

We obtained a total of 73 mutants, 24 of which were discarded because they contained a mutation introducing either a frameshift in the *mreB* orf or a stop codon leading to the expression of a truncated version of MreB. Only 12 false positive clones were not mutants for *mreB* but carried mutations on surrounding genes (*mreC*, *radC* and *maf*). Mutants in *mreC* were a fair possibility that we anticipated since MreC and MreB are supposed to act together in a complex (Defeu Soufo & Graumann, 2005; Divakaruni et al., 2007; Dominguez-Escobar et al., 2011). Mutants for *maf* and *radC* came more as a surprise since there is, so far, no evidences of their involvement in shape control, CW synthesis or interaction with MreBH (Attaiech, Granadel, Claverys, & Martin, 2008; Briley, Prepiak, Dias, Hahn, & Dubnau, 2011). Although these mutants may reveal to be interesting in the future, they were left aside for the present study. The 37 remaining clones presented 51 different amino-acid changes in MreB that were the subject of further investigation. It is worth noting that most clones (28) bear more than 1 SNP (single nucleotide polymorphism) either on *mreB* or on surrounding genes, preventing us to draw, for these mutants, a direct link between the phenotype observed and the presence of the mutation.

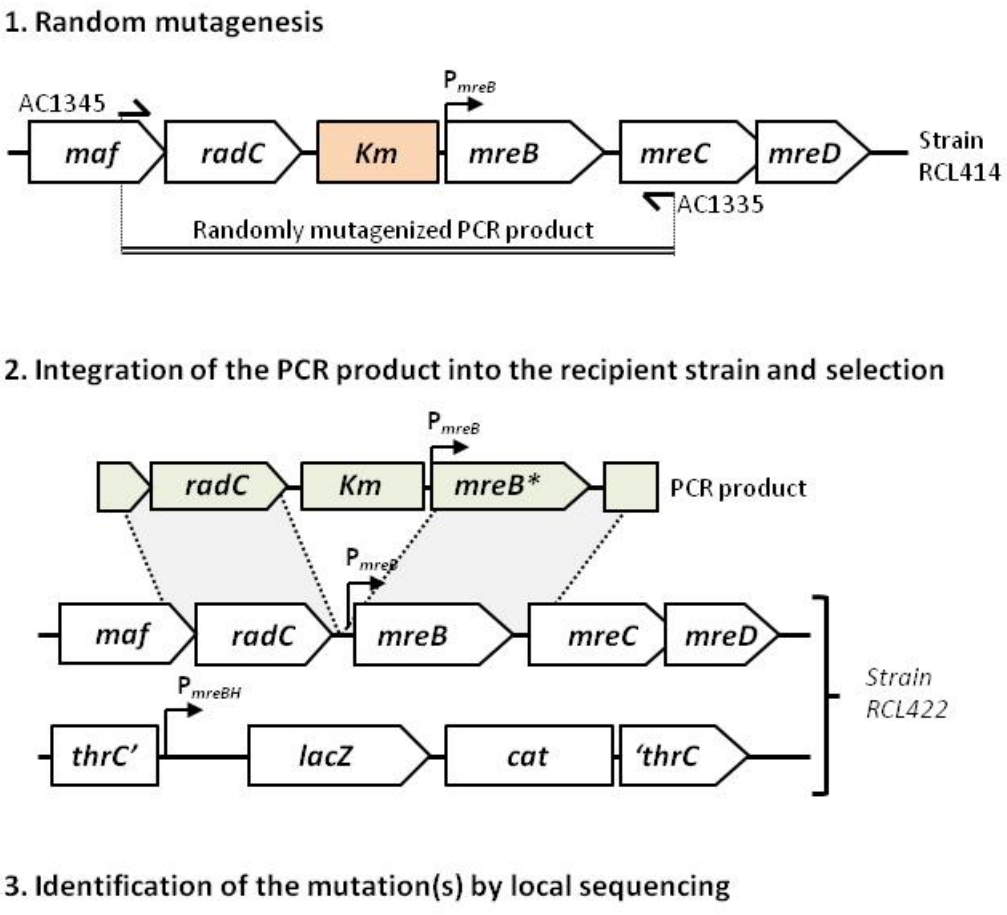

Figure 20 Principle of the *mreB* mutants screen. 1. A mutation-prone PCR is performed using primers AC1345/AC1335 on a strain containing a kanamycin resistance cassette (km) inserted between *radC* and *mreB* (RCL414). **2**. The resulting mutated PCR product is transformed and integrated by double cross-over recombination into the recipient *B. subtilis* strain bearing the reporter gene fusion at the *thrC* locus (RCL422). Loss-of-function *mreB* mutants are selected as kanamycin resistant blue clones (activation of P_{mreBH}) on LB-agar plates supplemented with Xgal and kanamycin. **3**. Mutations are mapped by sequencing the region from *maf* to *mreD*. PCR product is represented in green; light grey areas highlight regions of homology between the PCR fragment and the chromosome, allowing the recombination events to take place.

3.4.3. Site directed mutagenesis of *mreB*

In order to fully characterize the behavior of the selected MreB mutants, we needed to create translational fusions to GFP allowing in depth microscopy studies. Since most mutants carried several intra or intergenic SNPs, this engineering step was, in any case, required to individualize the mutations. We thus inserted into *B. subtilis gfp* fusions to *mreB* carrying single point mutations. In a first attempt, we tried to clone *gfp-mreB* fusions carrying SNP ectopically (at the *amyE* locus) under a xylose inducible promoter, in a strain that was deleted for endogenous *mreB*. This approach has been the method of choice since the early works from Carballido-López et al. in 2003 on the *mbl* paralog, until the beginning of our study. The task revealed to be far more difficult than anticipated and only generated a very limited number of clones (7) despite numerous attempts. This prompted us to change

strategy and, as it was revelaed by the results from the sequencing of the Δ*mreB* strain 3725 (see section 3.2.3), happened to be an astonishingly lucky change.

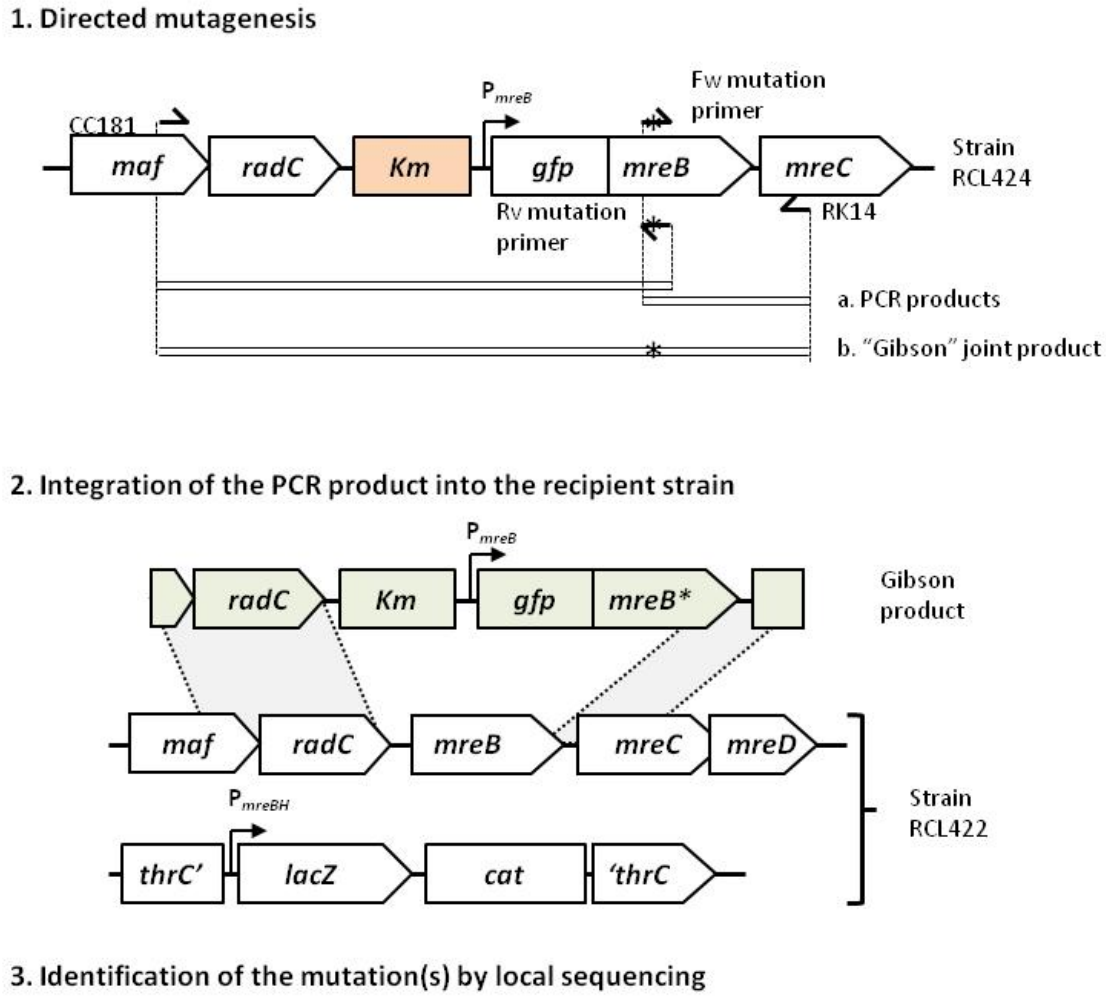

Figure 21 Site directed mutagenesis of *mreB*. 1. Site directed mutagenesis is performed by "Gibson" assembly of PCR fragments generated on DNA from a strain bearing a *km* resistance cassette before the natural *mreB* promoter, and the *gfp* gene fused in 5' of the *mreB* orf (RCL424). **a**. Two intermediate PCR products are generated using CC181/Rv mutation primer and Fw mutation primer/RK14, the mutation to introduce being bear on the overlapping forward and reverse primers. **b**. The resulting PCR products are assembled by the "Gibson" technique (see method), generating a single DNA fragment. **2**. The resulting mutated DNA product is transformed and integrated by double cross-over recombination into the recipient *B. subtilis* strain bearing the reporter gene fusion at the *thrC* locus (RCL422). **3**. Mutations are mapped by sequencing the region from *maf* to *mreD*. Gibson product is represented in green; light grey highlights regions of homology between the PCR fragment and the chromosome, allowing the recombination events to take place.

We then cloned mutated *gfp-mreB* at the natural locus under its own promoter, in place of the wild type *mreB* gene (Figure 21; see Material and Methods). This strategy of "*in locus*" cloning is quickly becoming the new paradigm in the field since it theoretically allows to maintain expression conditions as close as possible to those found in the WT strain.

Obtaining the mutants proved to be still difficult as they frequently acquired spontaneously extra mutations, a premature stop codon, or reverted to the wild type sequence. *In toto*, out of the 49 attempted constructions, 32 were successfully cloned and further characterized (Table 9). This suggests the possibility that some aberrant forms of MreB could be more harmful to *B. subtilis* cells than not having MreB at all. This hypothesis is strengthened by the fact that the mutagenesis was performed in the presence of Mg^{+2}, a condition known to allow *mreB* deletion mutant strains to support an almost wild type growth. In the course of this site directed mutagenesis, we noticed the recurrent, independent, appearance of additional mutations that drove two amino-acid changes (MreB$^{I168F\ I169W}$). Without entering into the molecular detail, we could link this to the existence of an unnoticed conserved stretch of amino-acids between MreB (TEVA**II**SL) and Maf (TEVA**FW**SL). We then decided to add these mutations to our list and created a MreB$^{I168F\ I169W}$ mutant (B58; table 9). All these *gfp-mreB* mutants will be here after called *mreB**.

RCL #	MreB* #	*mreB*	*thrC*
RCL422		*mreB*	P_{mreBH}*lacZ*
RCL424		*gfp-mreB*^{WT}	P_{mreBH}*lacZ*
RCL423		Δ*mreB*	P_{mreBH}*lacZ*
RCL425	B1	*gfp-mreB*^{I242N}	P_{mreBH}*lacZ*
RCL426	B2	*gfp-mreB*^{N88I}	P_{mreBH}*lacZ*
	B3	*gfp-mreB*^{M1T}	P_{mreBH}*lacZ*
RCL427	B4	*gfp-mreB*^{G56R}	P_{mreBH}*lacZ*
RCL428	B5	*gfp-mreB*^{K197E}	P_{mreBH}*lacZ*
RCL429	B6	*gfp-mreB*^{G160R}	P_{mreBH}*lacZ*
RCL430	B7	*gfp-mreB*^{E243G}	P_{mreBH}*lacZ*
	B9	*gfp-mreB*^{V107A}	P_{mreBH}*lacZ*
RCL431	B10	*gfp-mreB*^{S109P}	P_{mreBH}*lacZ*
RCL432	B11	*gfp-mreB*^{T41A}	P_{mreBH}*lacZ*
	B12	*gfp-mreB*^{S170P}	P_{mreBH}*lacZ*
RCL433	B14	*gfp-mreB*^{V114A}	P_{mreBH}*lacZ*
RCL434	B15	*gfp-mreB*^{I142T}	P_{mreBH}*lacZ*
RCL435	B16	*gfp-mreB*^{G216R}	P_{mreBH}*lacZ*
RCL436	B17	*gfp-mreB*^{A276G}	P_{mreBH}*lacZ*
RCL437	B18	*gfp-mreB*^{V72I}	P_{mreBH}*lacZ*
RCL438	B19	*gfp-mreB*^{G231D}	P_{mreBH}*lacZ*
RCL439	B20	*gfp-mreB*^{E31G}	P_{mreBH}*lacZ*
RCL440	B21	*gfp-mreB*^{V182A}	P_{mreBH}*lacZ*
RCL441	B22	*gfp-mreB*^{G14E}	P_{mreBH}*lacZ*
RCL442	B23	*gfp-mreB*^{K52R}	P_{mreBH}*lacZ*
	B24	*gfp-mreB*^{T176S}	P_{mreBH}*lacZ*
RCL443	B25	*gfp-mreB*^{S33T}	P_{mreBH}*lacZ*
RCL444	B26	*gfp-mreB*^{A51V}	P_{mreBH}*lacZ*
RCL445	B27	*gfp-mreB*^{I174M}	P_{mreBH}*lacZ*

RCL #	MreB* #	*mreB*	*thrC*
RCL446	B28	*gfp-mreB*^{D189G}	P_{mreBH}*lacZ*
RCL447	B29	*gfp-mreB*^{R66C}	P_{mreBH}*lacZ*
RCL448	B30	*gfp-mreB*^{I279V}	P_{mreBH}*lacZ*
	B31	*gfp-mreB*^{Y85H}	P_{mreBH}*lacZ*
RCL449	B32	*gfp-mreB*^{L171P}	P_{mreBH}*lacZ*
	B33	*gfp-mreB*^{M213V}	P_{mreBH}*lacZ*
	B34	*gfp-mreB*^{E274V}	P_{mreBH}*lacZ*
	B35	*gfp-mreB*^{T39A}	P_{mreBH}*lacZ*
	B36	*gfp-mreB*^{T58A}	P_{mreBH}*lacZ*
RCL450	B37	*gfp-mreB*^{T79M}	P_{mreBH}*lacZ*
	B38	*gfp-mreB*^{V299A}	P_{mreBH}*lacZ*
RCL451	B39	*gfp-mreB*^{D121E}	P_{mreBH}*lacZ*
	B40	*gfp-mreB*^{D130G}	P_{mreBH}*lacZ*
RCL452	B41	*gfp-mreB*^{I134V}	P_{mreBH}*lacZ*
RCL453	B42	*gfp-mreB*^{P151Q}	P_{mreBH}*lacZ*
	B43	*gfp-mreB*^{I159T}	P_{mreBH}*lacZ*
RCL454	B44	*gfp-mreB*^{P32L}	P_{mreBH}*lacZ*
	B45	*gfp-mreB*^{V35A}	P_{mreBH}*lacZ*
RCL455	B46	*gfp-mreB*^{V72A}	P_{mreBH}*lacZ*
RCL456	B47	*gfp-mreB*^{M155V}	P_{mreBH}*lacZ*
	B48	*gfp-mreB*^{V103I}	P_{mreBH}*lacZ*
	B49	*gfp-mreB*^{E262G}	P_{mreBH}*lacZ*
	B50	*gfp-mreB*^{G95A}	P_{mreBH}*lacZ*
	B51	*gfp-mreB*^{M202T}	P_{mreBH}*lacZ*
RCL457	B52	*gfp-mreB*^{N49S}	P_{mreBH}*lacZ*
RCL458	B53	*gfp-mreB*^{G60R}	P_{mreBH}*lacZ*
RCL461	B58	*gfp-mreB*$^{I168F\ I169W}$	P_{mreBH}*lacZ*

Table 9 List of strains carrying SNP in *gfp-mreB*, cloned at natural locus, and their controls used for phenotypic characterization. In grey, strains that could not be constructed. RCL numbers correspond to collection number. B* numbering will be used throughout

Both successfully cloned mutants and those that we did not achieve to clone bear mutations spatially spread all over the protein, on its surface and in the inner core of the protein (Figure 22). There is no apparent reason to attain the goal of creating a particular MreB*, other than perseverance.

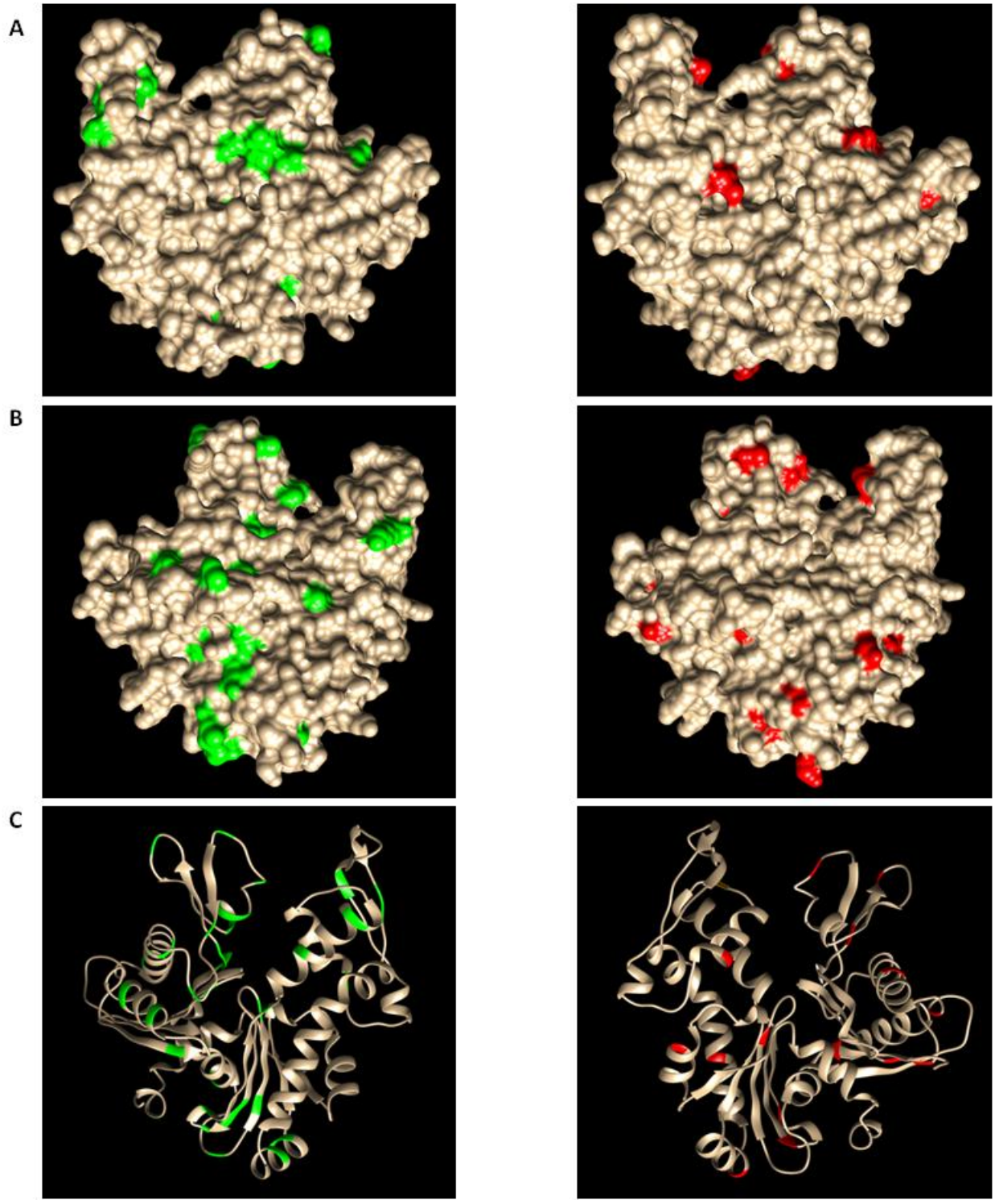

Figure 22 3D model of MreB showing the residues that we achieved to construct in green and those that we did not in red. We can see the surface of MreB on **A** (side 1) and **B** (side 2), while a ribbon model of MreB is shown in **C**. There is no apparent trend on the probability of constructing a SNP or not. Both groups of SNPs are localized in big areas of the protein's surface and interior and they are well spread. Some of the SNPs that we did not achieve to construct lay next to others that we did.

3.4.4. Phenotypic characterization reveals different categories of MreB*s

A systematic analysis of phenotypes was undertaken, comparing strains expressing *gfp-mreB** with their wild type counterpart (RCL424; *gfp-mreB*^{WT}) and the Δ*mreB* mutant (RCL243). We monitored: 1- growth from exponential to deep stationary phase in two rich complex media (LB and CH), 2- cell shape integrity by bright field microscopy, and 3- MreB dynamics by TIRF microscopy. As controls, the levels of GFP-MreB* proteins were estimated by western blot, and strains were also checked for the expression of the *mreBH* reporter fusion (see Materials and Methods). Finally the mutations were drawn onto a hypothetical 3D structure of the protein. *B. subtilis* MreB hasn't been crystallized yet, but a predicted tertiary structure was obtained using the modeling and prediction web tool Phyre2 (Kelley et al., 2015).

Based on these, we could regroup MreB*s into four main categories (Table 10): WT-like, Δ*mreB*-like, mutants with intermediate phenotypes between the 2 previous and mutants with more dramatic growth phenotypes than that of Δ*mreB* (WeB). For TIRFM acquisitions refer to appendix 4.

	MreB*	Mutation	Activation of P_{mreBH} [1]	Protein levels [2]	Growth		Cell morphology [5]	GFP-MreB [6]		
					CH [3]	LB [4]		Localization	Velocity	Density
WT-like	B1	I242N	L	+++	WT	WT	WT	P	WT	WT
	B2	N88I	L	+++	WT	WT	WT	P	WT	WT
	B7	E243G	L	+++	WT	WT	Interm	P	WT	WT
	B11	T41A	L	+++	WT	WT	WT	P	WT	WT
	B15	I142T	L	+++	WT	WT	WT	P	WT	WT
	B16	G216R	L	+++	WT	WT	WT-ish	P	WT	WT
	B18	V72I	L	+++	WT	WT	WT-ish	P	WT	WT
	B20	E31G	L	+++	WT	WT	WT	P	WT	WT
	B23	K52R	L	+++	WT	WT	Interm	P	WT	WT
	B25	S33T	L	+++	WT	WT	WT	P	WT	WT
	B27	I174M	L	+++	WT	WT	WT	P	WT	WT
	B28	D189G	L	+++	WT	WT	Interm	P	WT	WT
	B29	R66C	L	+++	WT	WT	Interm	P	WT	WT
	B37	T79M	L	+++	WT	WT	WT	P	WT	WT
	B39	D121E	L	+++	WT	WT	WT	P	WT	WT
	B41	I134V	L	+++	WT	WT	WT	P	WT	WT
	B44	P32L	L	+++	WT	WT	WT	P	WT	WT
	B52	N49S	L	+++	WT	WT	WT	P	WT	WT
Intermediates	B5	K197E	H	+++	Δ*mreB*	WT	Interm	P	WT	WT
	B14	V114A	H	+++	Δ*mreB*	WT	Interm.	Dif & P	WT	Very low
	B21	V182A	H	+++	Δ*mreB*	WT	WT	P	WT	WT
	B26	A51V	H	+++	WT	WT	Interm.	P	WT	WT
	B42	P151Q	H	+++	Δ*mreB*	WT	Interm.	Dif & P	Static	Low
	B47	M155V	H	++	atypical	WT	Interm.	P	WT	WT
	B53	G60R	H	+++	Δ*mreB*	WT	Interm.	P	WT	WT
Δ*mreB*-like	B6	G160R	H	++	Δ*mreB*	Δ*mreB*	Interm.	Dif	-	-
	B19	G231D	H	++	Δ*mreB*	Δ*mreB*	Δ*mreB*	Dif	-	-
	B22	G14E	H	+	Δ*mreB*	Δ*mreB*	Interm.	Dif	-	-
	B4	G56R	H	+++	Δ*mreB*	WT	Δ*mreB*	Dif & P	-	Very low
	B58	I168F I169W	H	+	Δ*mreB*	Δ*mreB*	Δ*mreB*	Dif & P	Static	Very low
WeB	B10	S109P	H	+	WeB	WeB	Interm	Dif & P	Some static	Very low
	B17	A276G	H	+++	WeB	WeB	Interm	P	Some static	WT
	B30	I279V	H	+++	WeB	WeB	Interm	P	WT	WT
	B46	V72A	H	+++	WeB	WeB	Interm	P	WT	WT
	B32	L171P	H	+	WeB	WT	WeB	Dif	-	-

Table 10 Classification of MreB*s based on their phenotypic characterization. [1] Expression of P_{mreBH} based on the color of the colony on LB plates supplemented with Xgal; L, low; H, high. [2] Estimated relative protein levels during exponential growth, based on western blot analysis. [3] Growth curve of cells grown in CH media at 37 °C; WeB stands for "Worst than Δ*mreB*". [4] Growth curve of cells grown in LB media at 37 °C. [5] Morphology of exponentially grown cells in CH media at 37 °C observed with bright field microscopy; interm. stands for intermediate phenotype between that of WT and Δ*mreB* strains. [6] GFP-MreB localization and dynamic properties qualitatively analyzed from TIRFM acquisitions; P, patches; Dif, diffusive.

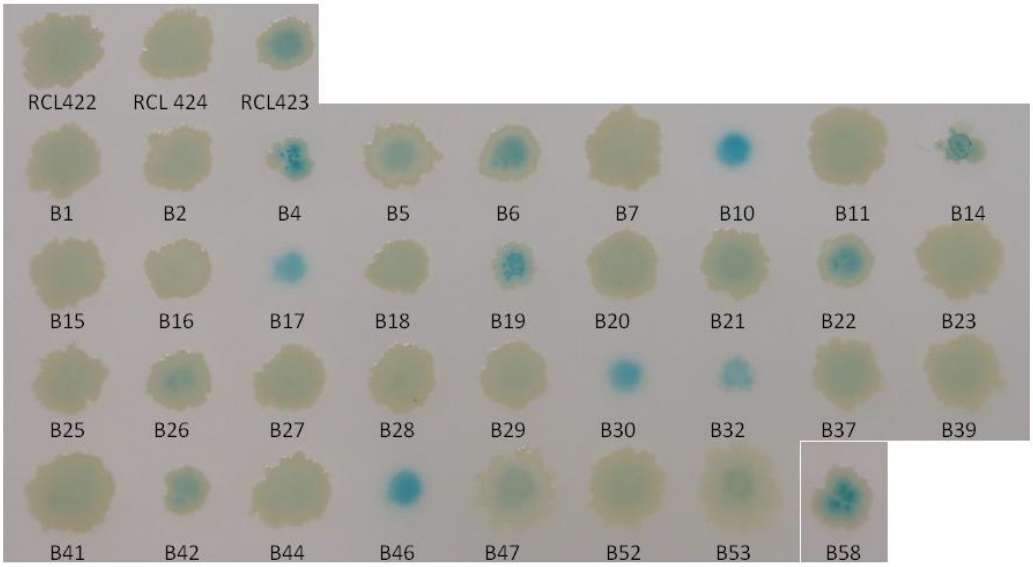

Figure 23 Comparative expression of P_{mreBH}*lacZ* in strains expressing *gfp-mreB, assayed by colorimetric assay on plate.** Expression of the reporter gene P_{mreBH}*lacZ* was tested on RCL422 (WT, P_{mreBH}*lacZ*), RCL424 (P_{mreB}*gfp-mreB*^{WT}, P_{mreBH}*lacZ*), RCL423 (Δ*mreB*, P_{mreBH}*lacZ) and all the MreB*s (*P_{mreB}*gfp-mreB**, *P_{mreBH}*lacZ), on LB-agar plates supplemented with Xgal after 12 h of incubation at 37 °C.*

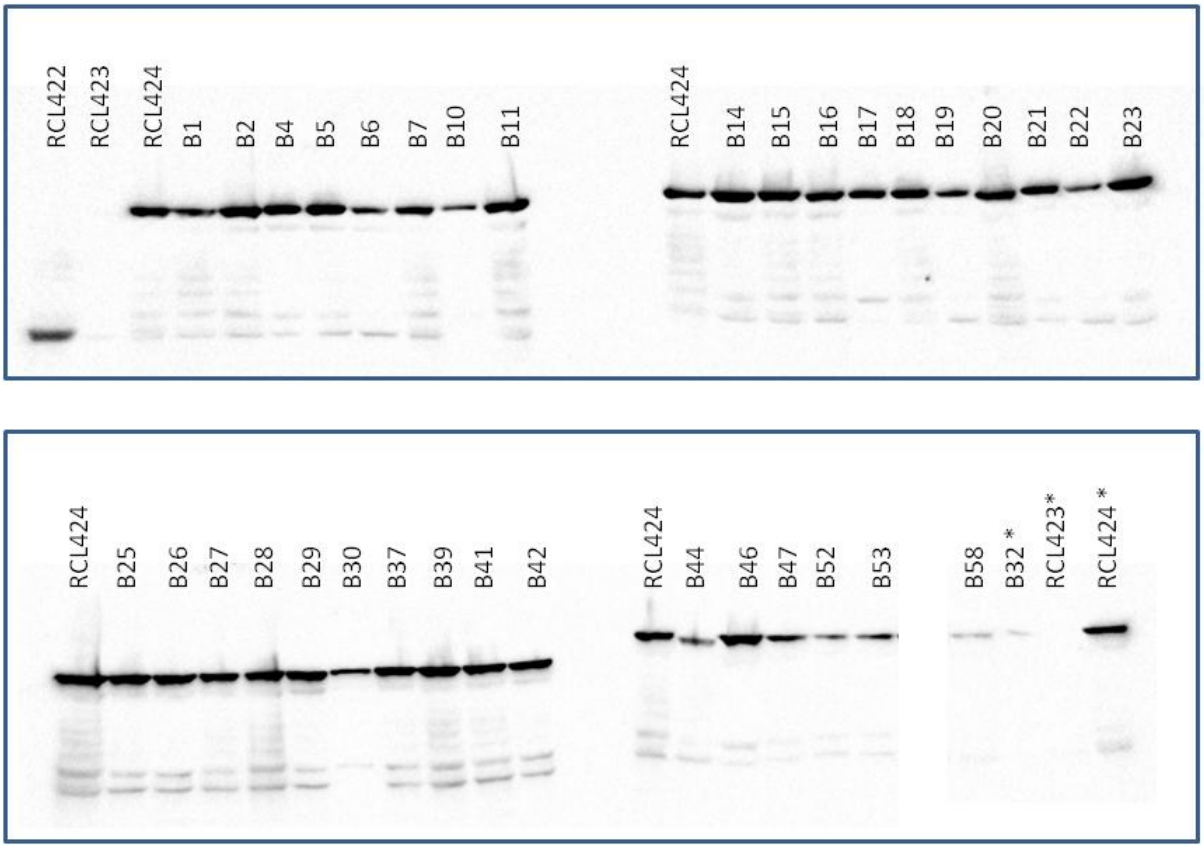

Figure 24 Comparative expression levels of GFP-MreB. Cell extracts from RCL422 (WT, P_{mreBH}*lacZ*), RCL424 (P_{mreB}*gfp-mreB*^{WT}, P_{mreBH}*lacZ*), RCL423 (Δ*mreB*, P_{mreBH}*lacZ*) and all the MreB*s (P_{mreB}*gfp-mreB**, P_{mreBH}*lacZ*), grown in CH media until an $OD_{600\ nm} \approx 0{,}2$. *, indicates cultures supplemented with 20 mM $MgSO_4$. Western inmunoblots were probed with antibodies raised againt MreB (note the presence of a lower band for RCL422 due to the absence of a GFP tag).

3.4.4.1 A range of phenotypes: from wild type- to Δ*mreB*-like

Arguably not the most interesting group of mutants, the 18 WT-like clones present no or very mild defects on every phenotype checked (Table 10, Figure 23-25). All but four derived from screened mutants bearing more than one SNP that could account for their original selection. B7, B16, B18 and B39, had only a single SNP in *mreB* suggesting that these false positives may have had extra mutation(s) outside of the sequenced area.

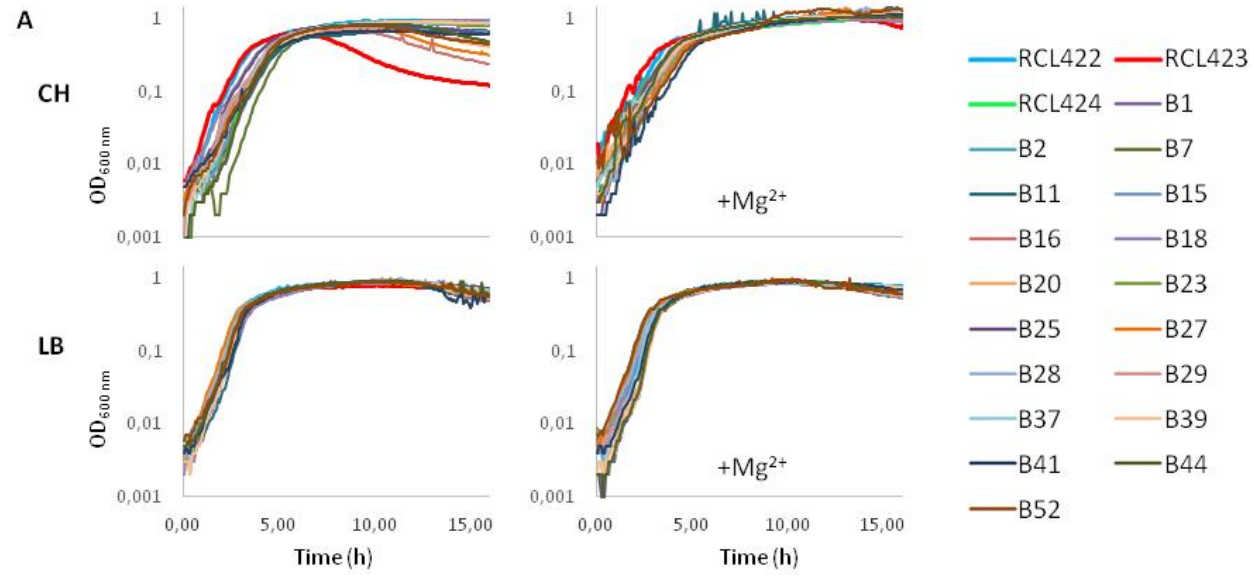

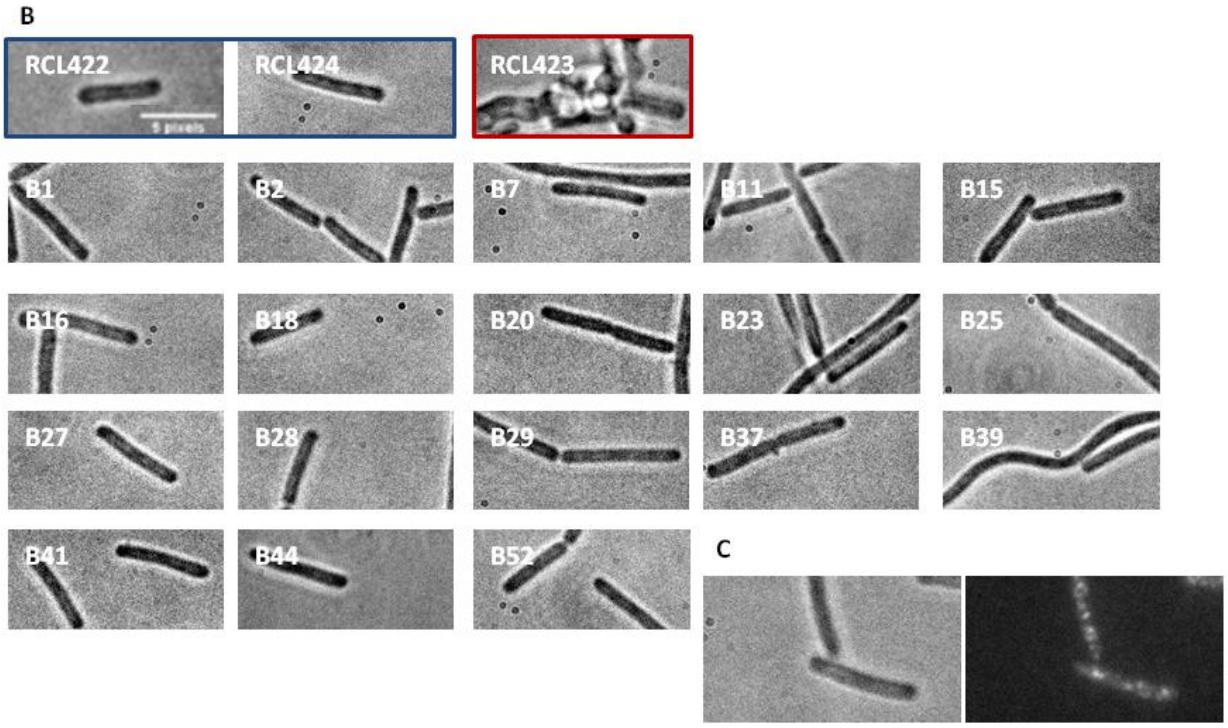

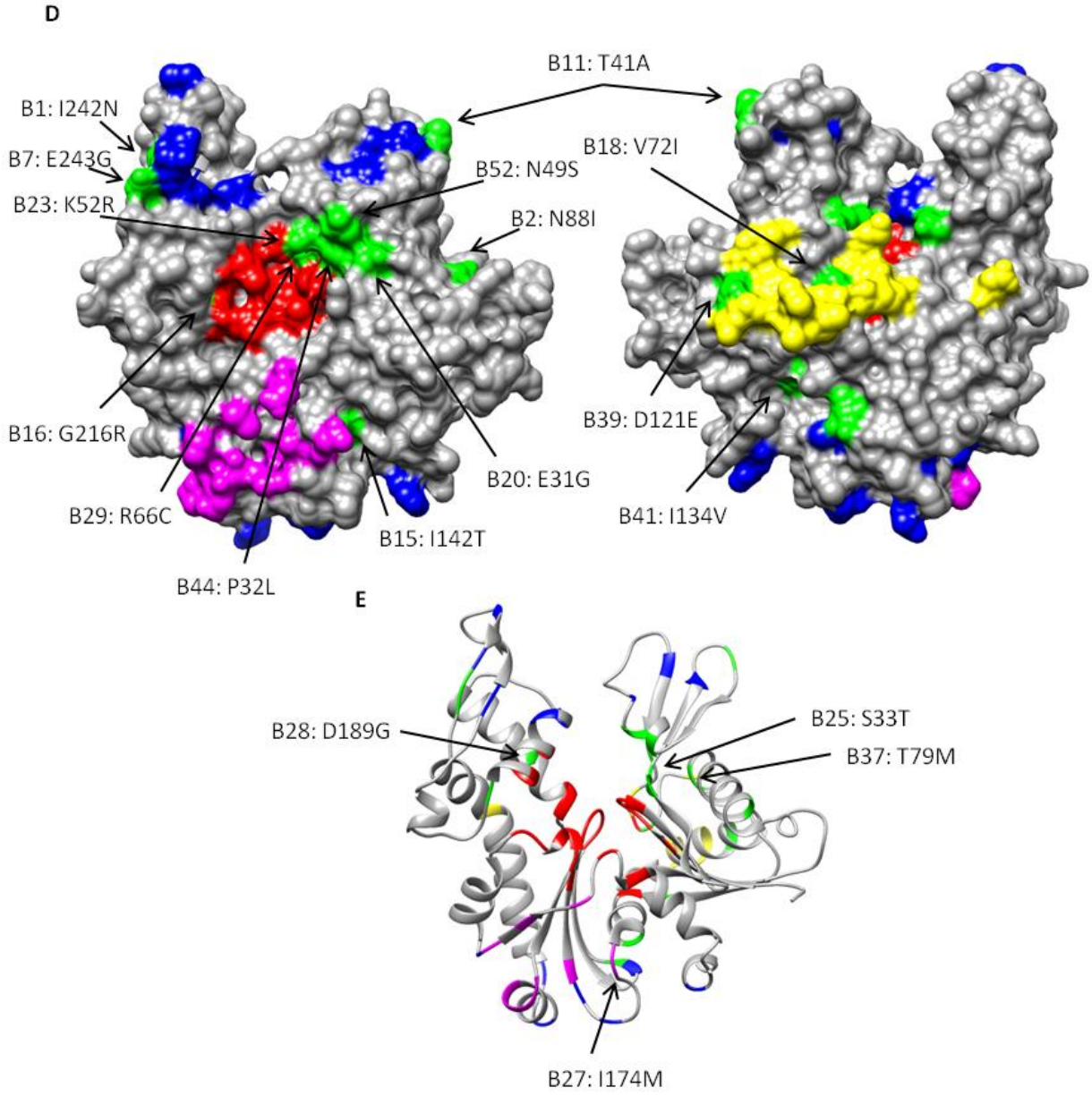

Figure 25 WT-like MreB*s: growth in CH or LB media (supplemented or not with $MgSO_4$), morphology and spatial localization on the protein. A. Growth curves of RCL422 (WT, P_{mreBH}*lacZ*), RCL424 (P_{mreB}*gfp-mreB*^{WT}, P_{mreBH}*lacZ*), RCL423 (Δ*mreB*, P_{mreBH}*lacZ*) and the 18 WT-like MreB*s, grown in CH (upper panels) or LB media (lower panels), supplemented with $MgSO_4$ (right panels) or not (left panels). **B.** Bright field microscopy images of control WT strains RCL422 and RCL424 (blue outline), Δ*mreB* strain RCL423 (red outline) and the 18 WT-like MreB* strains grown in CH media, and acquired during mid-exponential phase of growth (OD ≈ 0,2 - 0,3). **C.** Example of zoomed are of bright field and fluorescent signal of mutant B18. **D.** Mutated residues displayed on a 3D-structure model of MreB showing the surface of the protein, recto (left) and verso (right). Mutated residues in WT-like MreB* mutants (green) are designated by arrows while other colored residues signaled known or presumed aminoacids involved in: monomer:monomer interaction (blue), putative nucleotide binding area (red), putative RodZ interaction area (pink), and putative interfilament bundleing interface (yellow). **E.** MreB ribbon structure model (recto only) displaying mutated residues embedded in the structure and not visible on the surface display. The color code is the same than in D.

Conversely, the Δ*mreB*-like mutants B4, B6, B19 and B22 were almost indistinguishable from a deletion mutant of *mreB*: they presented strong shape defects and poor growth (reversed by the presence of Mg^{+2}), combined with strong induction of the P_{mreBH} *lacZ* reporter (Table 10, Figures 23, 24 and 26). In addition, the mutant B58, bearing the 2 amino-acid changes at position 168 169 (mutations that spontaneously and independently arose during the cloning process in many clones), presents an identical Δ*mreB*-like phenotype. Protein localization shows mostly soluble, diffusive signal instead of the typical patchy and dynamic localization observed with the wild type, strongly suggesting an inability of the mutants to form a complex with the PGEM. Two of the mutations (G14E -B22-, G160R -B6-) are predicted to be active site residues (van den Ent et al., 2001) lying in the putative nucleotide-binding pocket, which advocates for a role of ATP or GTP in MreB's function *in vivo*. Two other mutated residues (G56R -B4-, G231D -B19-) are present at the surface of domain IB and IIB (corresponding to domain 1 and 4 in G-actin) and were predicted to contact the previous subunit in the polymer (van den Ent et al., 2001). It suggests that this change may have altered the ability of the MreB*s B4 and B19 to polymerize. Finally, mutations 168-169 of mutant B58 lie deep in the core of MreB and may have simply compromised its tertiary structure. This is supported by the western blot analysis (Figure 24) showing that this strain has (with B32) the lowest levels of MreB of all the mutants. It should be noted that three other "Δ*mreB*-like" mutants described above also have slightly lower levels of MreB ("++" on Table 10) than that of the wild type, although not as low as in B58. Even though we cannot discard the possibility of these mutations slightly destabilizing the protein folding, we could also imagine that it is simply the mislocalization of the protein to the cytosol (instead of the usual membrane association) or their existence as monomers that facilitates their turnover.

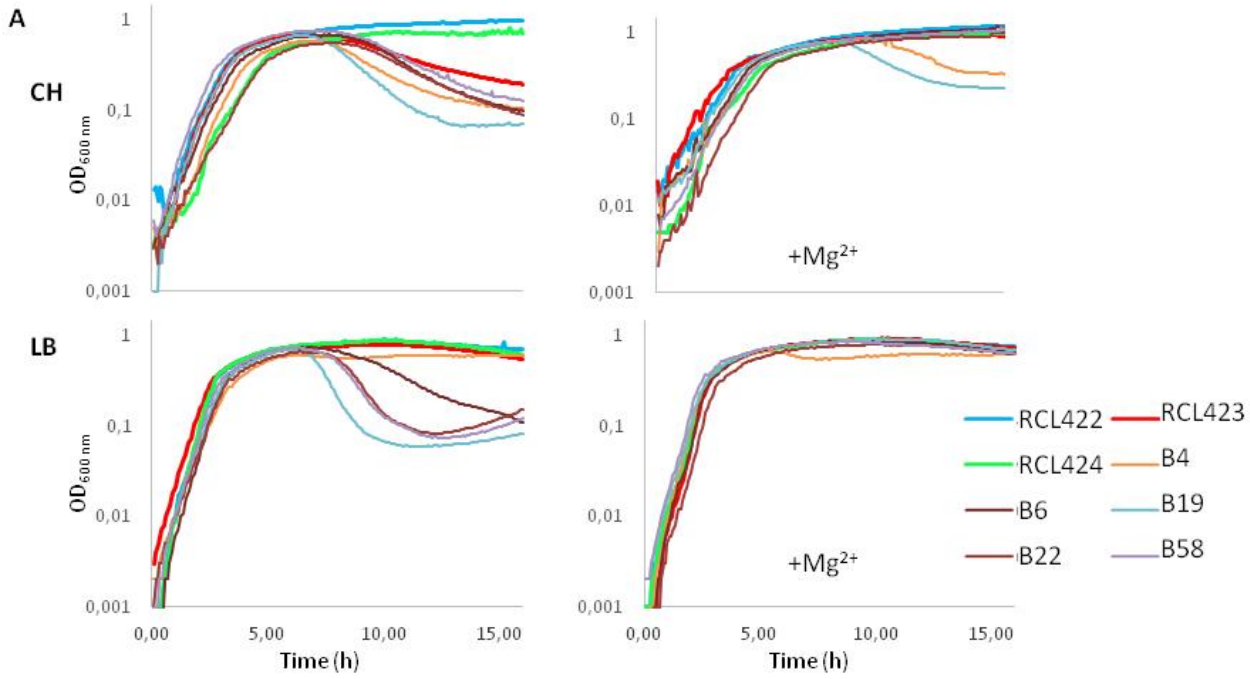
A
CH
LB
OD600 nm
1
0,1
0,01
0,001
+Mg2+
0,00
5,00
10,00
15,00
Time (h)
RCL422
RCL423
RCL424
B4
B6
B19
B22
B58

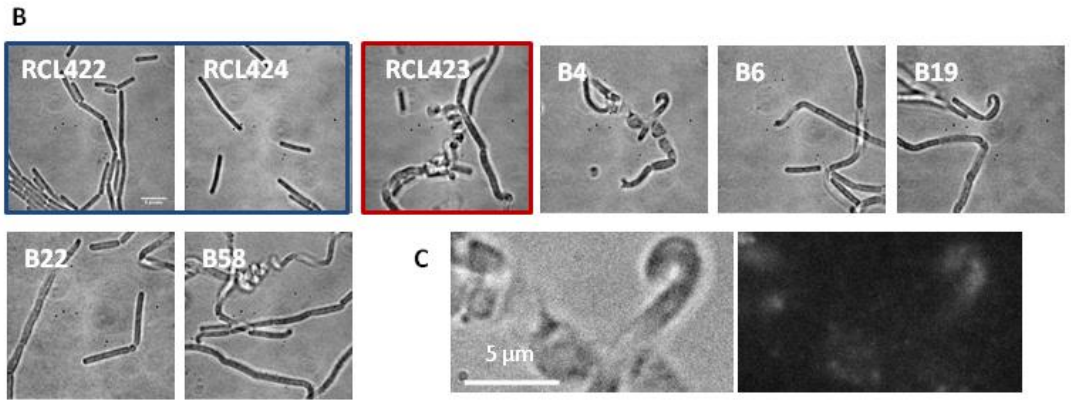
B
RCL422
RCL424
RCL423
B4
B6
B19
B22
B58
C
5 µm

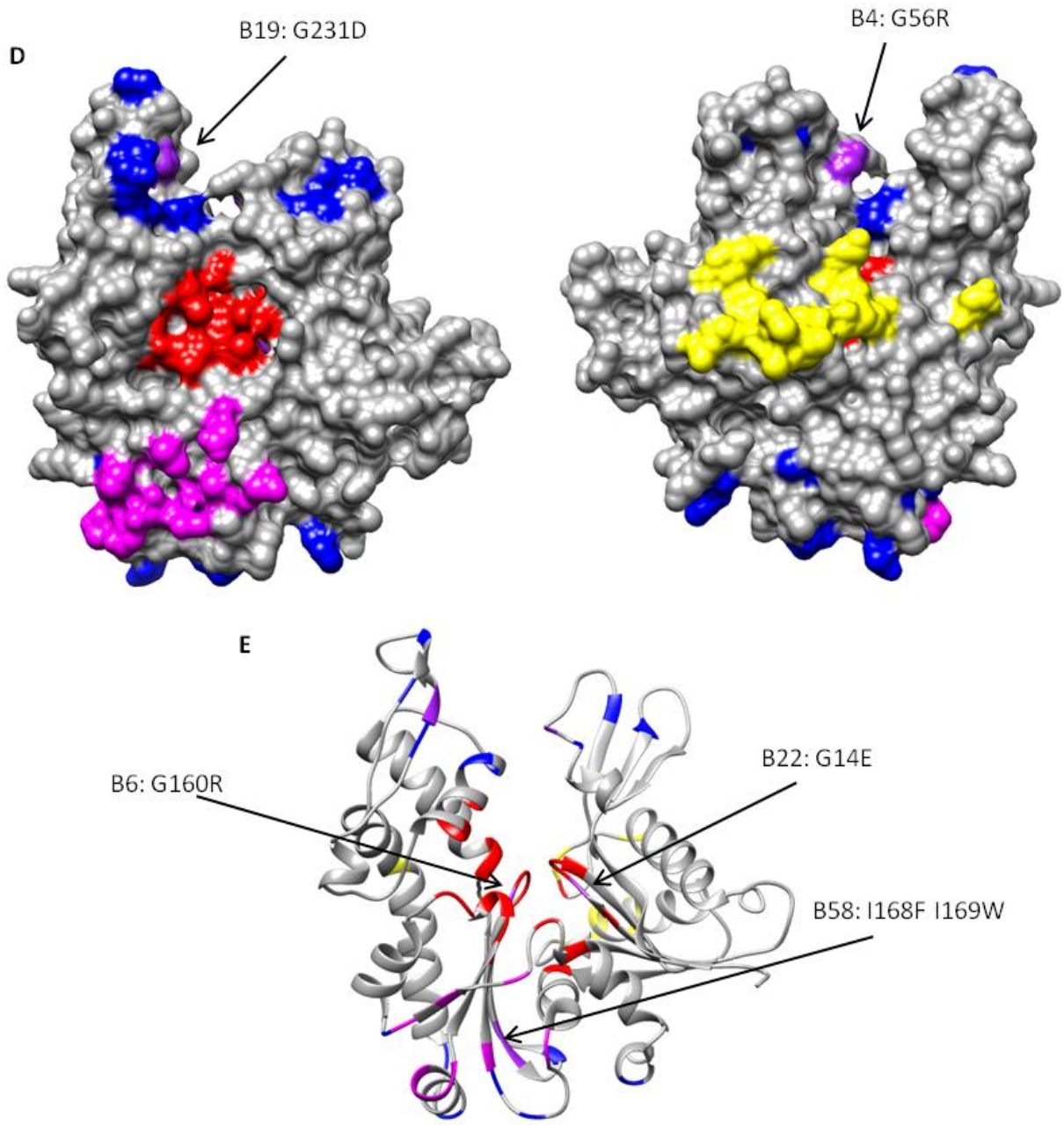

Figure 26 Δ*mreB*-like MreB*s: growth in CH or LB media (supplemented or not with $MgSO_4$), morphology and spatial localization on the protein. A. Growth curves of RCL422 (WT, P_{mreBH}*lacZ*), RCL424 (P_{mreB}*gfp-mreB*^{WT}, P_{mreBH}*lacZ*), RCL423 (Δ*mreB*, P_{mreBH}*lacZ*) and the 5 Δ*mreB*-like MreB*s grown in CH (upper panels) or LB media (lower panels), supplemented with $MgSO_4$ (right panels) or not (left panles). **B.** Bright field microscopy images of control WT strains RCL422 and RCL424 (blue outline), Δ*mreB* strain RCL423 (red outline) and the 5 Δ*mreB*-like MreB* strains grown in CH media, and acquired during mid-exponential phase of growth (OD ≈ 0,2 - 0,3). Mutant cells display an essentially Δ*mreB* shape. **C.** Example of zoomed are of bright field and fluorescent signal of mutant B4. **D.** Mutated residues displayed on a 3D-structure model of MreB showing the surface of the protein, recto (left) and verso (right). Mutated residues in Δ*mreB*-like MreB* mutants (purple) are designated by arrows while other colored residues signaled known or presumed aminoacids involved in: monomer:monomer interaction (blue), putative nucleotide binding area (red), putative RodZ interaction area (pink), and putative interfilament bundleing interface (yellow). **E.** MreB ribbon structure model (recto only) displaying mutated residues embedded in the structure and not visible on the surface display. The color code is the same than in D.

Finally, in addition to these WT or completely inactivated mutants, we obtained seven clones (B5, B14, B21, B26, B42, B47 and B53) with a gradation of intermediate phenotypes between these two extremes. In these, increased induction of P_{mreBH} *lacZ* roughly correlates with degradation of shape integrity and growth defect (Table 10, Figures 23, 24 and 27). As expected, the localization of MreB was patchy and dynamic and almost identical to wild type in strains with limited shape defect (B5, B21, B26, B47, B53), while strains B14 and B42 presented dimmer signal and increasing number of cells without MreB dynamics together with increasing shape defects (twisting, uncontrolled width, swelling cells). Mutations A51V, G60R and P151Q (in B26, B53 and B42 respectively) are again located in the surface, potentially responsible for monomer:monomer interaction: residues 60 and 151 were predicted to be "contacting residues" on the – (or pointed) and + (or barbed) side of the monomer, while residue 51 is in the direct vicinity of the contacting residues of the – side and, importantly, it is extremely well conserved from *B. subtilis* to eukaryotic actin (Figure 27D-F). Mutation V182A (B21) and V114A (B14) are two very highly conserved residues in MreBs from different organisms (according to an alignment performed using Clustal Omega (Goujon et al., 2010; Sievers et al., 2011) suggesting that they have an important role in the protein's stability or functionality, although their phenotype is not very severe. Both lie on the surface of the protein, away from the areas important for monomer:monomer interaction, and may be important for bundling of polymers (van den Ent et al., 2001). Interestingly, the mutation V114A precedes a triplet of charged amino-acid residues shown to be important in *Saccharomyces cerevisaie* (Wertman, Drubin, & Botstein, 1992). Unpublished results from our lab had previously shown that a *B. subtilis* mutant expressing GFP-MreB with a triple substitution (E115A-E116A-R117A), expressed as the only copy of MreB in the cell, showed strong defects both in growth and morphology (unpublished, Dominguez-Escobar et al.). Together, these results strongly suggest an important role of this area in the function of MreB, potentially through protein:protein interactions, either with other protein effectors or with other polymers of MreB.

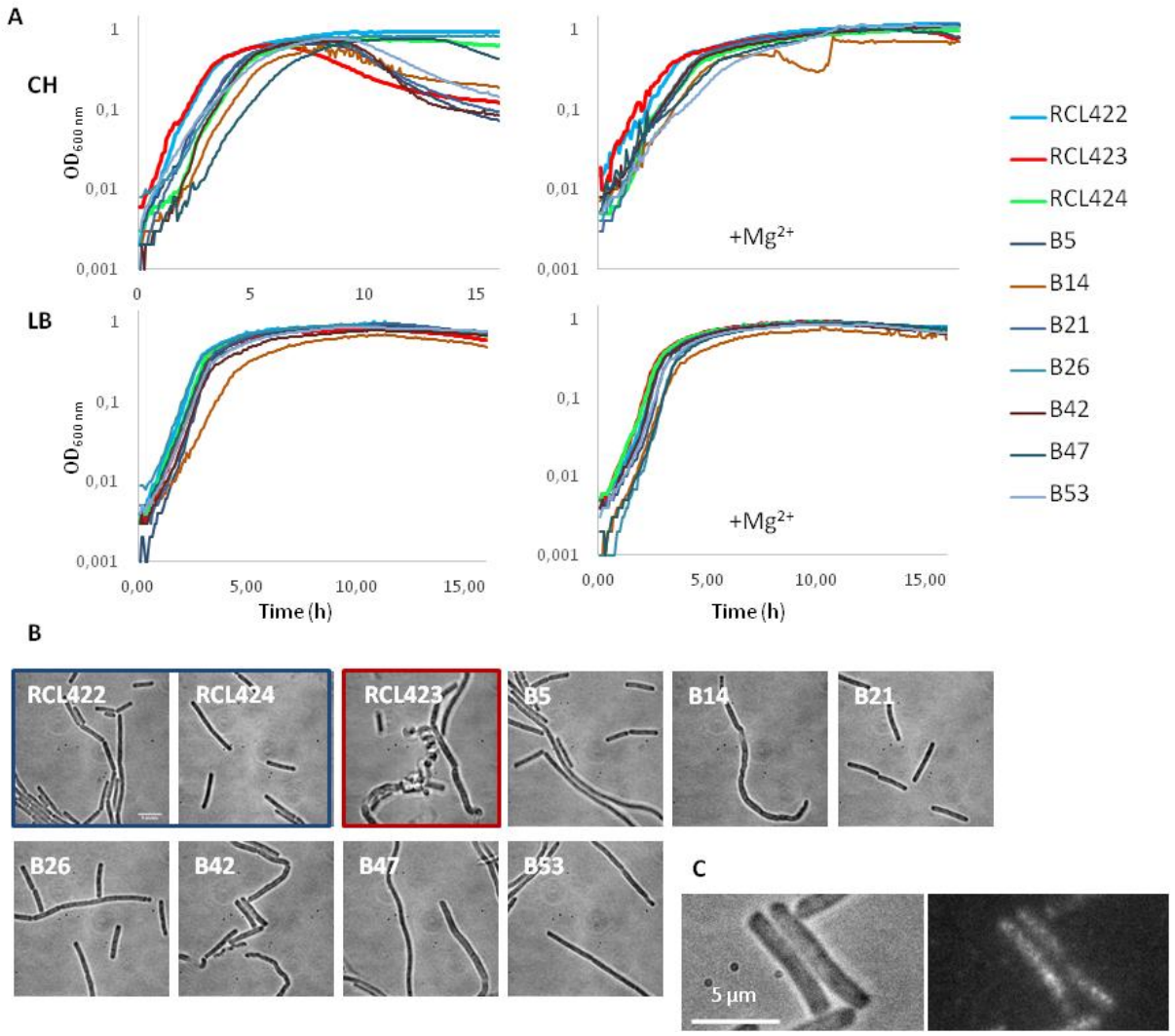
A
CH
LB
OD600 nm
1
0,1
0,01
0,001
0
5
10
15
0,00
5,00
10,00
15,00
Time (h)
+Mg2+
RCL422
RCL423
RCL424
B5
B14
B21
B26
B42
B47
B53
B
RCL422
RCL424
RCL423
B5
B14
B21
B26
B42
B47
B53
C
5 µm

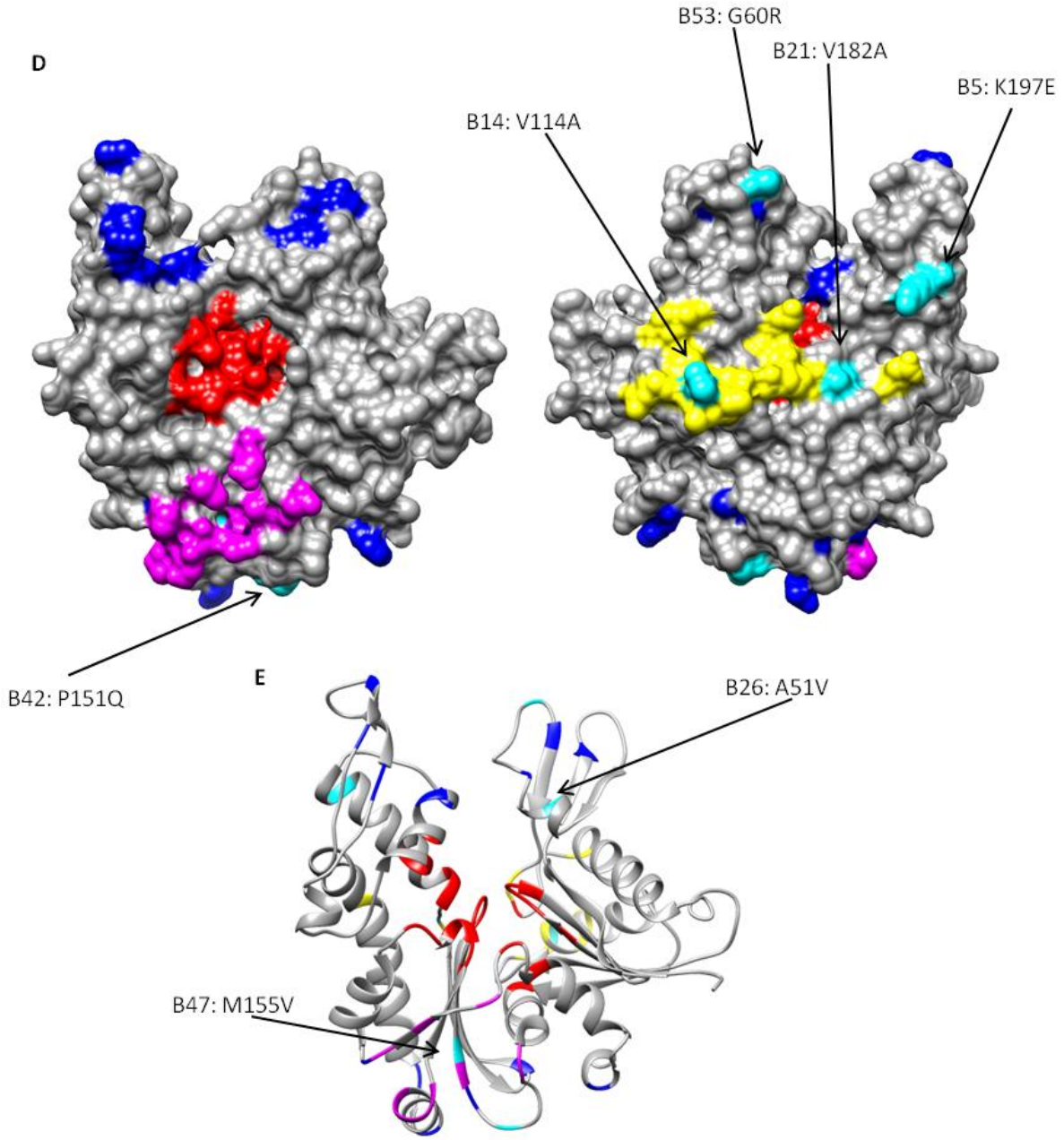

Figure 27 Intermediate MreB*s: growth in CH or LB media (supplemented or not with $MgSO_4$), morphology and spatial localization on the protein. A. Growth curves of RCL422 (WT, P_{mreBH}*lacZ*), RCL424 (P_{mreB}*gfp-mreB*^{WT}, P_{mreBH}*lacZ*), RCL423 (Δ*mreB*, P_{mreBH}*lacZ*) and the 7 intermediate MreB*s grown in CH (upper panels) or LB media (lower panels), supplemented with $MgSO_4$ (right panels) or not (left panels). **B.** Bright field microscopy images of control WT strains RCL422 and RCL424 (blue outline), Δ*mreB* strain RCL423 (red outline) and the 7 intermediate MreB* strains grown in CH media, and acquired during mid-exponential phase of growth (OD ≈ 0,2 - 0,3). Mutant cells display a range of morphological defects. **C.** Example of zoomed are of bright field and fluorescent signal of mutant B42. **D.** Mutated residues displayed on a 3D-structure model of MreB showing the surface of the protein, recto (left) and verso (right). Mutated residues in interrmediate MreB* mutants (cyan) are designated by arrows while other colored residues signaled known or presumed aminoacids involved in: monomer:monomer interaction (blue), putative nucleotide binding area (red), putative RodZ interaction area (pink), and putative interfilament bundleing interface (yellow). **E.** MreB ribbon structure model (recto only) displaying mutated residues embedded in the structure and not visible on the surface display. The color code is the same than in D.

3.4.4.2 Some *mreB* mutants present partial uncoupling of growth and localization defects

The five remaining mutants, hereafter named WeB (worst growth than Δ*mreB)*, are in many ways remarkable. Four (B10, B17, B30 and B46) present a common, very intriguing set of features: they present more dramatic growth defects than a Δ*mreB* strain, while having normal or mildly affected shape and MreB localization.(Table 10, Figures 23, 24 and 28). Indeed, bright field and TIRFM observations show that B46, B17 and B30 present mainly WT shapes with occasional polar swelling, and a majority of directionally moving MreB patches resembling that of the WT (Figure 28B). Only B10 presents a very slightly affected shape and a reduction in the number of patches with a few aberrant movements. However, their growth is severely affected both in CH and LB medium (Figure 28A). In CH, the mutants' optical density grows at a very slow pace, followed (to the exception of B30) by an equivalent decrease during “stationary phase”, suggesting an important cell lyses. In LB, growth in exponential phase is identical to that of the control strains, but an abrupt change occurs at the entry of the stationary phase, where the mutants quickly start to lyse. Remarkably these defects were not restored by the addition of magnesium, a trick known to restore Δ*mreB* growth defects (Figure 28A).

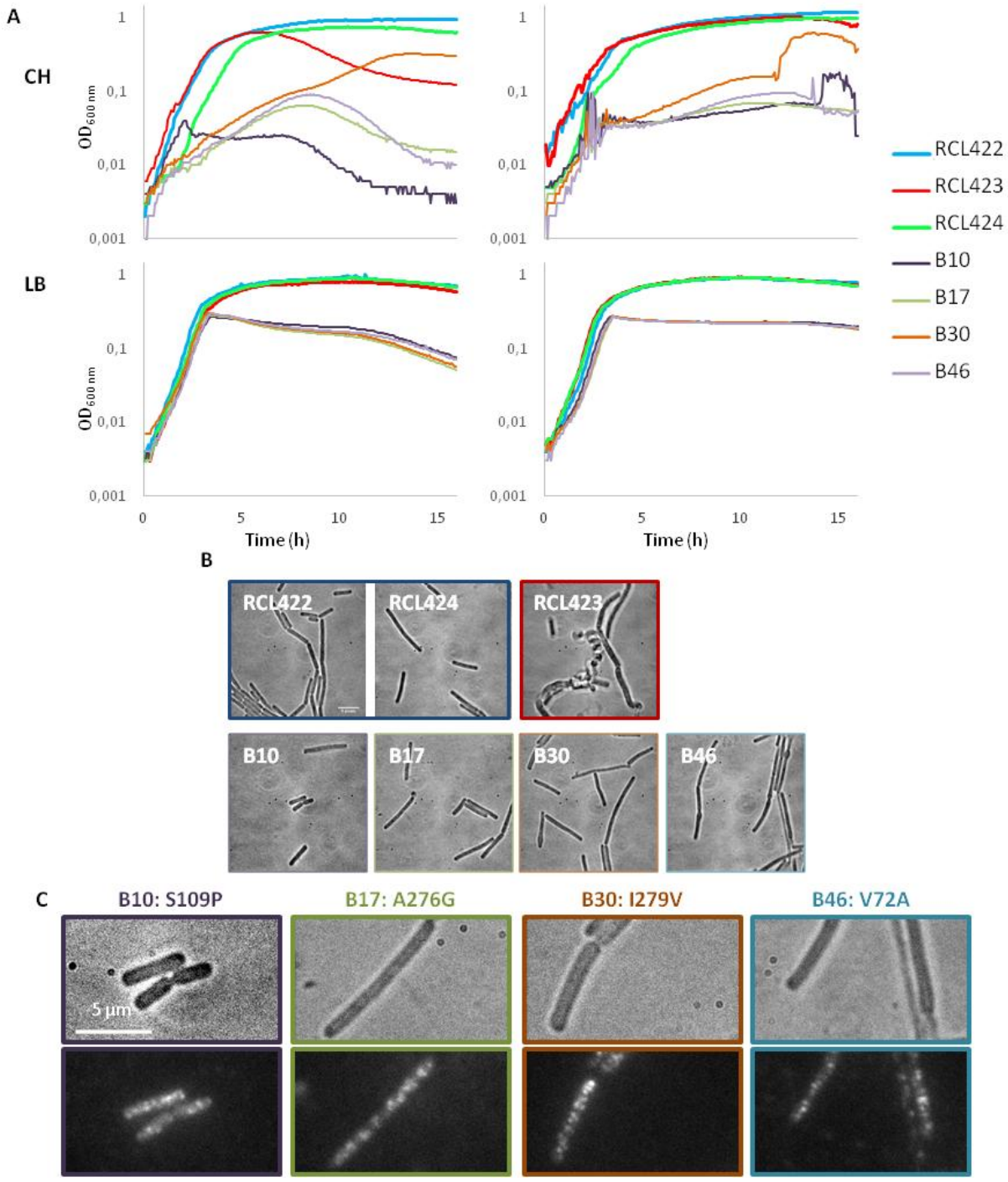
A
CH
LB
OD600 nm
1
0,1
0,01
0,001
0
5
10
15
Time (h)
RCL422
RCL423
RCL424
B10
B17
B30
B46
B
RCL422
RCL424
RCL423
B10
B17
B30
B46
C
B10: S109P
B17: A276G
B30: I279V
B46: V72A
5 µm

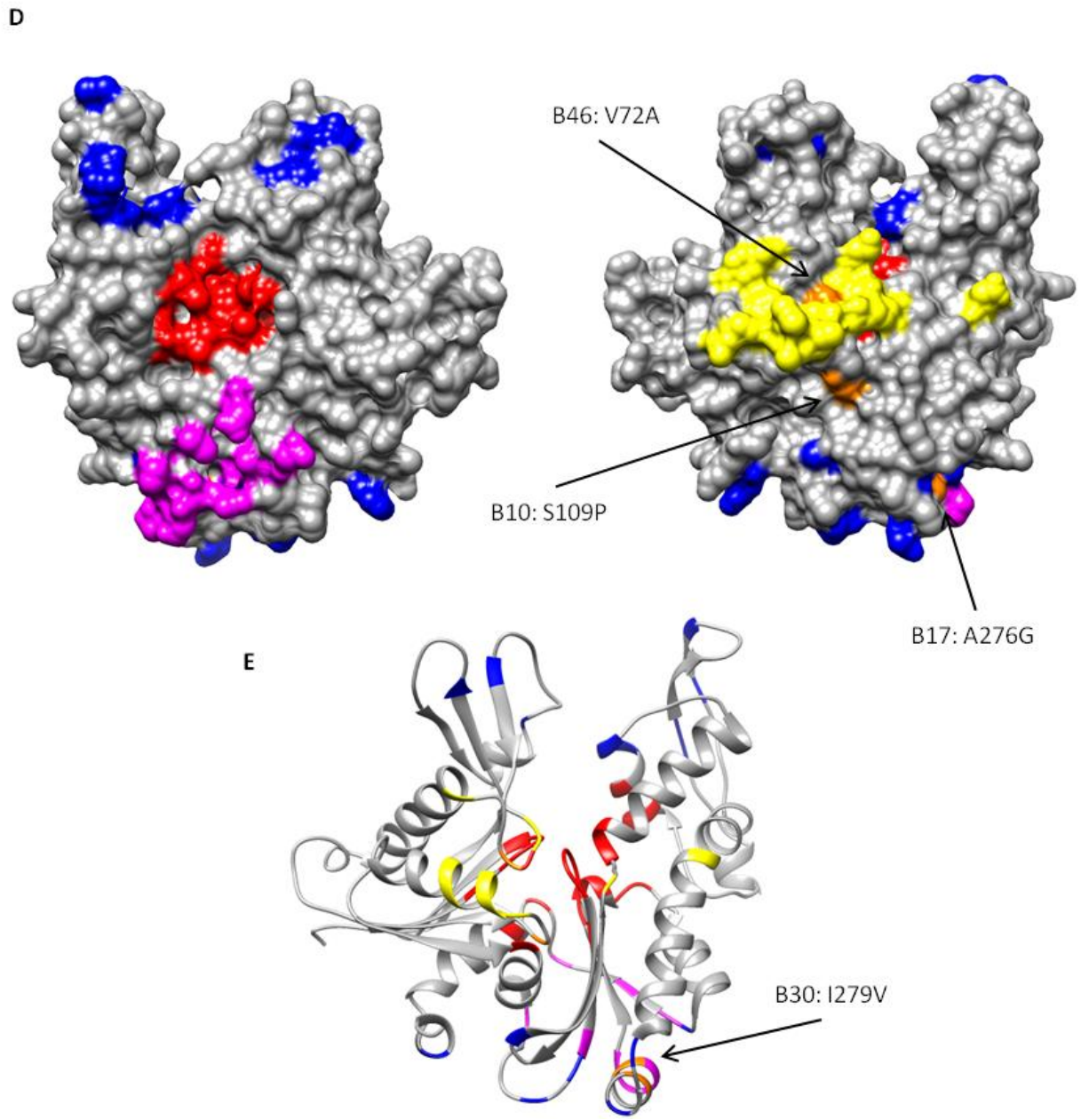

Figure 28 4 WeB MreB*s: growth in CH or LB media (supplemented or not with $MgSO_4$), morphology and spatial localization on the protein. A. Growth curves of RCL422 (WT, P_{mreBH}*lacZ*), RCL424 (P_{mreB}*gfp-mreB*^{WT}, P_{mreBH}*lacZ*), RCL423 (Δ*mreB*, P_{mreBH}*lacZ*) and 4 WeB MreB*s grown in CH (upper panels) or LB media (lower panels), supplemented with $MgSO_4$ (right panels) or not (left panels). **B.** Bright field microscope images of control WT strains RCL422 and RCL424 (blue outline), Δ*mreB* strain RCL423 (red outline) and the 4 WeB MreB* strains grown in CH media, and acquired at OD ≈ 0.1 – 0.2. Mutant cells display very mild morphological defects or none. **C.** Zoomed area of bright field and fluorescent signal of mutants B10, B17, B30 and B46. **D.** Mutated residues displayed on a 3D-structure model of MreB showing the surface of the protein, recto (left) and verso (right). Mutated residues in 4 WeB MreB* mutants (orange) are designated by arrows while other colored residues signaled known or presumed aminoacids involved in: monomer:monomer interaction (blue), putative nucleotide binding area (red), putative RodZ interaction area (pink), and putative interfilament bundleing interface (yellow). **E.** MreB ribbon structure model (verso only) displaying mutated residues embedded in the structure and not visible on the surface display. The color code is the same than in D.

Another very intriguing mutant is B32 (Table 10, Figures 23, 24 and 29). This mutant is in all aspects more affected than the mutant deleted for *mreB*. It causes a stronger activation of the P_{mreBH} *lacZ* reporter (Figure 23), barely grows and has a dramatic loss of cell shape control in CH medium (with almost no benefits from increasing Mg^{+2} concentration), and grows similarly to the deletion mutant in LB but with a pronounced lag (Figure 29). What is most surprising is that MreB is completely delocalized to the cytosol with the lowest protein levels of all the strains tested (Figure 24, Table 10), therefore, one could have expected the phenotypes of this strain to be identical to a Δ*mreB*. Thus, a strong hypothesis is that $MreB^{L171P}$ (B32) may have a dominant effect on other MreB isoforms, preventing them to associate to the membrane, and aggravating the phenotype of a simple Δ*mreB* under specific conditions present in CH, but not in LB.

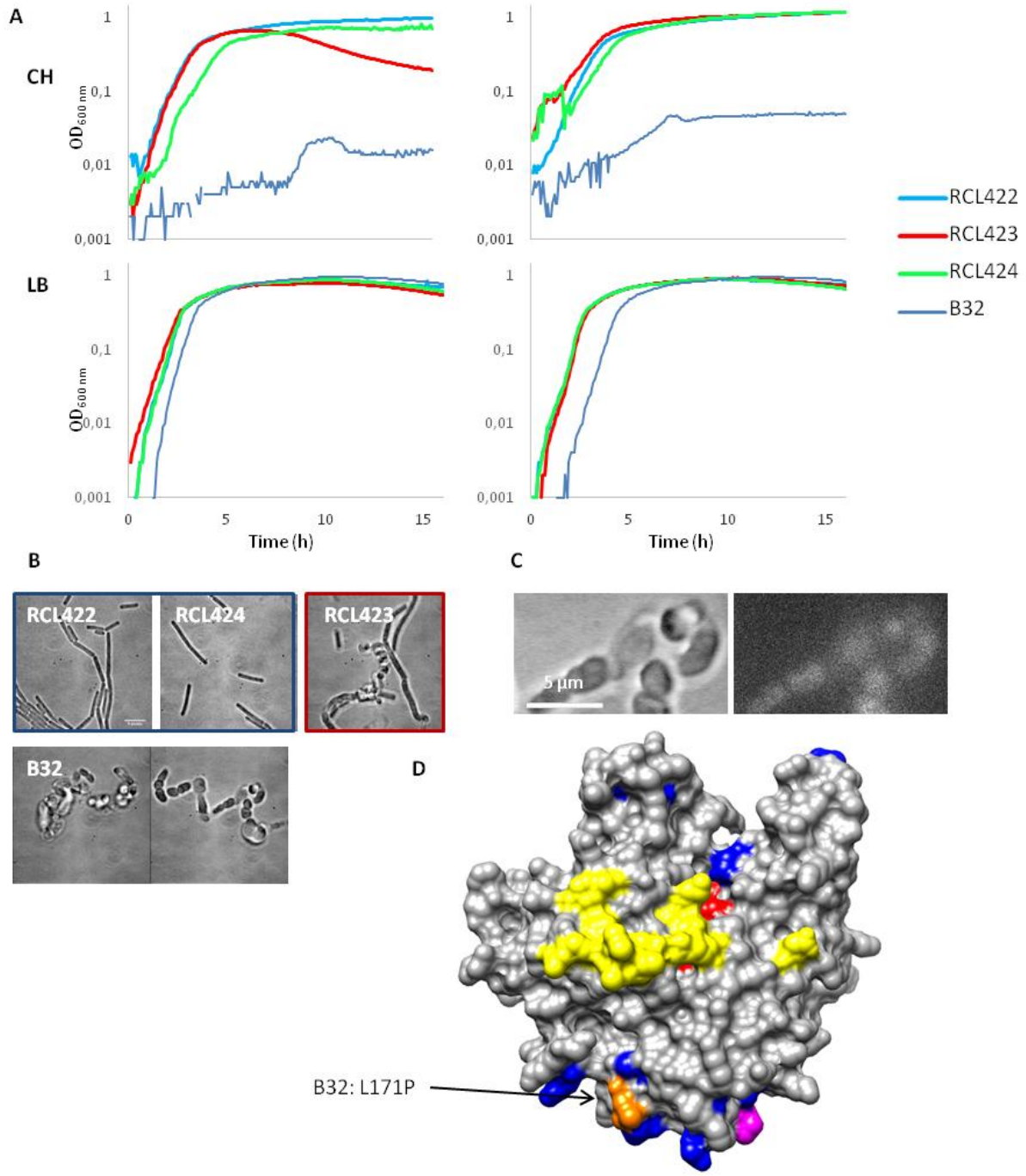

Figure 29 B32 MreB*: growth in CH or LB media (supplemented or not with $MgSO_4$), morphology and spatial localization on the protein. A. Growth curves of RCL422 (WT, P_{mreBH}*lacZ*), RCL424 (P_{mreB}*gfp-mreB*^{WT}, P_{mreBH}*lacZ*), RCL423 (Δ*mreB*, P_{mreBH}*lacZ*) and B32 MreB* grown in CH (upper panels) or LB media (lower panels), supplemented with $MgSO_4$ (right panels) or not (left panels). **B.** Bright field microscopy images of control WT strains RCL422 and RCL424 (blue outline), Δ*mreB* RCL423 strain (red outline) grown in CH media, and acquired during mid-exponential phase of growth (OD ≈ 0,2 - 0,3). B32 was grown in CH media and images were acquired after ~ 24 h growth, at an OD ≈ 0,1. Mutant cells display very severe morphological defects. **C.** Zoomed area of bright field and fluorescent signal of mutant B32. **D.** 3D-structure model of MreB showing the surface of the protein verso (right). B32 MreB* mutant (orange) is designated by an arrow while other colored residues signaled known or presumed aminoacids involved in: monomer:monomer interaction (blue), putative nucleotide binding area (red), putative RodZ interaction area (pink), and putative interfilament bundleing interface (yellow).

3.4.5. Growth defect of WeB and Δ*mreB* mutants can be suppressed by addition of fructose

The dramatic growth defect in CH and abrupt lysis at the entry of stationary phase in LB observed with the WeB mutants, pointed toward a defect in carbon source utilization. We had previously seen that *fruRKA* is overexpressed in Δ*mreB* (*fruK* is also overexpressed in Δ*mbl*). Therefore, we wondered if the addition of fructose could rescue the growth defect of the WeB mutants. As seen on Figure 30, all 5 WeB mutants benefit from the addition of 1,5% fructose and, to the exception of B32 that grew slightly slower, they recover a full WT-like growth. To our surprise, the Δ*mreB* strain is also completely reverted to WT growth, a phenomenon that was, so far, only observed when Mg^{+2} was added to the medium.

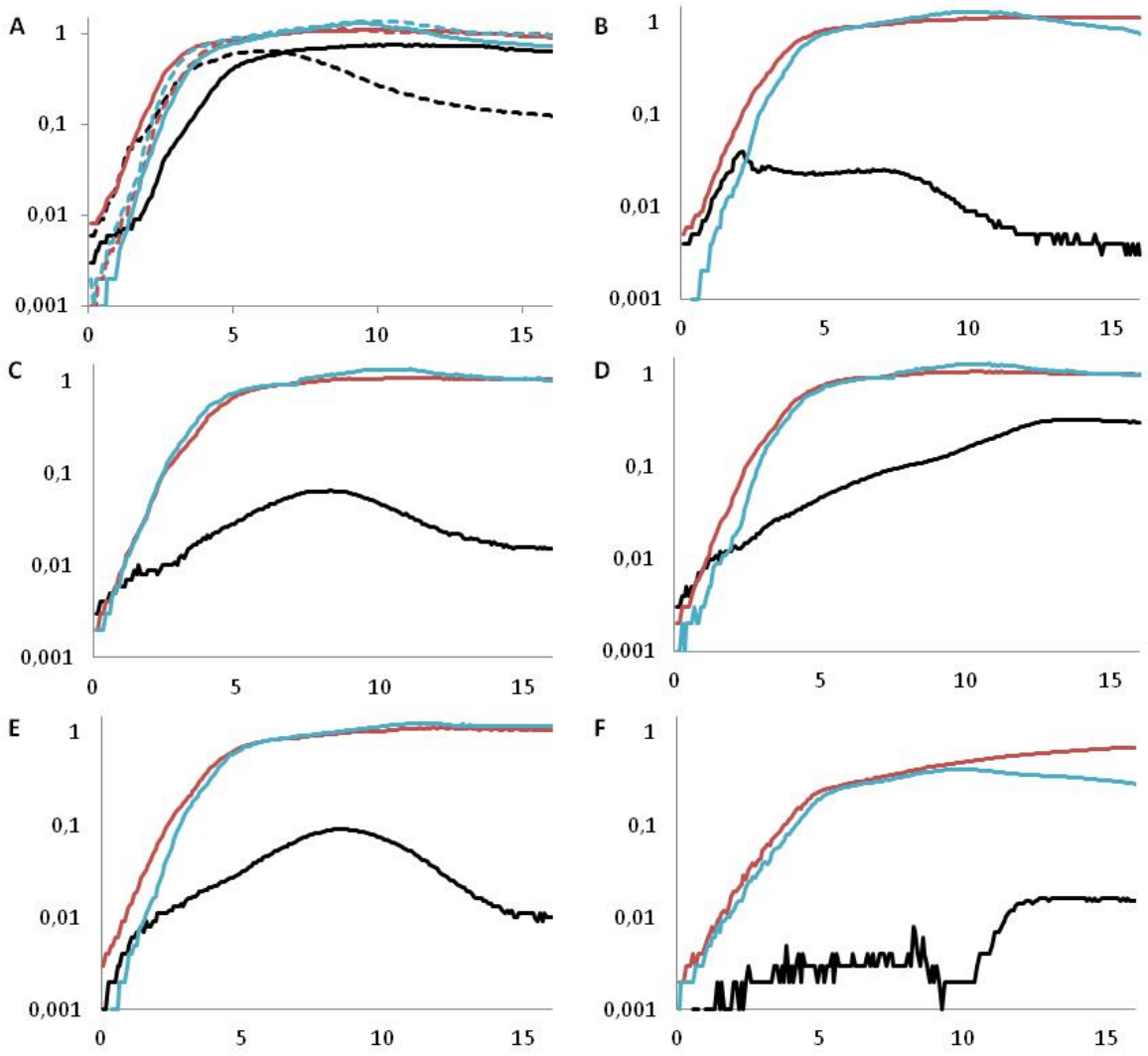

Figure 30 Effect on the growth of WeB and B32 MreB*s by the addition of 1,5 % fructose or 1,5 % glucose. Strains were grown in CH media (black lines), CH media supplemented with 1,5 % fructose (red lines) or CH supplemented with 1,5 % glucose (cyan lines). **A**. RCL424 (P_{mreB}*gfp-mreB*^{WT}, P_{mreBH}*lacZ*) in solid lines and RCL423 (Δ*mreB*, P_{mreBH}*lacZ*) in dashed lines; **B**. B10; **C**. B17; **D**. B30; **E**. B46; **F**. B32. All strains grow to a higher $OD_{600\ nm}$ when 1,5 % fructose or 1,5 % glucose is added to CH media. Δ*mreB* and all the MreB*s tested recover WT-like growth.

Next, we wondered if the improvement in growth was specifically due to the presence of fructose or to the presence of sugars in general, the bacterial preferred carbon source (Fondi, Bosi, Presta, Natoli, & Fani, 2016). As seen in Figure 30, the growth defect is also bypassed when mutants are grown in CH medium supplemented with 1,5 % glucose.

It is well-established that addition of Mg^{+2} restores growth and shape defects of Δ*mreB* cells (although the mechanism behind it is still unclear). We thus wondered if fructose could have the same benefits toward B32, a mutant that presented major morphology defects in CH medium (Figure 31A). Bright field images show that addition of extra Mg^{+2} to the medium confers a very mild improvement to B32's morphology, with some cells recovering short rod shapes (Figure 31B), while addition of fructose does not (Figure 31C). Thus, in B32, magnesium can partially restore shape without restoring growth while fructose dramatically improves growth without improving cell shape.

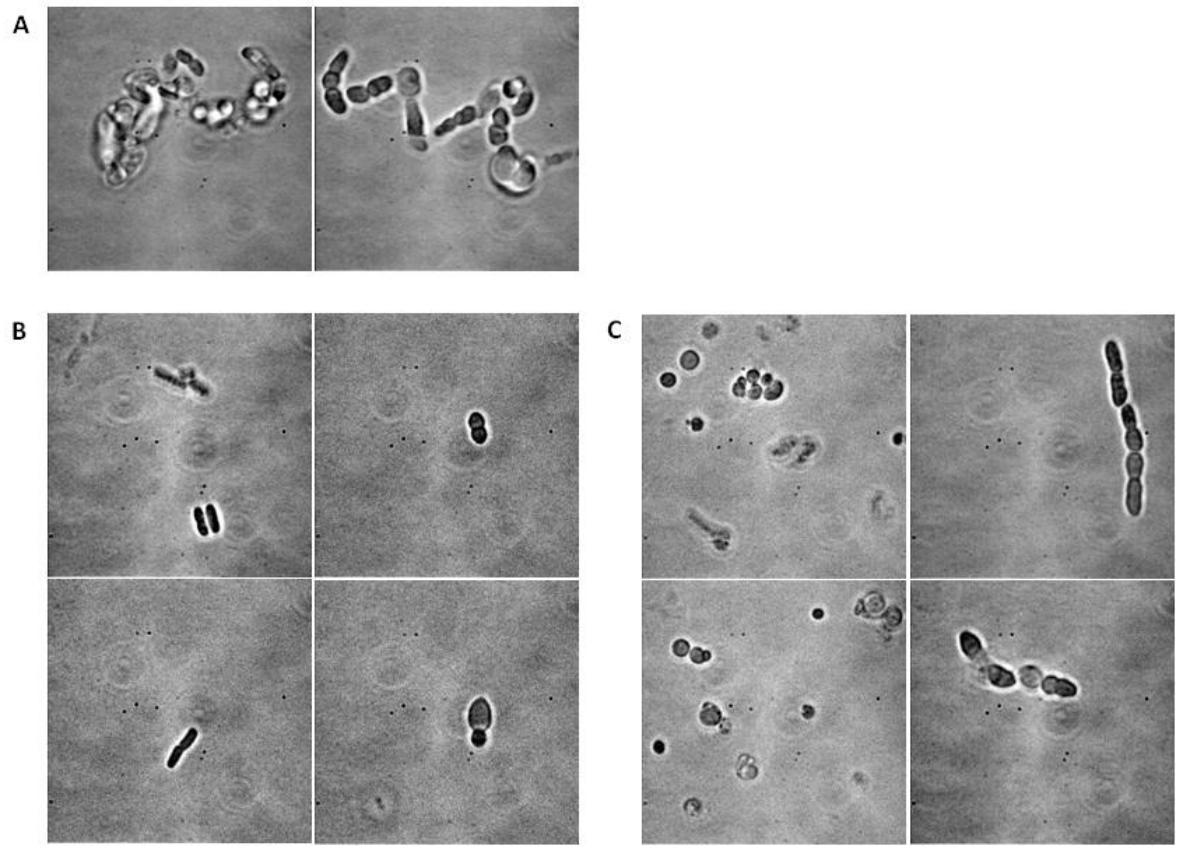

Figure 31 Comparative benefits of $MgSO_4$ or 1,5 % fructose on B3 mutant's shape defect. B32 was grown in CH medium either without supplements (**A**), supplemented with 20 mM $MgSO_4$ (**B**) or 1,5 % fructose (**C**). Bright field images were acquired at $OD_{600\ nm}$ = 0,1 – 0,2. Presence of high concentrations of $MgSO_4$, but not 1.5 % fructose, partially restores rod-shape morphology.

4. Discussion

4. Discussion

4.1 YdcH: a repressor/activator MarR transcription regulator?

The global approach we used revealed a very large number of genes affected, positively and negatively, by YdcH. Albeit surprising, several hypotheses can explain this result. A simple possibility would be that YdcH affects other regulators activity. This may be either through direct activation/repression of genes involved in other regulators activity or because the physiological alterations of the absence of *ydcH*, in turn, turned on/off such regulators. We could not find complete up- or down-regulated regulons but such regulons may be partially hidden by cross regulations of their genes.

Another hypothesis is that YdcH could act both as a repressor and activator of gene expression. Most described MarR TRs act as repressors and a few as activators (Grove, 2013). There are only two known MarR TRs that have both activities (Oh, Shin, & Roe, 2007; Tran et al., 2005). They act as repressors by binding to DNA sequences near the promoter regions of the repressed genes. When the environmental conditions are modified, they undergo a structural modification that causes a reduction of their affinity for DNA and makes them bind the RNA polymerase, enhancing its binding to the promoter region of the regulated gene. Hence, this is a possibility that may be worth checking in the future.

4.2 YdcH: a new transition state regulator

Several lines of evidence advocate for YdcH being a novel transition state regulator potentially helping the cell to adapt to environmental changes, in a similar way than AbrB or SigH (Britton et al., 2002; Phillips & Strauch, 2002). First, the pattern of expression of *ydcFGH* shows that the climax of expression (presumably when YdcH is inactive) coincides with the transition between exponential and stationary phase of growth (Figure 17). This is nicely confirmed by the dramatic difference between exponential and stationary phase global gene expression profiles. These show that the huge YdcH regulon is deregulated once cells have entered stationary phase (almost no more differences between WT and Δ*ydcH*). Not surprisingly, several genes regulated by another transition state regulator, AbrB, are also affected in absence of YdcH. Second, there is a large diversity of functions affected by YdcH (Figure 18) driving to a global reprogramming of gene expression, typical of such regulators (Strauch & Hoch, 1993). Third, among these many genes, a large subset is involved in carbon or amino-acids metabolism, both being dramatically affected at the entrance into stationary phase due to the depletion of some carbon sources. Interestingly, we noticed many genes of the YdcH regulon related to the synthesis of several bacteriotoxin: *albABCDEFG* (antilisterial bacteriocin subtilosin), *ntdR* (antibiotic kanosamine), *sdpA*, *sdpI* and *yknW* (SdpC toxin) and *yydGHIJ* (control of LiaR-LiaS system as a response to bacitracin). This could be a strategy for the cell to scavenge new resources from a depleted

environment (Abriouel, Franz, Ben Omar, & Galvez, 2011). All together, our results suggest that during transition from exponential to stationary phase of growth, YdcH repression is partially released (as observed with the expression of P_{ydc1}) leading to the activation/repression of a large set of genes, potentially leading to a reprogramming of the cell. We hypothesize that YdcH acts as a transition state regulator in *B. subtilis*, maybe acting both as activator and repressor. We can imagine YdcH being active during exponential growth, repressing its own expression and that of other TRs. This would cause the activation of those TRs that would then be able to act, positively or negatively, upon the more than 300 genes that appear differentially expressed in the Δ*ydcH* strain compared to the WT during stationary phase.

To go farther in our understanding of YdcH and its function(s) and to verify our hypothesis, we should identify the DNA sequence to which it binds, the "YdcH-box", in P_{ydc1}. We could then perform an *in silico* prediction of "YdcH-boxes" in other promoters in order to attempt a more precise characterization of the YdcH regulon. If YdcH causes a broad effect in the cell, by using the genome wide approach of RNAseq, we will recover the data of all the changes produced in the cell: those that are directly linked to YdcH and those that are caused indirectly (by genes controlled by YdcH). Pull-down experiments could also give us information about YdcH's function and effectors.

4.3 A library of MreB mutants with impaired functionality

We have developed a methodology to obtain MreB mutants and screen for their loss of functionality by means of the activation of P_{mreBH}. Although it is difficult to obtain MreB*s due to spontaneous acquisition of extra mutations or suppressor mutations, we successfully constructed a collection of mutants displaying a variety of phenotypes. In the future, by using different reporters of MreB functionality, we could enlarge our library and have a complete vision of how MreB performs its activity. Addition of Mg^{+2} and sugars during the process of mutagenesis could help recovering additional mutants. Finally, these mutants will be an asset for future biochemical studies to pinpoint the biochemical properties of *B. subtilis* MreB. Protein interaction could also be investigated through pulldown experiments or yeast two hybrid.

4.4 MreB may play a role in CW synthesis, cell morphology and cell metabolism

Despite years of extended efforts, MreB's exact function(s) remains elusive. By creating a genetic screen that selects for loss-of-function MreB mutants (MreB*s) in the Gram-positive bacterium model *B. subtilis*, we were able to circumvent this problem and make links between MreB structure and function. It is difficult to extract strong conclusions from our preliminary results, but we did succeed in the acquisition of some very interesting group of MreB mutants that hint MreB has more than one function in *B. subtilis*.

Structure-function correlations allow us to extract some conclusions. Mutants B6 (G160R) and B22 (G14E), from the Δ*mreB*-like group, are localized in the putative nucleotide binding site of MreB. Combining the localization and the results that prove the loss of function of these mutations (Figure 26) we can infer that this area and possibly the nucleotide binding activity of MreB are important form the correct functioning of the protein. MreB*s B19 (G231D), B4 (G56R), from the Δ*mreB*-like group, and B32 (L171P), from the WeB group, are in close vicinity of the putative protofilament area, were MreB monomers bind to other MreB monomers to form chains. These three mutants, as the ones mentioned above, show an impaired MreB function (Figure 26 and 29). We can, therefore, deduce that this area and probably the polymerization capability of MreB are important for the proper functioning of the protein.

Interestingly, some mutants show the uncoupling of shape defect and growth impairment. Four of the WeB MreB*s (B10, B17, B30 and B46) have nearly WT morphology and MreB localization while being strongly impaired in cell growth both in CH and LB media (Figure 28). As shown using *E. coli*, LB has presumably low quantities of sugars (estimated < 100 μM). Their depletion marks the end of the exponential phase of growth, when cells switch to amino-acids consumption (Sezonov et al., 2007). When *B. subtilis* is grown in LB, a diauxie can be observed around OD~0.5, that is presumably due to the exhaustion of sugars from the medium as well. This is precisely the point at which the growth of mutants B10, B17, B30 and B46 starts to decay. B10 and B46 are localized at the surface of MreB, in close vicinity of the putative interfilament interface; B17 is localized near the putative protofilament area. Lastly, B30 is mutated in an internal residue, near the putative polymerization area. Our hypothesis is that those MreB mutations are, somehow, preventing the cell to change from glycolysis to gluconeogenesis. A tempting possibility is that MreB would act as a checkpoint linking cell metabolism and CW synthesis. It is known that MreB interacts with proteins involved in the synthesis of CW precursors (Favini-Stabile et al., 2013; Rueff et al., 2014) and we think that there is an equilibrium maintained between cytosolic and polymerized membrane-associated MreB. It could be possible that MreB acts as a sensor of cell metabolic status to coordinate CW synthesis with the needs of the cell. This could explain why the shape and growth defects could be uncoupled.

This hypothesis is further reinforced by the results obtained from mutant B32. In this case we lose both WT morphology and MreB localization (Figure 29). In addition, high concentration of Mg^{+2} recovers its shape defect, but not its growth anomalies. On the other hand, addition of sugars improves its growth without affecting its morphology. There is previously reported evidence of association between CW synthesis and cell metabolism in bacteria. It has been shown that FtsZ is sensitive to pyruvate levels and that the deletion of a gene encoding a pyruvate kinase (*pyk*) in *B. subtilis* affects Z-ring formation and, consequently, division (Monahan, Hajduk, Blaber, Charles, & Harry, 2014). Lateral CW synthesis has also been connected to cellular metabolism (Foulquier, Pompeo, Bernadac, Espinosa, & Galinier, 2011; Gorke, Foulquier, & Galinier, 2005). YvcK has two distinct roles, one in

carbon metabolism and another in CW synthesis. The modification of its phosphorylation levels uncouples both functions. While its function in carbon metabolism is not affected by its phosphorylation levels, its capacity to correctly position PBP1 is. What is even more interesting is that YvcK, when overproduced, is capable of rescuing the Δ*mreB* mutant.

With all these data in mind, we hypothesize that MreB may act as a checkpoint between lateral CW synthesis and cell metabolism. MreB could have a second function in amino-acids metabolism that is being altered by our WeB mutations. The addition of sugars would allow these mutants to overcome the negative effects of having an altered amino-acids metabolism. Further verification will be done towards the identification of the specific metabolism process linked to MreB. We will grow the WeB MreB*s, were we have uncoupled MreB's role in cell morphology and cell metabolism, in defined minimal media supplemented with different carbon sources. We will also take advantage of the MreB mutant B32 that grows as the WT strain in LB to elucidate what is needed for that mutant to recover WT-like cell morphology and MreB dynamics.

4.5 Some MreB*s have atypical colony morphologies

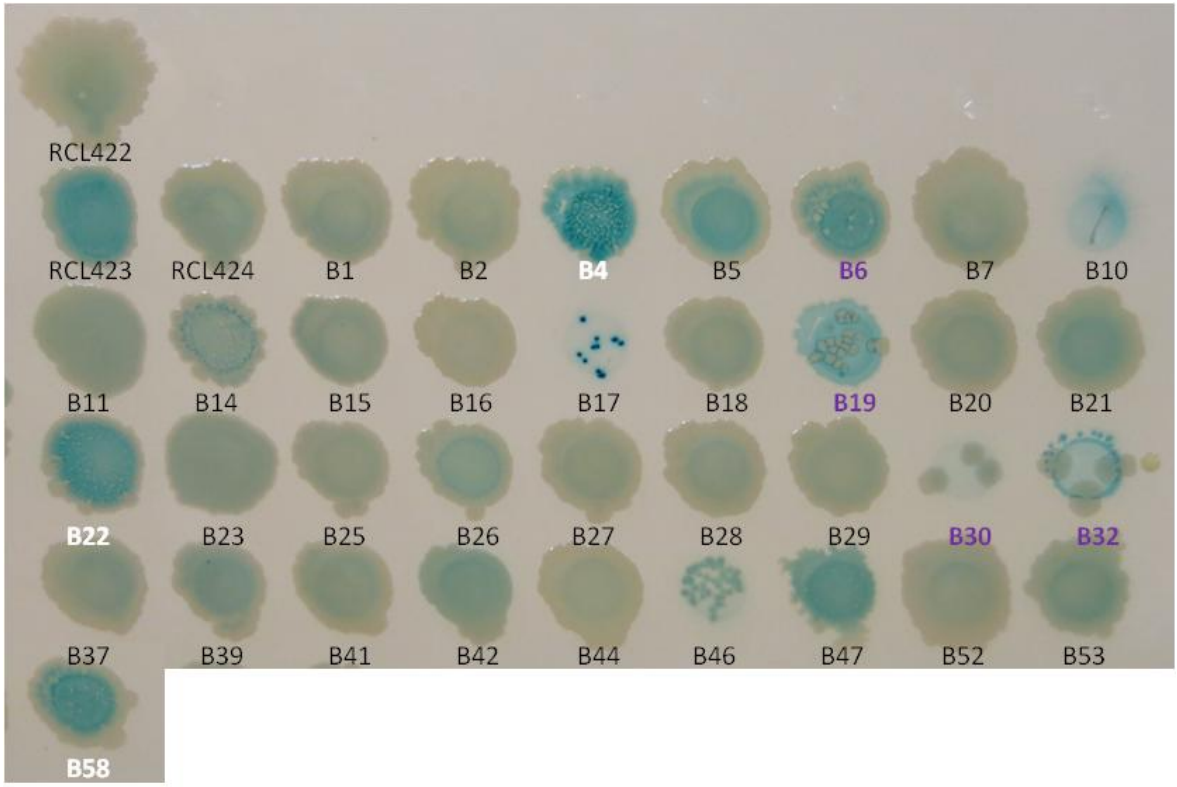

Figure 32 Development of divergent colony morphologies after extended growth. After > 24 h of growth of MreB*s on LB-agar plates, three different phenotypes start to develop: while most colonies keep a smooth and regular appearance, B4, B22 and B58 (white) display a wrinkled surface wnd B6, B19, B30 and B32 (purple) develop white overgrowing colonies that do not activate P_{mreBH}*lacZ*, suggesting the appearance of suppressor mutations.

When colonies of MreB*s are incubated on LB-agar plates for > 24 h at 37 °C, various colony phenotypes develop. Mutants B6 and B19 (from the Δ*mreB*-like group) and mutants B30 and B32 (from the WeB group), develop overgrowing colonies that do not turn on the reporter gene, probably through the acquisition of spontaneous mutations (Figure 32). It has been demonstrated that stress conditions increase the appearance of mutations in bacteria (Bridges, 1997; Hall, 1990) and that this process is boosted during stationary phase of growth (Sung & Yasbin, 2002). Thus, it is tempting to imagine that the stress induced by the presence of those MreB*s may, in turn, increase the mutation rate, favoring the appearance of suppressor mutations. It would be interesting to sequence these overgrowing colonies to verify where the spontaneous mutations occur and why the MreB* benefits from them.

Another observed anomaly is the "wrinkling" of the colony surface of mutants B22, B58 and, most strongly, B4 (all three from the Δ*mreB*-like group). The wrinkling of a colony surface has been shown to be linked with the formation of areas of increased cell death in the colony (Haussler & Fuqua, 2013) or with biofilm and motility defects (Bridier et al., 2011). This could be a possibility to investigate with these mutants.

4.6 Possible connection between the *mreB* deletion and the *ydcH* frame-shift

On the onset of this project was the specific induction of the *ydcFGH* operon observed in absence of *mreB*, calling for elucidation of the function of this potentially specific effector of MreB, as well as its mode of induction. The outcome, in the last weeks of the doctorate, was unexpected.

The strain 3725 is supposed to be a direct parent of the wild type *B. subtilis* 168, and has been used for many years in European labs on the field. Noticing several familiar mutations in the list of SNPs, we realized that one of these mutations, $SepF^{M11T}$ was reported to be required for *B. subtilis* to form L-forms (Dominguez-Cuevas, 2011), while several others (*sigI, walR, accC*) affect genes known or suspected to be involved in L-form and/or to be suppressor genes of *mreB* defects (Dominguez-Cuevas, 2011; Schirner, 2009; Mercier, 2013).

Although it was not possible to completely track the chain of events leading to the appearance of so many mutations in strain 3725, they all appeared in a time and location (Oxford) were L-form and the essential gene *mreB* were studied. It is then conceivable that they were unwittingly selected as suppressors. At the moment, it is unknown if the frameshift mutation in *ydcH* was fortuitous or selected because it improves the Δ*mreB* phenotype. But one can speculate that, if YdcH plays a role in state regulation facilitating the adaptation of the cell to changing conditions including carbon depletion as in phase transition (acting on ~60 genes involved in carbon metabolism) and if MreB is linking cell growth to carbon metabolism (see MreB mutagenesis section), then, this mutation may increase the

survival of the Δ*mreB* strain by modifying carbon and/or amino-acids metabolism and may not be incidental.

6. Appendices

Appendix 1: Phenotypic analysis of *ydcFGH*

Note to readers: the following experiments were realized with two marker-less ydcF *and* ydcG *mutants and a deletion-replacement mutant of* ydcH. *The two marker-less mutants were shown lately to have a different genetic background than the reference wild-type strain. As such, the present results can't be interpreted as the result of the deletions and for this reason were removed from the main text. They are presented here as purely informational regarding the work produced during the PhD.*

Following the construction *ydcF*, *ydcG* and *ydcH* mutants, a phenotypic analysis of these genes was undertaken by studying the effects of their deletion on a number of conditions: growth in different media, sporulation and competence. We also verified if they had morphological defects as they may be related to the morphogene *mreB*.

A1.1 *ydcF*, *-G* and *–H* deletion mutants are not impaired for cell morphology

MreB is a morphogene; when deleted, cells start to swell and deform until they lyse. As the expression of *ydcFGH* is activated in absence of MreB, we thought that the three genes might have a role in cell morphology maintenance. Deletion mutants of each of the genes were grown in MSM and CH media at 37 °C. Cell width were measured on phase contrast images acquired during exponential growth of these strains in MSM and both during exponential growth and stationary phase in CH media (Figure A1.1). In poor MSM medium a relatively high variability in cell width was observed and no significant differences between strains could be detected. However, a significantly thinner width was observed for *ydcF* and *ydcG* mutants compared to WT and Δ*ydcH* strains when grown in rich CH medium both in exponential and stationary phase.

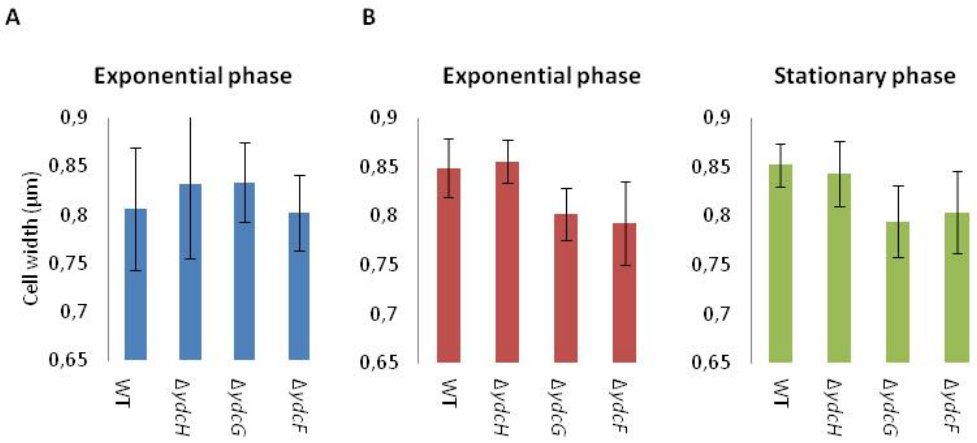

Figure A1.1 Width measurements of deletion mutants of *ydcF*, *ydcG* and *ydcH*. A. Cell width of WT (ABS2005), Δ*ydcF* (ASEC60), Δ*ydcG* (ASEC58) and Δ*ydcH* (ASEC56) strains during exponential phase of growth in MSM media. **B.** Cell width of the same strains during exponential and stationary phase in CH media.

A1.2. Defects during stationary phase

We next tested the deletion mutants for potential growth defect in various conditions. Extensive growths were recorded, from exponential to late stationary phase, in a set of complex and defined medium (see materials and methods for details). As shown on Figure A1.2, optical density of Δ*ydcF* and Δ*ydcG* cultures decrease during stationary phase in CH and MSM media, suggesting cell lysis. Note that this pattern is very similar to that observed with Δ*mreB* strain in CH (see results chapter MreB mutagenesis).

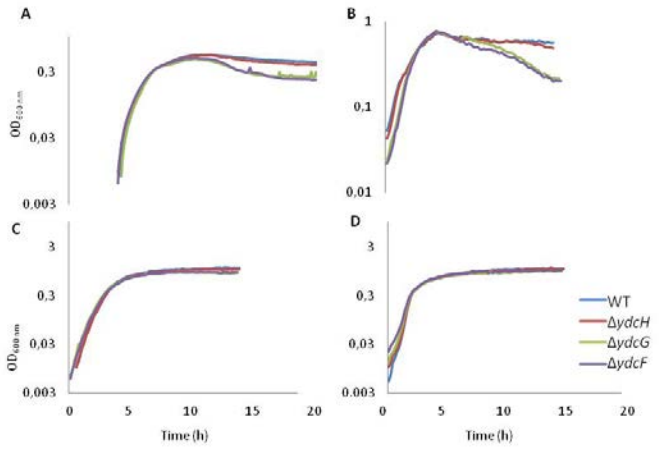

Figure A1.2 Growth of deletion mutants of *ydcF*, *ydcG* and *ydcH* in different media. WT (ABS2005), Δ*ydcF* (ASEC60), Δ*ydcG* (ASEC58) and Δ*ydcH* (ASEC56) strains were grown in CH media (**A**), MSM media (**B**), MC media (**C**) and LB media (**D**). Δ*ydcG* and Δ*ydcF* lyse during stationary phase when grown in CH and MSM media.

Then, we wondered if cell viability could be affected during stationary phase. To test this, we measured colony forming units of samples harvested at different points during cell growth: exponential, entry to stationary phase and late stationary phase (see materials and methods; Figure A1.3). Unfortunately, the accuracy of this approach was not sufficient to detect the difference observed with OD measurement.

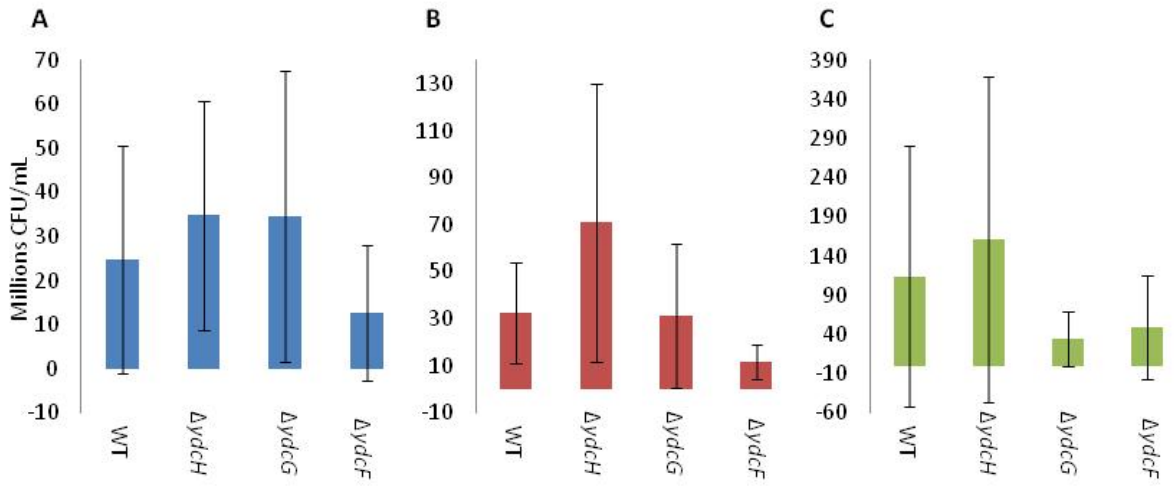

Figure A1.3 Viability of deletion mutants of *ydcF*, *ydcG* and *ydcH* in CH. Colony forming units per mL of culture were estimated by plating aliquots of WT (ABS2005), Δ*ydcF* (ASEC60), Δ*ydcG* (ASEC58) and Δ*ydcH* (ASEC56) strains harvested during exponential (**A**), entry into stationary phase (**B**) and late stationary phase (**C**).

A1.2.1 Sporulation

We reasoned that the observed decreased in OD during stationary phase may reflect a change in these strains in their ability to undertake one or several of the processes that take place during stationary phase. Indeed, at the entry into stationary phase, *B. subtilis* cells can follow different developmental pathways, helping them surviving in changing environments, such as competence for DNA transformation or sporulation (Maughan & Nicholson, 2004).

We first focused on sporulation because the process involves at late stages the release of a mature spore and the lysis of its nurturing mother cell, that could impact the OD. As shown on Figure A2.4A, mutants of *ydcF* and *ydcG* present a two to three fold increase in sporulation efficiency. WT *B. subtilis* are known to produce 10-50% spores (strain and medium depending) in optimal conditions due to a complex regulatory pathway allowing a fraction of the population to escape this long and costly process (Piggot & Hilbert, 2004). But the spores produced are virtually all viable. Consequently, an increase in spore frequency suggested a more efficient induction of the process, leading to a higher number of cells entering the sporulation pathway.

A	Spore frequency (%)	Number of spores (10^7/ml)
WT	56.7 ± 39	2,3
Δ*ydcH*	28.5 ± 25	3,44
Δ*ydcG*	105.3 ± 64	5,85
Δ*ydcF*	165.6 ± 80	8,5

B	Transformation rate	Ratio WT/*
WT	1,24E-05 ± 1,57E-05	
Δ*ydcH*	1,26E-05 ± 1,23E-05	3,02 ± 4,18
Δ*ydcG*	2,62E-04 ± 3,20E-04	0,33 ± 0,46
Δ*ydcF*	1,28E-03 ± 3,38E-04	0,01 ± 0,02

Figure A1.4 Stationary phase processes are affected in *ydcF*, and *ydcG* mutants. A. Sporulation assays were performed on WT (ABS2005), Δ*ydcF* (ASEC60), Δ*ydcG* (ASEC58) and Δ*ydcH* (ASEC56) strains as described in the method section, using the exhaustion method. Briefly, samples of 30h old cultures were plated before (giving the total number of cells) and after (giving the number of spores) heat kill. Spore frequency (spores/viable cells) and spore counts are calculated from CFU. **B**. Competence assays were performed on the same strains and as described in the method section. Briefly, samples were grown in competence media and plates in LB plates (giving total number of cells) and in LB plates supplemented with the antibiotic resistance that was introduced (giving the number of transformants). Transformation rate (transformants/total cells) was calculated from CFU.

A1.2.2 Competence

We finally decided to assay our mutants for their proficiency in developing natural competence for DNA transformation. This is a well-known ability of *B. subtilis* that develops in a subpopulation of cells at the entry of stationary phase in specific conditions (for review, see (Dubnau, 1991)). Our lab recently shows that absence of MreB affects the efficiency of transformation, albeit indirectly (Mirouze et al., 2015). Since we observed a difference in *ydcFGH* expression in a *mreB* deletion mutant, we wondered if the operon could play a role in competence development. Competence was tested through the two step method (see material and methods) in each deletion mutant: Δ*ydcF*, Δ*ydcG* and Δ*ydcH*. As presented on Figure A1.4B. The results obtained from these experiments were highly variable, which is demonstrated by the values of the error deviations.

Once we realized that strains mutant for *ydcF* and *ydcG* had a different genetic background than our WT *B. subtilis* strain, Δ*ydcF* and Δ*ydcG* were reconstructed (ASEC325 and ASEC327, respectively; see methods). Sporulation experiment assays as well as growth in MSM, CH and LB medium were repeated. No sporulation increase and no stationary phase survival defect could be detected with these strains, strongly suggesting that the differences observed in ASEC58 and ASEC60 were indeed due to differences in the strain background. We noticed that in this alternative background, the absence of several *rap* genes, notorious sporulation inhibitors (Pottathil & Lazazzera, 2003) whose deletion increase the ratio of sporulating cells. Thus, the absence of such genes is the most probable reason for the phenotypic differences observed.

Appendix 2: The absence of MreB is not responsible for P_{ydc1} induction

Note to readers: the study of the ydcFGH *operon was initiated because of its induction in the ⊿*mreB *background, suggesting a regulatory link between these two loci. After a long -genetic- hunt, we concluded that the induction of* ydcFGH *was in fact unlinked to* mreB*, and caused by one of the many mutations present, to our surprise, in strain 3725, most probably a frameshift in* ydcH*. We decided to present in the main text only the conclusion to this search. Here are presented in detail the various hypotheses and experiments realized that drove us to this unexpected result.*

As described on the results chapter *ydcFGH*, the reporter P_{ydc1}*lacZ* was not expressed on a WT context (strain ABS1990) and showed an increase in absence of *mreB* (strain ABS2054). As a reminder, the *mreB* gene is present in a three gene operon with two other essential genes, *mreC* and *mreD.* A whole genome transcriptional study from Nicolas *et al*. (Nicolas et al., 2012) also suggests the existence of longer transcripts originating from the *maf* promoter and going to the downstream *minCD* operon (Figure A3.1A).

A2.1. Absence of *mreB* complementation is not due to chromosomal positioning of the gene

To our surprise, we first noticed that an ectopic complementation at the *amyE* locus by either an inducible copy of *mreB* fused to *gfp* (*amyE*::P_{xyl} *gfpmreB*; strain ASEC9) or the *mreB* gene under its natural promoter (*amyE*::P_N *mreB*; strain ASEC16) failed to restore the repression of P_{ydc1} (Figure A3.1B.I). We then tested the possibility that the failed complementation could be due to the position of the ectopic locus (*amyE*) on the chromosome, potentially affecting the levels of MreB. Indeed, *amyE* is situated close to the origin of replication (position 327 618-329 597), *oriC*, while *mreB* is located at position 2 861 748-2 860 735. It is known that due to multiple replication forks, genes closer to *oriC* are in higher copy number than the ones close to the terminus, a property exploited by cells to adjust protein levels (Slager & Veening, 2016). To test this hypothesis, we expressed *mreB* from another locus, *bkdB*, a gene positioned very near *mreB* in the *B. subtilis* chromosome (position 2 498 070-2 496 796). Again, when *mreB* was expressed alone, the complementation failed and P_{ydc1} was overexpressed (Figure A3.1B.II; strains ASEC234 and ASEC236).

A *mreB* locus map

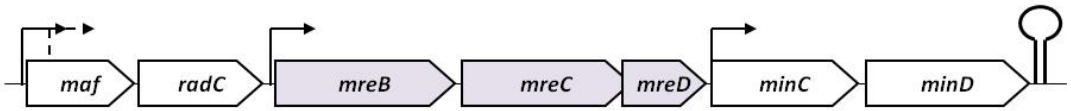

mreB (3725) mutant map

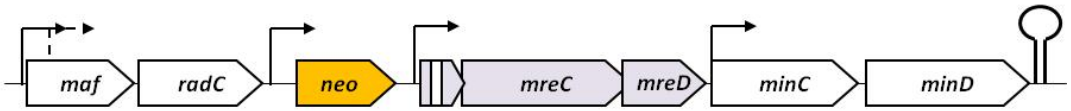

B

	maf-radC-mreB-mreC-mreD-minC	*amyE*	*bkdB*	Activation of P_{ydc1}
I	WT			-
	gfp-mreB			-
	km-mreB			-
	ΔmreB			+
	ΔmreB	P_{xyl}-*gfp-mreB*		+
	ΔmreB	P_N-*mreB*		+
II	*ΔmreB*		P_{xyl}-*gfp-mreB*	+
	ΔmreB		P_N-*mreB*	+
III	*ΔminC*			-
IV		*km*-P_{xyl}-*pep*		-
V	*ΔmreBCD*	P_N-*mreB-mreC-mreD*		-
	ΔmreB	P_N-*mreB-mreC-mreD*		+
VI	*ΔmreC*			-
VII	*mreCΩ*P_{xyl}-*gfp-mreC-mreD*			-
	mreDΩP_{xyl}-*gfp-mreD*			-
		P_{xyl}-*gfp-mreC*		-
		P_{xyl}-*gfp-mreD*		-

Figure A2.1 *B. subtilis* constructs bearing the reporter P_{ydc1}*lacZ*. A. Schematic view of the *mreB* locus and its neighboring genes in the wild type and the 3725 mutant strains. Results from (Nicolas et al., 2012) indicate that transcripts containing *mreB* originate upstream from *mreB* and *maf*, and extend up to *minD*. **B**. Various constructs made to link P_{ydc1} expression to the *mreB* locus. First column describes changes (deletions or cloning) at the *mreB* locus; the two middle columns show ectopic clonings at the *amyE* and *bkdR* loci; right column indicates the phenotype (induction of P_{ydc1}) of each corresponding strain as assayed by X-gal plating test (see materials and methods).

A2.2. *ydcFGH* induction is not due to decreased expression of *minC*

We then considered that the deletion of *mreB* could affect the expression levels of the downstream *minCD* genes which, in turn, could induce the overexpression of *ydcFGH*. However, deleting *minC* while leaving the *mreBCD* locus untouched (strain ASEC342) did not activated P_{ydc1} (Figure A3.1B.III).

A2.3. *ydcFGH* induction is not caused by the expression of a remnant peptide of MreB

Next, we wondered if the deletion of *mreB*, that had left a short peptide, could have a dominant effect on the expression of *ydcFGH*. Indeed, to avoid potential influence on the expression of the downstream essential *mreC* and *mreD* genes, *mreB* deletion mutant had been built without replacing the gene by an antibiotic resistance cassette. Instead, most of *mreB* was removed and a resistance gene to neomycin (*neo*) was cloned upstream of the *mreB* promoter to allow its selection (Formstone & Errington, 2005). During this process, the 30 N-terminal and 34 C-terminal nucleotides of *mreB* were kept but we discovered in between a small 21 nucleotide sequence of unknown origin. To test if the resulting DNA fragment (encoding a 28 amino-acid long peptide) was producing a perturbing RNA or peptide, we cloned a DNA fragment from *neo* up to *mreC* at the ectopic *amyE* locus under the control of P_{xyl} in a strain where the *mreBCD* locus was untouched (*amyE*::*km*-P_{xyl}-*pep*; strain ASEC266). This construction did not activate the expression of *ydcFGH* (Figure A3.1B.IV).

A2.4. *ydcFGH* induction is not caused by abnormal levels of MreCD

Intriguingly, we noticed that the repression of P_{ydc1} was maintained in cells expressing the entire *mreBCD* operon under its own promoter from the *amyE* locus, and deleted for the whole native *mreBCD* operon, while P_{ydc1} was highly activated in cells deleted for *mreB* only (Figure A3.1B.V; strains ASEC40 and ASEC20). We therefore hypothesized that an abnormal MreB/CD ratio could be the cause for P_{ydc1}'s induction. To test this, we first created a deletion of *mreC* (*mreD* is strictly essential but a *mreC* deletion can be made in the presence of high Mg^{+2} concentrations), but again, no induction of the P_{ydc1} was observed in this construct (Figure A3.1B.VI; strain ASEC7).

Since on our previous construct the cells where P_{ydc1} was induced carried two copies of *mreC* and *mreD*, we then wondered if the overexpression of *mreC*/*mreD* rather than the absence of them could cause the induction of P_{ydc1}. To check this possibility, we looked at the activation of P_{ydc1} when the expression of *mreCD* (strain ASEC115) or *mreD* (strain ASEC168) were under the control of a xylose dependent promoter at natural locus. Under these conditions, the *ydcFGH* operon wasn't overexpressed (Figure A3.1B.VII). As a second verification, we expressed GFPMreC/GFPMreD with a P_{xyl} promoter at *amyE* (*amyE*:: P_{xyl}-*gfpmreC*, strain ASEC109 and *amyE*:: P_{xyl}-*gfpmreD*, strain ASEC111) leaving the *mreBCD* locus untouched. By having an extra copy of the genes in addition to the gene at locus we were sure to have an excess of MreC/MreD in the cell. Again, P_{ydc1} wasn't activated in any of these genetic backgrounds either (Figure A3.1B.VII).

A2.5. Absence of the MreB protein is not the cause of *ydcFGH* induction

Altogether, these results indicated that the deletion in the *mreB* transcript rather than absence of the MreB protein was responsible for P_{ydc1} induction. To test this, a mutant was generated in which 3 stop codons were introduced at the beginning of the *mreB* orf -at the natural locus- (Figure A3.2B), in order to prevent protein synthesis with minimal perturbation of the *mreBCD* transcript (strain CCBS194). The absence of MreB synthesis in this strain was confirmed by western blotting using anti-MreB antibodies (Figure A3.2C, see materials and methods). In this construct, where the entire *mreBCD* transcript remains untouched to the exception of these three added codons, P_{ydc1} was not induced. These results apparently confirmed our hypothesis.

Suspecting a regulatory RNA to be the source of this regulation, and to pinpoint the area of the transcript responsible for it, we planned to create deletions of various sizes of the *mreB* orf. Surprisingly, the first construct obtained, combining the almost complete *mreB* deletion (strictly identical to that present in the Δ*mreB* strain (3725)) with the 3 stop codons did not induce P_{ydc1}; indicating that the deletion of *mreB* was not responsible for the phenotype either (Figure A3.2D; strain CCBS202).

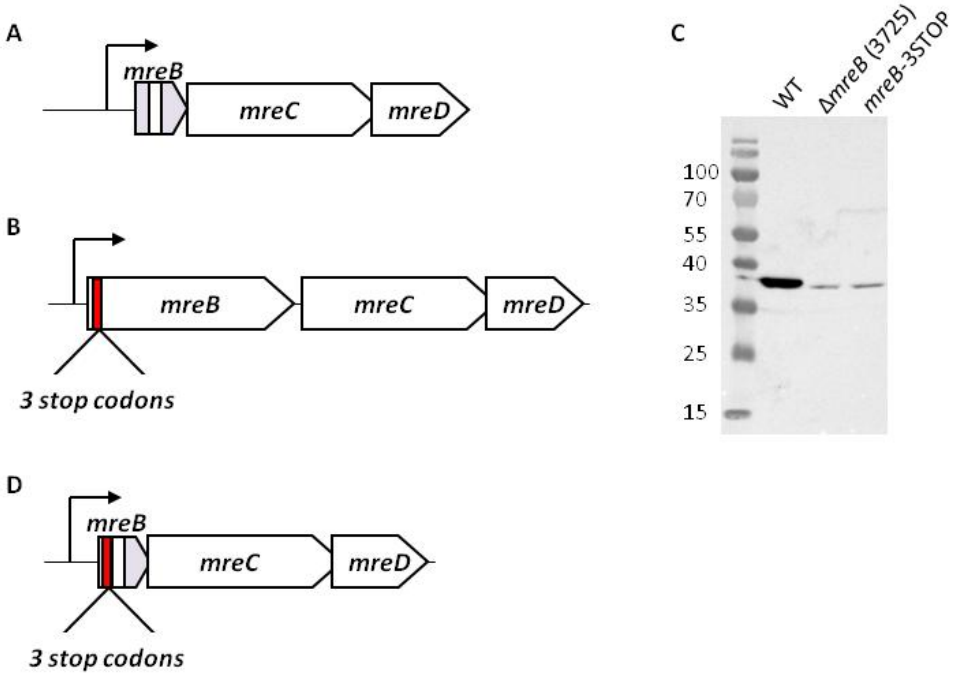

Figure A2.2 Construction of *B. subtilis* strains inactivated for *mreB*. A. Genetic map of the *mreB* locus in strain 3725. *mreB* was inactivated by removing nucleotides 31 to 977 and addition of 21 extragenic base pairs. **B**. Genetic map of the *mreB* locus in strain CCBS194. MreB synthesis was abolished by introducing 3 stop codons after the sixth base-pair of *mreB*. **C**. Western blot of strain CCBS194 (*mreB*-3STOP) showing the absence of MreB synthesis, comparable to that of strain 3725. **D**. Genetic map of the *mreB* locus in strain CCBS202 . In this strain, the 3 stop codons introduced in strain CCBS194 were combined with the deletion present in strain 3725.

A2.6. *ydcFGH* induction is unlinked to the *mreB* locus

This result being in complete disagreement with the results so far, we decided to check the genetic link between *mreB* and the induction of *ydcFGH*. For this, we either transformed strain Δ*mreB* (3725) with chromosomal DNA of the strain bearing the reporter fusion (ABS1990) or transformed ABS1990 with chromosomal DNA of strain 3725. When the reporter was passed into 3725, the reporter was systematically induced, indicating the overexpression of *ydcFGH*, as previously observed. When the reverse transformation was performed, none of the resulting clones displayed any induction of the reporter suggesting that the locus responsible for P_{ydc1} *lacZ* induction was not genetically linked to *mreB*.

We then sequenced the *ydcFGH* locus, who became an obvious candidate based on our transcriptional study (see results chapter *ydcFGH*), and found a frameshift mutation lying in the middle of *ydcH*. According to our results, inactivation of *ydcH* leads to induction of the expression of P_{ydc1}, thus such frameshift has a very high probably to explain the observed induction. Out of curiosity, we sequenced in parallel another locus of interest, *walR*, in which spontaneous mutations had been selected in the Δ*mreB* strain 3725 (Dominguez-Cuevas et al; Chastanet et al unpublished). To our surprise, strain 3725 carried also a mutation in this gene. We wondered how many mutations this long-used strain could be carrying, and undertook its complete sequencing. This revealed, to our astonishment, the presence of > 50 mutations.

Appendix 2: Differentially expressed genes in the Δ*ydcH* strain

Overexpressed genes in Δ*ydcH* during exponential growth				
Gene	**Expression difference**	**Function1**	**Function2**	**Regulated by**
ydcF	71,73	Unknown		
ydcG	17,56	Unknown		
yozL	14,32	Unknown		LexA
yosU	8,08	SP-beta prophage		
ykoL	6,46	Unknown		PhoP and TnrA
bhlB/yomA	6,45	SP-beta prophage		
yckD	6,38	Sporulation		SigF and SigG
cotC	6,28	Sporulation	spore coat protein	GerE, SigK and SpoIIID
cotX	5,96	Sporulation	spore crust assembly	GerE, GerR, SigE and SigK
yozH	5,77	Unknown		
yocC	5,47	Unknown		
ydjM/yzvA	5,39	Cell wall	May be involved in cell wall metabolism (WalR regulon)	WalR and PhoP
yonR	5,29	Regulation of gene expression	Xre family TR	
lrpA/yddO	5,26	Regulation of gene expression	Repression of glyA transcription and KinB-dependent sporulation	
sdpA/yvaW	5,21	Toxins, antitoxins and immunity against toxins	maturation of the SdpC toxin	AbrB, Rok and Spo0A
ykzB	4,99	Unknown		TnrA
yqbG	4,94	Skin element		
yjdG	4,87	Unknown		AbrB
yydH	4,86	ABC transporter	Control of LiaR-LiaS activity, processing of YydF	AbrB and Rok
ggaA	4,64	Biosynthesis of teichoic acid	Galactosamine-containing minor teichoic acid biosynthesis	
yabE	4,50	Cell wall	Similar to CW binding prot	Cis-acting RNA dependent on SigX and SigM
yydG	4,50	Regulation of gene expression	control of LiaR-LiaS activity	AbrB
yjzI	4,47	Unknown		
abrB/cpsX/tolB	4,34	Regulation of gene expression		
yopF	4,33	SP-beta prophage		
yxlA	4,32	Biosynthesis/acquisition of nucleotides		
yotD	4,25	SP-beta prophage		CsoR
tagA	4,24	Biosynthesis of teichoic acid		PhoP and WalR
yonS	4,23	SP-beta prophage		
ydzP	4,22	Unknown		
yisI	4,16	Protein phosphatase	Spo0A-P phosphatase, control of the phosphorelay	PchR
yoaQ	4,16	Unknown		
ypzA	4,13	Sporulation proteins		SigG

Overexpressed genes in Δ*ydcH* during exponential growth (continuation)				
Gene	**Expression difference**	**Function1**	**Function2**	**Regulated by**
pyrP	4,13	Transporters	uracil permease	PyrR
yopO	4,12	SP-beta prophage		
ygzA	4,10	Unknown		
S717/SR5	3,99	Anti-toxin	Antisense RNA to bsrE	
yjcM	3,91	Unknown		SigD, AbrB
ybeF	3,90	Unknown		
yknT/cse15	3,88	Sporulation Protein		SigE, SpoIIID
yozF	3,87	Unknown		
cotM/yneL	3,87	Sporulation proteins	resistance of the spore	SigE, SigK, GerE
yydI	3,86	ABC transporters	control of LiaR-LiaS activity	AbrB and Rok
immR/ydcN	3,86	Regulation of gene expression	Control of transfer of the mobile genetic element ICEBs1	
ybzH	3,84	Prophage 1		
tagB	3,84	Biosynthesis of teichoic acid		PhoP and WalR
xre	3,83	Regulation of gene expression	regulation of PBSX prophage gene expression (Xre family)	
ydcP	3,83	Prophages	Conjugation and replication of ICEBs1, helicase processivity factor	
yybL	3,82	ABC transporters	Permease	Rok
yugI	3,81	Unknown		RelA
rpsT/yqeO	3,81	Ribosomal proteins	ribosomal prot S20 (BS20)	
yddK	3,76	Unknown		
yotE	3,75	SP-beta prophage		
yhjM/ntdR	3,73	Biosynthesis of antibacterial compounds		AbrB
yopN	3,73	SP-beta prophage		
yneF/yoxG	3,73	Unknown		SpoOA
yoyI	3,72	SP-beta prophage		
yokC	3,72	SP-beta prophage		
yobD	3,69	Regulation of gene expression	similar to TR Xre family	
yoyA	3,68	Unknown		
ymzD	3,68	Unknown		
yqbC	3,68	Skin element		
yybM	3,66	Unknown		Rok
albG/ywhM	3,64	Biosynthesis of antibacterial compounds	Production of subtilosin	AbrB, ResD and Rok
yjzD	3,62	Unknown	putative toxin-antitoxin	
trnB-Met3/trnB-Ile1/trnE	3,62	tRNA	Transfer RNA-Met	
yozQ	3,61	Sporulation proteins		SigG
ypzI	3,61	Unknown		
degR/prtR	3,58	Regulation of degradative enzyme production	Positive effector of DegU-phosphate stability	SigD
yjiA	3,57	Unknown		

Overexpressed genes in Δ*ydcH* during exponential growth (continuation)				
Gene	**Expression difference**	**Function1**	**Function2**	**Regulated by**
ykvS	3,57	Unknown		
ykzT	3,57	Unknown		
pyrR	3,56	Biosynthesis/ acquisition of pyrimidine nucleotides	Transcriptional antiterminator of the pyr operon	PyrR
yorC	3,54	SP-beta prophage		LexA
sacV/ydzC/xis	3,54	Prophages and mobile genetic elements	Excision of the conjugative transposon ICEBs1 from the trnS-leu2 locus	ImmR
yrzM	3,53	Unknown		
yopM	3,52	SP-beta prophage		
lrpB/yddP	3,51	Regulation of gene expression	Repression of glyA transcription and KinB-dependent sporulation	
yxaC	3,50	Unknown	Holin-like auxiliary protein	
rpmGB/rpmG	3,49	Ribosomal proteins	Ribosomal protein L33b	
ynaE	3,49	Unknown		
phrE	3,48	Regulation of gene expression	Phosphatase (RapE) regulator	AbrB, CcpA, CodY, ComA and SigH
yokB	3,47	SP-beta prophage		
rpmB/yloT	3,45	Ribosomal proteins	ribosomal protein L28	
trnD-Ser/trnR	3,44	tRNA	Transfer RNA-Ser	
yxkC	3,43	Unknown		SigD and TnrA
ydcO	3,42	Unknown		
yybN	3,40	Unknown		Rok
immA/ydcM	3,40	Proteolysis	Ccontrol of ImmR activity, site-specific protease	
ylbN	3,39	Unknown	may be required for accumulation of 23S rRNA	
gerD	3,37	Unknown	Scaffold of the germinosome	SigF and SigG
ybfE	3,33	Unknown		
ydcL/int	3,32	Prophages	Excision of the conjugative transposon ICEBs1	
ggaB	3,31	Biosynthesis of teichoic acid	Galactosamine-containing minor teichoic acid biosynthesis	
ykyB/kre	3,31	Genetic competence	ComK repressor	ComK
ydfL	3,30	Regulation of gene expression		
yaaC	3,28	Sporulation protein		
yeeD	3,27	Unknown		
yopR	3,26	SP-beta prophage		
ydeB	3,26	Regulation of gene expression		
yoyJ	3,26	SP-beta prophage		
dps/ytkB	3,21	Acquisition of iron	Miniferritin	SigB
tagD	3,17	Biosynthesis of teichoic acid	Glycerol-3-phosphate cytidylyltransferase	PhoP and WalR
tagC/dinC	3,17	Biosynthesis of teichoic acid		LexA

Overexpressed genes in Δ*ydcH* during exponential growth (continuation)				
Gene	**Expression difference**	**Function1**	**Function2**	**Regulated by**
yopP	3,17	SP-beta prophage		
secE	3,16	Protein secretion	Protein translocase	
yncB	3,16	Unknown		
trnD-Trp/trnR	3,16	tRNA	Transfer RNA-Trp	
yonI	3,14	SP-beta prophage		
yopE	3,10	SP-beta prophage		
ydjO	3,09	Cell envelope stress proteins		SigW
yopA	3,08	SP-beta prophage		
sigX/ypuM	3,07	Sigma factors	Resistance to cationic antimcrobial peptides, RNA polymerase ECF-type sigma factor SigX	SigX and YvrHb reg; induced in stationary phase due to the production of toxic peptides (SdpC, SkfA)
pbuO/ytiP	3,06	Transporters	Paralog of PbuG	PurR
yraH	3,05	Unknown		
yhcN	3,05	Sporulation proteins		SigF and SigG
yopQ	3,04	SP-beta prophage		
yqaE/sknR	3,04	Skin element	transcriptional repressor (Xre family); essential in WT due to overexpression of the toxic proteins YqaH and YqaM	
yqkE	3,03	Unknown		
sdpI/yvaZ	3,02	Toxins, antitoxins and immunity against toxins		AbrB and SdpR
yydJ	3,00	ABC transporters	Control of LiaR-LiaS activity	AbrB and Rok
ypoP	3,00	Transcription factors and their control		
yopK	2,99	SP-beta prophage		
trnD-Cys/trnR	2,97	tRNA	translation, transfer RNA-Cys	
yvnA	2,97	Unknown		AbrB and CcpA
yjfB	2,97	Unknown		SigD
yezA	2,96	Unknown		
ligB/yoqV	2,96	SP-beta phage replication	DNA ligase (ATP dependent)	
rapI/yddL	2,96	Protein phosphatases	Control of transfer of the mobile genetic element ICEBs1	ComA
yfzA	2,96	Unknown		
rpsO	2,95	Ribosomal proteins	Ribosomal protein S15	
hbs/dbpA/hubA	2,92	DNA condensation/segregation	Non-specific DNA-binding protein Hbsu, DNA packaging	LexA and SigH
yxxD	2,92	Toxins, antitoxins and immunity against toxins based on similarity	Antitoxin	
ydeH	2,89	Unknown		AbrB
mgsR/yqgZ	2,86	Transcription factors and their control	Transcriptional regulator of a subset of the SigB general stress regulon, required for protection against oxidative stress	SigB and MgsR

Overexpressed genes in Δ*ydcH* during exponential growth (continuation)				
Gene	**Expression difference**	**Function1**	**Function2**	**Regulated by**
S903/rpmGC	2,83	Replaces L33 under conditions of zinc depletion		Zur
yonV	2,82	SP-beta prophage		
yoeC	2,81	Unknown		
yydD	2,80	Unknown		
yxjA/nupG	2,78	Transporters	Purine nucleosides transporter	G-box
yobL	2,78	Toxins, antitoxins and immunity against toxins/based on similarity		
yrdC	2,78	Unknown		
yorJ	2,78	SP-beta prophage		
yqaS	2,78	Skin element		SigD
mntR/yqhN	2,77	Trace metal homeostasis (Cu, Zn, Ni, Mn, Mo)	Regulation of manganese transport, transcriptional regulator (DtxR family)	MntR
sinR/sin/flaD	2,76	Transcription factors and their control	Transcriptional regulator (Xre family) of post-exponential-phase responses genes, control of biofilm formation	AbrB, ScoC and Spo0A
comC	2,74	Genetic competence	Late competence gene required for processing and translocation of ComGC, ComGD, ComGE and ComGG	ComK
yfmI	2,74	Transporters		AbrB and Spo0A
comK	2,74	Genetic competence	Competence transcription factor (CTF)	AbrB, CodY, ComK, DegU, Rok and Spo0A
yopC	2,72	SP-beta prophage		
yonT	2,72	toxins, antitoxins and immunity against toxins/ based on similarity	toxin	
yvzA	2,72	Unknown		
yqgW	2,71	Unknown		
ybfF	2,70	Unknown		
ywpF	2,70	Unknown		
ydeI	2,70	Unknown		
yosT	2,70	SP-beta prophage		
yhfM	2,70	sporulation proteins		
yqzF	2,68	Unknown		
sda	2,68	Phosphorelay	Sporulation inhibitor by preventing Spo0A-P	
ycxB	2,67	Unknown		
yfnC	2,65	Resistance against toxins based on similarity	similar to fosfomycin resistance protein	
ykvN	2,64	Transcription factors and their control	MarR/DUF24 family transcription regulator	
yorM	2,64	SP-beta prophage		
ynaB	2,63	Unknown		
yorE	2,61	SP-beta prophage		
ypbS	2,60	Unknown		
yurQ	2,60	Unknown		

Overexpressed genes in Δ*ydcH* during exponential growth (continuation)				
Gene	**Expression difference**	**Function1**	**Function2**	**Regulated by**
yorB	2,58	SP-beta prophage		
yozV	2,58	Unknown		
yceK	2,56	transcription factors and their control	similar to transcriptional regulator (ArsR family)	
yotM/yodV	2,56	SP-beta prophage		
yubF	2,54	Unknown		
yorS	2,54	SP-beta prophage		
yrkD	2,53	Unknown	similar to TR copper sensor	
yomO	2,49	SP-beta prophage		
yoqL	2,49	SP-beta prophage		
yobK	2,48	Toxins, antitoxins and immunity against toxins based on similarity	Inhibition of the cytotoxic activity of YobL	
tnrA/scgR	2,45	Biosynthesis, acquisition of amino acids	Transcriptional pleiotropic regulator (MerR family) involved in global nitrogen regulation	
yoyH	2,34	SP-beta prophage		
yvkN	2,33	Unknown	RAB11 family (control of membrane traficking)	
ywnA	2,29	Unknown		

Down-regulated genes in Δ*ydcH* during exponential growth				
Gene	**Expression difference**	**Function1**	**Function2**	**Regulated by**
gltX	2,09	Aminoacyl-tRNA synthetases	glutamyl-tRNA synthetase	SigA
yhcY	2,13	Protein kinases	two component sensor kinase	LiaR, SigA
yhfJ/lplJ	2,14	Biosynthesis of lipoic acid	Lipoate:protein ligase	
yvlA	2,14	Cell envelope stress proteins (controlled by SigM, V, W, X, Y)		SigW, AbrB
deaD/yxiN	2,16	RNA synthesis and degradation, DEAD-box RNA helicases	Important for adaptation to low temperatures	
mutSB/yshD	2,17	DNA repair, recombination	Probable DNA mismatch repair protein	
ywcD/gtcA/ipa-34d/gtaC	2,21	Biosynthesis of teichoic acid	Teichoic acid glycosylation protein	
murF/ydbQ	2,22	Biosynthesis of peptidoglycan	Peptidoglycan precursor biosynthesis	SigM
deoC/dra	2,24	Utilization of nucleotides	Deoxyribose-phosphate aldolase	CcpA, DeoR
dhbB	2,24	Acquisition of iron	Isochorismatase; biosynthesis of the siderophore bacillibactin	AbrB, Fur, Kre
ytlR	2,25	Unknown		SigD
moaE	2,29	Biosynthesis of molybdopterin (cofactor)		
cpgA/yloQ	2,29	Cell envelope and cell division	GTPase	
cheR	2,30	Protein modification	MCPs methyltransferase; motility, chemotaxis	
yhaN/sbcE	2,30	DNA repair/ recombination	DNA double-strand break repair and competence; SMC-like protein	LexA
yqeK	2,31	Unknown		

Down-regulated genes in Δ*ydcH* during exponential growth (continuation)				
Gene	**Expression difference**	**Function1**	**Function2**	**Regulated by**
yprA	2,33	DNA repair/ recombination/ based on similarity		
yloV	2,34	Phosphoproteins		
fmt/yloL	2,34	tRNA modification and maturation	Methionyl-tRNA formyltransferase; formylation of Met-tRNA(fMet)	
dnaI/ytxA/dnaY	2,34	DNA replication	Primosome component (helicase loader)	
ykuO	2,34	Unknown		Fur, NsrR, ResD, Kre
aroF	2,34	Biosynthesis, acquisition of amino acids	Chorismate synthase	
xtmB/ykxG	2,35	DNA replication	Phage DNA replication, PBSX terminase (large subunit)	Xpf
bglA	2,35	Utilization of beta-glucosides	6-phospho-beta-glucosidase	
motA/mot	2,36	Flagellar proteins	Paralog of MotP	SigD
resB/ypxB	2,36	Respiration	Part of the ResB-ResC haem translocase, cytochrome c biogenesis	CcpA, PhoP, ResD
rsmB/sun/yloM	2,36	rRNA modification and maturation, based on similarity	S-adenosyl-L-methionine-dependent 16S rRNA m5C967 methyltransferase	SigA
yusY	2,37	Unknown		
spoVT/yabL	2,37	Transcription factors and their control	Transcription activator and repressor of SigG-dependent genes	SigF, SigG
citZ/citA2	2,38	TCA cycle	Citrate synthase II	CcpA, CcpC
galK/ipa-35d	2,38	Utilization of galactose	Galactose utilization, galactokinase	
ypgQ	2,38	Unknown	Degradation of excessive or abnormal nucleotides	
yukB	2,39	Export of YukE	Membrane FtsK/SpoIIIE-like ATPase, part of the type VII protein secretion system	DegU
panB	2,40	Biosynthesis of coenzyme A	3-methyl-2-oxobutanoate hydroxymethyltransferase	
yvcQ/psdS	2,41	Protein kinases	Control of psdA-psdB in response to lipid II-binding lantibiotics, such as nisin and gallidermin	
engA/yphC	2,41	Ribosome assembly	GTPase essential for ribosome 50S subunit assembly	
gcvT/yqhI	2,41	Utilization of threonine/ glycine	Glycine utilization	Gly-box cooperative-riboswitch-
yqjZ	2,42	Unknown		
ycnE	2,42	Unknown		
crh/yvcM	2,43	Control of transcription factor (other than two-component system)	Regulating HPr	
yyaE	2,43	Electron transport, based on similarity	Paralogue of YoaE	
yuaG/floT/yuaH	2,44	Membrane dynamics	Membrane-associated scaffold protein, orchestration of physiological processes in lipid microdomains, involved in the control of membrane fluidity, confers (together with YuaF) resistance to cefuroxime	SigW

Down-regulated genes in Δ*ydcH* during exponential growth (continuation)				
Gene	**Expression difference**	**Function1**	**Function2**	**Regulated by**
queA	2,45	tRNA modification and maturation	S-adenosylmethionine tRNA ribosyltransferase	
mdh/citH	2,47	TCA cycle	malate dehydrogenase	CcpA, CcpC
pdxK/ywdB/ipa-52r/thiD	2,49	Biosynthesis of pyridoxal phosphate (cofactor)	Pyridoxine, pyridoxal, and pyridoxamine kinase	
yyzE	2,49	Unknown		
tepA/ymfB/ylxI	2,49	Protein secretion	Degradation of SASPs,orphan ClpP-like germination protease	SigG, SpoVT
tyrA	2,50	Biosynthesis, acquisition of aromatic amino acids	Prephenate dehydrogenase	TRAP
birA	2,50	Biosynthesis of fatty acids	Transcriptional repressor (BirA family)/ biotin-protein ligase	Spx
gmuE/ydhR	2,52	Utilization of glucomannan	Mannose kinase	AbrB, CcpA, GmuR
proB	2,53	Biosynthesis/ acquisition of proline	Glutamate 5-kinase	T-box
gmuD/ydhP	2,53	Utilization of glucomannan	Phospho-beta-mannosidase	AbrB, CcpA, GmuR
ykuN	2,54	Electron transport	Replaces ferredoxin under conditions of iron limitation, probably involved in electron transfer to nitric oxide synthase	Fur, NsrR, ResD, Kre
xynD	2,54	Utilization of other polymeric carbohydrates	arabinoxylan degradation	AbrB
ylmE	2,54	biofilm formation	control of the CoA pool	Spo0A
parE/grlB	2,55	DNA condensation/ segregation	subunit of DNA topoisomerase IV	LexA
atpF	2,56	ATP synthesis	part of the Fo complex (subunit b)	RelA
sigF/spoIIAC	2,56	sigma factors	RNA polymerase forespore-specific (early) sigma factor SigF	AbrB, SigF, SigG, SigH, SinR, Spo0A
yloN	2,57	rRNA modification and maturation, based on similarity	Adenosine methyltransferase for modification of 23S rRNA	
iscU/sufU/yurV	2,58	biosynthesis of iron-sulfur clusters	iron-sulfur cluster scaffold protein, receives iron from SufS, synthesis of Fe-S clusters	
sucC	2,58	ATP synthesis	TCA cycle	CcpA, RoxS
valS	2,58	aminoacyl-tRNA synthetases	valyl-tRNA synthetase	T-box, Efp-dependent proteins
ytpQ	2,59	Unknown		Spx
yuaF/NfeD2	2,59	membrane dynamics	NfeD2, role in maintaining membrane integrity during conditions of cellular stress, confers (together with FloT) resistance to cefuroxime	SigW
ylxH/flhG	2,59	motility and chemotaxis/ other	GTPase activating protein, activates FlhF, activates assembly of the flagellar C ring, control of flagellar basal body position	CodY, DegU, SigD, Spo0A
yknW	2,60	ABC transporters	modulates assembly of the YknX-YknY-YknZ ABC transporter for the export of the SdpC toxin	AbrB, SigW
cca/papS/ypjI	2,63	tRNA modification and maturation	tRNA nucleotidyltransferase, maturation of the single-copy tRNACys, which lacks an encoded CCA 3 end	Spx
icd/citC	2,64	TCA cycle	isocitrate dehydrogenase	CcpA, CcpC

Down-regulated genes in Δ*ydcH* during exponential growth (continuation)				
Gene	**Expression difference**	**Function1**	**Function2**	**Regulated by**
mobB	2,66	biosynthesis of molybdopterin (cofactor)	nitrate respiration, molybdopterin-guanine dinucleotide cofactor synthesis protein	
trpD	2,66	biosynthesis/ acquisition of aromatic amino acids	biosynthesis of tryptophan, anthranilate phosphoribosyltransferase	TRAP
yhbB/ygaQ	2,67	Unknown	spore coat protein, amidase	SigE
cysH	2,67	sulfur metabolism	sulfate reduction, phosphoadenosine phosphosulfate sulfotransferase	CymR, S-box
rseP/rasP/yluC	2,67	cell division	intramembrane protease, cleaves FtsL, RsiV and RsiW as well as signal peptides after release of the secreted proteins, control of SigV and SigW activity	
gcvPA/yqhJ/gcvP	2,68	utilization of threonine/ glycine	glycine decarboxylase (subunit 1)	Gly-box
yvcR/psdA	2,69	ABC transporters	export of lipid II-binding lantibiotics, such as nisin and gallidermin	PsdR, activated stat by internal toxic peptides (Sdp, SkfA)
xkdE	2,69	PBSX prophage		Xpf
pfkA/pfk	2,69	glycolysis	6-phosphofructokinase	
pheS	2,70	aminoacyl-tRNA synthetases	phenylalanyl-tRNA synthetase (alpha subunit)	T-box
ycbM	2,71	protein kinases	two-component sensor kinase	
acuB	2,71	Unknown		CcpA
artQ/yqiY	2,72	ABC transporters	high affinity arginine ABC transporter (permease)	
ytaF	2,72	Unknown		SigE
aroB	2,74	biosynthesis/ acquisition of aromatic amino acids	3-dehydroquinate synthase	
trmK/yqfN	2,74	tRNA modification and maturation	tRNA:m1A22 methyl transferase	
yszB/pheB/thrR	2,75	biosynthesis/ acquisition of aromatic amino acids	control of threonine biosynthesis, transcription repressor of threonine biosynthetic gene	
yqfA/floA	2,76	cell envelope stress proteins (controlled by SigM, V, W, X, Y)	flottilin-like protein (in addition to FloT), resistence protein (against sublancin), accessory role in resistance to cefuroxime	SigW
xtmA/ykxF	2,77	DNA replication prophage	PBSX terminase (small subunit), phage DNA replication	Xpf
xkdQ	2,78	PBSX prophage		
sdhA/citF	2,78	TCA cycle	succinate dehydrogenase (flavoprotein subunit)	FsrA
ynbB	2,79	Unknown		
malL/yvdL	2,80	utilization of starch/ maltodextrin	alpha-glucosidase	
ysmA	2,82	Unknown		
xtrA	2,83	PBSX prophage		Xre
yrhE	2,84	Unknown		
yxaB	2,85	biofilm formation	biofilm formation, survival of salt and ethanol stress	AbrB, SigB

Down-regulated genes in Δ*ydcH* during exponential growth (continuation)				
Gene	**Expression difference**	**Function1**	**Function2**	**Regulated by**
gmuF/ydhS	2,86	utilization of glucomannan	mannose-6-P-isomerase	AbrB, CcpA, GmuR
exuM/yjmB	2,86	transporters/ other		CcpA, ExuR
bioW	2,86	biosynthesis/ acquisition of biotin	pimeloyl-CoA synthase	BirA
xepA/xkdY	2,86	cell wall degradation/ turnover * autolysis	phage release, PBSX prophage lytic exoenzyme	
thiU/ykoF	2,88	ABC transporters	thiamine transporter (binding protein), uptake	Thi-box
truA/ybaH	2,88	tRNA modification and maturation	pseudouridylate synthase I	stringent response, RelA
purH/purJ	2,90	biosynthesis/ acquisition of purine nucleotides	phosphoribosylaminoimidazole carboxamide formyltransferase and inosine-monophosphate cyclohydrolase	G-box, PurR
gmuA/ydhN	2,91	phosphotransferase systems	glucomannan-specific phosphotransferase system, EIIA component	AbrB, CcpA, GmuR
folC	2,91	biosynthesis of folate	folyl-polyglutamate synthetase	T-box
sucD	2,91	ATP synthesis	succinyl-CoA synthetase (alpha subunit)	CcpA
hisH	2,93	biosynthesis/ acquisition of histidine	imidazole glycerol phosphate synthase (glutaminase subunit)	
prpC/yloO	2,95	protein phosphatases	antagonist of PrkC-dependent phosphorylation	
atpH	2,96	ATP synthesis	ATP synthase (subunit delta)	stringent response, RelA
yvrO	2,98	ABC transporters		AbrB, ComK
treA/treC	2,98	utilization of trehalose	phospho-alpha-glucosidase	CcpA, PhoP, TreR
xkdG	2,98	PBSX prophage		Xpf
nupC	3,02	transporters/ other	pyrimidine nucleoside transport protein	CcpA, DeoR
mutM/ytaE	3,04	DNA repair/ recombination	formamidopyrimidine-DNA glycosidase	
msmE	3,05	ABC transporters		CcpA
hisA	3,07	biosynthesis/ acquisition of histidine	phosphoribosylformimino-5-aminoimidazole carboxamide ribotide isomerase	
xkdF	3,07	PBSX prophage		Xpf
xkdJ	3,08	PBSX prophage		
gmuC/ydhO	3,08	phosphotransferase systems	glucomannan-specific phosphotransferase system, EIIC component	AbrB, CcpA, GmuR
rbsA	3,09	ABC transporters	ribose ABC transporter (ATP-binding protein), uptake	AbrB, CcpA
fadF/ywjF	3,10	utilization of fatty acids	FA degradation	FadR
iolE/yxdE	3,11	utilization of inositol	myo-inositol catabolism, 2-keto-myo-inositol dehydratase, dehydration of 2-keto-myo-inositol (2nd reaction)	CcpA, IolR
xkdH	3,12	PBSX prophage		Xpf
xhlA	3,13	PBSX prophage	host cell lysis upon induction of PBSX	
xkdS	3,13	PBSX prophage		

Down-regulated genes in Δ*ydcH* during exponential growth (continuation)				
Gene	**Expression difference**	**Function1**	**Function2**	**Regulated by**
thiQ/ylmB	3,14	biosynthesis/ acquisition of thiamine (cofactor)	thiamine salvage, N-formyl-4-amino-5-aminomethyl-2-methylpyrimidine deformylase	Thi-box
glcK/yqgR	3,14	utilization of trehalose	phosphorylation of the free glucose moiety resulting from cleavage of di-and oligosaccharides, glucose kinase (D-glucose:ATP)	
xkdI	3,14	PBSX prophage		Xpf
acuA	3,19	utilization of organic acids	protein acetylase for the control of AcsA activity, Gcn5-related N-acetyltransferase	CcpA
yxiI	3,20	Unknown		
xkdX	3,21	PBSX prophage		
etfB	3,22	electron transport/ other	fatty acid degradation, flavoprotein (beta subunit)	CcpA, FadR
yhcF	3,26	transcription factor/ other/ based on similarity		
trpF	3,26	biosynthesis/ acquisition of aromatic amino acids	synthesis of tryptophan, phosphoribosylanthranilate isomerase	TRAP
xkdR	3,30	PBSX prophage		
iolD/yxdD	3,42	utilization of inositol	myo-inositol catabolism, formation of 5-deoxy-D-glucuronic acid (3rd reaction)	CcpA, IolR
thiS/yjbS	3,43	biosynthesis/ acquisition of thiamine (cofactor)	sulfur carrier protein	Thi-box
rocG	3,43	utilization of arginine/ ornithine	arginine utilization, controls the activity of GltC, trigger enzyme: glutamate dehydrogenase (major)	AbrB, AhrC, CcpA, RocR, SigL
xkdC/ykxC	3,43	PBSX prophage		Xre
lplA	3,44	ABC transporters		
xhlB/xpaB	3,45	PBSX prophage	host cell lysis	
mtlD/mtlB	3,49	utilization of mannitol	mannitol-1-phosphate 5-dehydrogenase	MtlR
pyrF	3,63	biosynthesis/ acquisition of pyrimidine nucleotides	pyrimidine biosynthesis, orotidine-5-phosphate decarboxylase	PyrR
xkdW	3,64	PBSX prophage		
xkdK	3,65	PBSX prophage		Xpf
yulD/rhaM	3,68	Unknown	utilization of rhamnose, mutarotase	CcpA, RhaR
hisB	3,70	biosynthesis/ acquisition of histidine	imidazoleglycerol-phosphate dehydratase	
bioF	3,70	biosynthesis/ acquisition of biotin (cofactor)	8-amino-7-oxononanoate synthase	BirA
iolC/yxdC	3,74	utilization of inositol	myo-inositol catabolism, formation of 2-deoxy-5-keto-gluconic acid-6-phosphate (5th reaction)	CcpA, IolR
xkdB/ykxB	3,77	PBSX prophage		Xre
iolG/idh/iol	3,79	utilization of inositol	myo-inositol catabolism, inositol 2-dehydrogenase	CcpA, IolR

Down-regulated genes in Δ*ydcH* during exponential growth (continuation)				
Gene	**Expression difference**	**Function1**	**Function2**	**Regulated by**
lrgA/ysbA	3,79	Unknown		Kre, CcpA, LytT
yxiM	3,80	Unknown		
kdgK	3,84	utilization of hexuronate	utilization of galacturonic acid, 2-dehydro-3-deoxygluconokinase	CcpA, KdgR
tenI	3,97	biosynthesis/ acquisition of thiamine (cofactor)	thiazole tautomerase	Thi-box
bglH	3,98	utilization of beta-glucosides	salicin utilization, phospho-beta-glucosidase	CcpA, LicT
citT/yflQ	3,99	utilization of organic acids	two-component response regulator, regulation of citrate uptake	CitT
xkdD/ykxD	4,07	PBSX prophage		Xre
yjmC	4,10	may be involved in galacturonate utilization		CcpA, ExuR, SigE
mtlA	4,18	phosphotransferase systems	trigger enzyme: mannitol-specific phosphotransferase system, EIICB of the PTS; mannitol uptake and phosphorylation, control of MtlR activity	MtlR
licB/celA	4,30	phosphotransferase systems	trigger enzyme: lichenan-specific phosphotransferase system, EIIB component of the PTS; lichenan uptake and phosphorylation, control of LicR activity	CcpA, LicR
yesM	4,38	protein kinases	two-component sensor kinase	CcpA
mccB/yrhB	4,43	biosynthesis/ acquisition of cysteine	cystathionine lyase/ homocysteine gamma-lyase; methionine-to-cysteine conversion	CymR, Spx
mccA/yrhA	4,51	biosynthesis/ acquisition of cysteine	O-acetylserine-thiol-lyase, methionine-to-cysteine conversion	CymR, Spx
araL/yseA	4,58		detoxification of accidental accumulation of phosphorylated metabolites; sugar phosphate phosphatase	AraR, CcpA
levG	4,59	phosphotransferase systems	fructose-specific phosphotransferase system EIID component of the PTS; fructose uptake and phosphorylation	CcpA, LevR, SigL
iolB/yxdB	4,64	utilization of inositol	myo-inositol catabolism; formation of 2-deoxy-5-keto-gluconic acid (4th reaction)	CcpA, IolR
mdxE/yvdG	4,71	ABC transporters	maltodextrin ABC transporter, binding protein	
ykzM	4,73	PBSX prophage		
rbsD	5,13	ABC transporters	ribose uptake	AbrB, CcpA
ykzK	5,55	PBSX prophage		
levD	6,11	phosphotransferase systems	fructose-specific phosphotransferase system, EIIA component of the PTS, fructose uptake and phosphorylation	CcpA, LevR, SigL
mtlF	6,38	phosphotransferase systems	phosphotransferase system(PTS) mannitol-specific enzyme IIA component	MtlR

Down-regulated genes in Δ*ydcH* during exponential growth (continuation)				
Gene	**Expression difference**	**Function1**	**Function2**	**Regulated by**
sat/ylnB	6,52	sulfur metabolism	sulfate activation, sulfate adenylyltransferase	CymR, S-box
cysC/ylnC	7,16	sulfur metabolism	sulfate reduction and activation, adenylyl-sulfate kinase	CymR, S-box
yxeK	7,19	Unknown	sulphur metabolism	CymR
levF	7,25	phosphotransferase systems	fructose-specific phosphotransferase system, EIIC component of the PTS, fructose uptake and phosphorylation	CcpA, LevR, SigL
levE	7,43	phosphotransferase systems	fructose-specific phosphotransferase system, EIIB component of the PTS, fructose uptake and phosphorylation	CcpA, LevR, SigL
yxeN	8,86	ABC transporters	sulphur metabolism	CymR
yxeL/snaB	9,47	ABC transporters	sulphur metabolism	CymR
sumT/ylnD	9,87	biosynthesis of heme/ siroheme	siroheme biosynthesis , sulfite reduction	CymR, S-box
ydcH	13,68	Unknown		
acpK	14,40	biosynthesis of antibacterial compounds	polyketide biosynthesis, acyl carrier protein	AbrB, CodY

Overexpressed genes in Δ*ydcH* during stationary growth				
Gene	**Expression difference**	**Function1**	**Function2**	**Regulated by**
ydcF	6,50	Unknown		
ywzD	6,29	Unknown		
ywdA/ipa-51d	4,79	Unknown		CcpA, SacT
ydfQ	4,19	electron transport/ other/ based on similarity		
sacA/ipa-50d	3,26	utilization of sucrose	phosphosucrase	
ydcG	3,18	Unknown		
albB/ywhR	3,18	biosynthesis of antibacterial compounds	antilisterial bacteriocin (subtilosin) production	AbrB, ResD, Rok
albE/ywhO	2,80	biosynthesis of antibacterial compounds	antilisterial bacteriocin (subtilosin) production; processing protease	AbrB, ResD, Rok
albC/ywhQ	2,77	biosynthesis of antibacterial compounds	export of antilisterial bacteriocin (subtilosin); ABC transporter	AbrB, ResD, Rok
albA/ywiA	2,71	biosynthesis of antibacterial compounds	antilisterial bacteriocin (subtilosin) production; radical S-adenosylmethionine enzyme	AbrB, ResD, Rok
albD/ywhP	2,65	biosynthesis of antibacterial compounds	export of antilisterial bacteriocin (subtilosin); ABC transporter; membrane protein	AbrB, ResD, Rok
albF/ywhN	2,57	biosynthesis of antibacterial compounds	antilisterial bacteriocin (subtilosin) production	AbrB, ResD, Rok
yflI	2,39	Unknown		
rsbRD/yqhA	2,17	control of sigma factors	probably part of the stressosome, negative regulator of SigB activity	
ywzB	2,17	Unknown		
albG/ywhM	1,81	biosynthesis of antibacterial compounds	antilisterial bacteriocin (subtilosin) production; U	AbrB, ResD, Rok
yozB	1,71	Unknown		

Down-regulated genes in Δ*ydcH* during stationary growth				
Gene	**Expression difference**	**Function1**	**Function2**	**Regulated by**
fadN/yusL	2,79	utilization of fatty acids	fatty acid degradation	CcpA, FadR, SdpR
yoqL	3,11	SP-beta prophage		
yonT	3,29	toxins, antitoxins and immunity against toxins/ based on similarity	Toxin	as-yonT (antisense RNA)
yotM/yodV	3,45	SP-beta prophage		
yoqY	3,52	SP-beta prophage		
yoqR	4,21	SP-beta prophage		
iolT/ydjK	4,23	transporters	major transporter of inositol; myo-inositol uptake	IolR
yoqK	5,43	SP-beta prophage		
ydcQ/conQ	5,72	Prophages and mobile genetic elements	conjugative transfer of ICEBs1, coupling protein, part of the type IV secretion system for DNA transfer	
yfnG	5,93	sporulation		GerE, SigK
ykzV	57,58	Unknown		
ydcH	114,98	Unknown		

Appendix 4: MreB*s TIRFM acquisitions

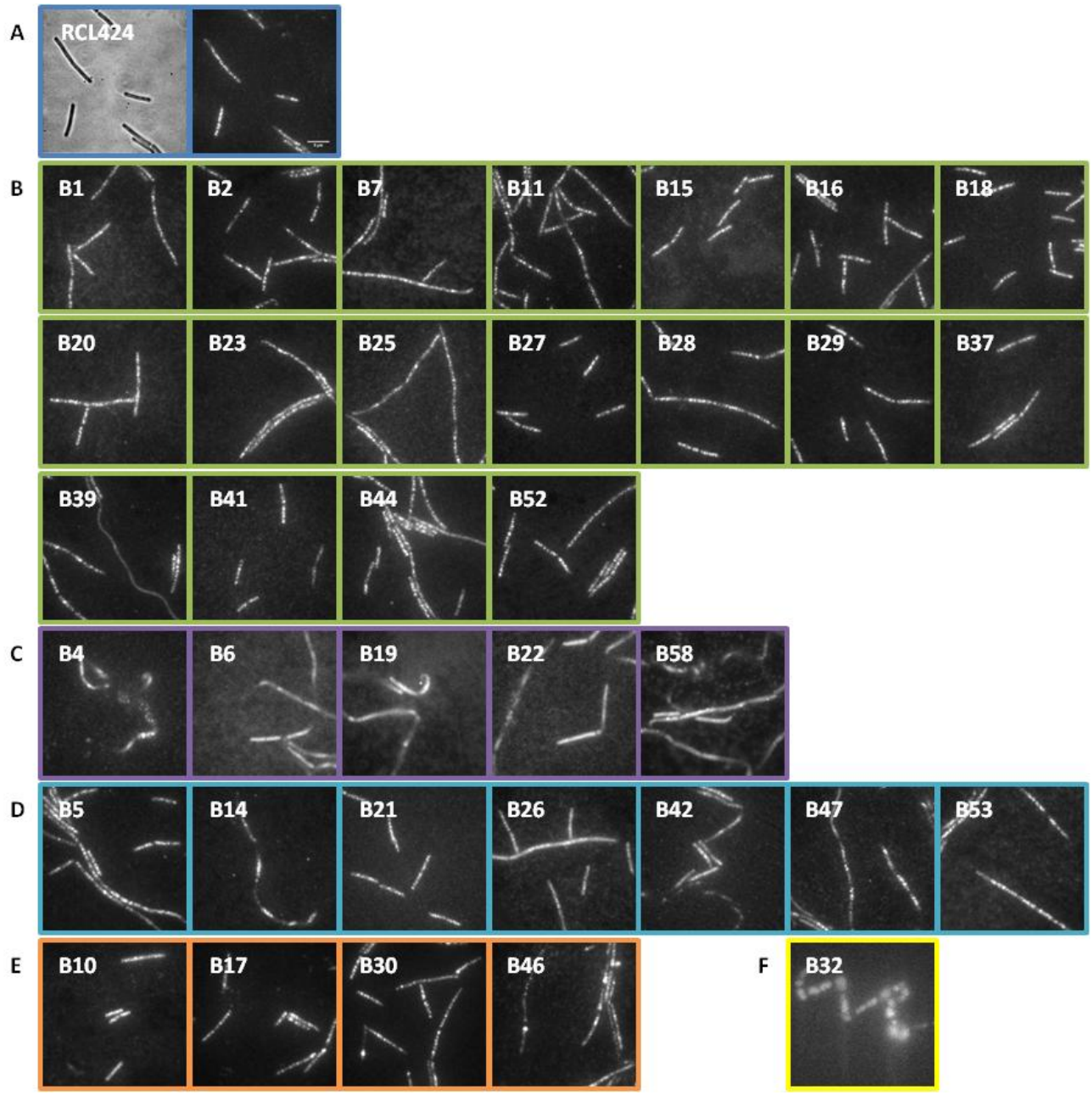

Figure A4 TIRFM acquisitions of MreB*s. Control strain RCL424 (P_{mreB}*gfp-mreB*^{WT}, P_{mreBH}*lacZ*) and the 35 MreB*s mutants were grown in CH media and acquired during mid-exponential growth (OD ≈ 0,2 - 0,3). **A**. Bright field (left panel) and TIRFM acquisition (right panel) of control strain RCL424 (dark blue). **B**. TIRFM acquisitions corresponding to bright field images from Figure 19 in the text of the 18 WT-like MreB*s (green). They form dynamic patches of MreB. **C**. TIRFM acquisitions corresponding to bright field images from Figure 20 in the text of the 5 Δ*mreB*-like MreB*s (purple). They all have delocalized GFP-MreB signal. **D**. TIRFM acquisitions corresponding to bright field images from Figure 21 in the text of the 7 intermediate MreB*s (cyan). They show a variety of localized and delocalized GFP-MreB. **E**. TIRFM acquisitions corresponding to bright field images from Figure 22 in the text of 4 of the WeB MreB*s (orange). They form MreB dynamic patches in a WT-ish manner. **F**. TIRFM acquisition corresponding to the bright field image in Figure 23 in the text of the MreB* mutant B32 (yellow). GFP-MreB has a delocalized signal.

7. Bibliography

7. Bibliography

Abriouel, H., Franz, C. M., Ben Omar, N., & Galvez, A. (2011). Diversity and applications of *Bacillus* bacteriocins. *FEMS Microbiol Rev, 35*(1), 201-232. doi: 10.1111/j.1574-6976.2010.00244.x

Altschul, S. F., Madden, T. L., Schaffer, A. A., Zhang, J., Zhang, Z., Miller, W., & Lipman, D. J. (1997). Gapped BLAST and PSI-BLAST: a new generation of protein database search programs. *Nucleic Acids Res, 25*(17), 3389-3402.

Attaiech, L., Granadel, C., Claverys, J. P., & Martin, B. (2008). RadC, a misleading name? *J Bacteriol, 190*(16), 5729-5732. doi: 10.1128/JB.00425-08

Ausmees, N., Kuhn, J. R., & Jacobs-Wagner, C. (2003). The bacterial cytoskeleton: an intermediate filament-like function in cell shape. *Cell, 115*(6), 705-713.

Balzer, D., Pansegrau, W., & Lanka, E. (1994). Essential motifs of relaxase (TraI) and TraG proteins involved in conjugative transfer of plasmid RP4. *J Bacteriol, 176*(14), 4285-4295.

Barko, S., Szatmari, D., Bodis, E., Turmer, K., Ujfalusi, Z., Popp, D., . . . Nyitrai, M. (2016). Large-scale purification and *in vitro* characterization of the assembly of MreB from *Leptospira interrogans*. *Biochim Biophys Acta, 1860*(9), 1942-1952. doi: 10.1016/j.bbagen.2016.06.007

Bean, G. J., & Amann, K. J. (2008). Polymerization properties of the *Thermotoga maritima* actin MreB: roles of temperature, nucleotides, and ions. *Biochemistry, 47*(2), 826-835. doi: 10.1021/bi701538e

Bean, G. J., Flickinger, S. T., Westler, W. M., McCully, M. E., Sept, D., Weibel, D. B., & Amann, K. J. (2009). A22 disrupts the bacterial actin cytoskeleton by directly binding and inducing a low-affinity state in MreB. *Biochemistry, 48*(22), 4852-4857. doi: 10.1021/bi900014d

Becker, E., Herrera, N. C., Gunderson, F. Q., Derman, A. I., Dance, A. L., Sims, J., . . . Pogliano, J. (2006). DNA segregation by the bacterial actin AlfA during *Bacillus subtilis* growth and development. *EMBO J, 25*(24), 5919-5931. doi: 10.1038/sj.emboj.7601443

Bennet, M., Bertinetti, L., Neely, R. K., Schertel, A., Kornig, A., Flors, C., . . . Faivre, D. (2015). Biologically controlled synthesis and assembly of magnetite nanoparticles. *Faraday Discuss, 181*, 71-83. doi: 10.1039/c4fd00240g

Bern, M., Beniston, R., & Mesnage, S. (2016). Towards an automated analysis of bacterial peptidoglycan structure. *Anal Bioanal Chem*. doi: 10.1007/s00216-016-9857-5

Bertonati, C., Punta, M., Fischer, M., Yachdav, G., Forouhar, F., Zhou, W., . . . Rost, B. (2009). Structural genomics reveals EVE as a new ASCH/PUA-related domain. *Proteins, 75*(3), 760-773. doi: 10.1002/prot.22287

Bertsche, U., Breukink, E., Kast, T., & Vollmer, W. (2005). *In vitro* murein peptidoglycan synthesis by dimers of the bifunctional transglycosylase-transpeptidase PBP1B from *Escherichia coli*. *J Biol Chem, 280*(45), 38096-38101. doi: 10.1074/jbc.M508646200

Beveridge, T. J. (1999). Structures of gram-negative cell walls and their derived membrane vesicles. *J Bacteriol, 181*(16), 4725-4733.

Bhavsar, A. P., & Brown, E. D. (2006). Cell wall assembly in *Bacillus subtilis*: how spirals and spaces challenge paradigms. *Mol Microbiol, 60*(5), 1077-1090. doi: 10.1111/j.1365-2958.2006.05169.x

Bi, E., Dai, K., Subbarao, S., Beall, B., & Lutkenhaus, J. (1991). FtsZ and cell division. *Res Microbiol, 142*(2-3), 249-252.

Born, P., Breukink, E., & Vollmer, W. (2006). *In vitro* synthesis of cross-linked murein and its attachment to sacculi by PBP1A from *Escherichia coli*. *J Biol Chem, 281*(37), 26985-26993. doi: 10.1074/jbc.M604083200

Bridges, B. A. (1997). Microbial genetics. Hypermutation under stress. *Nature, 387*(6633), 557-558. doi: 10.1038/42370

Bridier, A., Le Coq, D., Dubois-Brissonnet, F., Thomas, V., Aymerich, S., & Briandet, R. (2011). The spatial architecture of *Bacillus subtilis* biofilms deciphered using a surface-associated model and *in situ* imaging. *PLoS One, 6*(1), e16177. doi: 10.1371/journal.pone.0016177

Briley, K., Jr., Prepiak, P., Dias, M. J., Hahn, J., & Dubnau, D. (2011). Maf acts downstream of ComGA to arrest cell division in competent cells of *B. subtilis*. *Mol Microbiol, 81*(1), 23-39. doi: 10.1111/j.1365-2958.2011.07695.x

Britton, R. A., Eichenberger, P., Gonzalez-Pastor, J. E., Fawcett, P., Monson, R., Losick, R., & Grossman, A. D. (2002). Genome-wide analysis of the stationary-phase sigma factor (sigma-H) regulon of *Bacillus subtilis*. *J Bacteriol, 184*(17), 4881-4890.

Brown, S., Santa Maria, J. P., Jr., & Walker, S. (2013). Wall teichoic acids of Gram-positive bacteria. *Annu Rev Microbiol, 67*, 313-336. doi: 10.1146/annurev-micro-092412-155620

Cabeen, M. T., & Jacobs-Wagner, C. (2010). The bacterial cytoskeleton. *Annu Rev Genet, 44*, 365-392. doi: 10.1146/annurev-genet-102108-134845

Carballido-Lopez, R. (2006). The bacterial actin-like cytoskeleton. *Microbiol Mol Biol Rev, 70*(4), 888-909. doi: 10.1128/MMBR.00014-06

Carballido-Lopez, R., Formstone, A., Li, Y., Ehrlich, S. D., Noirot, P., & Errington, J. (2006). Actin homolog MreBH governs cell morphogenesis by localization of the cell wall hydrolase LytE. *Dev Cell, 11*(3), 399-409. doi: 10.1016/j.devcel.2006.07.017

Cava, F., & de Pedro, M. A. (2014). Peptidoglycan plasticity in bacteria: emerging variability of the murein sacculus and their associated biological functions. *Curr Opin Microbiol, 18*, 46-53. doi: 10.1016/j.mib.2014.01.004

Chang, Y. M., Chen, C. K., Ko, T. P., Chang-Chien, M. W., & Wang, A. H. (2013). Structural analysis of the antibiotic-recognition mechanism of MarR proteins. *Acta Crystallogr D Biol Crystallogr, 69*(Pt 6), 1138-1149. doi: 10.1107/S0907444913007117

Chastanet, A., & Carballido-Lopez, R. (2012). The actin-like MreB proteins in *Bacillus subtilis*: a new turn. *Front Biosci (Schol Ed), 4*, 1582-1606.

Cleveland, D. W. (1982). Treadmilling of tubulin and actin. *Cell, 28*(4), 689-691.

Coltharp, C., & Xiao, J. (2017). Beyond force generation: Why is a dynamic ring of FtsZ polymers essential for bacterial cytokinesis? *Bioessays, 39*(1), 1-11. doi: 10.1002/bies.201600179

Cowles, K. N., & Gitai, Z. (2010). Surface association and the MreB cytoskeleton regulate pilus production, localization and function in *Pseudomonas aeruginosa*. *Mol Microbiol, 76*(6), 1411-1426. doi: 10.1111/j.1365-2958.2010.07132.x

de Pedro, M. A., & Cava, F. (2015). Structural constraints and dynamics of bacterial cell wall architecture. *Front Microbiol, 6*, 449. doi: 10.3389/fmicb.2015.00449

Defeu Soufo, H. J., & Graumann, P. L. (2004). Dynamic movement of actin-like proteins within bacterial cells. *EMBO Rep, 5*(8), 789-794. doi: 10.1038/sj.embor.7400209

Defeu Soufo, H. J., & Graumann, P. L. (2005). *Bacillus subtilis* actin-like protein MreB influences the positioning of the replication machinery and requires membrane proteins MreC/D and other actin-like proteins for proper localization. *BMC Cell Biol, 6*(1), 10. doi: 10.1186/1471-2121-6-10

Defeu Soufo, H. J., Reimold, C., Linne, U., Knust, T., Gescher, J., & Graumann, P. L. (2010). Bacterial translation elongation factor EF-Tu interacts and colocalizes with actin-like MreB protein. *Proc Natl Acad Sci U S A, 107*(7), 3163-3168. doi: 10.1073/pnas.0911979107

Deng, A., Lin, W., Shi, N., Wu, J., Sun, Z., Sun, Q., . . . Wen, T. (2016). *In vitro* assembly of the bacterial actin protein MamK from ' *Candidatus* Magnetobacterium casensis' in the phylum Nitrospirae. *Protein Cell, 7*(4), 267-280. doi: 10.1007/s13238-016-0253-x

Derman, A. I., Becker, E. C., Truong, B. D., Fujioka, A., Tucey, T. M., Erb, M. L., . . . Pogliano, J. (2009). Phylogenetic analysis identifies many uncharacterized actin-like proteins (Alps) in bacteria: regulated polymerization, dynamic instability and treadmilling in Alp7A. *Mol Microbiol, 73*(4), 534-552. doi: 10.1111/j.1365-2958.2009.06771.x

Divakaruni, A. V., Baida, C., White, C. L., & Gober, J. W. (2007). The cell shape proteins MreB and MreC control cell morphogenesis by positioning cell wall synthetic complexes. *Mol Microbiol, 66*(1), 174-188. doi: 10.1111/j.1365-2958.2007.05910.x

Dmitriev, B. A., Toukach, F. V., Schaper, K. J., Holst, O., Rietschel, E. T., & Ehlers, S. (2003). Tertiary structure of bacterial murein: the scaffold model. *J Bacteriol, 185*(11), 3458-3468.

Doi, M., Wachi, M., Ishino, F., Tomioka, S., Ito, M., Sakagami, Y., . . . Matsuhashi, M. (1988). Determinations of the DNA sequence of the *mreB* gene and of the gene products of the *mre* region that function in formation of the rod shape of *Escherichia coli* cells. *J Bacteriol, 170*(10), 4619-4624.

Dominguez-Cuevas, P., Porcelli, I., Daniel, R. A., & Errington, J. (2013). Differentiated roles for MreB-actin isologues and autolytic enzymes in *Bacillus subtilis* morphogenesis. *Mol Microbiol, 89*(6), 1084-1098. doi: 10.1111/mmi.12335

Dominguez-Escobar, J., Chastanet, A., Crevenna, A. H., Fromion, V., Wedlich-Soldner, R., & Carballido-Lopez, R. (2011). Processive movement of MreB-associated cell wall biosynthetic complexes in bacteria. *Science, 333*(6039), 225-228. doi: 10.1126/science.1203466

Dubnau, D. (1991). Genetic competence in *Bacillus subtilis*. *Microbiol Rev, 55*(3), 395-424.

Dufresne, K., & Paradis-Bleau, C. (2015). Biology and assembly of the bacterial envelope. *Adv Exp Med Biol, 883*, 41-76. doi: 10.1007/978-3-319-23603-2_3

Egan, A. J., Cleverley, R. M., Peters, K., Lewis, R. J., & Vollmer, W. (2016). Regulation of bacterial cell wall growth. *FEBS J*. doi: 10.1111/febs.13959

Ehlert, K., & Holtje, J. V. (1996). Role of precursor translocation in coordination of murein and phospholipid synthesis in *Escherichia coli*. *J Bacteriol, 178*(23), 6766-6771.

Ellison, D. W., & Miller, V. L. (2006). Regulation of virulence by members of the MarR/SlyA family. *Curr Opin Microbiol, 9*(2), 153-159. doi: 10.1016/j.mib.2006.02.003

Erickson, H. P., Anderson, D. E., & Osawa, M. (2010). FtsZ in bacterial cytokinesis: cytoskeleton and force generator all in one. *Microbiol Mol Biol Rev, 74*(4), 504-528. doi: 10.1128/MMBR.00021-10

Errington, J. (2015). Bacterial morphogenesis and the enigmatic MreB helix. *Nat Rev Microbiol, 13*(4), 241-248. doi: 10.1038/nrmicro3398

Esue, O., Cordero, M., Wirtz, D., & Tseng, Y. (2005). The assembly of MreB, a prokaryotic homolog of actin. *J Biol Chem, 280*(4), 2628-2635. doi: 10.1074/jbc.M410298200

Favini-Stabile, S., Contreras-Martel, C., Thielens, N., & Dessen, A. (2013). MreB and MurG as scaffolds for the cytoplasmic steps of peptidoglycan biosynthesis. *Environ Microbiol, 15*(12), 3218-3228. doi: 10.1111/1462-2920.12171

Fenton, A. K., & Gerdes, K. (2013). Direct interaction of FtsZ and MreB is required for septum synthesis and cell division in *Escherichia coli*. *EMBO J, 32*(13), 1953-1965. doi: 10.1038/emboj.2013.129

Fenton, A. K., Lambert, C., Wagstaff, P. C., & Sockett, R. E. (2010). Manipulating each MreB of *Bdellovibrio bacteriovorus* gives diverse morphological and predatory phenotypes. *J Bacteriol, 192*(5), 1299-1311. doi: 10.1128/JB.01157-09

Figge, R. M., Divakaruni, A. V., & Gober, J. W. (2004). MreB, the cell shape-determining bacterial actin homologue, co-ordinates cell wall morphogenesis in *Caulobacter crescentus*. *Mol Microbiol, 51*(5), 1321-1332. doi: 10.1111/j.1365-2958.2003.03936.x

Fink, G., Szewczak-Harris, A., & Lowe, J. (2016). SnapShot: The bacterial cytoskeleton. *Cell, 166*(2), 522-522 e521. doi: 10.1016/j.cell.2016.06.057

Fondi, M., Bosi, E., Presta, L., Natoli, D., & Fani, R. (2016). Modelling microbial metabolic rewiring during growth in a complex medium. *BMC Genomics, 17*(1), 970. doi: 10.1186/s12864-016-3311-0

Formstone, A., Carballido-Lopez, R., Noirot, P., Errington, J., & Scheffers, D. J. (2008). Localization and interactions of teichoic acid synthetic enzymes in *Bacillus subtilis*. *J Bacteriol, 190*(5), 1812-1821. doi: 10.1128/JB.01394-07

Formstone, A., & Errington, J. (2005). A magnesium-dependent *mreB* null mutant: implications for the role of *mreB* in *Bacillus subtilis*. *Mol Microbiol, 55*(6), 1646-1657. doi: 10.1111/j.1365-2958.2005.04506.x

Foulquier, E., Pompeo, F., Bernadac, A., Espinosa, L., & Galinier, A. (2011). The YvcK protein is required for morphogenesis via localization of PBP1 under gluconeogenic growth conditions in *Bacillus subtilis*. *Mol Microbiol, 80*(2), 309-318. doi: 10.1111/j.1365-2958.2011.07587.x

Frirdich, E., & Gaynor, E. C. (2013). Peptidoglycan hydrolases, bacterial shape, and pathogenesis. *Curr Opin Microbiol, 16*(6), 767-778. doi: 10.1016/j.mib.2013.09.005

Gaballah, A., Kloeckner, A., Otten, C., Sahl, H. G., & Henrichfreise, B. (2011). Functional analysis of the cytoskeleton protein MreB from *Chlamydophila pneumoniae*. *PLoS One, 6*(10), e25129. doi: 10.1371/journal.pone.0025129

Gan, L., Chen, S., & Jensen, G. J. (2008). Molecular organization of Gram-negative peptidoglycan. *Proc Natl Acad Sci U S A, 105*(48), 18953-18957. doi: 10.1073/pnas.0808035105

Garner, E. C., Bernard, R., Wang, W., Zhuang, X., Rudner, D. Z., & Mitchison, T. (2011). Coupled, circumferential motions of the cell wall synthesis machinery and MreB filaments in *B. subtilis*. *Science, 333*(6039), 222-225. doi: 10.1126/science.1203285

Gibson, D. G., Young, L., Chuang, R. Y., Venter, J. C., Hutchison, C. A., 3rd, & Smith, H. O. (2009). Enzymatic assembly of DNA molecules up to several hundred kilobases. *Nat Methods, 6*(5), 343-345. doi: 10.1038/nmeth.1318

Gorke, B., Foulquier, E., & Galinier, A. (2005). YvcK of *Bacillus subtilis* is required for a normal cell shape and for growth on Krebs cycle intermediates and substrates of the pentose phosphate pathway. *Microbiology, 151*(Pt 11), 3777-3791. doi: 10.1099/mic.0.28172-0

Goujon, M., McWilliam, H., Li, W., Valentin, F., Squizzato, S., Paern, J., & Lopez, R. (2010). A new bioinformatics analysis tools framework at EMBL-EBI. *Nucleic Acids Res, 38*(Web Server issue), W695-699. doi: 10.1093/nar/gkq313

Govindarajan, S., & Amster-Choder, O. (2016). Where are things inside a bacterial cell? *Curr Opin Microbiol, 33*, 83-90. doi: 10.1016/j.mib.2016.07.003

Grove, A. (2013). MarR family transcription factors. *Curr Biol, 23*(4), R142-143. doi: 10.1016/j.cub.2013.01.013

Gumbart, J. C., Beeby, M., Jensen, G. J., & Roux, B. (2014). *Escherichia coli* peptidoglycan structure and mechanics as predicted by atomic-scale simulations. *PLoS Comput Biol, 10*(2), e1003475. doi: 10.1371/journal.pcbi.1003475

Hall, B. G. (1990). Spontaneous point mutations that occur more often when advantageous than when neutral. *Genetics, 126*(1), 5-16.

Haussler, S., & Fuqua, C. (2013). Biofilms 2012: new discoveries and significant wrinkles in a dynamic field. *J Bacteriol, 195*(13), 2947-2958. doi: 10.1128/JB.00239-13

Hayhurst, E. J., Kailas, L., Hobbs, J. K., & Foster, S. J. (2008). Cell wall peptidoglycan architecture in *Bacillus subtilis*. *Proc Natl Acad Sci U S A, 105*(38), 14603-14608. doi: 10.1073/pnas.0804138105

Hodgkin, J., & Kaiser, D. (1979). Genetics of gliding motility in *Myxococcus xanthus* (Myxobacterales): Two gene systems control movement. *Molecular and General Genetics MGG, 171*(2), 177-191. doi: 10.1007/BF00270004

Howard, J., & Hyman, A. A. (2003). Dynamics and mechanics of the microtubule plus end. *Nature, 422*(6933), 753-758. doi: 10.1038/nature01600

Ingerson-Mahar, M., Briegel, A., Werner, J. N., Jensen, G. J., & Gitai, Z. (2010). The metabolic enzyme CTP synthase forms cytoskeletal filaments. *Nat Cell Biol, 12*(8), 739-746. doi: 10.1038/ncb2087

Ingerson-Mahar, M., & Gitai, Z. (2012). A growing family: the expanding universe of the bacterial cytoskeleton. *FEMS Microbiol Rev, 36*(1), 256-266. doi: 10.1111/j.1574-6976.2011.00316.x

Islam, S. T., & Mignot, T. (2015). The mysterious nature of bacterial surface (gliding) motility: A focal adhesion-based mechanism in *Myxococcus xanthus*. *Semin Cell Dev Biol, 46*, 143-154. doi: 10.1016/j.semcdb.2015.10.033

Jones, L. J., Carballido-Lopez, R., & Errington, J. (2001). Control of cell shape in bacteria: helical, actin-like filaments in *Bacillus subtilis*. *Cell, 104*(6), 913-922.

Juers, D. H., Matthews, B. W., & Huber, R. E. (2012). LacZ beta-galactosidase: structure and function of an enzyme of historical and molecular biological importance. *Protein Sci, 21*(12), 1792-1807. doi: 10.1002/pro.2165

Kawai, Y., Asai, K., & Errington, J. (2009). Partial functional redundancy of MreB isoforms, MreB, Mbl and MreBH, in cell morphogenesis of *Bacillus subtilis*. *Mol Microbiol, 73*(4), 719-731. doi: 10.1111/j.1365-2958.2009.06805.x

Kawai, Y., Daniel, R. A., & Errington, J. (2009). Regulation of cell wall morphogenesis in *Bacillus subtilis* by recruitment of PBP1 to the MreB helix. *Mol Microbiol, 71*(5), 1131-1144. doi: 10.1111/j.1365-2958.2009.06601.x

Kelley, L. A., Mezulis, S., Yates, C. M., Wass, M. N., & Sternberg, M. J. (2015). The Phyre2 web portal for protein modeling, prediction and analysis. *Nat Protoc, 10*(6), 845-858. doi: 10.1038/nprot.2015.053

Kim, S. J., Chang, J., & Singh, M. (2015). Peptidoglycan architecture of Gram-positive bacteria by solid-state NMR. *Biochim Biophys Acta, 1848*(1 Pt B), 350-362. doi: 10.1016/j.bbamem.2014.05.031

Kramer, N. E., Smid, E. J., Kok, J., de Kruijff, B., Kuipers, O. P., & Breukink, E. (2004). Resistance of Gram-positive bacteria to nisin is not determined by lipid II levels. *FEMS Microbiol Lett, 239*(1), 157-161. doi: 10.1016/j.femsle.2004.08.033

Krasper, L., Lilie, H., Kublik, A., Adrian, L., Golbik, R., & Lechner, U. (2016). The MarR-Type Regulator Rdh2R Regulates rdh Gene Transcription in *Dehalococcoides mccartyi* Strain CBDB1. *J Bacteriol, 198*(23), 3130-3141. doi: 10.1128/JB.00419-16

Kruse, T., Moller-Jensen, J., Lobner-Olesen, A., & Gerdes, K. (2003). Dysfunctional MreB inhibits chromosome segregation in *Escherichia coli*. *EMBO J, 22*(19), 5283-5292. doi: 10.1093/emboj/cdg504

Kuhn, J., Briegel, A., Morschel, E., Kahnt, J., Leser, K., Wick, S., . . . Thanbichler, M. (2010). Bactofilins, a ubiquitous class of cytoskeletal proteins mediating polar localization of a cell wall synthase in *Caulobacter crescentus*. *EMBO J, 29*(2), 327-339. doi: 10.1038/emboj.2009.358

Laloux, G., & Jacobs-Wagner, C. (2014). How do bacteria localize proteins to the cell pole? *J Cell Sci, 127*(Pt 1), 11-19. doi: 10.1242/jcs.138628

Larsen, R. A., Cusumano, C., Fujioka, A., Lim-Fong, G., Patterson, P., & Pogliano, J. (2007). Treadmilling of a prokaryotic tubulin-like protein, TubZ, required for plasmid stability in *Bacillus thuringiensis*. *Genes Dev, 21*(11), 1340-1352. doi: 10.1101/gad.1546107

Lecoq, L., Bougault, C., Hugonnet, J. E., Veckerle, C., Pessey, O., Arthur, M., & Simorre, J. P. (2012). Dynamics induced by beta-lactam antibiotics in the active site of Bacillus subtilis L,D-transpeptidase. *Structure, 20*(5), 850-861. doi: 10.1016/j.str.2012.03.015

Lee, T. K., Tropini, C., Hsin, J., Desmarais, S. M., Ursell, T. S., Gong, E., . . . Huang, K. C. (2014). A dynamically assembled cell wall synthesis machinery buffers cell growth. *Proc Natl Acad Sci U S A, 111*(12), 4554-4559. doi: 10.1073/pnas.1313826111

Li, Z., Trimble, M. J., Brun, Y. V., & Jensen, G. J. (2007). The structure of FtsZ filaments in vivo suggests a force-generating role in cell division. *EMBO J, 26*(22), 4694-4708. doi: 10.1038/sj.emboj.7601895

Lin, L., & Thanbichler, M. (2013). Nucleotide-independent cytoskeletal scaffolds in bacteria. *Cytoskeleton (Hoboken), 70*(8), 409-423. doi: 10.1002/cm.21126

Lowe, J., & Amos, L. A. (2009). Evolution of cytomotive filaments: the cytoskeleton from prokaryotes to eukaryotes. *Int J Biochem Cell Biol, 41*(2), 323-329. doi: 10.1016/j.biocel.2008.08.010

Lutkenhaus, J. (2007). Assembly dynamics of the bacterial MinCDE system and spatial regulation of the Z ring. *Annu Rev Biochem, 76*, 539-562. doi: 10.1146/annurev.biochem.75.103004.142652

Makarova, K. S., & Koonin, E. V. (2010). Two new families of the FtsZ-tubulin protein superfamily implicated in membrane remodeling in diverse bacteria and archaea. *Biol Direct, 5*, 33. doi: 10.1186/1745-6150-5-33

Maughan, H., & Nicholson, W. L. (2004). Stochastic processes influence stationary-phase decisions in *Bacillus subtilis*. *J Bacteriol, 186*(7), 2212-2214.

Mauriello, E. M., Mouhamar, F., Nan, B., Ducret, A., Dai, D., Zusman, D. R., & Mignot, T. (2010). Bacterial motility complexes require the actin-like protein, MreB and the Ras homologue, MglA. *EMBO J, 29*(2), 315-326. doi: 10.1038/emboj.2009.356

Mayer, J. A., & Amann, K. J. (2009). Assembly properties of the *Bacillus subtilis* actin, MreB. *Cell Motil Cytoskeleton, 66*(2), 109-118. doi: 10.1002/cm.20332

Meeske, A. J., Sham, L. T., Kimsey, H., Koo, B. M., Gross, C. A., Bernhardt, T. G., & Rudner, D. Z. (2015). MurJ and a novel lipid II flippase are required for cell wall biogenesis in *Bacillus subtilis*. *Proc Natl Acad Sci U S A, 112*(20), 6437-6442. doi: 10.1073/pnas.1504967112

Meighen, E. A. (1993). Bacterial bioluminescence: organization, regulation, and application of the *lux* genes. *FASEB J, 7*(11), 1016-1022.

Mirouze, N., Ferret, C., Yao, Z., Chastanet, A., & Carballido-Lopez, R. (2015). MreB-dependent inhibition of cell elongation during the escape from competence in *Bacillus subtilis*. *PLoS Genet, 11*(6), e1005299. doi: 10.1371/journal.pgen.1005299

Mohammadi, T., van Dam, V., Sijbrandi, R., Vernet, T., Zapun, A., Bouhss, A., . . . Breukink, E. (2011). Identification of FtsW as a transporter of lipid-linked cell wall precursors across the membrane. *EMBO J, 30*(8), 1425-1432. doi: 10.1038/emboj.2011.61

Monahan, L. G., Hajduk, I. V., Blaber, S. P., Charles, I. G., & Harry, E. J. (2014). Coordinating bacterial cell division with nutrient availability: a role for glycolysis. *MBio, 5*(3), e00935-00914. doi: 10.1128/mBio.00935-14

Muchova, K., Chromikova, Z., & Barak, I. (2013). Control of *Bacillus subtilis* cell shape by RodZ. *Environ Microbiol, 15*(12), 3259-3271. doi: 10.1111/1462-2920.12200

Munoz-Espin, D., Serrano-Heras, G., & Salas, M. (2012). Role of host factors in bacteriophage phi29 DNA replication. *Adv Virus Res, 82*, 351-383. doi: 10.1016/B978-0-12-394621-8.00020-0

Mura, A., Fadda, D., Perez, A. J., Danforth, M. L., Musu, D., Rico, A. I., . . . Massidda, O. (2016). Roles of the essential protein FtsA in cell growth and division in *Streptococcus pneumoniae*. *J Bacteriol*. doi: 10.1128/JB.00608-16

Neuhaus, F. C., & Baddiley, J. (2003). A continuum of anionic charge: structures and functions of D-alanyl-teichoic acids in Gram-positive bacteria. *Microbiol Mol Biol Rev, 67*(4), 686-723.

Nicolas, P., Mader, U., Dervyn, E., Rochat, T., Leduc, A., Pigeonneau, N., . . . Noirot, P. (2012). Condition-dependent transcriptome reveals high-level regulatory architecture in *Bacillus subtilis*. *Science, 335*(6072), 1103-1106. doi: 10.1126/science.1206848

Noguchi, N., Yanagimoto, K., Nakaminami, H., Wakabayashi, M., Iwai, N., Wachi, M., & Sasatsu, M. (2008). Anti-infectious effect of S-benzylisothiourea compound A22, which inhibits the actin-like protein, MreB, in *Shigella flexneri*. *Biol Pharm Bull, 31*(7), 1327-1332.

Nurse, P., & Marians, K. J. (2013). Purification and characterization of *Escherichia coli* MreB protein. *J Biol Chem, 288*(5), 3469-3475. doi: 10.1074/jbc.M112.413708

Oh, S. Y., Shin, J. H., & Roe, J. H. (2007). Dual role of OhrR as a repressor and an activator in response to organic hydroperoxides in *Streptomyces coelicolor*. *J Bacteriol, 189*(17), 6284-6292. doi: 10.1128/JB.00632-07

Olshausen, P. V., Defeu Soufo, H. J., Wicker, K., Heintzmann, R., Graumann, P. L., & Rohrbach, A. (2013). Superresolution imaging of dynamic MreB filaments in *B. subtilis*--a multiple-motor-driven transport? *Biophys J, 105*(5), 1171-1181. doi: 10.1016/j.bpj.2013.07.038

Ouellette, S. P., Karimova, G., Subtil, A., & Ladant, D. (2012). *Chlamydia* co-opts the rod shape-determining proteins MreB and Pbp2 for cell division. *Mol Microbiol, 85*(1), 164-178. doi: 10.1111/j.1365-2958.2012.08100.x

Ouzounov, N., Nguyen, J. P., Bratton, B. P., Jacobowitz, D., Gitai, Z., & Shaevitz, J. W. (2016). MreB orientation correlates with cell diameter in *Escherichia coli*. *Biophys J, 111*(5), 1035-1043. doi: 10.1016/j.bpj.2016.07.017

Percy, M. G., & Grundling, A. (2014). Lipoteichoic acid synthesis and function in Gram-positive bacteria. *Annu Rev Microbiol, 68*, 81-100. doi: 10.1146/annurev-micro-091213-112949

Petek, N. A., & Mullins, R. D. (2014). Bacterial actin-like proteins: purification and characterization of self-assembly properties. *Methods Enzymol, 540*, 19-34. doi: 10.1016/B978-0-12-397924-7.00002-9

Phillips, Z. E., & Strauch, M. A. (2002). *Bacillus subtilis* sporulation and stationary phase gene expression. *Cell Mol Life Sci, 59*(3), 392-402.

Pichoff, S., & Lutkenhaus, J. (2005). Tethering the Z ring to the membrane through a conserved membrane targeting sequence in FtsA. *Mol Microbiol, 55*(6), 1722-1734. doi: 10.1111/j.1365-2958.2005.04522.x

Piggot, P. J., & Hilbert, D. W. (2004). Sporulation of *Bacillus subtilis*. *Curr Opin Microbiol, 7*(6), 579-586. doi: 10.1016/j.mib.2004.10.001

Pisabarro, A. G., de Pedro, M. A., & Vazquez, D. (1985). Structural modifications in the peptidoglycan of *Escherichia coli* associated with changes in the state of growth of the culture. *J Bacteriol, 161*(1), 238-242.

Pogliano, J. (2008). The bacterial cytoskeleton. *Curr Opin Cell Biol, 20*(1), 19-27. doi: 10.1016/j.ceb.2007.12.006

Popp, D., Narita, A., Maeda, K., Fujisawa, T., Ghoshdastider, U., Iwasa, M., . . . Robinson, R. C. (2010). Filament structure, organization, and dynamics in MreB sheets. *J Biol Chem, 285*(21), 15858-15865. doi: 10.1074/jbc.M109.095901

Pottathil, M., & Lazazzera, B. A. (2003). The extracellular Phr peptide-Rap phosphatase signaling circuit of *Bacillus subtilis*. *Front Biosci, 8*, d32-45.

Pradel, N., Santini, C. L., Bernadac, A., Fukumori, Y., & Wu, L. F. (2006). Biogenesis of actin-like bacterial cytoskeletal filaments destined for positioning prokaryotic magnetic organelles. *Proc Natl Acad Sci U S A, 103*(46), 17485-17489. doi: 10.1073/pnas.0603760103

Radeck, J., Fritz, G., & Mascher, T. (2016). The cell envelope stress response of *Bacillus subtilis*: from static signaling devices to dynamic regulatory network. *Curr Genet*. doi: 10.1007/s00294-016-0624-0

Reimold, C., Defeu Soufo, H. J., Dempwolff, F., & Graumann, P. L. (2013). Motion of variable-length MreB filaments at the bacterial cell membrane influences cell morphology. *Mol Biol Cell, 24*(15), 2340-2349. doi: 10.1091/mbc.E12-10-0728

Rueff, A. S., Chastanet, A., Dominguez-Escobar, J., Yao, Z., Yates, J., Prejean, M. V., . . . Carballido-Lopez, R. (2014). An early cytoplasmic step of peptidoglycan synthesis is associated to MreB in *Bacillus subtilis*. *Mol Microbiol, 91*(2), 348-362. doi: 10.1111/mmi.12467

Ruiz, N. (2015). Lipid flippases for bacterial peptidoglycan biosynthesis. *Lipid Insights, 8*(Suppl 1), 21-31. doi: 10.4137/LPI.S31783

Ruiz, N. (2016). Filling holes in peptidoglycan biogenesis of *Escherichia coli*. *Curr Opin Microbiol, 34*, 1-6. doi: 10.1016/j.mib.2016.07.010

Sauvage, E., Kerff, F., Terrak, M., Ayala, J. A., & Charlier, P. (2008). The penicillin-binding proteins: structure and role in peptidoglycan biosynthesis. *FEMS Microbiol Rev, 32*(2), 234-258. doi: 10.1111/j.1574-6976.2008.00105.x

Sauvage, E., & Terrak, M. (2016). Glycosyltransferases and transpeptidases/penicillin-binding proteins: valuable targets for new antibacterials. *Antibiotics (Basel), 5*(1). doi: 10.3390/antibiotics5010012

Schirner, K., & Errington, J. (2009). The cell wall regulator {sigma}I specifically suppresses the lethal phenotype of *mbl* mutants in *Bacillus subtilis*. *J Bacteriol, 191*(5), 1404-1413. doi: 10.1128/JB.01497-08

Sezonov, G., Joseleau-Petit, D., & D'Ari, R. (2007). *Escherichia coli* physiology in Luria-Bertani broth. *J Bacteriol, 189*(23), 8746-8749. doi: 10.1128/JB.01368-07

Sham, L. T., Butler, E. K., Lebar, M. D., Kahne, D., Bernhardt, T. G., & Ruiz, N. (2014). Bacterial cell wall. MurJ is the flippase of lipid-linked precursors for peptidoglycan biogenesis. *Science, 345*(6193), 220-222. doi: 10.1126/science.1254522

Siegel, S. D., Liu, J., & Ton-That, H. (2016). Biogenesis of the Gram-positive bacterial cell envelope. *Curr Opin Microbiol, 34*, 31-37. doi: 10.1016/j.mib.2016.07.015

Sievers, F., Wilm, A., Dineen, D., Gibson, T. J., Karplus, K., Li, W., . . . Higgins, D. G. (2011). Fast, scalable generation of high-quality protein multiple sequence alignments using Clustal Omega. *Mol Syst Biol, 7*, 539. doi: 10.1038/msb.2011.75

Silhavy, T. J., Kahne, D., & Walker, S. (2010). The bacterial cell envelope. *Cold Spring Harb Perspect Biol, 2*(5), a000414. doi: 10.1101/cshperspect.a000414

Slager, J., & Veening, J. W. (2016). Hard-wired control of bacterial processes by chromosomal gene location. *Trends Microbiol, 24*(10), 788-800. doi: 10.1016/j.tim.2016.06.003

Sonkaria, S., Fuentes, G., Verma, C., Narang, R., Khare, V., Fischer, A., & Faivre, D. (2012). Insight into the assembly properties and functional organisation of the magnetotactic bacterial actin-like homolog, MamK. *PLoS One, 7*(5), e34189. doi: 10.1371/journal.pone.0034189

Strauch, M. A., & Hoch, J. A. (1993). Transition-state regulators: sentinels of *Bacillus subtilis* post-exponential gene expression. *Mol Microbiol, 7*(3), 337-342.

Sung, H. M., & Yasbin, R. E. (2002). Adaptive, or stationary-phase, mutagenesis, a component of bacterial differentiation in *Bacillus subtilis*. *J Bacteriol, 184*(20), 5641-5653.

Swulius, M. T., Chen, S., Jane Ding, H., Li, Z., Briegel, A., Pilhofer, M., . . . Jensen, G. J. (2011). Long helical filaments are not seen encircling cells in electron cryotomograms of rod-shaped bacteria. *Biochem Biophys Res Commun, 407*(4), 650-655. doi: 10.1016/j.bbrc.2011.03.062

Swulius, M. T., & Jensen, G. J. (2012). The helical MreB cytoskeleton in *Escherichia coli* MC1000/pLE7 is an artifact of the N-Terminal yellow fluorescent protein tag. *J Bacteriol, 194*(23), 6382-6386. doi: 10.1128/JB.00505-12

Tanaka, K., Henry, C. S., Zinner, J. F., Jolivet, E., Cohoon, M. P., Xia, F., . . . Noirot, P. (2013). Building the repertoire of dispensable chromosome regions in *Bacillus subtilis* entails major refinement of cognate large-scale metabolic model. *Nucleic Acids Res, 41*(1), 687-699. doi: 10.1093/nar/gks963

Tipper, D. J., & Strominger, J. L. (1965). Mechanism of action of penicillins: a proposal based on their structural similarity to acyl-D-alanyl-D-alanine. *Proc Natl Acad Sci U S A, 54*(4), 1133-1141.

Toro-Nahuelpan, M., Muller, F. D., Klumpp, S., Plitzko, J. M., Bramkamp, M., & Schuler, D. (2016). Segregation of prokaryotic magnetosomes organelles is driven by treadmilling of a dynamic actin-like MamK filament. *BMC Biol, 14*(1), 88. doi: 10.1186/s12915-016-0290-1

Tran, H. J., Heroven, A. K., Winkler, L., Spreter, T., Beatrix, B., & Dersch, P. (2005). Analysis of RovA, a transcriptional regulator of *Yersinia pseudotuberculosis* virulence that acts through antirepression and direct transcriptional activation. *J Biol Chem, 280*(51), 42423-42432. doi: 10.1074/jbc.M504464200

Turner, R. D., Hobbs, J. K., & Foster, S. J. (2016). Atomic force microscopy analysis of bacterial cell wall peptidoglycan architecture. *Methods Mol Biol, 1440*, 3-9. doi: 10.1007/978-1-4939-3676-2_1

Typas, A., Banzhaf, M., Gross, C. A., & Vollmer, W. (2011). From the regulation of peptidoglycan synthesis to bacterial growth and morphology. *Nat Rev Microbiol, 10*(2), 123-136. doi: 10.1038/nrmicro2677

Ursell, T. S., Nguyen, J., Monds, R. D., Colavin, A., Billings, G., Ouzounov, N., . . . Huang, K. C. (2014). Rod-like bacterial shape is maintained by feedback between cell curvature and cytoskeletal localization. *Proc Natl Acad Sci U S A, 111*(11), E1025-1034. doi: 10.1073/pnas.1317174111

van den Ent, F., Amos, L. A., & Lowe, J. (2001). Prokaryotic origin of the actin cytoskeleton. *Nature, 413*(6851), 39-44. doi: 10.1038/35092500

van Heijenoort, J. (1998). Assembly of the monomer unit of bacterial peptidoglycan. *Cell Mol Life Sci, 54*(4), 300-304. doi: 10.1007/s000180050155

van Heijenoort, Y., Gomez, M., Derrien, M., Ayala, J., & van Heijenoort, J. (1992). Membrane intermediates in the peptidoglycan metabolism of *Escherichia coli*: possible roles of PBP 1b and PBP 3. *J Bacteriol, 174*(11), 3549-3557.

van Teeffelen, S., & Gitai, Z. (2011). Rotate into shape: MreB and bacterial morphogenesis. *EMBO J, 30*(24), 4856-4857. doi: 10.1038/emboj.2011.430

van Teeffelen, S., Wang, S., Furchtgott, L., Huang, K. C., Wingreen, N. S., Shaevitz, J. W., & Gitai, Z. (2011). The bacterial actin MreB rotates, and rotation depends on cell-wall assembly. *Proc Natl Acad Sci U S A, 108*(38), 15822-15827. doi: 10.1073/pnas.1108999108

Vazquez-Torres, A. (2012). Redox active thiol sensors of oxidative and nitrosative stress. *Antioxid Redox Signal, 17*(9), 1201-1214. doi: 10.1089/ars.2012.4522

Vollmer, W., Blanot, D., & de Pedro, M. A. (2008). Peptidoglycan structure and architecture. *FEMS Microbiol Rev, 32*(2), 149-167. doi: 10.1111/j.1574-6976.2007.00094.x

Vollmer, W., & Holtje, J. V. (2004). The architecture of the murein (peptidoglycan) in Gram-negative bacteria: vertical scaffold or horizontal layer(s)? *J Bacteriol, 186*(18), 5978-5987. doi: 10.1128/JB.186.18.5978-5987.2004

Wachi, M., Doi, M., Tamaki, S., Park, W., Nakajima-Iijima, S., & Matsuhashi, M. (1987). Mutant isolation and molecular cloning of mre genes, which determine cell shape, sensitivity to mecillinam, and amount of penicillin-binding proteins in *Escherichia coli*. *J Bacteriol, 169*(11), 4935-4940.

Wertman, K. F., Drubin, D. G., & Botstein, D. (1992). Systematic mutational analysis of the yeast ACT1 gene. *Genetics, 132*(2), 337-350.

White, C. L., Kitich, A., & Gober, J. W. (2010). Positioning cell wall synthetic complexes by the bacterial morphogenetic proteins MreB and MreD. *Mol Microbiol, 76*(3), 616-633. doi: 10.1111/j.1365-2958.2010.07108.x

Young, K. D. (2014). Microbiology. A flipping cell wall ferry. *Science, 345*(6193), 139-140. doi: 10.1126/science.1256585

Résumé de la thèse

L'acquisition et le maintient de la forme bactérienne ont été consciencieusement étudiés pendant une très longue période. Néanmoins, il reste encore beaucoup de questions sans réponse. Les bactéries Gram-positives présentent une couche externe rigide (la paroi cellulaire) qui permet de préserver la pression osmotique interne et la morphologie cellulaire. La paroi cellulaire (CW) est principalement formée par un maillage de polymères de sucres, le peptidoglycane (PG), sur lequel sont accrochés des acides téichoïques. L'absence de cette barrière essentielle provoque la perte de forme et, finalement, la lyse de la cellule. L'intégrité du CW est par conséquent d'une importance vitale pour les bactéries.

La structure ainsi que la synthèse correcte du CW dépendent de supposées machineries d'élongation du peptidoglycane (PGEM) chargées d'assembler le réseau du PG. Le fonctionnement et la composition des PGEMs restent incertains, mais on sait qu'ils dépendent d'une protéine essentielle : MreB, une protéine procaryote similaire à l'actine. MreB est suspectée de contrôler l'activité et/ou l'assemblage des PGEMs, mais sa fonction exacte comme son mode de régulation sont actuellement inconnus. J'utilise *Bacillus subtilis*, le modèle des bactéries Gram-positives, pour mieux comprendre les fonctions de MreB via i- le développement et l'utilisation d'un criblage génétique pour l'identification de mutants de *mreB* non fonctionnels et ii- l'étude d'un effecteur potentiel de MreB.

(i) MreB a été étudié pendant près de deux décennies et pourtant, sa (ses) fonction(s) reste(nt) mal comprise(s). Comme les approches biochimiques se sont révélées particulièrement difficiles jusqu'à présent, la plupart des études se sont concentrées sur la localisation cellulaire et la dynamique de la protéine. Au cours de mes travaux, j'ai conçu un criblage génétique au moyen duquel j'ai obtenu une collection de mutants de *mreB* fonctionnellement déficients, chez *B. subtilis*. La caractérisation de ces mutants a révélé de nombreux résidus importants pour le fonctionnement de la protéine. De façon intéressante, mes résultats indiquent que certains mutants ont conservé leurs propriétés dynamiques (suggérant une association fonctionnelle aux PGEMs) en plus d'une morphologie de type sauvage, tout en étant fortement affectés pour la croissance. Des résultats préliminaires indiquent que ces mutants sont compromis dans leur capacité à utiliser certaines sources de carbone, reliant MreB au métabolisme cellulaire. Ceci suggère l'existence soit d'un point de contrôle, soit d'un couplage entre le métabolisme du carbone et l'expansion du CW chez *B. subtilis*.

(ii) Des résultats non publiés de notre groupe ont révélé l'existence d'un opéron non caractérisé (*ydcFGH*) dont l'expression est fortement induite en absence de *mreB*, par comparaison à la souche sauvage. J'ai 1- mis en évidence la cause probable de l'induction de cet opéron en l'absence de MreB, révélant ainsi l'existence de nombreuses mutations dans la souche Δ*mreB* et 2- réalisé une caractérisation poussée de chaque gène de l'opéron *ydcFGH*. Bien que le lien exact entre MreB et *ydcFGH* soit encore inconnu, nos résultats suggèrent un rôle potentiel d'YdcH dans le contrôle du

métabolisme du carbone et l'adaptation à la phase stationnaire. À la lumière de mes données issues du criblage génétique (i), ces résultats indiquent un lien fort entre MreB et le métabolisme du carbone.

Thesis abstract

Acquisition and maintenance of the bacterial shape has been conscientiously studied for a long time. Nevertheless, there are still many unanswered questions. Gram-positive bacteria present a rigid external coating (cell wall) that allows them to preserve internal osmotic pressure and cell morphology. The cell wall (CW) is mainly formed by the peptidoglycan meshwork (PG), that confers its structure to the CW, to which are connected teichoic acids. The absence of this essential barrier causes the loss of shape and, ultimately, lysis of the cells. Integrity of the CW is, therefore, a matter of vital importance for bacteria.

Proper CW synthesis and structure depends on the so-called peptidoglycan elongation machineries (PGEM) in charge of building the PG meshwork. The precise composition and functioning of the PGEM is not completely understood but they rely on a key player: MreB, a conserved prokaryotic actin-like protein. MreB is suspected to control PGEM activity and/or assembly but its precise function and mode of regulation are currently unknown. I used *Bacillus subtilis*, the model for Gram-positive bacteria, to gain a better understanding of MreB functions via i- the development and use of a genetic screen for loss-of-function mutants of *mreB* and ii- the study of a potential effector of MreB.

(i) MreB has been studied for almost two decades now and still, little is known about its function(s). Since biochemical approaches proved to be difficult so far, most of the studies have focused on cellular localization and dynamics of the protein. Here, I have designed a genetic screen by means of which I have obtained a collection of functionally impaired *mreB* mutants in *B. subtilis*. Characterization of these mutants revealed numerous key residues for the functioning of the protein. Interestingly, my results indicate that some mutants have kept their dynamic properties (suggesting functional association to the PGEM) together with a wild type shape, while being strongly affected for growth. Preliminary results indicate an impaired ability to use certain carbon sources linking MreB to cellular metabolism. This suggests the existence of either a checkpoint or a coupling between carbon metabolism and CW expansion in *B. subtilis*.

(ii) Unpublished results from our group revealed the existence of an uncharacterized operon (*ydcFGH*), whose expression is highly induced in the absence of *mreB* by comparison to the wild type. I have 1- deciphered the cause of *ydcFGH* induction in the absence of MreB, revealing the existence of multiple mutations in the Δ*mreB* strain and 2- realized a thorough characterization of each gene of the *ydcFGH* operon. Although the exact link between MreB and *ydcFGH* is yet unknown, my results suggest a potential role of YdcH in the control of carbon metabolism and adaptation to stationary phase. In light of my mutagenesis screen data (i), these results are pointing towards a strong link between MreB and carbon metabolism.

université PARIS-SACLAY | ÉCOLE DOCTORALE Structure et dynamique des systèmes vivants (SDSV)

Titre : Développement d'un criblage fonctionnel de mutants de MreB chez *Bacillus subtilis* et caractérisation d'un effecteur putative de *mreB*

Mots clés : microbiologie, *Bacillus subtilis*, MreB, peptidoglycan

Résumé : Les bactéries sont de minuscules organismes présentes partout : l'air, le sol, notre peau ou dans nos intestins. Si la plupart sont neutres, voir bénéfiques pour notre organisme, d'autres sont malheureusement malfaisantes. Parce que les bactéries ont, de plus, une grande capacité à échapper aux traitements, nous devons en permanence découvrir de nouveaux remèdes et approfondir notre compréhension de la façon dont elles fonctionnent.

Une cible privilégiée des antibactériens est la paroi des bactéries. Celle-ci, telle une carapace, les protège, mais constitue aussi leur talon d'Achille, sa destruction compromettant leur survie. Ce projet consiste à mieux comprendre comment cette paroi est assemblée en étudiant les machines moléculaires qui la fabrique, et en particulier certaines parties de ces machines (protéines) dont la fonction reste incomprise. Je me concentre également sur la façon dont d'autres fonctions cellulaires sont affectées lorsque ces machines sont défectueuses.

Title : Development of a functional screen for MreB mutants in *Bacillus subtilis* and characterization of a putative *mreB* effector

Keywords : microbiology, *Bacillus subtilis*, MreB, peptidoglycan

Abstract : Bacteria are tiny organisms found everywhere: in the air, soil, our skin or in our intestines. If most of them are neutral, even beneficial for us, others are less innocuous. Because they have a great ability to escape treatments by developing mechanisms of resistance, we always need to discover new cures, and deepen our understanding of how bacteria function.

A preferred target of antibacterial compounds is the bacterial wall. This wall is like a shell, protecting them. But as such, it also constitutes their Achilles heel as they can't survive without it. This project aims to understand how this wall is assembled by studying the molecular machines that makes it, and in particular parts of these machines (proteins), which functions are still unknown. I also focus on how other functions of the cell are altered when these proteins are defective.